

**Development of Thermoplastic Composite Tubes for  
Large Deformation**

**Bijan Derisi**

A Thesis

in

The Department

of

Mechanical and Industrial Engineering

Presented in Partial Fulfillment of the Requirements

For the Degree of Doctor of Philosophy at

Concordia University

Montreal, Quebec, Canada

June 2008

© Bijan Derisi, 2008



Library and  
Archives Canada

Bibliothèque et  
Archives Canada

Published Heritage  
Branch

Direction du  
Patrimoine de l'édition

395 Wellington Street  
Ottawa ON K1A 0N4  
Canada

395, rue Wellington  
Ottawa ON K1A 0N4  
Canada

*Your file* *Votre référence*  
*ISBN: 978-0-494-45654-5*  
*Our file* *Notre référence*  
*ISBN: 978-0-494-45654-5*

**NOTICE:**

The author has granted a non-exclusive license allowing Library and Archives Canada to reproduce, publish, archive, preserve, conserve, communicate to the public by telecommunication or on the Internet, loan, distribute and sell theses worldwide, for commercial or non-commercial purposes, in microform, paper, electronic and/or any other formats.

The author retains copyright ownership and moral rights in this thesis. Neither the thesis nor substantial extracts from it may be printed or otherwise reproduced without the author's permission.

**AVIS:**

L'auteur a accordé une licence non exclusive permettant à la Bibliothèque et Archives Canada de reproduire, publier, archiver, sauvegarder, conserver, transmettre au public par télécommunication ou par l'Internet, prêter, distribuer et vendre des thèses partout dans le monde, à des fins commerciales ou autres, sur support microforme, papier, électronique et/ou autres formats.

L'auteur conserve la propriété du droit d'auteur et des droits moraux qui protègent cette thèse. Ni la thèse ni des extraits substantiels de celle-ci ne doivent être imprimés ou autrement reproduits sans son autorisation.

---

In compliance with the Canadian Privacy Act some supporting forms may have been removed from this thesis.

Conformément à la loi canadienne sur la protection de la vie privée, quelques formulaires secondaires ont été enlevés de cette thèse.

While these forms may be included in the document page count, their removal does not represent any loss of content from the thesis.

Bien que ces formulaires aient inclus dans la pagination, il n'y aura aucun contenu manquant.

  
**Canada**

## **Abstract**

### **Development of Thermoplastic Composite Tubes for Large Deformation**

**Bijan Derisi, Ph.D.**

**Concordia University, 2008**

Composites have proved their great potentials for many aerospace applications, where the high performance can justify the high cost. However, the brittleness of the composites has been a main drawback for many applications that require large deformation, high failure strain and extensive energy absorption before final fracture.

The objective of this research is to present a solution to the brittleness of the composites in tubular form and to introduce a composite tube that shows the same strength, stiffness and failure strain as its high grade Aluminum 7075-T6 counterpart tube.

One application of this research can be in the development of composite landing gear for helicopters. Up to date, almost all helicopter landing gears are made of high strength aluminum, and despite their major issues in maintenance and fabrication, aluminum landing gears have remained the only choice for the helicopter manufacturing industry. Substitution of aluminum landing gear for helicopters with a thermoplastic composite landing gear is really a challenge, but if this can be done, it would be for the first time in the world!

Through this research, the mechanical behavior of flat plate Carbon AS4/PEKK is characterized, and the potential mechanisms for large deformation of composite laminates are sought. The outcomes are used to design a composite tube that shows the same strength, stiffness and deformability as its high grade aluminum counterpart. The

accuracy of the design is verified through progressive failure by ANSYS analysis and experimental work.

Strain Controlled Design is introduced as a new design technique to substitute for the traditional stiffness-controlled techniques whenever large deformation from composite laminates is expected. The analytical techniques for stress analysis of composite tubes are reviewed, and the cumbersomeness of the method is highlighted.

Finally, a simplified technique is presented to analyze composite tubes as a sandwich panel model. The results of the analysis are compared with the ANSYS and experimental results. Agreement between three methods is demonstrated. Moreover, guidelines for the design of composite tubes that exhibit large deformation before failure are presented.

## Acknowledgement

First, I would like to thank Concordia University for providing me the opportunity to conduct this research and meet a unique scientist in the complex world of composites, Professor S.V. Hoa. I have to appreciate all the supports and encouragements he has provided for me through four years of hard work and challenge. I am also grateful to my co-supervisor, Dr. M. Hojjati, and members of the research committee, Dr. F. Haghghat, Dr. M. Pugh, and Dr. R. Sedaghati for their great feedback and support through this effort.

I use this opportunity to thank people in CRIAQ, Bell Helicopter, Cytec and NRC-AMTC who collaborated in this project and helped me to overcome numerous obstacles. Meanwhile many thanks to School of Graduate Studies of Concordia University and the donors of the following awards, which I have been honored to receive:

- Port of Montreal Award in Transportation Studies;
- JW McConnell Memorial Award;
- Canada Steamship Lines Inc.: Award in Transportation Studies;
- Campaign for a New Millennium Graduate Scholarship;
- Power Corporation of Canada Graduate Fellowships;
- Teaching Fellowship: Faculty of Engineering and Computer Science of Concordia University;

I would also like to thank the research assistants and associates at CONCOM especially Mr. M. Mourtazov and Dr. M. Xie who willingly assisted me through this work.

Last but not the least, I have to present my deep appreciation to my great family who have been supportive and encouraging through my life until I have achieved this honor.

To

*Eternal souls of my Parents*

# Table of Content

<b>List of Figures.....</b>	<b>xii</b>
<b>List of Tables.....</b>	<b>xxi</b>
<b>Nomenclature.....</b>	<b>xxii</b>
<b>Chapter 1:</b>	
<b><u>Introduction</u> .....</b>	<b>1</b>
1-1 Background.....	1
1-2 Design challenges associated with aluminum landing gear.....	4
1-3 Objective and plans of the research.....	7
1-4 Structure of composites.....	9
1-5 Selection of materials.....	17
1-5.1 Reinforcements.....	18
1-5.2 Matrices.....	26
1-5.3 PolyEtherKetoneKetone (PEKK).....	30
1-5.4 Carbon AS4/PEKK composite.....	34
1-6 Fabrication process of Carbon/PEKK composites.....	37
1-6.1 Compression molding.....	41
1-6.2 Automated fiber placement.....	44

## **Chapter 2:**

<b><u>Review of Analytical Techniques for Composite Tubes</u></b> .....	49
2-1 Introduction.....	49
2-2 Previous works .....	51
2-3 Definition of terms and general equations.....	52
2-3.1 General Hooke's law for anisotropic bodies .....	55
2-3.2 General Hooke's law for orthotropic bodies .....	55
2-3.3 Transformation of elastic constants.....	57
2-4 Analysis of anisotropic tubes.....	58
2-4.1 Displacements and strain functions.....	63
2-4.2 Stress functions.....	65
2-4.3 Solving the differential equations.....	67
2-4.4 Stresses and displacement functions.....	70
2-5 Analytical solution for composite tubes.....	72
2-6 equilibrium of an anisotropic cantilever beam.....	78
2-7 Summary and conclusion.....	80

## **Chapter 3:**

<b><u>Characterization of the Mechanical Properties of Carbon AS4/PEKK Composite</u></b> ..	82
3-1 Introduction.....	82
3-2 Manufacturing and testing of the composite laminates.....	85
3-3 Mechanical Properties in the Fiber Direction, $0^\circ$ .....	96

3-4	Mechanical properties in the transverse direction, 90°	100
3-5	Mechanical properties of quasi isotropic laminates	106
3-6	Mechanical properties of $\pm 45^\circ$ laminates	112
3-7	Mechanical properties of $\pm 30^\circ$ laminates	116
3-8	Mechanical behavior of $[30^\circ/\text{Resin}/-30^\circ/\text{Resin}]_{2s}$	121
3-9	Mechanical behavior of $[\pm 30^\circ/\pm 45^\circ]_s$	124
3-10	Mechanical properties of $\pm 25^\circ$ laminates	127
3-11	Mechanical properties of $\pm 20^\circ$ laminates	128
3-12	Summary and discussion	130

**Chapter 4:**

	<b><u>A Procedure for Bending Test of the Tubes</u></b>	136
4-1	Introduction	136
4-2	Design and manufacturing of the fixture	140
4-3	Three-point bending test of aluminum tubes	146
4-3.1	Aluminum tubes test 1: No pad	147
4-3.2	Aluminum tubes test 2: Rubber pad	153
4-3.3	Aluminum tubes test 3: Composite pad	156
4-4	Results from three bending tests on aluminum tubes	159

## **Chapter 5:**

<b><u>Design of the Composite Tubes for Large Deformation</u></b> .....	162
5-1 Introduction.....	162
5-2 Design and testing the first composite tube.....	164
5-3 Design of a composite tube for large deformation.....	170
5-3.1 Strain controlled design.....	172
5-3.2 Design for the strength and stiffness.....	174
5-3.3 Stress analysis according to CLT.....	177
5-4 Design, manufacturing and testing the second composite tube.....	182
5-4.1 Design of the layup.....	183
5-4.2 Stress analysis of the layup.....	184
5-4.3 Testing and failure analysis second composite tube.....	186
5-4.4 Testing the second composite tube: first run .....	190
5-4.5 Testing the second composite tube: second run.....	192
5-4.6 Testing the second composite tube: third run .....	193
5-4.7 Testing the second composite tube: fourth run .....	194
5-4.8 Final test on the second composite tube.....	195
5-4.9 Analysis of the results.....	201
5-4.10 Summary and conclusions.....	208
5-5 Design and manufacturing the third composite tube.....	210
5-5.1 Design of the layup.....	211

5-5.2	Stress analysis of the layup.....	213
5-5.3	Testing the third composite tube.....	219
5-5.4	Failure analysis of the third tube.....	222
5-6	Design and testing the fourth composite tube.....	226
5-6.1	Layup of the tube .....	227
5-6.2	Stress analysis of the layup.....	228
5-6.3	Testing and the results.....	232
5-7	ANSYS results.....	239
5-8	Extraction of design procedure.....	241
<b>Chapter 6:</b>		
<b><u>Summary and Conclusions</u>.....</b>		
6-1	Summary.....	250
6-2	Conclusion.....	252
6-3	Contribution.....	253
6-4	Process for design.....	255
6-5	Future work.....	258
<b>References.....</b>		
		260

**Appendices:**

Appendix A: Compression Mold Drawings.....267

Appendix B: Installation of Strain Gauges on Thermoplastic Composites.....269

Appendix C: Three-Point Bending Fixture Drawings.....277

Appendix D: Four-Point Bending Fixture Drawings .....290

## List of Figures

Figure 1-1	Helicopter landing gear.....	2
Figure 1-2	Bell Model 429 with sleigh type skid gear, Minderhoud (2008).....	3
Figure 1-3	Bell Model 427 with conventional skid gear, Minderhoud (2008).....	3
Figure 1-4	A typical thermoplastic resin in (a) liquid (b) solid forms.....	15
Figure 1-5	A typical thermosetting resin in (a) liquid (b) solid forms.....	16
Figure 1-6	Application of para-aramid fibers, Hearle (2002).....	21
Figure 1-7	Structure of high strength PAN based carbon fiber, Morgan (2005).....	23
Figure 1-8	Strength-modulus profile of carbon fibers, Hearle (2002).....	25
Figure 1-9	Filament wound (In-situ consolidated) PEKK/Carbon AS4 towpreg .....	32
Figure 1-10	Application of PEKK polymer in interior design.....	33
Figure 1-11	Mechanical Properties of thermoplastic polymers.....	36
Figure 1-12	Different forms of Carbon AS4/PEKK prepreg.....	38
Figure 1-13	Processing profile for thermoplastic composite.....	39
Figure1-14	Wabash compression molding machine.....	42
Figure1-15	A mold for processing thermoplastic composites by compression molding.....	42
Figure1-16	Time-temperature profile for processing carbon AS4/ PEKK composite.....	43
Figure 1-17	The processing head for fiber placement system, Morgan (2005).....	44

Figure 1-18	Fiber placement head, Lamontia et al (2002).....	46
Figure 1-19	Temperature and pressure profiles for fiber placement process, Lamontia et al (2002).....	47
Figure 1-20	The fiber placement machine at AMTC-NRC.....	48
Figure 2-1	Anisotropic tube subjected to bending, twisting and axial load.....	59
Figure 2-2	Cross section of a composite tube having $N$ layers.....	73
Figure 2-3	A cantilever anisotropic beam.....	78
Figure 3-1	Preform of Carbon/AS4 PEKK for compression molding.....	85
Figure 3-2	Variation in the ply stiffness by variation in the fiber direction.....	86
Figure 3-3	A sample installed at the MTS machine ready for the tensile test.....	88
Figure 3-4	Grinding and polishing equipment.....	89
Figure 3-5	Fracture of the fibers due to a high processing pressure.....	91
Figure 3-6	A resin rich area in a Carbon AS4/ PEKK laminate.....	92
Figure 3-7	Micrograph of $[0/45/90/-45]_s$ laminate in 0 direction.....	93
Figure 3-8	A typical mold for compression molding.....	94
Figure 3-9	Schematic debulking of a laminate inside a mold.....	95
Figure 3-10	Strength of Carbon AS4/PEKK $0^\circ$ laminate.....	96
Figure 3-11	Stress-strain curves of Carbon AS4/PEKK specimens in fiber direction.....	97
Figure 3-12	Fractured samples of Carbon AS4/PEKK $0^\circ$ laminate after tensile tests.....	98

Figure 3-13	The variation of Poisson's ratio by axial strain.....	99
Figure 3-14	Micrograph of Carbon AS4/PEKK in 0° Direction.....	100
Figure 3-15	Tensile Strength of Carbon AS4/PEKK laminate 90° directions.....	101
Figure 3-16	Tensile Strength of Carbon AS4/PEKK laminate in 90° direction.....	102
Figure 3-17	Propagation of the cracks parallel to the fiber direction and debonding.....	103
Figure 3-18	Fracture of 90 degree Carbon AS4/PEKK laminate.....	104
Figure 3-19	Micrographs in the fiber and transverse directions.....	105
Figure 3-20	Processing temperatures at different stages of the fabrication.....	107
Figure 3-21	Strength of carbon AS4/PEKK quasi isotropic laminates.....	108
Figure 3-22	Fractured samples of quasi isotropic laminate after tensile test.....	109
Figure 3-23	Stress-Strain curve of carbon AS4/PEKK quasi isotropic laminate.....	110
Figure 3-24	Micrograph of [0/45/90/-45] <sub>s</sub> laminate in 0 direction.....	111
Figure 3-25	Stress-Strain curve of carbon AS4/PEKK [±45°] <sub>2s</sub> laminate.....	113
Figure 3-26	Stress-Strain curve of carbon AS4/PEKK [±45°] <sub>2s</sub> laminate.....	114
Figure 3-27	A carbon AS4/PEKK [±45°] <sub>2s</sub> laminate specimen after tensile test.....	115
Figure 3-28	Strength of Carbon AS4/PEKK [±30°] <sub>2s</sub> laminates.....	117
Figure 3-29	Stress-strain curves of Carbon AS4/PEKK [±30°] <sub>2s</sub> specimens.....	118
Figure 3-30	Fracture of Carbon AS4/PEKK [±30°] <sub>2s</sub> specimens after tensile test.....	119
Figure 3-31	Measuring the rotation of the fibers during the tensile test.....	120
Figure 3-32	Stress- strain curves for Carbon/PEKK [30°/Resin/-30°/Resin] <sub>2s</sub> laminate.....	121

Figure 3-33	Fracture of carbon AS4/PEKK $[30^\circ/\text{Resin}/-30^\circ/\text{Resin}]_{2s}$ specimens by tensile tests.....	123
Figure 3-34	Stress-strain curves of carbon AS4/PEKK $[\pm 30^\circ/\pm 45^\circ]_s$ specimens.....	125
Figure 3-35	Fracture of carbon AS4/PEKK $[\pm 30^\circ/\pm 45^\circ]_s$ specimens by tensile tests.....	126
Figure 3-36	Delamination areas between the $\pm 30^\circ$ and $\pm 45^\circ$ layers.....	126
Figure 3-37	Stress- strain curves for Carbon/PEKK $[\pm 25^\circ]_{2s}$ laminate.....	128
Figure 3-38	Stress- strain curves for Carbon/PEKK $[\pm 20^\circ]_{2s}$ laminate.....	129
Figure 3-39	Fractured pieces of $[\pm 20^\circ]_{2s}$ laminate specimens after tensile test.....	130
Figure 3-40	Theoretical prediction of stress- strain curves for $[90/(\pm 45^\circ)_3/0]_{2s}$ laminate.....	132
Figure 3-41	Test results for stress- strain curves of $[90/(\pm 45^\circ)_3/0]_{2s}$ laminate.....	133
Figure 3-42	Stress-Strain curves of medium angle Carbon/PEKK laminates.....	134
Figure 3-43	Stress-Strain curves of low angle Carbon/PEKK laminate.....	135
Figure 4-1	Schematic dimensions of helicopter landing gear: Front Cross Tube....	138
Figure 4-2	Four point bending test set up on MTS machine.....	141
Figure 4-3	Strain distribution in the aluminum tube.....	143
Figure 4-4	Deflection of the tube.....	144
Figure 4-5	Assembly drawing of the fixture for 3 point bending test.....	145
Figure 4-6	Test set up of aluminum tube: test 1.....	147
Figure 4-7	Two double strain gauges installed on the bottom line of the tube.....	148
Figure 4-8	Deformation of aluminum tube during bending test.....	149

Figure 4-9	Force-axial strain at mid span and at 12cm offset from midpoint.....	150
Figure 4-10	Force circumferential strain in mid span and 12cm offset.....	151
Figure 4-11	Localized deformations at the loading nose.....	151
Figure 4-12	Bearing stress is the only cause of deformation at supporting points.....	152
Figure 4-13	Test set up for second test; wire meshed rubber under loading nose.....	153
Figure 4-14	Deformation of the second aluminum tube.....	154
Figure 4-15	Local deformation at the loading nose during the test of second tube....	155
Figure 4-16	Bending force versus axial strain.....	155
Figure 4-17	Test set up with composite pad under load applicator.....	156
Figure 4-18	Surfaces of the tube and the fiberglass pad after the test.....	157
Figure 4-19	Force-axial strain at the mid span and at 12 cm offset from midpoint....	158
Figure 4-20	Force-circumferential strain at the mid-span and at 12 cm offset.....	159
Figure 4-21	Different pads affect the behavior of the aluminum tubes in bending....	161
Figure 5-1	Set up for the four point bending test.....	164
Figure 5-2	Force- longitudinal strain at the mid-span of $[90^{\circ}_{20}/0^{\circ}_{20}]$ composite tube.....	165
Figure 5-3	Brittle fracture of the first composite tube.....	166
Figure 5-4	Deformation of the tube is mostly due to the rigid body motion.....	167
Figure 5-5	Fracture occurred at the loading noses.....	168
Figure 5-6	Schematic presentation of harsh landing.....	171
Figure 5-7	Linear strain distribution at the thickest cross section of the landing gear front skid tube where ID 56mm (2.25") OD 88mm (3.5").....	172

Figure 5-8	Strain distribution in the composite tube.....	174
Figure 5-9	Aluminum and composite tubes cross sections; Dimensions in mm.....	175
Figure 5-10	Cross sections AA' and BB' for the aluminum and composite tubes.....	177
Figure 5-11	Aluminum and composite sandwich panels.....	178
Figure 5-12	Laying up a tapered fiber glass pad on the composite tube.....	186
Figure 5-13	Location of strain gauges at the bottom line and 45° offset.....	187
Figure 5-14	Four <i>T</i> strain gauges installed on the second composite tube.....	187
Figure 5-15	Testing the second composite tube: first run.....	190
Figure 5-16	Load-axial strain at the midpoint and at 12 cm offset.....	191
Figure 5-17	Load-circumferential strain at the mid point and at 12 cm offset.....	191
Figure 5-18	Load-Axial strain at the mid point and at 12 cm offset at 45°.....	192
Figure 5-19	Load-Circumferential strain at the mid point and at 12 cm offset in 45°.....	192
Figure 5-20	Load-Axial strain at the mid point and at 12 cm offset at 0°.....	193
Figure 5-21	Load-Circumferential strain at the mid point and at 12 cm offset at 0°..	193
Figure 5-22	Load-Axial strain at the mid point and at 12 cm offset at 45° .....	194
Figure 5-23	Load-Circumferential strain at the mid point and at 12 cm offset at 45°.....	194
Figure 5-24	(a) Small dent at the support points, (b) No delamination or failure in strain gauges.....	195
Figure 5-25	(a) Final test set up, (b) Maximum strain is 1.5% at this stage.....	197
Figure 5-26	(a) Maximum strain is 3% (b) Maximum strain is 3.5%.....	198
Figure 5-27	Load-Axial strain at 0° .....	199

Figure 5-28	Load-Axial strain in at 45° .....	199
Figure 5-29	Load-Circumferential strain at 0° .....	200
Figure 5-30	Load-Circumferential strain at 45° .....	200
Figure 5-31	Schematic deformation of the composite beam during the test.....	201
Figure 5-32	Cross section of the second composite tube and its failure sequence.....	203
Figure 5-33	Fracture of the inner ring during the test.....	205
Figure 5-34	(a) Fracture of the inner ring (b) Delamination of the layers.....	205
Figure 5-35	Fracture of the tube in compression zone.....	206
Figure 5-36	Crack propagation and local buckling at the mid span.....	207
Figure 5-37	Foot prints of the fiberglass pad on the tube.....	207
Figure 5-38	Load– longitudinal strain curves at midpoints of the aluminum and second composite tubes.....	208
Figure 5-39	Crack propagation was very limited: No crack in section 3.....	209
Figure 5-40	Failure of 90° layer releases the constraint on adjacent layers.....	212
Figure 5-41	Cross sections of the aluminum and composite panels.....	214
Figure 5-42	Failure process of the aluminum panel.....	216
Figure 5-43	Failure process of the third composite panel.....	217
Figure 5-44	Sequence of failure for the third composite tube.....	218
Figure 5-45	Test set up for the third composite tube.....	219
Figure 5-46	Bending test of third composite tube.....	220
Figure 5-47	Force deflection curves for aluminum and third composite tubes.....	221
Figure 5-48	Failure of the innermost layer due to the radial load.....	222
Figure 5-49	Fracture of 90° layer due to radial and circumferential stresses.....	223

Figure 5-50	Damage at loading nose for third composite tube.....	223
Figure 5-51	Force-strain curves of aluminum and third composite tubes.....	225
Figure 5-52	Aluminum linear to reinforce the fourth composite tube.....	226
Figure 5-53	Failure process of the aluminum panel.....	228
Figure 5-54	Failure process of the fourth composite panel.....	230
Figure 5-55	Sequence of failure for the fourth composite tube.....	231
Figure 5-56	Test set up for the fourth composite tube.....	232
Figure 5-57	Bending test of the fourth composite tube.....	233
Figure 5-58	Schematic representation of the bending of the fourth composite tube..	234
Figure 5-59	The aluminum liner inside the fourth composite tube.....	235
Figure 5-60	Delamination and fracture of the layers at the mid span of the fourth composite tube.....	236
Figure 5-61	A, B, C & D Failure due to compression stresses.....	237
Figure 5-62	The fourth composite tube kept the load level during the test.....	238
Figure 5-63	Force-strain curves of aluminum and fourth composite tubes.....	238
Figure 5-64	Geometry of layered element SOLID46.....	240
Figure 5-65	Ansys model of the fourth composite tube, Dusheng (2008).....	240
Figure 5-66	Force-axial strain of the fourth composite tube in comparison to that of aluminum tube.....	241
Figure 5-67	Design flowchart for deformable composite tubes.....	249

## List of Tables

Table 1-1	Properties of high performance ceramic materials, Chawla (2003).....	13
Table 1-2	Typical properties of aramid fibers, Tuttle (2004).....	19
Table 1-3	Typical properties of glass fibers, Hearle (2002).....	22
Table 1-4	Mechanical properties of selected carbon fibers, Tuttle (2004).....	24
Table 1-5	Characteristics of three common thermoplastic polymers.....	35
Table 1-6	Mechanical properties of Carbon AS4/PEKK composite.....	37
Table 3-1	Polishing steps to prepare samples for taking micrograph.....	90
Table 3-2	Tensile test results of carbon AS4/PEKK quasi isotropic laminate.....	108
Table 4-1	Mechanical properties of aluminum 7075- T6.....	
Table 4-2	Specifications of aluminum tube DN 80, SCH 80.....	
Table 5-1	Strength and Failure strain of Carbon AS4/PEKK composite laminates.....	173
Table 5-2	Materials properties.....	178
Table 5-3	General design parameters of the aluminum and composite tubes.....	180
Table 5-4	Design parameters of the second aluminum and composite tubes.....	185
Table 5-5	Test plan for the second composite tube.....	189
Table 5-6	Design parameters of the aluminum and third composite tubes.....	215
Table 5-7	Design parameters of the aluminum and fourth composite tubes.....	228

## Nomenclature

### Lower case

$a_n$	Inner radius of $n^{\text{th}}$ layer
$b_n$	Outer radius of $n^{\text{th}}$ layer
$r$	Radial distance from the center of the tube
$u_r$	Displacement function in the radial direction
$u_\theta$	Displacement function in the hoop direction
$u_z$	Displacement function in the z direction
$u'_r$	Rigid body displacement in the radial direction
$u'_\theta$	Rigid body displacement in the hoop direction
$w'$	Rigid body displacement in the z direction

### Upper case

$C_{ij}$	Terms of stiffness matrix
$E_i$	Elastic Modulus of the laminate
$F$	Stress function
$G_{ij}$	Shear Modulus of the laminate
$I$	Moment of Inertia of the tube
$J$	Polar Moment of Inertia of the tube
$L_i$	Differential operators
$M_x$	Bending Moment around x axis
$M_y$	Bending Moment around y axis

$N$	Number of layers of the composite tube
$P$	Axial force
$R$	Body force
$S_{ij}$	Terms of compliance matrix
$T$	Twisting torque
$Z$	Body force

### Greek symbols

$\Theta$	Body force
$\beta_{ij}$	Reduced elastic constants
$\Phi$	Stress function
$\sigma_r$	Normal radial stress
$\sigma_{rz}$	Shear stress in cylindrical coordinate $rz$ plane
$\sigma_{r\theta}$	Shear stress in cylindrical coordinate $r\theta$ plane
$\sigma_x$	Normal stress in the $x$ direction
$\sigma_y$	Normal stress in the $y$ direction
$\sigma_z$	Normal stress in the $z$ direction
$\varepsilon$	Longitudinal strain of the tube
$\varepsilon_x$	Axial strain in the $x$ direction
$\varepsilon_y$	Axial strain in the $y$ direction
$\varepsilon_z$	Axial strain in the $z$ direction
$\tau_{xy}$	Shear stress in $xy$ plane
$\tau_{xz}$	Shear stress in $xz$ plane
$\tau_{yz}$	Shear stress in $yz$ plane

$\gamma_{xy}$	Shear strain in $xy$ plane
$\gamma_{yz}$	Shear strain in $yz$ plane
$\gamma_{xz}$	Shear strain in $xz$ plane
$\theta$	Angular coordinate
$\nu_{ij}$	Poisson's ratio in material coordinate system
$\kappa_x$	Curvature in the plane normal to $x$ direction
$\kappa_y$	Curvature in the plane normal to $y$ direction
$\vartheta$	Rotation per unit of length of the tube

# **Chapter 1**

## **Introduction**

### **1-1 Background**

In December 2004, the kick-off meeting for two challenging projects on the development of thermoplastic composites for aerospace applications was held in the Concordia Center for Composites, CONCOM, in the Mechanical and Industrial Engineering Department of Concordia University. The collaborators were Bell Helicopter, Bombardier, Concordia University, AMTC National Research Council of Canada and École de Technologie Supérieure.

The motivation for this research was to find a solution for one of these projects: the development of a thermoplastic composite landing gear for helicopters. The concern and necessity for such a development was raised by Bell Helicopter Textron Company. Figure 1-1 shows the aluminum helicopter landing gear. Currently most landing gears are

made of aluminum and despite their major problems, are used worldwide by the industry. In fact, composites are not considered a reliable substitution for aluminum to serve in such a heavy duty structure due to their brittleness.

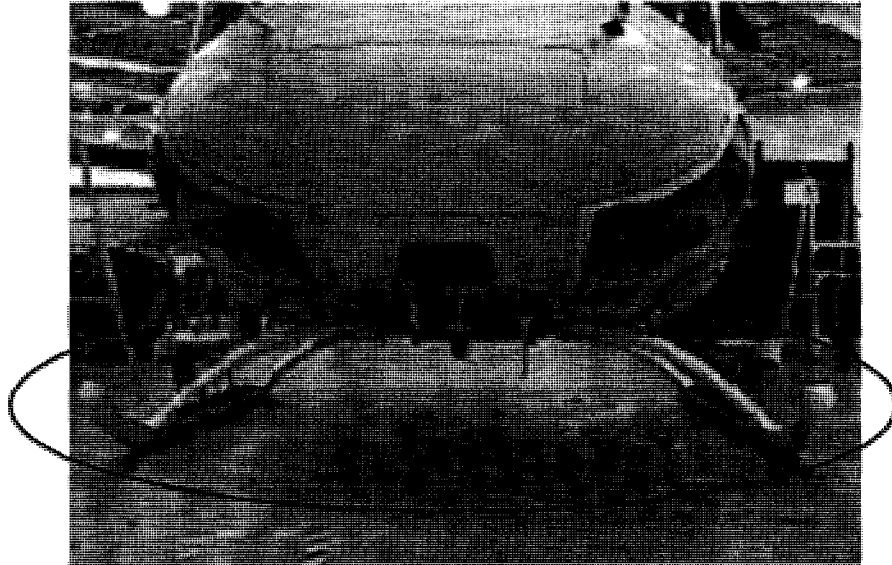


**Figure 1-1: Helicopter landing gear**

Bell had recently introduced a sleigh type skid landing gear for use on its new Model 429 civil helicopter as shown in Figure 1-2. The new landing gear has improved dynamic behavior and benefits from a lower weight, Minderhoud (2008). However, it still has some of the problems of conventional landing gear such as its fabrication process and corrosion control. The conventional landing gear used in all other Bell models consist of parallel forward and aft cross tubes, which are connected by two longitudinal skid tubes that are slightly extended forward of the front cross tube, Minderhoud (2008). Figure 1-3 shows Model 427 with a conventional skid gear.



**Figure 1-2: Bell Model 429 with sleigh type skid gear, Minderhoud (2008)**

The function of the cross tubes is to absorb energy in hard landings by plastic deformation. The skid tubes, however, provide stability to the cross tubes when placed outboard enough to suppress the rolling motions, Isaac (2008). Energy absorption during hard landings is a crucial design factor for helicopter landing gear. Keeping the stress level low ensures a satisfactory fatigue life; however, the stiffness should be high enough to avoid critical ground resonance modes, Minderhoud (2008).



**Figure 1-3: Bell Model 427 with conventional skid gear, Minderhoud (2008)**

## **1-2 Design challenges associated with aluminum landing gear**

Helicopter production skid landing gears are typically fabricated in high strength aluminum alloys to exploit the relatively high strength to weight ratio of these materials. Aluminum alloys also exhibit a non linear strain to failure characteristic that provides a measure of energy absorption during heavy or crash landing conditions.

These structures do however present significant challenges associated with manufacturing defects and in service damage or corrosion that might affect the overall structural life. Companies like Bell Helicopter address these issues through careful process control, extensive corrosion protection surface treatments and in some cases in service retirement criteria but this can make manufacturing expensive and add to the direct operating costs of helicopter owners.

One of the main issues of the current aluminum landing gear is the fabrication process, which is currently very costly and labor intensive. The conventional landing gears consist of two curved cross tubes with varying thicknesses connected together by two longitudinal skid tubes. The thickness of the cross tubes varies from 16mm in the thickest section to about 3 mm in the thinnest. An acid-etching technique is employed to make such a varying thickness. The tube is immersed in a pool of chemicals. As the acid etches the tube, it is taken out very slowly from the bath, and as a result, varying thickness is achieved. The thickness reduction at each point is proportional to the time that the tube is in the bath. First, one side of the cross tube is processed (for example the left hand side, LHS) and after that the other side. The work is carried out by companies who are specialized in the field. However, the process is very long and expensive, and a very intensive quality control is required. It is often difficult to get the proper thickness

tolerances because much material must be removed from the tube; any deviation between the center line of the inner and outer surfaces of the tubes becomes important. Nevertheless, the main difficulty with chemical milling is that it becomes more and more difficult to perform due to the environmental legislation and costly due to all regulatory preventions to be taken. There are fewer and fewer companies that can meet all the requirements related to chemical milling. This is the reason why chemical milling is less and less used. It is expected that this process will no longer be used at all, except in some special cases, which of course makes it more and more expensive. This is an important reason to find other ways to fabricate the helicopter cross tubes. If composites could be deployed, fabrication, by some techniques such as fiber placement, could be fast and considerably less expensive.

The second challenge for aluminum landing gear is the corrosion. It has been observed that spot corrosion is a primary source of failure in normal landings. Corroded parts especially inside the tube are hard to detect and prevent. Those parts weaken the structure and create stress concentrations. If the aircraft has a slightly harsh landing, cracks propagate in the landing gear and abrupt failure becomes inevitable. Corrosion has remained a great concern in the design of helicopter landing gear even though some new heat treatment has improved the performance of the structure. Therefore, in each design much attention must be paid to corrosion prevention. By employing polymer matrix composites the possibility for spot corrosion failure is reduced considerably.

The third challenge is fatigue prevention. Typically, landing gears are subjected to low cycle fatigue loading. Maneuver recognition and event sequence are important parameters in modeling the damage accumulation process, Rhoads et al. (2008). The

design requirements for the cross tubes are rather contradictory. On one side, stress levels must be kept as high as possible to get high energy absorption through plastic deformation while, on the other hand, the stress level must be lowered to avoid the fatigue problems. It is noteworthy that aluminum like most of the other nonferrous alloys does not show an endurance limit. Thus fatigue will ultimately occur regardless of the magnitude of the stress, and fracture will take place under dynamic and fluctuating stresses, Callister (2003). To reduce this possibility, shot-peening and cold worked holes are employed to retard the crack growth; the damage tolerance of the surface of the cross tubes is very small. In other words, even small scratches on the surface can increase the risk of corrosion failure while the repair would remain expensive.

Finally, accumulated residual strain can be a maintenance issue for the aluminum landing gear. In fact, the yield strain for aluminum is typically less than 0.7%. After a certain number of landings, permanent deformation is observed in the cross tubes, and this may jeopardize the normal performance of the helicopter. Hence, the structure may need to be replaced. This can increase the maintenance cost of the helicopters and is not desirable. Thermoplastic composites might show better elastic recovery for higher strains up to 1%. To avoid all these issues, a composite landing gear seems to be a potential solution. It is light due to the low density of the composites, strong, corrosion resistant, durable, and finally it is an environmental friendly product. However, the main drawbacks of the composites compared to aluminum are the brittleness, low toughness and low fracture strain. These downsides have prevented most researchers from approaching the problem. Substitution of aluminum with thermoplastic composites is really a challenge, but if this can be done, it would be for the first time in the world!

### **1-3 Objective and plans of the research**

Aluminum landing gears have serious technical issues. Their fabrication is getting to be more and more difficult and expensive due to the environmental legislation. Failure due to corrosion is a permanent concern, and fatigue prevention is difficult. Composites have proved their great potential for aerospace applications, where the higher performance can justify the higher initial investment. The ultimate objective of the project is to demonstrate the feasibility of composite landing gear.

For this research, the goal was set to design a composite tube that could show the same strength, stiffness and deformability as its aluminum counterpart tube. If this can be done, the next phase of the overall project for Bell would be implementation of the design into a curved composite tube to serve as landing gear.

A feasibility study in the structural design starts with understanding the nature of the loads and the working condition of the structure. When the loads are known, the designer would be able to select proper materials for the structure, considering other design parameters such as weight, cost, manufacturing and maintenance. Stress analysis, optimization of the design and testing the prototypes are the next steps.

As such, the first step of this research was to select a proper composite, which could be employed in the design and manufacturing of helicopter landing gear. Therefore, the first chapter of this study was devoted to a review of the common composites, their behaviors and characteristics. Accordingly, Carbon AS4/PEKK was selected as the material to be used in manufacturing the first helicopter landing gear. Nevertheless, the material was new in the market, and there was no reliable database on its mechanical characteristics.

As such, in order to collect required design data, some effort was devoted to characterization of the material. The results are summarized in Chapter 3.

Once the material was known, the second step was the stress analysis of the structure and finding out the appropriate cross sections and layups. Analytical and numerical methods may be used in the design and analysis of the composite tubes. Concerning the analytical work, most studies on the stress analysis of composite tubes are limited to small strains and elastic stresses. It is obvious that the behavior of the landing gear, especially during hard landings, is far beyond these limits. However, understanding the state of stress and strain in the elastic limit still could provide the designer with a preliminary vision. As such, in Chapter 2, the common procedures for analysis of anisotropic and composite tubes were reviewed. The review showed that despite all efforts to simplify the analytical work, the equations and systems of unknowns remain very complex, and solving such equations is a cumbersome task.

Moreover, the available analytical techniques only tackle the analysis of straight, uniform cross section tubes subjected to uniform loading while, in contrary, the landing gears are curved tubes with varying cross sections subjected to non-uniform loadings. Therefore, it was obvious that numerical methods must be used. Computer programs such as ANSYS enable the designer to determine the state of stress and strain, deformations and to some extent the modes of failure. For example, if the interlaminar shear stresses are known, it is possible to design a laminate that fails due to delamination. Though delamination is not a favorable fracture mode in many cases, it could be desirable here to dissipate the energy during harsh landings. Current aluminum landing gears absorb shocks through large deformation and plastic strains. Nonetheless, composites are brittle and low in toughness.

It was predicted that delamination might be used as a source to absorb energy and reduce the effects of harsh landings on the passengers and the structure. As such, parallel to this research ANSYS analysis of the composite tubes was done by Xu (2008). The results have always been in confirmation with the special analytical method presented in this research and the experimental data. Chapters 4 and 5 are dedicated to design, analysis and three point bending test of the aluminum and composite tubes. The goal was to design a composite tube that is equivalent to an aluminum 7075-T6 tube. A successful design requires that both tubes show the same strength, stiffness and failure strain, with possible weight savings.

#### **1-4 Structure of composites**

Composites consist of one or more discontinuous phases embedded in a continuous phase. The discontinuous phase is usually hard, stiff and strong and is called the reinforcement. The stiffness and load carrying capacity of the composite is highly dependent on the properties and volume fraction of this phase. For the case of unidirectional fiber composites, however, orientation of the fibers is also crucial. In fact, properties of the fibrous composite such as strength and stiffness could be more than twenty times stronger in the fiber direction rather than the transverse direction, Callister (2003).

Despite the fact that fibers are load carrying elements of composites, they can not be loaded directly due to their small cross-sectional dimensions. Moreover, fibers are not capable to transmit loads from one to another if they are not embedded in a continuous medium. Furthermore, fibers are very weak in compression due to the buckling, and it is

impossible to keep dry fibers together and make a structure. These limitations are overcome by embedding the fibers in a matrix to form a composite. The matrix binds the fibers together, transfers loads between them by shear mechanism, and protects them from environmental attack and damage due to handling. Transverse stiffness and strength, shear and compression properties, chemical properties and service temperature of composites are highly dependent on the matrix properties. Finally, the chemical characteristics of the matrix such as melting and curing temperature, viscosity, and reactivity with fibers, limit the choice of fabrication process, Agarwal et al. (2006). Composites can be classified into three main categories: Metal Matrix Composites, Ceramic Matrix Composites and Polymer Matrix Composites. In order to find a suitable material for the landing gear, general characteristics of these three groups are reviewed briefly hereinafter.

### **Metal Matrix Composites, MMCs**

Metals are the most versatile engineering material known and used by humans since ancient times. High strength, high stiffness, high toughness, good impact resistance and relative insensitivity to temperature change are unique characteristics of metals. In their composite form, metals can play the role of matrix for high temperature applications. Such composites can be expected to have higher specific stiffness and strength, good damage tolerance capabilities, and good fatigue resistance as compared to the traditional alloys. As a result, metal matrix composites have attracted much research interests in recent years. The main advantage of MMCs over monolithic alloys is that their properties

can be customized according to the properties of their constituents, Liu (2007). However, it is not hard to see why MMCs are still a small segment of composite industry.

Despite their promising properties, some factors limit the use of metals as matrix in composites. High density is one of the main problems. Composites are known as advanced materials due to their high specific strength and stiffness. High specific properties of common composites are due to the low density of polymer and ceramic matrices rather than the high strength and stiffness of the fibers. However, the density of most metal alloys usually is 3 to 4 times that of polymers. Moreover, the manufacturing process of MMCs will be more complicated and more expensive than common metal alloys.

On the other hand, obtaining higher strength, stiffness or wear resistance should not considerably affect the ductility and toughness of the initial metals. Furthermore, an advanced composite with high mechanical properties requires more than suitable materials for fibers and matrix. The effective bonding between matrix and fiber is also crucial. Achieving an effective bond, however, needs more precise fabrication process and higher quality control that often ends to higher manufacturing cost, Taliercio (2007).

Low density of aluminum and titanium ( $2.7 \text{ g/cm}^3$  and  $4.5 \text{ g/cm}^3$  respectively) has made these metals the best choices as a metal matrix. In terms of reinforcement, metal matrix composites can employ either discontinuous particles and whiskers or continuous fibers. The most common discontinuous reinforcements are SiC,  $\text{Al}_2\text{O}_3$  and  $\text{TiB}_2$  in both whisker and particulate forms. On the other hand, most of continuous reinforcements are non-metals such as carbon, mica and drawn silica; however, continuous metal filaments such as tungsten and stainless steel are also employed, Taya & Arsenault (1989).

Metal matrix composites have the potential to be used for some aerospace applications. However, the cost will be much higher than that of a monolithic metal alloys. As such, their use will be restricted to cost-effective applications, where the strength-stiffness saving justifies the higher cost. Indeed, metal matrix composites must be created when required properties are impossible to be achieved by any other treatment methods on one individual constituent, Taya & Arsenault (1989).

### **Ceramic Matrix Composites, CMCs**

Ceramics are non-metallic inorganic materials, and they are usually processed at very high temperatures during their fabrication. Ceramic materials may be categorized into two classes: traditional or conventional ceramics such as brick, pottery and tiles and advanced or high performance ceramics such as oxides, nitrides and carbides of silicon, aluminum, zirconium and titanium. Ceramics are used wherever wear resistance, hardness, corrosion resistance, high-temperature capability, high strength and finally, high stiffness is required. However, monolithic ceramics are susceptible to fracture due to their extreme brittleness and low toughness, Chawla (2003).

Under mechanical or thermal loadings, ceramics do not demonstrate any plasticity or large deformation, and catastrophic failure can be their usual fracture mode. So far, particle reinforced ceramic matrix composites have received great attention due to their improved fracture toughness and thermal shock resistance and isotropic properties for a variety of high temperature, high stress and severe erosion applications in aerospace, hot engine, and energy conversion devices, Wang et al. (2004) and Liu et al. (2007). On the

other hand, embedding fibers and whiskers into monolithic ceramics can improve energy absorption of the composite due to fiber/matrix debonding and crack deflection.

Table 1-1 lists some important high performance ceramic materials, which are used in making ceramic matrix composites. High resistance to heat, chemicals and wear is the common characteristics of these materials. However, these high characteristics require more difficult and more expensive fabrication process. Some of these expensive processing techniques are: CVD (chemical vapor deposition), CVI (chemical vapor infiltration) and Sol–Gel, Farooqi and Sheikh (2006).

Properties	Tensile strength MPa	Young's Modulus GPa	Toughness $K_{IC}$ , MPa m <sup>1/2</sup>
Alumina (99% purity)	300	340	4.5
Alumina & 25% SiC	900	390	8.0
Lithiumaluminosilicate Glass-ceramic	160	86	1.1
Lithiumaluminosilicate & 50% SiC CF	640	135	17.0

**Table 1-1: Properties of high performance ceramic materials, Chawla (2003).**

### **Polymer Matrix Composites, PMCs**

Polymers are undoubtedly the most common matrices used in the development of fiber composites. Polymers used as matrix materials are usually known as resins. For most

composites, the volume fraction of the resin is about 30 to 40 percent. The main advantages of polymer matrices are their low density, ease of processing, good chemical resistance, minimum effects on fiber properties due to their low processing temperature and relatively low cost. The applications of polymers, however, are restricted by their low strength and stiffness, low service temperature and susceptibility to ultraviolet light. Glass transition temperature of the polymer,  $T_g$ , plays an important role in manufacturing and performance of the polymer matrix composites. Generally, lower  $T_g$  means that the polymer transforms to a soft rubbery state from its stiff and glassy state at lower temperatures, and this is detrimental to the composite. The service temperature of the composites must be always below its  $T_g$  and the matrix must be in a glassy state. If such, the matrix is better capable of transferring loads to the fibers, provides support against fiber buckling, and maintains alignment of the fibers, Hyer (1998).

Polymer matrices, depending on their molecular structures as a solid material, are divided into two major categories: thermosetting and thermoplastic polymers. For thermoplastic polymers, upon raise in the temperature and thermal energy, the average distance between individual molecular chains is increased. As such, molecular mobility is increased and macroscopic stiffness is reduced. Eventually, at melting temperature, polymer chains can slide freely past each other and the polymer transforms to viscous liquid, Tuttle (2004). Thermoplastic polymers usually soften or melt on heating over a temperature range and regain their original solid form upon cooling. Melting and solidification of thermoplastic polymers is a reversible and repeatable process. At the microscopic level, thermoplastic polymers consist of linear or/and branched-chain molecules. The bonding between molecules inside a chain is usually strong. In contrast,

the bonding of adjacent chains is usually very weak. The structure of thermoplastic polymers can be amorphous or semicrystalline. The preform thermoplastic composites can be easily reshaped by application of heat and pressure. The most common thermoplastic polymers are: polyether-ether- ketone, PEEK, polyether- ketone- ketone, PEKK, polyphenylene sulfide, PPS, polyethylene, nylons, polyamide and polyimide. Figure 1-4 typically shows the structure of thermoplastic polymers in molten and solid forms.

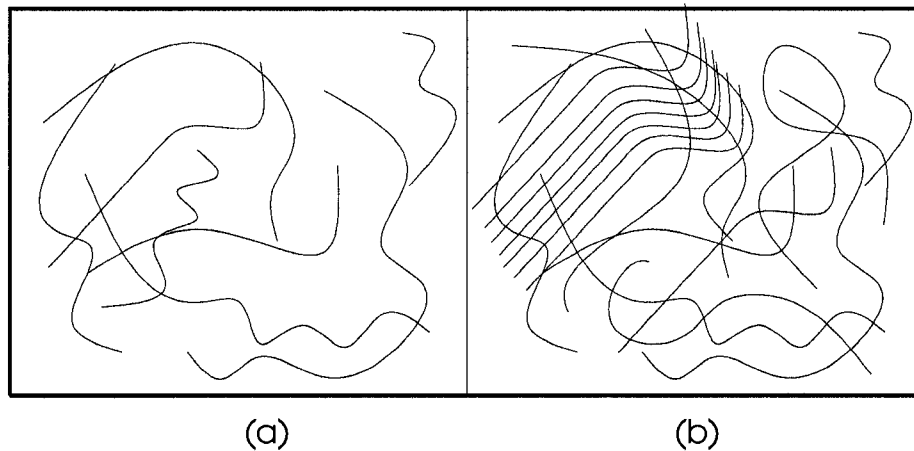


**Figure 1-4: A typical thermoplastic resin in (a) liquid (b) solid forms.**

In contrast to thermoplasts, thermosetting polymers transform in an irreversible chemical change as the temperature is raised, and make a solid structure if the polymer is kept at its curing temperature. Before curing, thermosets are low viscous fluids, consisting small molecule chains about 2-10 repeat units, Tuttle (2004). However, when the temperature is increased, due to a polymerization process, molecular weight and viscosity increase, and

a cross-linked network is developed, Rodriguez (1989). Most commercially available thermosetting composites are cured at temperature of either 120°C or 175°C.

After the polymer is completely cured and the chains are cross-linked, application of heat and pressure would not result in melting or reforming of a thermosetting composite, Strong (2000). However, if a cross-linked polymer is heated, the structural stiffness of the polymer may reduce slightly. Further application of heat results in breakage of covalent bonds of the molecular chains and cross-links. At this point, the degradation of the material is very likely. Figure 1-5 shows the structure of a typical thermosetting polymer in liquid and cross-linked forms.

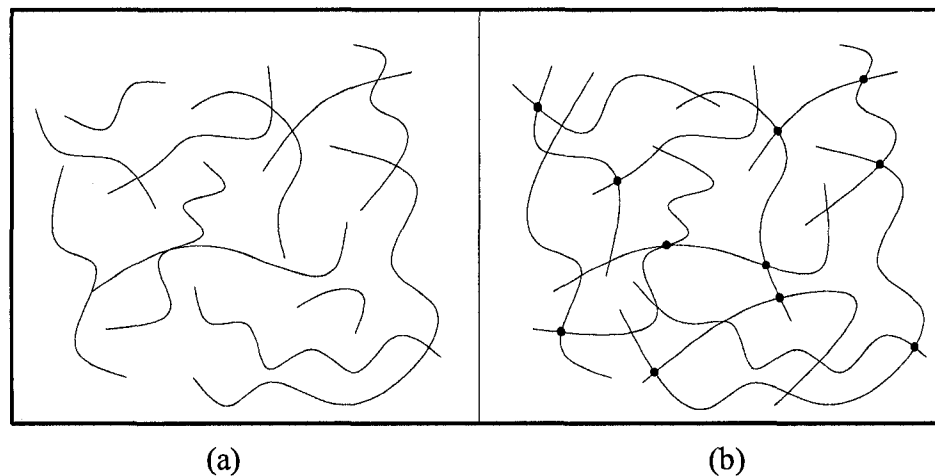


**Figure 1-5: A typical thermosetting resin in (a) liquid (b) solid form.**

Thermosetting polymers are the most used matrix system in composite industry. Low melt viscosity, good fiber impregnation, low processing temperature and lower cost compared to thermoplastic resins are some of the reasons for popularity of thermosetting

polymers. Some examples of thermosetting resins include epoxies, polyesters, phenolics, melamine, silicone and polyimides, Hyer (1998).

### **1-5 Selection of materials**

There is no doubt that composites are in their best years of research and development. For any application, there are choices for matrix and reinforcement, from the natural fibers to nanotubes as reinforcement, and variety of polymers, metals and ceramics as matrices. However, an industrial project needs a realistic design and commercial materials! In the scientific world, the options for material selection are enormous, but when it comes to industry, the design shall be limited to the products that have reasonable price for raw material and manufacturing. They should also be reliable, certifiable and available in the market. These are simply the reasons for the domination of fiberglass composites in the transport and civil industry whereas the use of carbon fiber composites is limited to aerospace applications, where higher performance can justify the higher price.

As discussed in Section 1-4, three major types of composites are metal matrix composites, ceramic matrix composite and polymer matrix composites. Keeping in mind the general characteristics of each group, obviously ceramic matrix composites, due to their low deformability, low toughness and catastrophic fracture, have no place in the selection of a proper material for landing gear. Metal matrix composites, which have similar characteristics and fabrication process to metals, can barely solve any of the current aluminum landing gear issues. As such, the choice for a composite landing gear will be limited to the polymer matrix composites. Restricting the discussion to the practical materials that are reliable, certifiable, available and relatively low in price, the potential options for reinforcement and matrix phase are reviewed hereinafter.

### **1-5.1 Reinforcements**

Three major types of reinforcements are particles, whiskers and fibers. Technologically, the most important composites are those reinforced by fibers. Fiber-reinforced composites, FRCs, are capable to demonstrate high mechanical properties such as high specific strength and stiffness. Mechanical characteristics of FRCs depend on many parameters including fiber properties, fiber orientation, position, density and geometry as well as the mechanical and chemical properties of the matrix. The highest performance and mechanical characteristics are achieved by employing high volume fractions of uniformly distributed, unidirectional and continuous fibers, Callister (2003).

Aramid, glass and carbon fibers are the most popular fibers with the highest applications in the structural and aerospace industries. These fibers are usually in mass production by reliable manufacturers. They have relatively reasonable price and often result in high performance composites. As such, hereinafter the discussion is limited to selection of fibers in continuous form.

#### **Aramid Fibers**

Various types of polymer fibers such as nylon, polyester and rayon have proved their applications for many years as reinforcement in automobile tires, large balloons, body armor and rubber-coated fabrics, Agarwal et al. (2006). In the 1960s, aromatic polyamides, however, became breakthrough materials in the market as compared to all other polymer fibers. In 1971, DuPont introduced a high strength, high stiffness, aramid fiber commercialized under the trade name Kevlar. The achievement to develop aramid

fibers into a very advanced reinforcement was brought into the field in part by Kwolek (1974, 1989), Blades (1975) and Tanner et al. (1989).

Aramid fibers are manufactured by extrusion of the polymer, following by stretching and drawing treatment. The rigid linear molecular chains, which are held together in the transverse direction by weak hydrogen bonds, are highly oriented in the fiber axis direction. This results in very strong mechanical properties in the fiber direction and very low transverse and compression strength. However, fiber properties can be altered by applying different solvent additives, varying the spinning conditions and post-spinning heat treatments, Agarwal (2006).

Kevlar 29, 49 and 149, Twaron and Twaron HM are the best known aramid fibers in the market. Typical properties of these fibers are listed in Table 1-2.

Properties	Kevlar 149	Kevlar 49	Kevlar 129	Kevlar 29
Specific Gravity	1.44	1.44	1.44	1.44
Young's Modulus, GPa	186	124	96	68
Tensile strength, MPa	3440	3700	3380	2930
Tensile elongation, %	2.5	2.8	3.3	3.6

**Table 1-2: Typical properties of aramid fibers, Tuttle (2004).**

Characteristics of aramid fibers are very unique. Tensile strength and modulus of these fibers are significantly higher than those of earlier organic fibers while fiber elongation is

lower. Aramid fibers do not melt. Application of heat results in decomposition of the material at 500°C. Glass transition temperature of this aromatic material is about 360°C that is high enough to facilitate the application of the fiber in thermal insulation products.

The main draw back of aramid fibers is their highly anisotropic structure that leads to low longitudinal shear modulus and poor transverse properties. Moreover, under compression loading, weak hydrogen bonds are not capable of preventing fibers from forming kink bands that relieve the axial stress in the fiber. Therefore in this case the maximum compression stress never exceeds 450 MPa while tensile strength easily reaches to above 2500 MPa, Andrews et al. (1997). However, poor compression strength can be somehow compensated if the fiber is used in hybrid form with glass or carbon fibers.

The aramid fibers have found their applications in a wide variety of composite structures. In the prepreg form, all types of Kevlar have been extensively used in manufacturing of high-performance composite structures. Prepregs of aramid fiber are commercially available in the forms of woven fabric and unidirectional tape. The resin is mostly epoxy even though the polyester is also used. The prepreg must be cured at high-temperature-pressure cycles in autoclave to flow, consolidate, and cure. Continuous aramid fibers are also used in filament winding. The fibers pass wet epoxy resin before being laid up on a mandrel. Nevertheless, the wet lay up of aramid composites is the most popular manufacturing technique in the construction of marine laminates, Wardle (2003). Figure 1-6 illustrates different applications of aramid fiber composites.

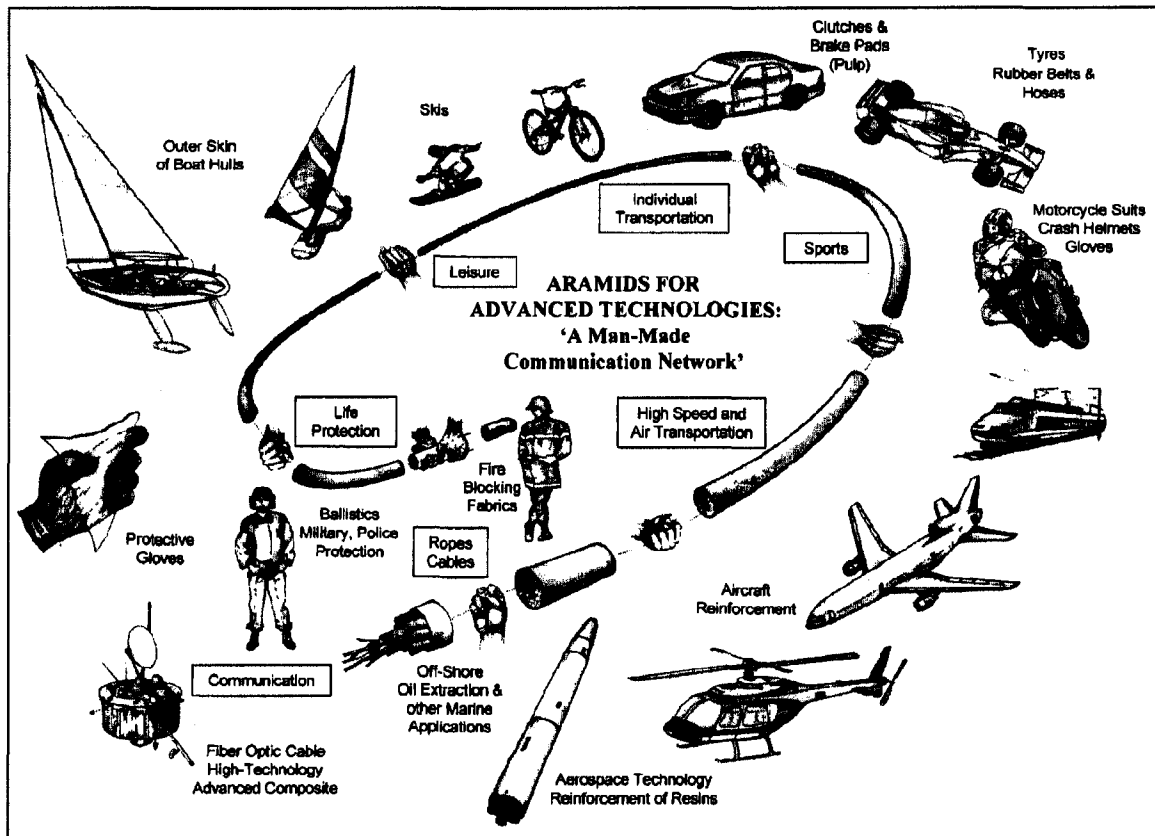


**Figure 1-6: Application of para-aramid fibers, Hearle (2002).**

### **Glass Fibers**

Ceramic are expected to be opaque brittle objects such as tiles and whitewares. However, despite their transparency, glasses are also a very well-known group of ceramics. Noncrystalline silicates account for the main part of the glass structure; however, other oxides such as  $\text{CaO}$ ,  $\text{Na}_2\text{O}$ ,  $\text{K}_2\text{O}$  and  $\text{Al}_2\text{O}_3$  may be found in the structures, Callister (2003). Glass fibers are also noncrystalline materials with a short-range structure that has no distinctive microstructure or molecular orientation, so their mechanical properties are isotropic.

Properties	E-Glass	S-Glass	S2-Glass
Specific Gravity	2.55	2.5	2.49
Young's Modulus, GPa	72	87	86
Tensile strength, MPa	1500-3000	3500	4000
Tensile elongation, %	1.8-3.2	4	5.4

**Table 1-3: Typical properties of glass fibers, Hearle (2002).**

Glass fibers, in continuous and discontinuous forms, are the most common reinforcement for polymer matrix composites. Glass fibers are low in cost, have high specific strength, and at elevated temperatures up to 350°C, they retain at least 50% of their mechanical properties including strength and stiffness, Wang et al. (2007). Good moisture and corrosion resistance (except for strong alkalis and acids) and high fracture strain are some of the other distinctive characteristics of glass fibers. Three dominant types of glass fibers in the market are E-Glass, mainly used for electrical applications, C-Glass, used for chemical resistant products, and S-Glass, which are widely used for structural applications. Glass fibers are widely used in marine and automobile industries where low price is a crucial factor. The main drawback of the glass fibers is relatively low stiffness (72 GPa) and higher density as compared to carbon fibers.

## Carbon fibers

Carbon fibers are the most important types of reinforcement for advanced composites especially in the aerospace industry. In the year 2000, it was estimated that the available industries require 45000 tons of carbon fibers for variety of their products while the manufactures were barely capable of producing 25000 tons of different forms of carbon fiber. In contrast to increasing demand for carbon fibers, the price reduces considerably every year due to the innovation in processing techniques, Hearle [2002].

Carbon fibers are polymer-based fibers and are produced by treating organic fibers (precursors) under high temperature and tension, leading to highly ordered carbon structure. The most common precursors include rayon, polyacrylonitrile (PAN) and pitch; however, rayon-based carbon fibers are no longer in production and so are of historical interest only, Morgan (2005). Figure 1-7 illustrates a typical structure of carbon fibers.

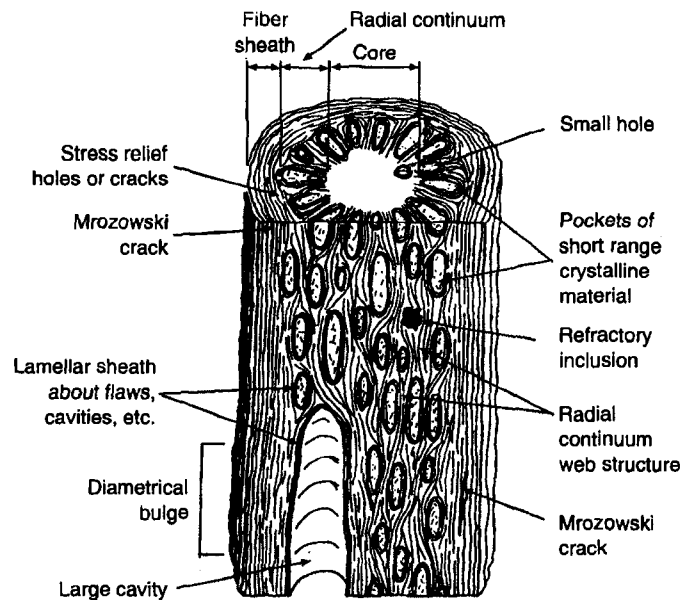


**Figure 1-7: Structure of high strength PAN based carbon fiber, Morgan (2005).**

Manufacturing techniques and processing parameters such as temperature and pressure highly affect the properties of carbon fibers. As such, each year a lot of research is conducted on the development of higher quality and lower price carbon fibers. In open literature, Dresselhaus et al. (1998) thoroughly reviews physical properties of carbon fibers, Donnet et al (1998) covers the treatment of carbon fiber technologies, and Peebles (1994) gives an exceptional review on formation, structure and properties of carbon fibers. Today, there is a rich variety of carbon fibers available in the market, and the physical properties including strength and stiffness are very versatile. Table 1-4 presents the mechanical properties of selected carbon fibers.

Properties	Low modulus	High modulus	Ultra high modulus
Specific Gravity	1.8	1.9	2.2
Young's Modulus, GPa	230	370	900
Tensile strength, MPa	3450	2480	3800
Tensile elongation, %	1.1	0.5	0.4

**Table 1-4: Mechanical properties of selected carbon fibers, Tuttle (2004).**

Carbon fibers are available in many grades and forms with a wide range of properties. While pitch-based fibers show very high modulus, PAN-based fibers demonstrate superior strength, Figure 1-8. The low density of carbon fibers is a crucial factor in producing composites with good specific properties, which is a highly valued parameter

for the aerospace applications. Good thermal stability in the absence of O<sub>2</sub>, low thermal expansion coefficient, excellent creep resistance, low electrical receptivity, biocompatibility and good chemical resistance are some of the spectacular features of carbon fibers, Morgan (2005).

However, despite many distinctive characteristics of carbon fibers, there are a few negative aspects. The cost of carbon fibers is much higher than that of glass and aramid fibers. Carbon fibers show very low strain to failure, about 1.5%, while glass and aramid fibers fracture at over 3% and 2.2% strain respectively. Composites reinforced by carbon fibers show lower impact resistance than the ones reinforced by aramid fibers. The compressive strength of carbon fibers is about 25% lower than their tensile strength. Oxidization in air could be problematic for high temperature applications, and finally anisotropic behavior in the axial and transverse directions can be an issue.

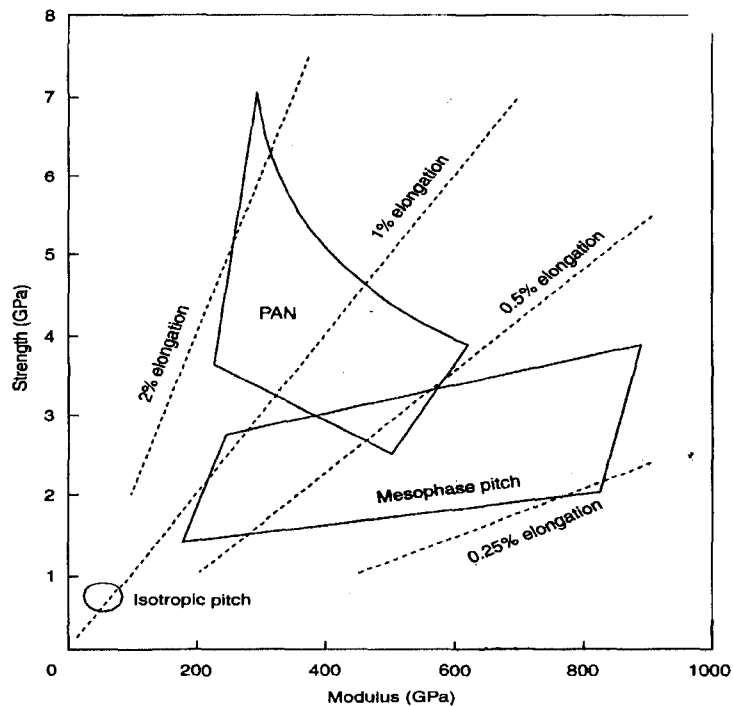


**Figure 1-8: Strength-modulus profile of carbon fibers, Hearle (2002).**

### **1-5.2 Matrices**

As discussed earlier, metal and ceramic matrices are not suitable materials for a composite landing gear for many reasons, so the discussion, hereinafter, is limited to the common commercially available polymer matrices. Polymers are the most widely used matrix material for composites. Their low cost, ease of processing, good chemical and corrosion resistance, and low specific gravity are the underlying reasons for their popularity and wide use by the industry. Nevertheless, low strength, low modulus, susceptibility to the ultraviolet light, and low working temperature restrict their use. The polymer matrices are usually divided into two general classifications: thermosetting and thermoplastic polymers. Characteristics of two very common thermosets, polyesters and epoxies, and two common thermoplasts poly-ether-ether- ketone (PEEK) and poly-ether- ketone- ketone (PEKK) are discussed hereinafter.

#### **Polyesters**

A polyester resin is an unsaturated (reactive) polyester solid dissolved in polymerizable monomer such as styrene. Unsaturated polyesters are long-chain linear polymers containing a number of carbon double bonds. They are made by a condensation reaction between a glycol (ethylene, propylene, or diethylene glycol) and an unsaturated dibasic acid (maleic or fumaric). The chemical structure of polyesters can be modified or tailored by choosing different processing techniques or diverse raw materials. Due to their good mechanical properties and relatively low cost, polyesters have conquered the market of composite industry especially for commercial products. As such, the term fiberglass sometimes refers to a composite made of glass fiber and polyester resin.

Polyesters are generally the lowest cost matrices for composites, and low cost has given rise to their wide usage. However, their lower temperature capability, lower resistance to hostile environment, and lower physical and mechanical properties as compared to other available resins have limited their use in advanced composites.

## **EPOXIES**

Epoxy resins are low-molecular weight organic liquids containing a number of epoxide groups, which are three-member rings with one oxygen and two carbon atoms. A curing agent is mixed into the liquid epoxy to polymerize the polymer and form a solid, network of cross-linked polymer. Epoxy systems, like polyesters, can be cured at room temperature. The curing temperature is mainly determined by the type of curing agent. However, higher degree of cross-linking is usually achieved by adding heat, which accelerates the curing as well. Besides the degree of cross-linking, the properties of a cured epoxy resin depend on the chemical composition of the epoxy pre-polymer, which can be modified greatly, as well as on the curing-agent molecule.

Epoxy resins are the most common matrices for advanced composites and for a variety of demanding applications. Excellent adhesion, good strength, low shrinkage, good corrosion resistance and processing versatility are some of the underlying reasons for epoxies popularity. Epoxies may be more expensive than polyesters and in high temperature applications may not perform as well as polyimides, but their overall properties are excellent. Epoxies have good adhesion to the fibers and properly transfer loads to the reinforcement. Moreover, epoxies are doing a fine job in protecting the reinforcement from adverse environmental effects.

The mechanical and physical properties of epoxy matrices are highly dependent on the relative concentration of active epoxy sites in the resin and reactive sites in the hardener. With a large excess of epoxy groups over reactive sites on the curing agent, the physical properties of the product are generally not as good as those of highly cross-linked products. The best properties, however, are achieved when there is one epoxy group for each hardener reactive site. On the other hand, when the concentration of curing agent reactive sites exceeds the number of epoxy groups, the material forms a resin with similar properties to thermoplastic polymers, and physical properties again reduce.

Despite having many outstanding properties, epoxies are still thermosetting polymers and suffer from their lower toughness. Improving the toughness of an epoxy matrix, however, usually contradicts improving other physical properties of the matrix. On the one hand, cross-link density must be lowered to give more flexibility to the molecular chains and improve the toughness while high strength and stiffness of the matrix are only achieved with relatively high cross-link density.

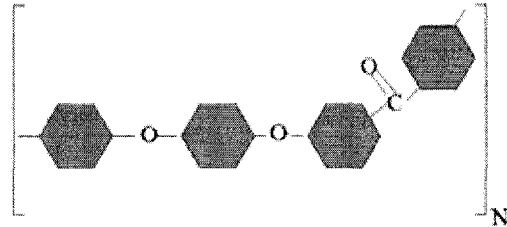
In general, epoxies are dominant matrix systems for advanced composites and aerospace applications due to their adaptability to manufacturing methods and overall excellent physical and mechanical properties. The main shortcoming of epoxy matrices is their relatively low toughness. As such, wherever the toughness is not the main issue, the use of epoxy systems is advised.

### **PolyEtherEtherKetone (PEEK)**

One of the uniquely developed thermoplastic resin material for use in composites is PolyEtherEtherKetone known worldwide as PEEK. The resin has inherent thermal and

mechanical capabilities beyond the conventional industrial thermoplastic polymers, which make it usually more costly than their conventional counterparts. The main advantage of PEEK over other ordinary thermoplasts is its high glass transition temperature, which gives the polymer good mechanical performance at elevated temperatures, and in some cases, even better than cross-linked thermosets.

PEEK is taking its name from the type of linkage between the benzene rings. As it can be seen below, PEEK has two ether (C-O-C) linkages attached to one ketone (C-C=O) linkage in its structure and, therefore, is called polyetheretherketone.



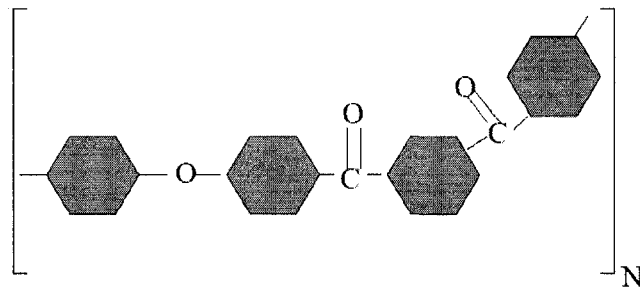
PEEK is characterized as a highly aromatic resin with a very high  $T_g$  that gives the polymer very good thermal stability. High crystallinity gives the polymer relatively high modulus and creep resistance. While the polymer is loaded by tensile forces, the loads are immediately resisted by the rigid and strong crystalline structure rather than merely by amorphous regions. Moreover, the crystalline structure, at least in part, increases the resistance of the polymer to many solvents and environmental attacks.

On the other hand, the amorphous regions of the polymer have an excellent contribution in increasing the flexibility and ductility of the polymer. Composites made by PEEK have far greater toughness and impact resistance in comparison with thermosetting composites. The combination of good water resistance and good toughness is very desirable in many applications where a hot/wet environment is dominant.

### 1-5.3 PolyEtherKetoneKetone (PEKK)\*

PolyEtherKetoneKetone or PEKK has all the outstanding properties of PEEK while its cost is much lower, its  $T_g$  is higher and its processing temperature is 50°C lower than that of PEEK polymers. As a result, a considerable saving in the fabrication cost and energy consumption can be made due to the lower processing temperature of the polymer. At the beginning of this research, the material was not very well known by the industry due to its limited database in the composite form. However, the lack of database can be interpreted as a great opportunity for universities, including Concordia, to take part in producing knowledge that will be highly used in the most advanced parts of the worldwide industry.

The material of interest is called Poly-Ether-Ketone-Ketone (PEKK) due to its one ether (C-O-C) and two ketone (C-C=O) linkages in the structure of the polymer as shown below:



The material was first introduced by DuPont in 1980s, and it took it just a few years to be launched into the market in mass production. In general, PEKK is a semi-crystalline polymer with very high  $T_g$  and moderate processing temperature around 350° C.

---

\* Most of the information of Section 1-5.3 has been adapted from Cyttec Engineered Materials presentations provided for this research and a brochure published by Cyttec Fiberite (1999), and it is reported here for the sake of completeness.

PEKK has very high strength and stiffness and shows good environmental resistance, good paintability and low moisture absorbance. Currently, 400,000 kg of PEKK polymers is in service on various aircraft projects. Even though the polymer behavior has been extensively characterized, in the composite form limited data are available.

A high performance semicrystalline thermoplastic resin that is part of the PEKK family is called CYPEK, and it is produced by Cytec Engineered Material. According to the manufacturer, the physical characteristics of the polymer make it a suitable material in a wide range of applications where excellent chemical, mechanical, and electrical performances are required at elevated temperatures. The polymer can be extruded, molded and thermoformed in conventional equipment providing excellent service and significant use and processing economies.

PEKK demonstrates high toughness and excellent stiffness. Impact resistance, cut-through and abrasion resistance of the polymer is beneficial for primary structures where harsh loads are dominant. Reinforced by carbon fibers, the compound still shows toughness and impact resistant even though higher tensile strength, stiffness and creep resistance of the fibers considerably limits the flexibility of the polymer. Two different grades of the polymer are available in the market. They differ from each other in their degree of crystallinity and vary from a dimensionally stable product to improved temperature and solvent resistance performance.

PEEK can be processed by conventional methods such as injection molding, transfer molding, compression molding, melt extrusion, etc. It can be extruded over aluminum or copper wire, plated with tin, nickel or silver. Finally, it is easily pigmented with both organic and inorganic pigments due to its lower processing temperature.

While the price of PEKK is considerably less than PEEK, its processing temperature is lower and its mechanical and chemical properties are in competence with PEEK, PEKK has found numerous applications in the plastic and composite industry. In electrical applications, it can be used for signal, control, communication and power wiring in mass transportation; in back panel wiring; oil well logging cable; in control and instrumentation wiring for chemical plants and utilities; and to injection mold coil forms, connectors, relay parts, switch components and insulators. The excellent mechanical properties of the polymer provide good service in such items as sealing rings, tubing (Figure 1-9), fasteners, interior decoration of airplanes (Figure 1-10), pipe linings, pump vanes and bearings.

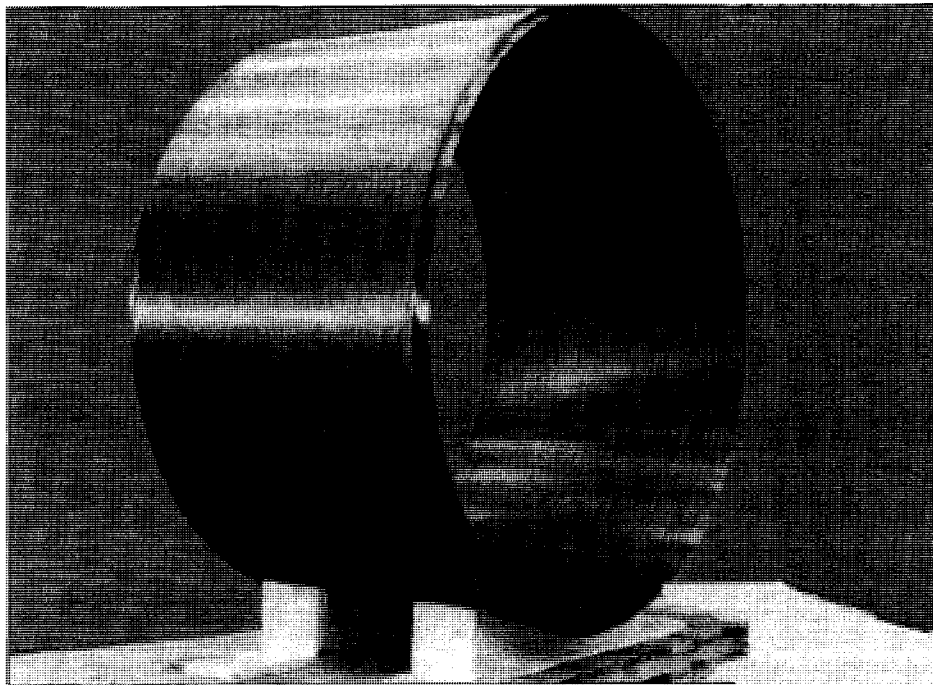


**Figure 1-9: Filament wound (In-situ consolidated) PEKK/Carbon AS4 towpreg (Provided by Cytec Engineered Materials).**

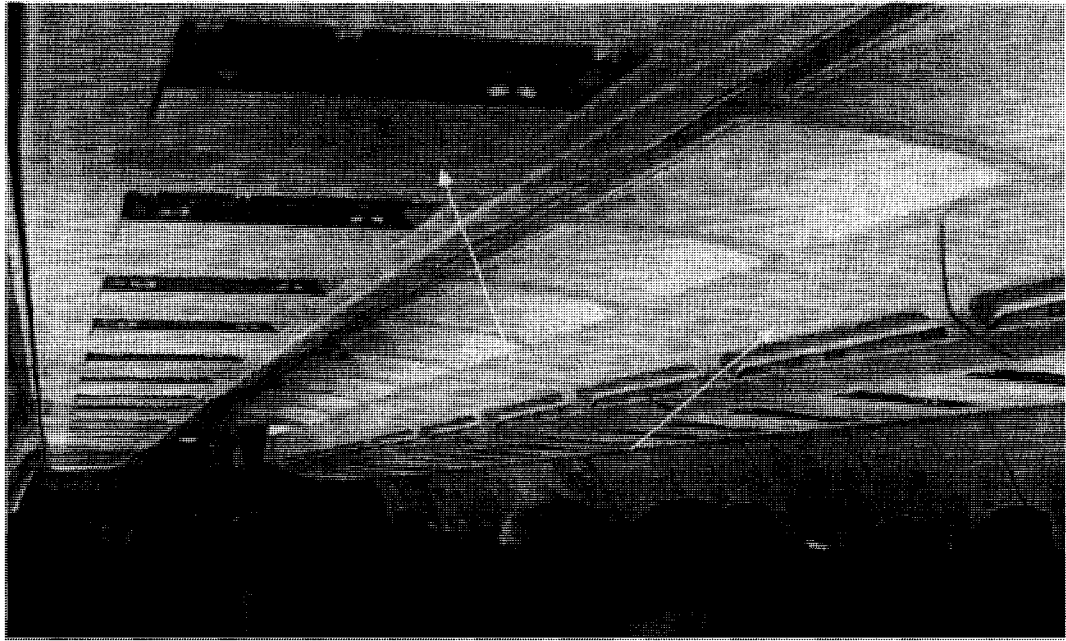


**Figure 1-10: Application of PEKK polymer in interior design  
(Provided by Cytec Engineered Materials).**

#### **1-5.4 Carbon AS4/PEKK composites**

Current landing gear are made of high grade Aluminum 7075-T6 with very high strength. The composite to be used in the landing gear must have high strength and stiffness in tension and compression and good shear properties to allow some ductility. Among fibers, Aramid is very poor in compression and shear. Glass fibers have the same stiffness and almost the same density as aluminum. So, both Aramid and glass fibers were eliminated from selection of materials.

On the other hand, carbon fibers have very high strength and stiffness in tension while their properties in compression still fall in a reasonable range. The Young's modulus of average carbon fiber/thermoplastic composites in the longitudinal direction (140 GPa) is about twice the Young's modulus of aluminum (70 GPa). As such, it is possible to produce an angle ply laminate that shows the same stiffness as aluminum plate. However, there is no guarantee that this special angle laminate can illustrate the required fracture strain and toughness.

#### **Selection of the matrix**

While selecting the type of reinforcement for a composite landing gear did not involve much ambiguity, selecting a proper matrix was very complex, and any choice could be controversial. Nevertheless, it was decided to focus on thermoplastic matrices due to their fast fabrication process. Moreover, thermoplastic polymers have higher toughness and damage tolerance than thermosetting polymers. Excellent solvent resistance and very low moisture absorption, high temperature properties, outstanding fire resistance and very low smoke generation, superior wear resistance, indefinite shelf life, room temperature

storage and being recyclable are some of the other exceptional characteristics of thermoplastic polymers. Furthermore, the structure and the material achieve their maximum mechanical properties right after fabrication, and there is no need for curing time. Tables 1-5 and Figure 1-11 illustrate the characteristics and mechanical properties of four common thermoplastic polymers: PEI, PPS, PEEK and PEKK. Finally, even though some properties of PEEK were superior to other polymers, PEKK was selected as the matrix as it provides outstanding balance of temperature performance, processing, temperature, mechanical properties, environmental resistance, fire resistance, low smoke and toxicity emission, paintability and its considerable lower cost than other thermoplastic polymers.

	PEI	PPS	PEEK	PEKK
<b>Morphology</b>	<b>Amorphous</b>	<b>Semi-Crystalline</b>	<b>Semi-Crystalline</b>	<b>Semi-Crystalline</b>
<b>Tg (°C)</b>	<b>217</b>	<b>90</b>	<b>143</b>	<b>156</b>
<b>Typical Process Temperature (°C)</b>	<b>330</b>	<b>325</b>	<b>390</b>	<b>340</b>
<b>Comments</b>	<ul style="list-style-type: none"> <li>✓ High Tg</li> <li>✓ Moderate Processing Temperature</li> <li>* <i>Environmental resistance</i></li> </ul>	<ul style="list-style-type: none"> <li>✓ Excellent environmental resistance</li> <li>✓ Moderate Processing Temperature</li> <li>* <i>Low Tg</i></li> <li>* <i>Low Toughness</i></li> <li>* <i>Poor Paint Adhesion</i></li> </ul>	<ul style="list-style-type: none"> <li>✓ Extensive database</li> <li>✓ Excellent environmental resistance</li> <li>✓ High toughness</li> <li>* <i>High process temperature</i></li> <li>* <i>High polymer cost</i></li> </ul>	<ul style="list-style-type: none"> <li>✓ Excellent environmental resistance</li> <li>✓ High toughness</li> <li>✓ Lower process temperature than PEEK</li> <li>✓ Bonding and painting</li> <li>* <i>Limited database in composite form</i></li> </ul>

**Table 1-5: Characteristics of three common thermoplastic polymers (Provided by Cytac Engineered Materials).**

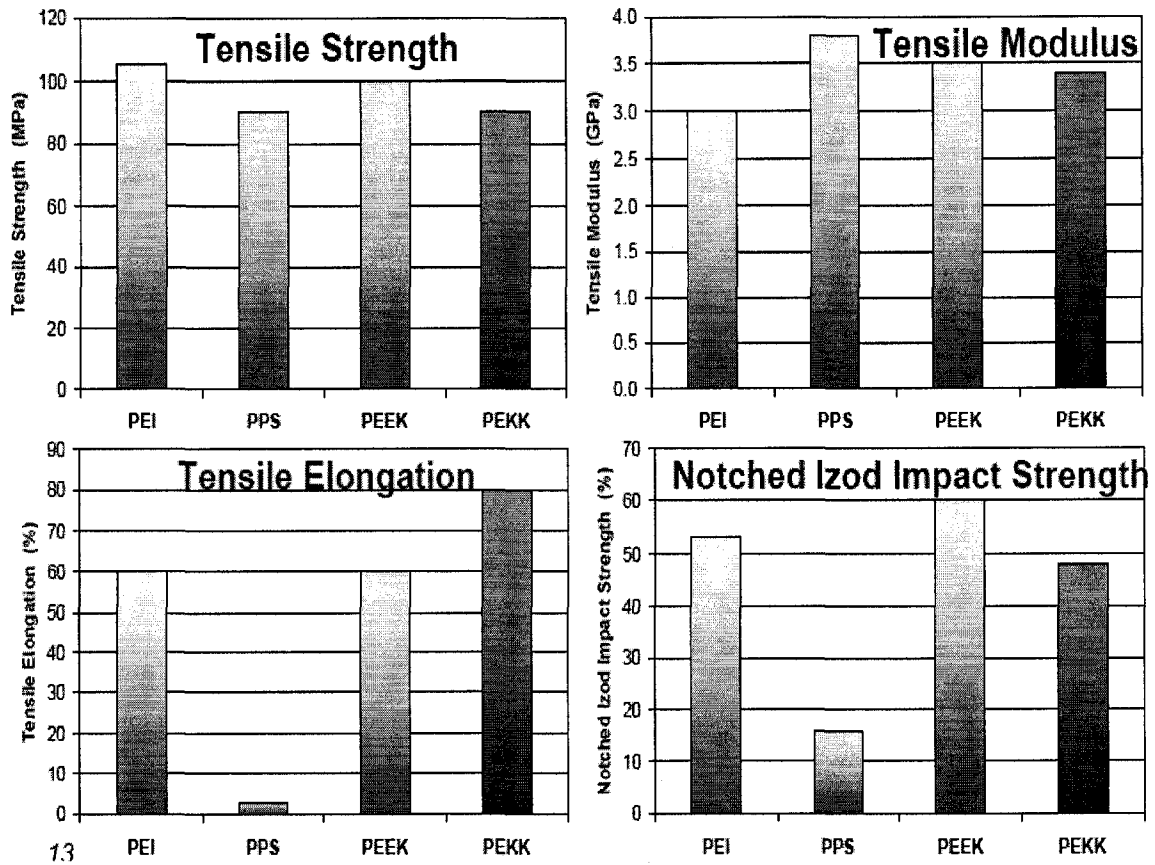


**Figure 1-11: Mechanical Properties of thermoplastic polymers (Provided by Cytec Engineered Materials).**

Carbon AS4/PEKK is a very high performance thermoplastic composite. This composite has a good balance of mechanical and physical properties. Table 1-6 shows the mechanical properties of this composite in the longitudinal and transverse directions. Properties of S2 Glass/PEKK composite have also been presented to show the superiority of carbon fiber composites for advanced applications over glass fiber composites, which are vastly used in low-to-moderate performance applications. The main shortcoming of carbon AS4/PEKK composite, however, is considerably lower strength in compression than in tension while for the glass fiber composite the difference is not very high.

Property	Units	PEKK/ AS4 Carbon	PEKK/ S-2 Glass
<b>0° Tension: ASTM D3039</b>			
Modulus	GPa	133	51.8
Strength	MPa	2050	1675
Poisson's ratio	-	0.30	0.27
<b>0° Compression: SACMA SRM-1</b>			
Modulus	GPa	124	20.1
Strength	MPa	1350	1213
<b>90° Tension: ASTM D3039</b>			
Modulus	GPa	9.47	20.1
Strength	MPa	56	48
<b>In-Plane Shear: ASTM D3518</b>			
Modulus	GPa	5.56	7.0
Strength	MPa	131	108
<b>Short-Beam Shear: ASTM D2344</b>			
Strength	MPa	98	74

**Table 1-6: Mechanical properties of Carbon AS4/PEKK composite.  
(Provided by Cytec Engineered Materials).**

### **1-6 Fabrication process of Carbon/PEKK composites**

As discussed earlier, the material selected for manufacturing the composite landing gear is Carbon AS4/PEKK, which is an advanced thermoplastic composite. Thermoplastic composites are famous for their rapid fabrication, no involvement of chemistry during the process, potential for manufacturing complex parts and integrating fabrication and assembly in one single step.

Cytec Engineered Materials provided the research project with two forms of the material: 300mm wide tape for fabrication of the plates and 6mm-wide strip for fabrication of the tubes. Figure 1-12 illustrates different forms of Carbon AS4/PEKK prepreg. The wide tape was used for manufacturing of the composite plates by compression molding

technique. The plates were cut into standard specimens for performing tensile tests and characterization of the material. On the other hand, 6 mm slit tapes were used to fabricate the tubes using a fiber placement machine at AMTC-NRC.

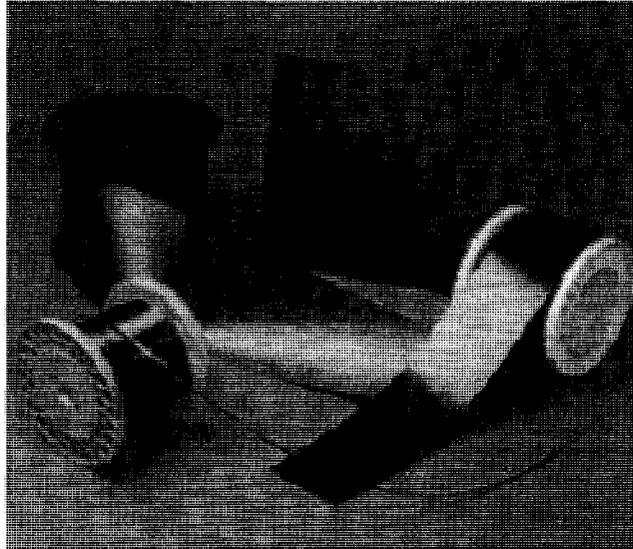


**Figure 1-12: Different forms of Carbon AS4/PEKK prepreg**

In general, the processing of thermoplastic composites consists of three steps: heating or melting, consolidation and solidification. Figure 1-13 schematically illustrates the pressure-temperature profile in terms of time for a typical thermoplastic composite process.

### **Melting**

Processing of thermoplastic composites starts with heating the prepreg in order to melt the matrix resin and bond the surfaces. When composite contains solvents or volatiles in its matrix the process must be slow. In all other cases rapid heating is preferred for short processing cycles, Gutowski (1997). In contrast to compression molding, filament

winding and fiber placement are very rapid processes. In these cases the prepreg is in motion and requires very rapid heating. As such, employment of hot shoes, infrared heating and focused laser heating is recommended, Saferis et al. (1986). However, for compression molding, the prepregs are heated and melted inside a mold, usually made of steel, and melting may last several minutes. The top and the bottom of the mold are usually isothermal plates that provide the composite with uniform heating rates.

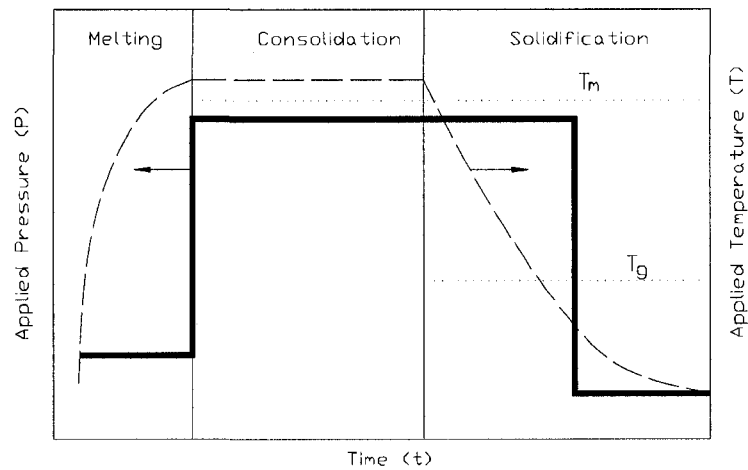


**Figure 1-13: Processing profile for thermoplastic composite.**

### **Consolidation**

After the prepregs melt, an external pressure is applied to the composite to de-bulk the prepregs and squeeze out entrapped air. The pressure also helps to suppress void formation and uniformly disperse the fibers. As a result of consolidation step, a void-free composite part through the bonding of prepreg tapes or complete impregnation of co-mingled tows is obtained. Due to the de-bulking during consolidation, the thickness of

the composite is reduced. When a thermoplastic prepreg lay-up is compressed above its melting temperature, the pressure brings the prepregs into intimate contact and eliminates any free space between the plies, Gutowski (1997). When the prepregs are in intimate contact and the polymer can flow, the plies of the prepreg can adhere to one another by the molecular diffusion of the matrix. Voyutskii (1963) called this healing process autohesion. According to him, during autohesion prepregs bond together and the interlaminar shear strength increases. During the process, the pressure must be sustained as long as the resin is in the molten or rubbery stages to prevent elastic recovery of the matrix and subsequent void formation through the composite.

### **Solidification**

During consolidation a part is formed; however, like other plastics, thermoplastic matrix composite has to be cooled to solidify and form the structure. During solidification, the processing pressure must be maintained until the temperature of the composite is below its matrix glass transition temperature. Application of the pressure prevents void formation within the resin, restricts the elastic recovery of the fibers and more importantly keeps the structure at the desired dimensions, Gutowski (1997).

Moreover, solidification has a significant impact on the mechanical properties of the thermoplastic composites, most of them semicrystalline materials. The degree of crystallinity affects the strength and stiffness of the composite in the transverse direction and improves the chemical and environmental resistance of the composite. The degree of crystallization, however, depends on the temperature and cooling rate during solidification. A slow cooling rate gives more chance to the polymer chains to align with

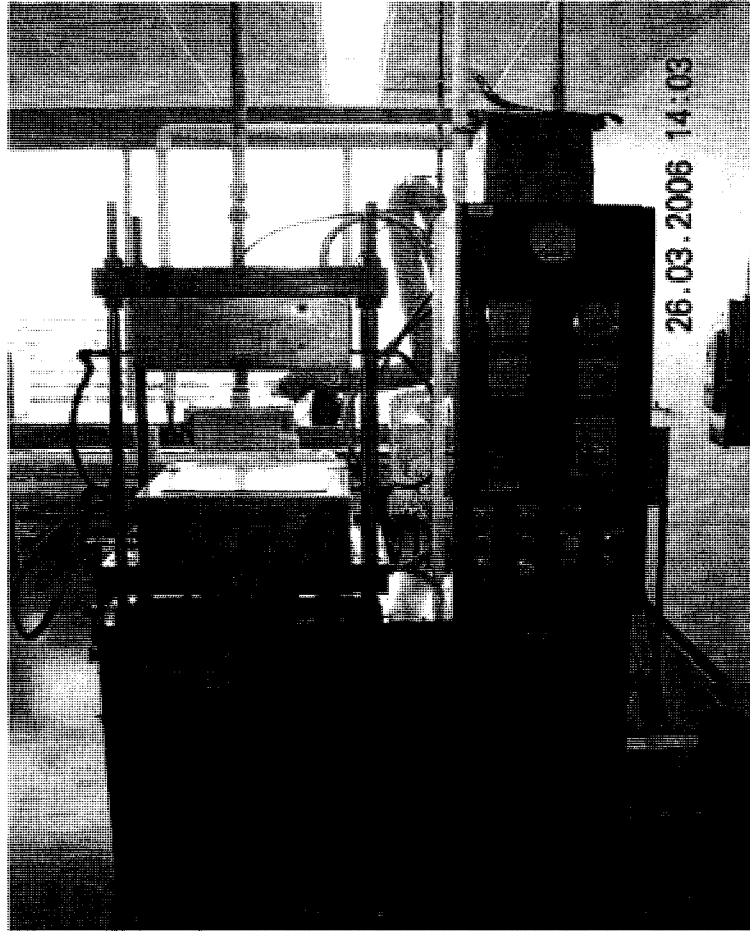
each other and produce some crystalline areas within the polymer matrix. However, this slows down the process, adds cost and to some certain level reduces the ductility of the composite.

Hereinafter, the general characteristics of two fabrication techniques, which are used in developing the samples for the experimental parts of this research, are discussed: the compression molding technique and the automated fiber placement.

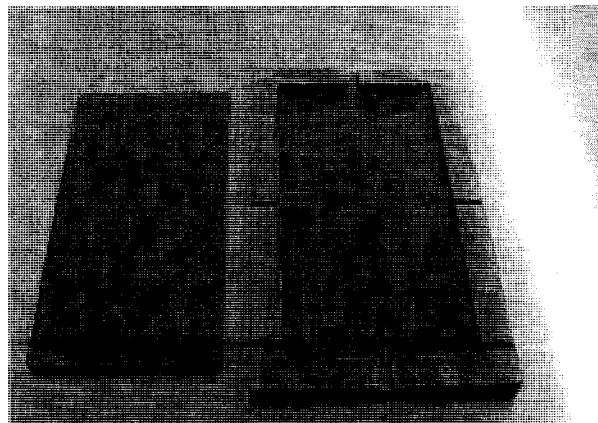
### **1-6.1 Compression molding**

Figure 1-14 shows a Wabash compression molding machine, which is available at CONCOM facilities at Concordia University. The machine can apply 30 tons of pressure while the temperature at platens can reach up to 537° C (1000° F). The machine has air and water cooling options; however, the cooling rate is not adjustable. The rates for air and water cooling are 2° C/min and 6° C/min respectively. Due to the restrictions of the machine, for temperatures above 245° C, the cooling must be done either by air or combination of air and water while below this temperature fast cooling by water only is possible. The processing temperature and pressure for carbon AS4/PEKK are around 345° C and 1000 KPa respectively.

The machine is used for fabrication of 150mm by 300mm carbon AS4/ PEKK composite plates. Figure 1-15 shows the corresponding mold; the drawing and detailed design of the mold are presented in Appendix A. The mold has been designed as male-female counterparts to assure applied pressure is totally transferred to the laminate. One slot at each side enables the extra resin (if any) to come out while the pressure is applied; moreover, the installation of thermocouples would be possible.



**Figure1-14: Wabash compression molding machine.**



**Figure1-15: A mold for processing thermoplastic composites by compression molding.**

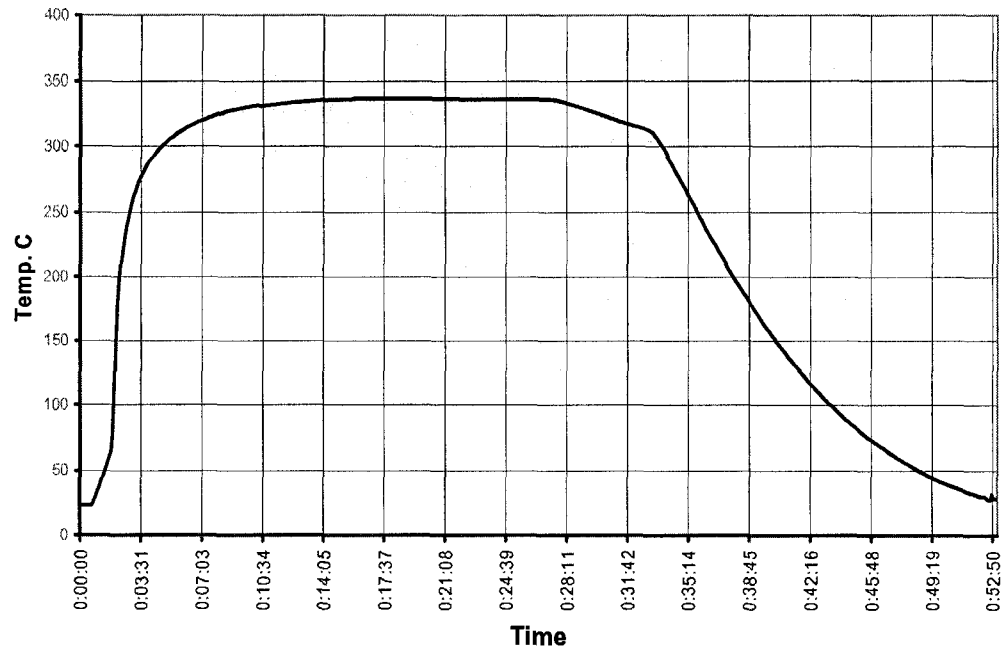


**Figure1-16: Time-temperature profile for processing carbon AS4/ PEKK composite.**

Figure 1-16 illustrates the time-temperature profile that was used for processing of the material and manufacturing of the plates. According to Cytec, the best processing temperature for the material is about 345° C. As such, the mold was kept at this temperature for 15 min to assure a proper consolidation. After consolidation, both air and water cooling systems were used to bring the laminates to room temperature. The pressure during the melting process was just a contact pressure while during the consolidation it was increased to 1000 KPa. However, during solidification, it is recommended to increase the pressure. In fact, as the temperature drops during the cooling period, the matrix shrinks. Therefore the chance to create some voids inside the laminate is increased. Nevertheless by increasing the pressure by 20%, the risk for such phenomenon is diminished.

## 1-6.2 Automated fiber placement

Fiber Placement is an automated manufacturing process for composites. For the case of thermoplastics, melting, consolidation and solidification of the pre-impregnated fibers on even complex tooling mandrels occur at once for any layers to be laid up. Advanced fiber placement machine can be used for fabrication of composite structures in different scales. Layup of thermoset or thermoplastic tows or slit tapes onto a mandrel or inside a mold is possible. Using the advanced fiber placement machines layup of the complex structures such as isogrids is now possible. Not long time ago, production of complex composite parts required extensive hand lay-up, which resulted in very expensive and time consuming processes. However, fiber placement machines combine the advantages of filament winding and the advance technology of automated robotic systems to demonstrate a fast and reliable fabrication process. Figure 1-17 shows the processing head for fiber placement system.

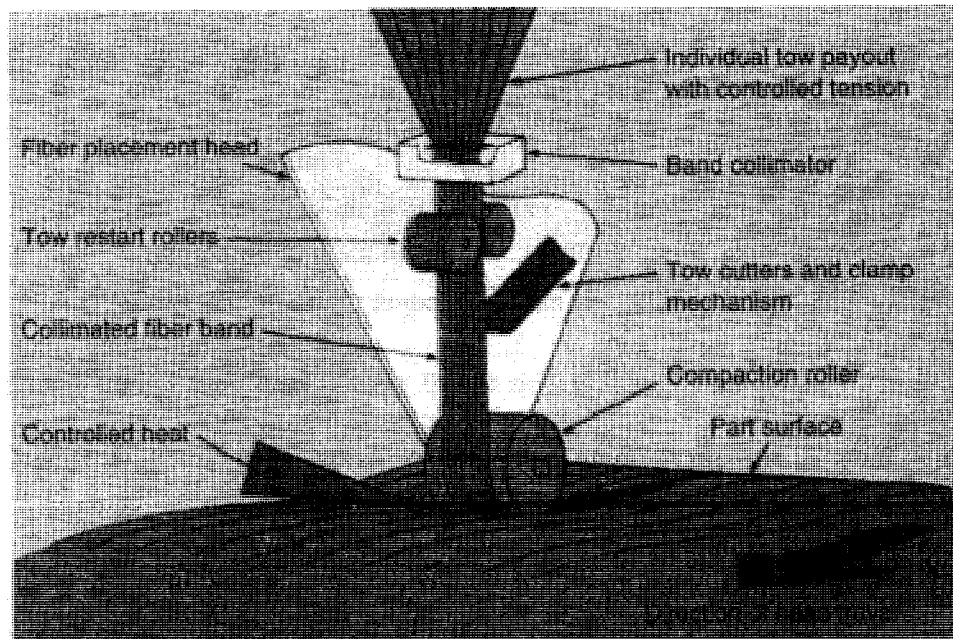


Figure 1-17: The processing head for fiber placement system, Morgan (2005).

Due to the reduction of manufacturing time and manpower and avoiding physical rework, the cost of products manufactured by fiber placement is less. Moreover, fibers can be laid up at any angle, and tows can be added or removed when necessary. The main challenge, however, is to create proper data and program the machine. This task is cumbersome and despite the considerable progress made, yet it remains prone to error.

One advantage of fiber placement machines is to dispense the tows at different speeds. As such, it would be possible for the machine to properly layup the tapes on the curved surfaces. A seven axis capability (roll, pitch, yaw, mandrel, arm tilt, carriage and crossfeed) positions the tows at the desired angles at up to 30 m/min to maximize the strength and minimize weight, Morgan (2005).

As the fibers are placed, the material and the structure are built. The slit tape is released from a spool on the machine. A torch preheats the tape, and a compaction device, which is usually a roller, applies direct contact between the incoming materials in the fiber placement head and the substrate material. According to Automated Dynamic Corporation, which is the main manufacturer of fiber placement systems, this approach provides the best degree of compaction with the lowest amount of damage to the material being placed. Heat is added to the incoming material and already deposited substrate at the pressure point of the compaction roller. Upon receiving the heat, the matrix viscosity is reduced, and the polymer can flow. Then the roller applies the pressure the materials are compacted. As such, tacking and debulking of the material occur simultaneously, Pasanen et al (1997). Figure 1-18 schematically shows a fiber placement head. From left to right, four devices are observed: a torch that is the main heat source and preheats the substrate; the trim heat source that heats the slit tape and the substrate to melting point;

the hot roller that applies heat and pressure to consolidate the laminates, and finally the cold roller that cools down the laminate while keeping the high pressure to assure proper solidification.

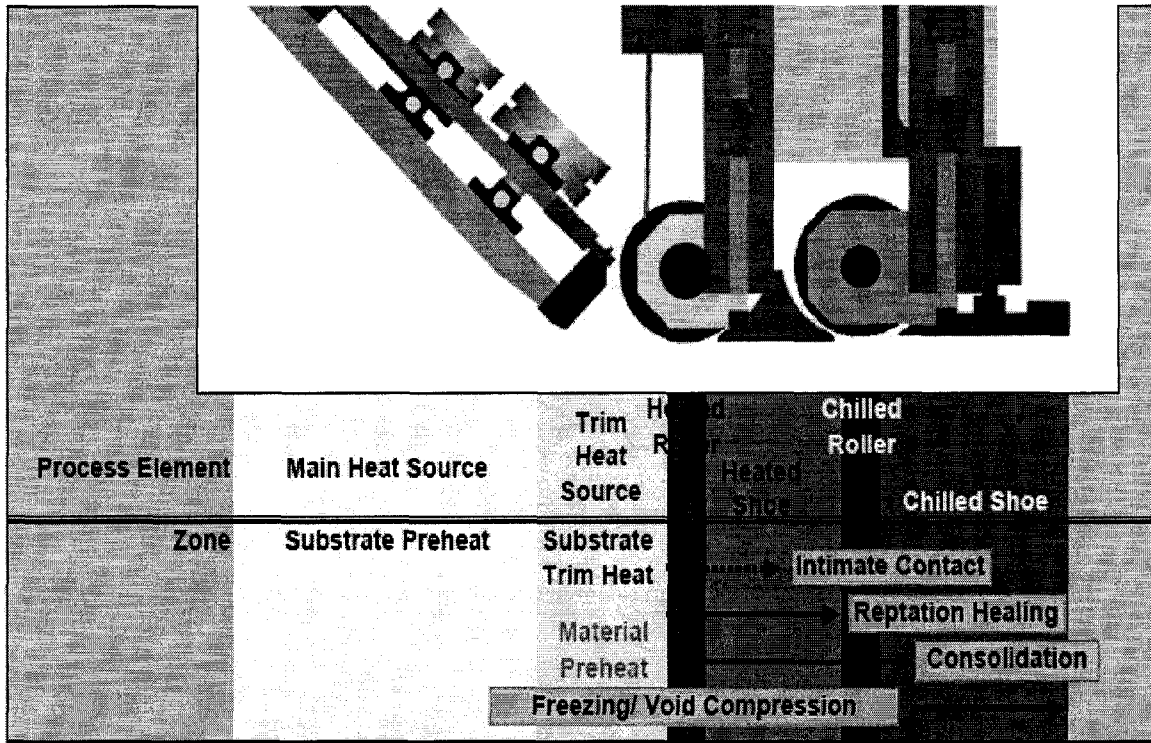
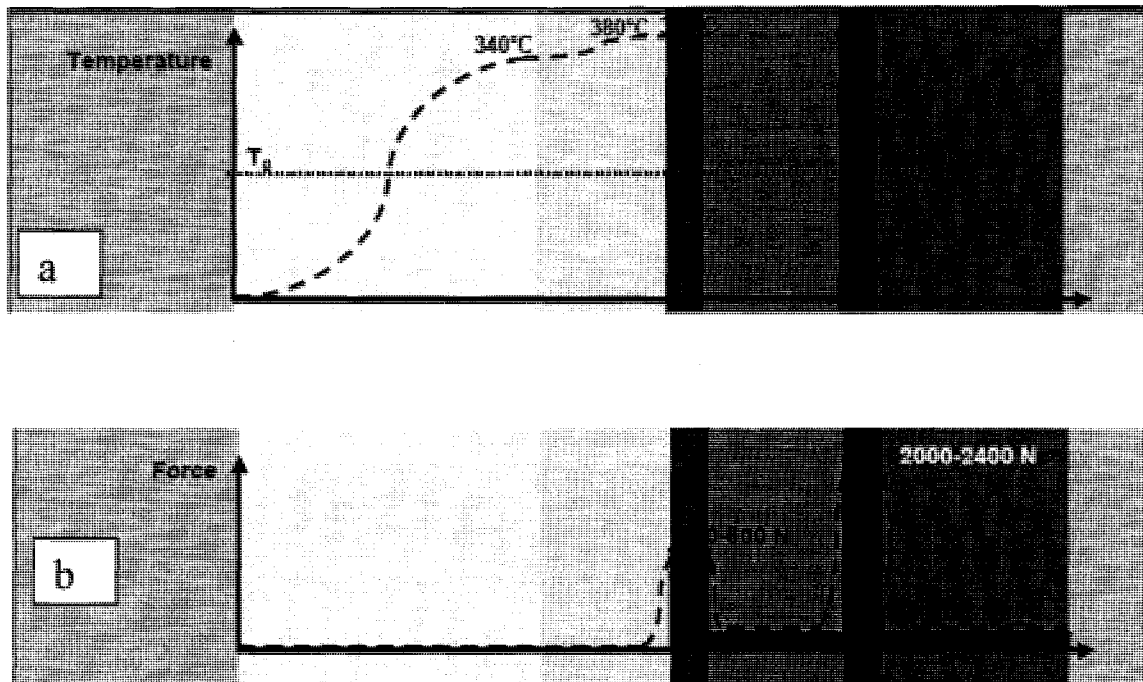


Figure 1-18 : Fiber placement head, Lamontia et al (2002).

Figures 1-19 a & b typically demonstrate the temperature and pressure profiles during the process. It is obvious that depending on the materials the values of temperature and pressure would vary. For carbon AS4/ PEKK prepreg the processing temperature is about 345°C. The pressure, however, can slightly vary. The higher pressure results in lower thickness at each ply as the tape can spread through the length. Normally a pressure around 500N is applied for manufacturing composite tubes.



**Figure 1-19: Temperature and pressure profiles for fiber placement process, Lamontia et al (2002).**

Fiber placement process has been successfully employed to fabricate both thermoset and thermoplastic composites for many aerospace applications. Fiber placement can be applied to both closed and open sections such as tubes and flat panels. AMTC-NRC has a fiber placement machine and provides aerospace companies with different fabrication services. For the goal of this research a few straight Carbon AS4/PEKK tubes were made by AMTC. The material was provided by Cytec Engineered Materials. The design of the tubes including the layups and dimensions was done in this research, and AMTC carried out the fabrication. Figure 1-20 illustrates the fiber placement machine installed at AMTC facilities in Montreal, Canada.

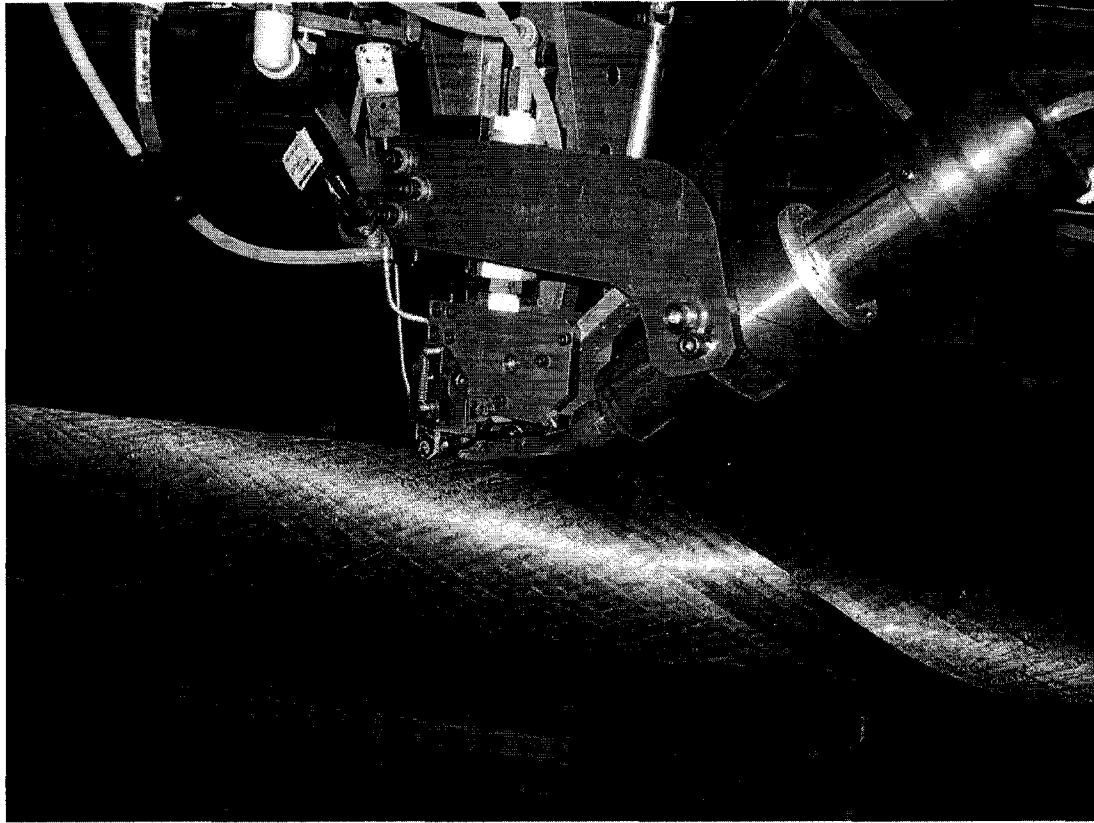


**Figure 1-20: The fiber placement machine at AMTC-NRC**

## **Chapter 2**

### **Review of Analytical Techniques for Composite Tubes**

#### **2-1 Introduction**

Stress analysis of a composite structure is often a complex and intricate task. Three reasons are widely mentioned for such a complexity. First, the governing equations for a composite structure are much more complicated than those of the structures made of isotropic materials. Second, as the material and structure are made at the same time, many more parameters are involved. For example, analyzing a metal structure, the designers are not concerned about the variation in material properties. The main concerns, however, might be the stress level, deformations and reliability of the joints and fasteners. Different samples of the same standard materials more or less show the same characteristics no matter in which factory they are made. In contrast, fabrication of a composite structure and the required composite material, which is built from resin and

fibers, is done simultaneously. As such, parameters involved in fabrication including temperature, pressure, humidity, time and quality control can play a significant role in the physical and mechanical properties of the material and, as a result, the behavior of the structure. Finally, a major source of intricacy is the layerwise failure of composite materials. In fact, as soon as a layer fails, a sort of delamination happens or a crack propagates in the plies, material properties and sometimes the governing equations could be different. This readily adds a lot of complexity to the analysis of composite structures.

Due to these three sources of complexity, application of finite element softwares to predict the behavior of composite structures beyond the first ply failure is a cumbersome task and very time consuming. As such, ANSYS analysis was carried out in a separate work parallel to this research by Xu (2008). At each stage, the required dimensions of tubes and the corresponding layups were designed according to Strain Controlled Analysis method presented in this work. Meanwhile ANSYS was used to predict the force deflection curves for the tubes subjected to bending loads. Through progressive failure, it was possible to predict the behavior of the tube beyond first ply failure.

While finite element analysis was done by ANSYS, in this work, a special analytical method was developed to carry out the design of the composite tubes. The method was verified through experimental work and finite element analysis. To achieve this method, nonetheless, it was necessary to have a thorough understanding of the behavior of anisotropic and composite tubes subjected to bending loads. As such, the available analytical techniques to analyze composite tubes were reviewed.

## 2-2 Previous works

In terms of design and stress analysis of composite tubes, as much as it can be found in the open literature, studies are limited to the small strains and elastic limit. The core of main works is the evaluation of displacements and stresses of a straight uniform thickness tube under uniform and constant loading. In other words, axial, torsional and bending loads are constant through out the span of the tube and not a function of the axial coordinate.

Most of the works are based on the basic equations of anisotropic elasticity in the cylindrical coordinate system presented by Lekhnitskii (1981). When the tube is in the state of generalized plane strain or generalized torsion, it can be analyzed by the Lekhnitskii stress function approach. The main problem of this method is that displacement expression in terms of stress functions are very complicated, especially when layerwise anisotropy is studied. Jolicoeur and Cardou (1994) and Chouchaoui and Ochoa (1999) developed Lekhnitskii functions into layerwise cylinders. In their method, each layer is analyzed first and then interfacial continuity and boundary conditions are satisfied. Though the method is straightforward, when many layers are involved, the system of equations will be huge and a lot of constants in the stress and displacement expressions must be determined. The other approach is to derive the governing equations in terms of displacements. In this case, the stress functions are very complicated, and still one has to deal with a lot of equations. Ting (1996, 1999) and Chen et al. (2000) studied a cylindrical anisotropic circular tube subjected to pressure, shear, torsion and extension for axisymmetric deformation of a homogeneous tube assuming the stresses are just a function of radial distance. Mamalis et al. (1995) presented a theoretical analysis for the

prediction of the ultimate bending strength for tubes of various composite materials subjected to bending. Gay and Hoa (2002) presented a method for the analysis of composite beams with an arbitrary cross section. However, each layer of this composite beam was made of isotropic materials and followed the generalized Hooke's law for linear small strains. Xia et al. (2002) developed an exact solution for multi-layered filament-wound composite tubes under pure bending. Finally, Tarn and Wang (2001) studied a laminate composite tube under extension, torsion, bending and shearing using a state space approach. They assumed that tractions do not vary axially. To avoid a system matrix to be dependent on  $r$ , they took  $r\sigma_r, r\sigma_{rz}, r\sigma_{r\theta}$  as the state variables and cast the field equations into a first order matrix equation with respect to  $r$ . As a result, the system matrix was then independent of  $r$ , so that the solution for the laminated tube using the method of matrix algebra in conjunction with the transfer matrix was possible.

### **2-3 Definition of terms and general equations**

Before going into the analytical analysis of composite tubes, it is necessary to have a common understanding of some frequent terms used in the analysis of anisotropic bodies. Though most of the composites can be categorized as orthotropic materials, the basic equations needed to analyze a composite tube are derived from the governing equations of anisotropic bodies. Definitions are based on Lekhnitskii (1981):

#### **Elastic properties**

Elastic properties are the parameters of the material that define the relations between the strain and stress components at any point inside the region of an elastic body. Considering small strains, the body is taken to be a continuous medium following the

generalized Hooke's law. Regarding the elastic properties all media are divided, on the one hand, into homogeneous and non-homogeneous, and, on the other hand, into isotropic and anisotropic.

A homogeneous anisotropic body has the same elastic properties at different points; however, these properties are different for different directions through a given point. Directions with similar elastic properties are called elastically equivalent directions.

### **Rectilinear and curvilinear anisotropy**

For a rectilinear anisotropic body all parallel directions are elastically equivalent; that is, all elements of the same size in the form of rectangular parallelepipeds with respective parallel faces deform identically under similar loading.

Despite rectilinear anisotropic bodies, a homogeneous medium is said to have curvilinear anisotropy if its elastically equivalent directions are not parallel but obey some other rules. Cylindrical and spherical anisotropy are of greatest practical interest.

### **Cylindrical anisotropy**

A very practical case of cylindrical anisotropy is encountered in the analysis of composite tubes. In fact a composite tube, with  $N$  number of layers, might be considered as an assembly of  $N$  coaxial anisotropic tubes bounded together at their interfaces. As such, it will be of a great interest in this research to know the behavior of an anisotropic tube under different loadings.

Considering an anisotropic tube, let a straight line  $g$  that can pass through the generator of the tube be the axis of anisotropy. If cylindrical anisotropy exists, all directions parallel to  $g$  and passing through different points are elastically equivalent; all normal directions to  $g$  (radial directions) are also equivalent; moreover, all directions orthogonal to the first two

(tangential directions) are equivalent. For a cylindrical anisotropic body, all infinitesimal elements bounded with three pairs of surfaces, whose normal vectors are the above mentioned directions, are equivalent and deform identically under similar loading.

### **Plane of elastic symmetry**

Assume that through each arbitrary point of a body there passes a plane with respect to that, elastic properties of symmetrical directions are equivalent. This plane is called plane of elastic symmetry and normal to this plane is called principle direction of elasticity.

Consider a homogenous anisotropic body. If there passes a plane of elastic symmetry at a point, normal to this plane, let say  $z$ , is a principle direction due to homogeneity. As such, there will be no coupling between out-of-plane shear stresses,  $\tau_{xz}$  and  $\tau_{yz}$ , with extensional strains,  $\varepsilon_x$  and  $\varepsilon_y$ , and in-plane shear strain  $\gamma_{xy}$ .

### **Generalized plane strain**

Consider a homogeneous cylindrical body having general rectilinear or cylindrical anisotropy. Assume that  $z$  axis coincides with the generator of the cylinder and  $r - \theta$  plane is normal to the generator. Loosely speaking, if at each point of the body there is a plane of elastic symmetry normal to the generator, under a uniform loading the planes of the cross section remain plane; in this case, the state of strain is known as plane strain. However, if the planes of elastic symmetry do not exist or are not parallel to  $r - \theta$  plane, the cross sections will warp and do not remain planes. Yet, if all the cross sections deform identically, the state of strain is described as generalized plane strain.

### 2-3.1 General Hooke's law for anisotropic bodies

In the general case of anisotropy, each strain component is a linear function of all six stress components. Referring to a Cartesian coordinate system, for a homogeneous anisotropic body that follows the generalized Hooke's law, the state of strain and stress for any arbitrary element are related as follows:

$$\begin{Bmatrix} \varepsilon_x \\ \varepsilon_y \\ \varepsilon_z \\ \gamma_{yz} \\ \gamma_{xz} \\ \gamma_{xy} \end{Bmatrix} = \begin{bmatrix} S_{11} & S_{12} & S_{13} & S_{14} & S_{15} & S_{16} \\ S_{12} & S_{22} & S_{23} & S_{24} & S_{25} & S_{26} \\ S_{13} & S_{23} & S_{33} & S_{34} & S_{35} & S_{36} \\ S_{14} & S_{24} & S_{34} & S_{44} & S_{45} & S_{46} \\ S_{15} & S_{25} & S_{35} & S_{45} & S_{55} & S_{56} \\ S_{16} & S_{26} & S_{36} & S_{46} & S_{56} & S_{66} \end{bmatrix} \begin{Bmatrix} \sigma_x \\ \sigma_y \\ \sigma_z \\ \tau_{yz} \\ \tau_{xz} \\ \tau_{xy} \end{Bmatrix} \quad (1)$$

The square six by six matrix is called the compliance matrix. For a homogeneous body elastic properties,  $S_{ij}$ , are invariable and are called elastic constants. Thanks to the symmetry of stress and strain tensors, the compliance matrix has no choice but to be symmetric. As such, the number of independent elastic constants reduces from 36 to 21. However, Novozhilov (1961) states that, geometrically, all coordinate systems are equivalent and symmetry may be observed even in the most general case of anisotropy; as a result, it can be shown that the number of independent elastic constants is not 21 but 18.

### 2-3.2 General Hooke's law for orthotropic bodies

A macroscopically homogeneous anisotropic body that has three mutually orthogonal planes of elastic symmetry at each point of the body is called an orthotropic body. As the

body is homogeneous, any plane parallel to one of these planes is also the plane of elastic symmetry. Taking the coordinate axes normal to the planes of elastic symmetry, the compliance matrix is considerably simplified. Leaving out the derivation, which can be found in the books of many authors including Love (1927) and Decolon (2002), the generalized Hooke's law for an orthotropic body can be expressed as follows:

$$\begin{Bmatrix} \varepsilon_x \\ \varepsilon_y \\ \varepsilon_z \\ \gamma_{yz} \\ \gamma_{xz} \\ \gamma_{xy} \end{Bmatrix} = \begin{bmatrix} S_{11} & S_{12} & S_{13} & 0 & 0 & 0 \\ S_{12} & S_{22} & S_{23} & 0 & 0 & 0 \\ S_{13} & S_{23} & S_{33} & 0 & 0 & 0 \\ 0 & 0 & 0 & S_{44} & 0 & 0 \\ 0 & 0 & 0 & 0 & S_{55} & 0 \\ 0 & 0 & 0 & 0 & 0 & S_{66} \end{bmatrix} \begin{Bmatrix} \sigma_x \\ \sigma_y \\ \sigma_z \\ \tau_{yz} \\ \tau_{xz} \\ \tau_{xy} \end{Bmatrix} \quad (2)$$

Based on engineering constants,  $E_i$ ,  $G_{ij}$  and  $\nu_{ij}$ , Equation (2) is written as

$$\begin{aligned} \varepsilon_x &= \frac{1}{E_1} \sigma_x - \frac{\nu_{21}}{E_2} \sigma_y - \frac{\nu_{31}}{E_3} \sigma_z, \\ \varepsilon_y &= -\frac{\nu_{12}}{E_1} \sigma_x + \frac{1}{E_2} \sigma_y - \frac{\nu_{32}}{E_3} \sigma_z, \\ \varepsilon_z &= -\frac{\nu_{13}}{E_1} \sigma_x - \frac{\nu_{23}}{E_2} \sigma_y + \frac{1}{E_3} \sigma_z, \\ \gamma_{yz} &= \frac{\tau_{yz}}{G_{23}}; \gamma_{xz} = \frac{\tau_{xz}}{G_{13}}; \gamma_{xy} = \frac{\tau_{xy}}{G_{12}} \end{aligned} \quad (3)$$

Though the number of independent elastic constants in these equations looks to be 12, M. W. Hyer (1998) and many other authors used Maxwell-Betti reciprocal theorem to

show that  $\frac{\nu_{ij}}{E_i} = \frac{\nu_{ji}}{E_j}$ . As a result, the number of independent elastic constants reduces to 9

as can be seen in Equation (2).

### 2-3.3 Transformation of elastic constants

Composite unidirectional lamina may be considered as orthotropic bodies; however, in most engineering cases, a laminate must include different angle ply laminae to attain enough strength and stiffness in all directions. As such, coordinate axes are not always normal to the planes of elastic symmetry. Leaving out the derivation, which can be found in the books of many authors including Decolon (2002) and Cristescu et al. (2004), the generalized Hooke's law for an orthotropic lamina rotated around z axis, normal to the plane of the lamina, can be expressed as follows:

$$\begin{Bmatrix} \varepsilon_x \\ \varepsilon_y \\ \varepsilon_z \\ \gamma_{yz} \\ \gamma_{xz} \\ \gamma_{xy} \end{Bmatrix} = \begin{bmatrix} C_{11} & C_{12} & C_{13} & 0 & 0 & C_{16} \\ C_{12} & C_{22} & C_{23} & 0 & 0 & C_{26} \\ C_{13} & C_{23} & C_{33} & 0 & 0 & C_{36} \\ 0 & 0 & 0 & C_{44} & C_{45} & 0 \\ 0 & 0 & 0 & C_{45} & C_{55} & 0 \\ C_{16} & C_{26} & C_{36} & 0 & 0 & C_{66} \end{bmatrix} \begin{Bmatrix} \sigma_x \\ \sigma_y \\ \sigma_z \\ \tau_{yz} \\ \tau_{xz} \\ \tau_{xy} \end{Bmatrix} \quad (4)$$

A case of great interest is when a lamina is rotated around the axis normal to the plane of the lamina. For example, if a tube or a cylindrical pressure vessel is made by filament winding or fiber placement techniques, the radial axis is normal to the plane of the laminate. Considering the helix angle for each layer, one can say that a lamina is rotated around the radial axis as much as the wind angle of the lamina. However, the  $r$  axis still remains as a principle direction of elasticity. As a result, there will be a coupling between extensional strains and in plane shear stress, on the one hand, and out-plane shear stresses

and strains, on the other hand. Using a cylindrical coordinate system, the generalized Hooke's law for this case is presented in the following sections.

#### **2-4 Analysis of anisotropic tubes**

Almost all the major studies in the analysis of composite tubes are based on the work of Lekhnitskii (1981). As such, it is noteworthy to review his work and the common fundamentals of other studies though different people used different approaches to solve the complex sets of the governing equations.

A main common assumption among all works is that the composite tube is in the state of generalized plane strain, the loads are constant and not varying along the  $z$ -axis, and there is no shear load resultant. That is, the curvature of the tube is constant through the length of the tube, and stresses and strains are functions of  $r$  and  $\theta$  only and independent of  $z$ . However, for anisotropic materials, bending of the tube is accompanied by some warping of the cross section even if just bending load is applied, Jolicoeur and Cardou (1994).

#### **Description of the problem**

Figure 2-1 shows a homogeneous orthotropic tube, with internal and external radii  $a$  and  $b$ , subjected to bending moments  $M_x$  and  $M_y$ , twisting torque  $T$  and axial force  $P$ . It is obvious that the internal forces in any cross section of a symmetric member are equivalent to the above mentioned loading and do not vary through the length of the tube. That is, no shear load resultant is involved. As a result, the tube will have constant curvatures of the center line in  $XZ$  and  $YZ$  planes and will undergo the following global deformations: axial strain  $\varepsilon$ , rotation per unit length  $\vartheta$ , and curvatures of the center line

$\kappa_x$  and  $\kappa_y$ . Moreover, it is assumed that the axis of anisotropy is aligned with the  $z$  axis, so the mechanical properties of the cylinder are axially symmetric; that is, the tube has cylindrical anisotropy. In other words, while using cylindrical coordinate system, elastic properties are constant. Finally, it is assumed that the elastic body will undergo small strains, and stresses and strains are functions of  $r$  and  $\theta$  only and are independent of  $z$ .

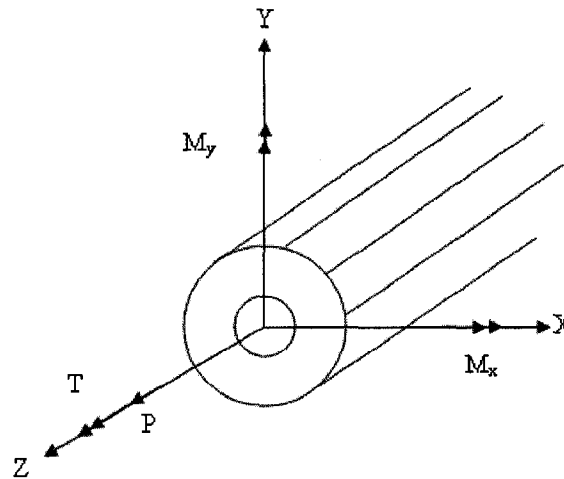


**Figure 2-1: Anisotropic tube subjected to bending, twisting and axial load**

In his book, “The Theory of Elasticity of an Anisotropic Body,” Lekhnitskii (1981) developed the governing equations for the analysis of a single-layer-anisotropic cylinder. However, those equations can be employed to analyze helically wound fibrous tubes if each layer is considered as a cylinder with orthotropic properties, which can be considered as a special case of anisotropy. Finally, compatibility equations at the interface of adjacent layers must be applied to avoid interference or separation of the layers.

Hereinafter, the general governing equations of anisotropic tubes are reviewed, and finally, extension of the method for the analysis of composite tubes is presented.

## Equilibrium equations

The basic equations of equilibrium in the cylindrical coordinates are

$$\begin{aligned}\frac{\partial \sigma_r}{\partial r} + \frac{1}{r} \frac{\partial \tau_{r\theta}}{\partial \theta} + \frac{\partial \tau_{rz}}{\partial z} + \frac{\sigma_r - \sigma_\theta}{r} + R &= 0 \\ \frac{\partial \tau_{r\theta}}{\partial r} + \frac{1}{r} \frac{\partial \sigma_\theta}{\partial \theta} + \frac{\partial \tau_{\theta z}}{\partial z} + \frac{2\tau_{r\theta}}{r} + \Theta &= 0 \\ \frac{\partial \tau_{rz}}{\partial r} + \frac{1}{r} \frac{\partial \tau_{\theta z}}{\partial \theta} + \frac{\partial \sigma_z}{\partial z} + \frac{\tau_{rz}}{r} + Z &= 0\end{aligned}\tag{5}$$

$R$ ,  $\Theta$  and  $Z$  denote the body forces. For the case in hand stresses do not vary in the  $z$  axis.

Assuming that body forces are absent, equations of equilibrium are simplified to

$$\begin{aligned}\frac{\partial \sigma_r}{\partial r} + \frac{1}{r} \frac{\partial \tau_{r\theta}}{\partial \theta} + \frac{\sigma_r - \sigma_\theta}{r} &= 0 \\ \frac{\partial \tau_{r\theta}}{\partial r} + \frac{1}{r} \frac{\partial \sigma_\theta}{\partial \theta} + \frac{2\tau_{r\theta}}{r} &= 0 \\ \frac{\partial \tau_{rz}}{\partial r} + \frac{1}{r} \frac{\partial \tau_{\theta z}}{\partial \theta} + \frac{\tau_{rz}}{r} &= 0\end{aligned}\tag{6}$$

## Strain displacement relations

Though based on the assumptions made, strains are independent of  $z$ , displacements still might be a function of axial position. If displacements are small and the body is continuous, strains are related to the components of displacement as follows

$$\begin{aligned}
\varepsilon_r &= \frac{\partial u_r}{\partial r} \\
\varepsilon_\theta &= \frac{1}{r} \frac{\partial u_\theta}{\partial \theta} + \frac{u_r}{r} \\
\varepsilon_z &= \frac{\partial u_z}{\partial z}
\end{aligned} \tag{7a}$$

$$\begin{aligned}
\gamma_{\theta z} &= \frac{\partial u_\theta}{\partial z} + \frac{1}{r} \frac{\partial u_z}{\partial \theta} \\
\gamma_{rz} &= \frac{\partial u_z}{\partial r} + \frac{\partial u_r}{\partial z} \\
\gamma_{r\theta} &= \frac{1}{r} \frac{\partial u_r}{\partial \theta} + \frac{\partial u_\theta}{\partial r} - \frac{u_\theta}{r}
\end{aligned} \tag{7b}$$

### Stress-Strain relations

As the body is considered elastic and only small strains are of interest, it can be assumed that the state of stress is linearly dependent on the state of strain, and the material follows the generalized Hooke's law. Unidirectional fiber composites, as could be seen in helically wound fibrous bodies, show orthotropic behavior in material coordinate system. The compliance matrix for such a material consists of nine independent elastic constants. However, as the material coordinates for each layer are not necessarily coincident with the global coordinate system, the transformed compliance matrix has 13 terms derived from the nine independent terms. The constitutive equation then is expressed as follows:

$$\begin{Bmatrix} \varepsilon_r \\ \varepsilon_\theta \\ \varepsilon_z \\ \gamma_{\theta z} \\ \gamma_{rz} \\ \gamma_{r\theta} \end{Bmatrix} = \begin{bmatrix} C_{11} & C_{12} & C_{13} & C_{14} & 0 & 0 \\ C_{12} & C_{22} & C_{23} & C_{24} & 0 & 0 \\ C_{13} & C_{23} & C_{33} & C_{34} & 0 & 0 \\ C_{14} & C_{24} & C_{34} & C_{44} & 0 & 0 \\ 0 & 0 & 0 & 0 & C_{55} & C_{56} \\ 0 & 0 & 0 & 0 & C_{56} & C_{66} \end{bmatrix} \begin{Bmatrix} \sigma_r \\ \sigma_\theta \\ \sigma_z \\ \tau_{\theta z} \\ \tau_{rz} \\ \tau_{r\theta} \end{Bmatrix} \tag{8}$$

The difference observed between Equations (4) and (8) is due to the axis of rotation. The helix angle is the angle between fiber direction, which is direction 1 in the material coordinate system, and longitudinal direction, which is  $z$  in global coordinate system. As such, it is obvious that each lamina is rotated around  $r$  axis by its helix angle.

It must be notified that Equations (6) to (8) are the governing equations for each individual cylindrical layer of the composite tube and must be solved as a system of equations for all layers simultaneously; besides, compatibility equations at the interfaces of the layers must be applied. Finally, boundary conditions must be applied in order to find the state of stress and strain and displacement components at each point of the body.

### Reduced elastic constants

To solve this system of equations, Lekhnitskii (1981) employs some functions with unknown constants to define the relations between displacements and stresses and finally applies the geometrical restrictions and compatibility equations to determine the unknowns. Function  $D$  is introduced as

$$D = C_{13}\sigma_r + C_{23}\sigma_\theta + C_{33}\sigma_z + C_{34}\tau_{\theta z} \quad (9)$$

where  $D$  is a function of  $r$  and  $\theta$  only seeing that stress components are not a function of  $z$ . As such,  $\sigma_z$  can be defined in terms of  $D$  and other stress components as follows:

$$\sigma_z = \frac{1}{C_{33}} [D - C_{13}\sigma_r - C_{23}\sigma_\theta - C_{34}\tau_{\theta z}] \quad (10)$$

Moreover, the reduced elastic constants are defined as follows:

$$\beta_{ij} = C_{ij} - \frac{C_{i3}C_{3j}}{C_{33}} \quad (11)$$

It can be easily seen that for orthotropic materials some  $\beta_{ij}$  terms are zero.

$$\begin{aligned}\beta_{15} = \beta_{16} = \beta_{25} = \beta_{26} = \beta_{35} = \beta_{36} = \beta_{45} = \beta_{46} = 0 \\ \beta_{i3} = \beta_{3j} = 0\end{aligned}\tag{12}$$

#### 2-4.1 Displacement and strain functions

Displacement components  $u_r, u_\theta$  and  $u_z$  are obtained by integration of Equation (7) where Equation (8) is used to express the strain components based on stresses. The detail of this procedure is given by Lekhnitskii (1981); however, the results are presented here for further references. It can be shown that the displacement components can be presented as follows:

$$\begin{aligned}u_r &= -\frac{z^2}{2}(\kappa_x \sin \theta - \kappa_y \cos \theta) + U + u'_r \\ u_\theta &= -\frac{z^2}{2}(\kappa_x \cos \theta + \kappa_y \sin \theta) + \mathcal{G}rz + V + u'_\theta \\ u_z &= z(\kappa_x r \sin \theta - \kappa_y r \cos \theta + \varepsilon) + W + w'\end{aligned}\tag{13}$$

In these equations,  $U, V$  and  $W$  are functions of  $r$  and  $\theta$  only and represent displacements caused by strains in axial position  $z = 0$ ; however, function  $W$  represents warping and rotation of the cross section. If not zero,  $W$  indicates that the Bernoulli-Euler hypothesis is not valid. Moreover,  $\kappa_x$  and  $\kappa_y$  are curvatures of the tube after deformation due to bending moments  $M_x$  and  $M_y$  respectively. Finally,  $u'_r, u'_\theta$  and  $w'$  are rigid body displacements and can be defined as

$$\begin{aligned}
u'_r &= z(-\omega_1 \sin \theta + \omega_2 \cos \theta) + u'_0 \cos \theta + v'_0 \sin \theta \\
u'_\theta &= z(-\omega_1 \cos \theta - \omega_2 \sin \theta) - \omega_3 r - u'_0 \sin \theta + v'_0 \cos \theta \\
w'_z &= r(\omega_1 \sin \theta - \omega_2 \cos \theta) + w'_0
\end{aligned} \tag{14}$$

where  $u'_0, v'_0, w'_0, \omega_1, \omega_2$  and  $\omega_3$  represent translations and rotations of the body with respect to the three coordinate axes. Though in the analysis of isotropic tubes all of these constants are set equal to zero, in the analysis of composite or anisotropic tubes this results in incompatibility in the radial and tangential displacements of the cylinders; yet,  $\omega_1$  and  $w'_0$  may still be set zero, but the body must be set free to translate in  $X$ - $Y$  plane to ensure compatibility of the deformed cylinders.

Substitution of Equation (13) into (7) and using the reduced elastic constants results in the following equations, which can be integrated to find  $U, V$  and  $W$  if stresses are known functions of  $r$  and  $\theta$ :

$$\begin{aligned}
\varepsilon_r &= \frac{\partial U}{\partial r} = \beta_{11} \sigma_r + \beta_{12} \sigma_\theta + \beta_{14} \tau_{\alpha z} + \frac{C_{13}}{C_{33}} D \\
\varepsilon_\theta &= \frac{1}{r} \frac{\partial V}{\partial \theta} + \frac{U}{r} = \beta_{12} \sigma_r + \beta_{22} \sigma_\theta + \beta_{24} \tau_{\alpha z} + \frac{C_{23}}{C_{33}} D \\
\varepsilon_z &= \frac{\partial u_z}{\partial z} = D
\end{aligned} \tag{15a}$$

$$\begin{aligned}
\gamma_{\alpha z} &= \frac{1}{r} \frac{\partial W}{\partial \theta} + \mathcal{G}r = \beta_{14} \sigma_r + \beta_{24} \sigma_\theta + \beta_{44} \tau_{\alpha z} + \frac{C_{34}}{C_{33}} D \\
\gamma_{rz} &= \frac{\partial W}{\partial r} = \beta_{55} \tau_{rz} + \beta_{56} \tau_{r\theta} \\
\gamma_{\alpha z} &= \frac{1}{r} \frac{\partial U}{\partial \theta} + \frac{\partial V}{\partial r} - \frac{V}{r} = \beta_{56} \tau_{rz} + \beta_{66} \tau_{r\theta}
\end{aligned} \tag{15b}$$

while  $D$ , which is a function of  $r$  and  $\theta$  only, can be expressed as follows:

$$D = \kappa_x r \sin \theta - \kappa_y r \cos \theta + \varepsilon \quad (16)$$

#### 2-4.2 Stress functions

By eliminating  $U$ ,  $V$  and  $W$  from Equations (15a) and (15b), a system of two equations is derived that only contains the stresses. However, solving the system of two equations, forcing the interface and boundary conditions into the closed form solutions and finding the stresses and displacements is a very intricate task. As such, to solve the equations for one single anisotropic tube, Lekhnitskii (1981) introduces two stress functions and relates them to stress components by the relations shown in Equation (17). Extension of the method for layer-wise cylinders was done by Jolicoeur and Cardou (1994), and also Chouchaoui and Ochoa (1999).

$$\begin{aligned} \sigma_r &= \frac{1}{r} \frac{\partial F}{\partial r} + \frac{1}{r^2} \frac{\partial^2 F}{\partial \theta^2} \\ \sigma_\theta &= \frac{\partial^2 F}{\partial r^2} \\ \tau_{r\theta} &= \frac{1}{r^2} \frac{\partial F}{\partial \theta} - \frac{1}{r} \frac{\partial^2 F}{\partial r \partial \theta} \end{aligned} \quad (17)$$

$$\tau_{rz} = \frac{1}{r} \frac{\partial \Phi}{\partial \theta}$$

$$\tau_{\theta z} = \frac{1}{r} \frac{\partial \Phi}{\partial \theta}$$

After eliminating  $U$ ,  $V$  and  $W$  and substituting stress functions, a system of two differential equations is derived, which just maintains the stress functions:  $F$  and  $\Phi$ . The system of differential equations may be expressed as follows:

$$\begin{aligned}
L_4 F + L_3 \Phi &= G_1(r, \theta) \\
L_3 F + L_2 \Phi &= G_2(r, \theta)
\end{aligned} \tag{18}$$

$L_4, L_3, L'_3$  and  $L_2$  are differential operators;  $F$  and  $\Phi$  are stress functions, and  $G_1$  and  $G_2$  are the non-homogenous terms of the differential equations. For orthotropic materials, some of the elastic constants are zero that results in a simplified form for the differential operators. Jolicoeur and Cardou (1994) and Chouchaoui and Ochoa (1999) used the following notations:

$$\begin{aligned}
L_4 &= -\beta_{22} \frac{\partial^4}{\partial r^4} - (2\beta_{12} + \beta_{66}) \frac{1}{r^2} \frac{\partial^4}{\partial r^2 \partial \theta^2} - \beta_{11} \frac{1}{r^4} \frac{\partial^4}{\partial \theta^4} - 2\beta_{22} \frac{1}{r} \frac{\partial^3}{\partial r^3} + \\
&(2\beta_{12} + \beta_{66}) \frac{1}{r^3} \frac{\partial^3}{\partial r \partial \theta^2} + \beta_{11} \frac{1}{r^2} \frac{\partial^2}{\partial r^2} - (2\beta_{11} + 2\beta_{12} + \beta_{66}) \frac{1}{r^4} \frac{\partial^2}{\partial \theta^2} - \beta_{11} \frac{1}{r^3} \frac{\partial}{\partial r} \\
L_3 &= \beta_{24} \frac{\partial^3}{\partial r^3} + (\beta_{14} + \beta_{56}) \frac{1}{r^2} \frac{\partial^3}{\partial r \partial \theta^2} + (\beta_{14} - 2\beta_{24}) \frac{1}{r} \frac{\partial^2}{\partial r^2} \\
L'_3 &= \beta_{24} \frac{\partial^3}{\partial r^3} + (\beta_{14} + \beta_{56}) \frac{1}{r^2} \frac{\partial^3}{\partial r \partial \theta^2} + (\beta_{14} + \beta_{24}) \frac{1}{r} \frac{\partial^2}{\partial r^2} - (\beta_{14} + \beta_{56}) \frac{1}{r^3} \frac{\partial^2}{\partial \theta^2} \\
L_2 &= -\beta_{44} \frac{\partial^2}{\partial r^2} - \beta_{55} \frac{1}{r^2} \frac{\partial^2}{\partial \theta^2} - \beta_{44} \frac{1}{r} \frac{\partial}{\partial r}
\end{aligned} \tag{19}$$

Moreover  $G_1(r, \theta)$  and  $G_2(r, \theta)$  can be expressed by the following equations:

$$\begin{aligned}
G_1(r, \theta) &= \frac{2}{r} \frac{C_{13} - C_{23}}{C_{33}} (\kappa_x \sin \theta - \kappa_y \cos \theta) \\
G_2(r, \theta) &= \frac{C_{34}}{C_{33}} (2\kappa_x \sin \theta - 2\kappa_y \cos \theta + \frac{\varepsilon}{r}) - 2\mathcal{G}
\end{aligned} \tag{20}$$

### 2-4.3 Solving the differential equations

As  $F$  and  $\Phi$  are functions of both  $r$  and  $\theta$ , separation of variables technique is employed to solve Equation (18). Stress functions then may be stated as follows:

$$\begin{aligned} F &= f_1(r)(\kappa_x \sin \theta - \kappa_y \cos \theta) + f_2(r) \\ \Phi &= \varphi_1(r)(\kappa_x \sin \theta - \kappa_y \cos \theta) + \varphi_2(r) \end{aligned} \quad (21)$$

By substitution of Equations (20) and (21) into (18), two distinct systems of ordinary differential equations are obtained. The first system, which is in terms of  $f_1$  and  $\varphi_1$ , is the Cauchy-Euler type and represents a pure bending problem while the second system only consists of  $f_2$  and  $\varphi_2$  and represents an axisymmetric tension-torsion and even pressure problem.

$$\begin{aligned} &[\beta_{22} \frac{d^4}{dr^4} + 2\beta_{22} \frac{1}{r} \frac{d^3}{dr^3} - (\beta_{11} + 2\beta_{12} + \beta_{66}) \frac{1}{r^2} \frac{d^2}{dr^2} + (\beta_{11} + 2\beta_{12} + \beta_{66}) \frac{1}{r^3} \frac{d}{dr} - \\ &(\beta_{11} + 2\beta_{12} + \beta_{66}) \frac{1}{r^4}] f_1 + \\ &[-\beta_{24} \frac{d^3}{dr^3} + (\beta_{14} - 2\beta_{24}) \frac{1}{r} \frac{d^2}{dr^2} + (\beta_{14} + \beta_{56}) \frac{1}{r^2} \frac{d}{dr}] \varphi_1 = \frac{2}{r} \frac{C_{13} - C_{23}}{C_{33}} \end{aligned} \quad (22a)$$

$$\begin{aligned} &[-\beta_{24} \frac{d^3}{dr^3} - (\beta_{14} + \beta_{24}) \frac{1}{r} \frac{d^2}{dr^2} + (\beta_{14} + \beta_{56}) \frac{1}{r^2} \frac{d}{dr} - (\beta_{14} + \beta_{56}) \frac{1}{r^3}] f_1 + \\ &[\beta_{44} \frac{d^2}{dr^2} + \beta_{44} \frac{1}{r} \frac{d}{dr} - \beta_{55} \frac{1}{r^2}] \varphi_1 = 2 \frac{C_{34}}{C_{33}} \end{aligned} \quad (22b)$$

The homogeneous part of Equation (22) can be written in the simplified form

$$\begin{aligned} D_4 f_1 + D_3 \varphi_1 &= 0 \\ D_3 f_1 + D_2 \varphi_1 &= 0 \end{aligned} \quad (23)$$

where  $D_4, D_3, D_3'$  and  $D_2$  are differential operators of order four, three and two respectively. Using systematic elimination technique for solving system of equations it can be shown

$$\begin{aligned} (D_4 D_2 - D_3 D_3') f_1 &= D_6 f_1 = 0 \\ (D_3 D_3' - D_4 D_2) \varphi_2 &= D_6 \varphi_1 = 0 \end{aligned} \quad (24)$$

where  $D_6$  is a sixth order differential operator. As such, it is obvious that System (22) is of the Cauchy-Euler type. Solution of this system, including homogenous and non-homogenous parts, can be expressed as follows:

$$\begin{aligned} f_1 &= \sum_{i=1}^4 \frac{K_i}{m_i} r^{m_i+1} + K_5 r + K_6 r \ln r + \frac{\mu_1}{2} r^3 \\ \varphi_1 &= \sum_{i=1}^4 K_i g_i r^{m_i} + K_6 \frac{\beta_{56}}{\beta_{66}} + \mu_2 r^2 \end{aligned} \quad (25)$$

where  $m_i$  are the roots of the characteristic equation and can be derived from

$$am^6 + bm^4 + cm^2 = 0 \quad (26)$$

$$m_{1,2,3,4} = \pm \sqrt{\frac{-b \pm \sqrt{b^2 - 4ac}}{2a}}, \quad m_5 = m_6 = 0 \quad \text{while } a, b \text{ and } c \text{ are defined as:}$$

$$\begin{aligned} a &= \beta_{22} \beta_{44} - \beta_{24}^2 \\ b &= \beta_{24} (2\beta_{14} + \beta_{24} + 2\beta_{56}) - \beta_{44} (\beta_{11} + 2\beta_{12} + \beta_{22} + \beta_{66}) - \beta_{22} \beta_{55} + \beta_{14}^2 \\ c &= \beta_{55} (\beta_{11} + 2\beta_{12} + \beta_{22} + \beta_{66}) - \beta_{56}^2 \end{aligned}$$

Moreover  $g_i$  and  $\mu_i$  can be expressed with the following equations:

$$g_i = \frac{\beta_{24} m_i^3 + (\beta_{14} + \beta_{24}) m_i^2 - \beta_{56}}{\beta_{44} m_i^2 - \beta_{55}}, \quad i = 1 \text{ to } 4 \quad (27)$$

$$\begin{Bmatrix} \mu_1 \\ \mu_2 \end{Bmatrix} = \begin{bmatrix} -2\beta_{14} - 6\beta_{24} + \beta_{56} & 4\beta_{44} - \beta_{55} \\ -\beta_{11} - 2\beta_{12} + 3\beta_{22} - \beta_{66} & 2\beta_{14} - 2\beta_{24} + \beta_{56} \end{bmatrix}^{-1} \frac{1}{C_{33}} \begin{Bmatrix} 2C_{34} \\ C_{13} - C_{23} \end{Bmatrix} \quad (28)$$

On the other hand, the second system is only consisting of  $f_2$  and  $\varphi_2$ . The system represents an axisymmetric tension-torsion and even pressure problem

$$\begin{aligned} & [\beta_{22} \frac{d^4}{dr^4} + 2\beta_{22} \frac{1}{r} \frac{d^3}{dr^3} - \beta_{11} \frac{1}{r^2} \frac{d^2}{dr^2} + \beta_{11} \frac{1}{r^3} \frac{d}{dr}] f_2 - \\ & [\beta_{24} \frac{d^3}{dr^3} - (\beta_{14} - 2\beta_{24}) \frac{1}{r} \frac{d^2}{dr^2}] \varphi_2 = 0 \end{aligned} \quad (29a)$$

$$[-\beta_{24} \frac{d^3}{dr^3} - (\beta_{14} + \beta_{24}) \frac{1}{r} \frac{d}{dr}] f_2 + [\beta_{44} \frac{d^2}{dr^2} + \beta_{44} \frac{1}{r} \frac{d}{dr}] \varphi_2 = \frac{\varepsilon}{r} \frac{C_{34}}{C_{33}} - 2\vartheta \quad (29b)$$

The general solution of this system can be derived in a similar manner

$$\begin{aligned} f_2 &= \sum_{i=1}^2 \frac{K_i'}{m_i' + 1} r^{m_i' + 1} + K_3' + K_4' r + \frac{K_5'}{2} r^2 + \frac{\mu_3}{3} \vartheta r^3 \\ \varphi_2 &= \sum_{i=1}^2 \frac{K_i' g_i'}{m_i'} r^{m_i'} + K_4' \frac{\beta_{11}}{\beta_{14}} \ln r + K_5' \frac{\beta_{14} + \beta_{24}}{\beta_{44}} r + K_6' + \frac{C_{34}}{C_{33} \beta_{44}} \varepsilon r + \frac{\mu_4}{2} \vartheta r^2 \end{aligned} \quad (30)$$

Again  $m_i'$  are the roots of the characteristic equation

$$m_{1,2}' = \pm \sqrt{\frac{\beta_{11} \beta_{44} - \beta_{14}^2}{\beta_{22} \beta_{44} - \beta_{24}^2}}$$

$g_i'$  and  $\mu_3$  and  $\mu_4$  can be expressed with the following equations:

$$g_i' = \frac{\beta_{14} + \beta_{24} m_i'}{\beta_{44}}; \quad i = 1, 2 \quad (31)$$

$$\begin{Bmatrix} \mu_3 \\ \mu_4 \end{Bmatrix} = \begin{bmatrix} \beta_{14} + 2\beta_{24} & -\beta_{44} \\ 4\beta_{22} - \beta_{11} & \beta_{14} - 2\beta_{24} \end{bmatrix}^{-1} \begin{Bmatrix} 1 \\ 0 \end{Bmatrix} \quad (32)$$

## Complete general solution

The complete general solution of system (18) for the stress functions is achieved by substitution of (25) and (30) into Equation (21)

$$F = (\kappa_x \sin \theta - \kappa_y \cos \theta) \left\{ \sum_{i=1}^4 \frac{K_i}{m_i} r^{m_i+1} + K_5 r + K_6 r \ln r + \frac{\mu_1}{2} r^3 \right\} + \sum_{i=1}^2 \frac{K'_i}{m'_i + 1} r^{m'_i+1} + K'_3 + K'_4 r + \frac{K'_5}{2} r^2 + \frac{\mu_3}{3} \mathcal{R}^3 \quad (33)$$

$$\Phi = (\kappa_x \sin \theta - \kappa_y \cos \theta) \left\{ \sum_{i=1}^4 K_i g_i r^{m_i} + K_6 \frac{\beta_{56}}{\beta_{66}} + \mu_2 r^2 \right\} + \sum_{i=1}^2 \frac{K'_i g'_i}{m'_i} r^{m'_i} + K'_4 \frac{\beta_{11}}{\beta_{14}} \ln r + K'_5 \frac{\beta_{14} + \beta_{24}}{\beta_{44}} r + K'_6 + \frac{C_{34}}{C_{33} C_{44}} \varepsilon r + \frac{\mu_4}{2} \mathcal{R}^2$$

$k_i$  and  $k'_i$  are constants that must be determined by satisfying compatibility and interface conditions between the layers.

### 2-4.4 Stresses and displacement functions

By substituting  $F$  and  $\Phi$  from (33) into (17) stress components are obtained

$$\begin{aligned} \sigma_r &= (\kappa_x \sin \theta - \kappa_y \cos \theta) \left( \sum_{i=1}^4 K_i r^{m_i-1} + \mu_1 r \right) + \sum_{i=1}^2 K'_i r^{m'_i-1} + \mu_3 \mathcal{R} + \mu_5 \varepsilon \\ \sigma_\theta &= (\kappa_x \sin \theta - \kappa_y \cos \theta) \left( \sum_{i=1}^4 K_i (m_i + 1) r^{m_i-1} + 3\mu_1 r \right) + \sum_{i=1}^2 K'_i m'_i r^{m'_i-1} + 2\mu_3 \mathcal{R} + \mu_5 \varepsilon \quad (34) \\ \sigma_z &= \frac{1}{C_{33}} [\kappa_x r \sin \theta - \kappa_y r \cos \theta + \varepsilon - C_{13} - C_{23} \sigma_\theta - C_{34} \tau_{\theta z}] \end{aligned}$$

$$\begin{aligned}
\tau_{r\theta} &= (\kappa_x \cos \theta + \kappa_y \sin \theta) \left( - \sum_{i=1}^4 K_i r^{m_i-1} - \mu_1 r \right) \\
\tau_{rz} &= (\kappa_x \cos \theta + \kappa_y \sin \theta) \left( \sum_{i=1}^4 K_i g_i r^{m_i-1} + \mu_2 r \right) \\
\tau_{\theta z} &= (\kappa_x \sin \theta - \kappa_y \cos \theta) \left( - \sum_{i=1}^4 K_i g_i m_i r^{m_i-1} - 2\mu_2 r \right) - \sum_{i=1}^2 K'_i g'_i r^{m'_i-1} - \mu_4 \mathcal{R} - \\
&\left( \mu_5 \frac{\beta_{14} + \beta_{24}}{\beta_{44}} + \frac{C_{34}}{C_{33}\beta_{44}} \right) \mathcal{E}
\end{aligned} \tag{34Cont.}$$

where constant  $\mu_5$  is defined as follows:

$$\mu_5 = \frac{C_{34}(\beta_{24} - \beta_{14}) + \beta_{44}(C_{13} - C_{23})}{C_{33}[\beta_{14}^2 - \beta_{24}^2 + \beta_{44}(\beta_{22} - \beta_{11})]} \tag{35}$$

Equation (15) relates  $U$ ,  $V$ , and  $W$ , which are functions of  $r$  and  $\theta$  only, into stress components in differential forms. Substitution of Equation (34) in (15) and consequent integration gives the following expressions for  $U$ ,  $V$ , and  $W$ .

$$\begin{aligned}
U &= (\kappa_x \sin \theta - \kappa_y \cos \theta) \left( \sum_{i=1}^4 K_i U'_i r^{m_i} + U'_5 r^2 \right) + \sum_{i=1}^2 K'_i U''_i r^{m'_i} + U''_3 \mathcal{R}^2 + U''_4 \mathcal{E} \\
V &= (\kappa_x \cos \theta + \kappa_y \sin \theta) \left( \sum_{i=1}^4 K_i V'_i r^{m_i} + V'_5 r^2 \right) \\
W &= (\kappa_x \cos \theta + \kappa_y \sin \theta) \left( \sum_{i=1}^4 K_i W'_i r^{m_i} + W'_5 r^2 \right)
\end{aligned} \tag{36}$$

$U'_i, U''_i, V'_i$  and  $W'_i$  are constants derived from the material elastic constants:  $C_{ij}, \beta_{ij}$ ; roots of the characteristic equations:  $m_i, m'_i$ ; and constants  $g_i$  and  $\mu_i$ . Finally, while stresses are readily available by Equation (34), simple substitution of (36) in Equation (13) gives displacement components at any point of the body.

## 2-5 Analytical solution for composite tubes

Equations (34) and (13) give the state of stress and displacement for one individual orthotropic hollow cylinder. A composite tube with  $N$  layers may be considered as  $N$  coaxial tubes, and as long as the boundary conditions are satisfied, the above mentioned equations can be applied for each layer or namely each cylinder.

Boundary conditions depend on the type of bonding between cylinders. Jolicoeur and Cardou (1994) studied two cases: perfect bonding that means no slip between the layers and also a case of no friction. With either case, they assume the pressure between layers remains high enough to prevent any sort of debonding or loss of contact between layers. On the other hand, Chouchaoui and Ochoa (1999), who also studied the analysis of composite tubes, assume a perfect bonding between layers with no slip. These two authors have almost used the same scheme for extension of the analytical solution of an anisotropic tube into an analytical solution for composite tubes. Their method is comprehensive enough to give some ideas for the design and analysis of a thermoplastic composite landing gear thus it is noteworthy to be reviewed hereinafter. Nonetheless, a few other authors have developed their work by other techniques. Among them are J. Tarn and Y. Wang (2001) who used a state space approach to study a composite tube under extension, torsion, bending and shear loading. However, their method is not presented here.

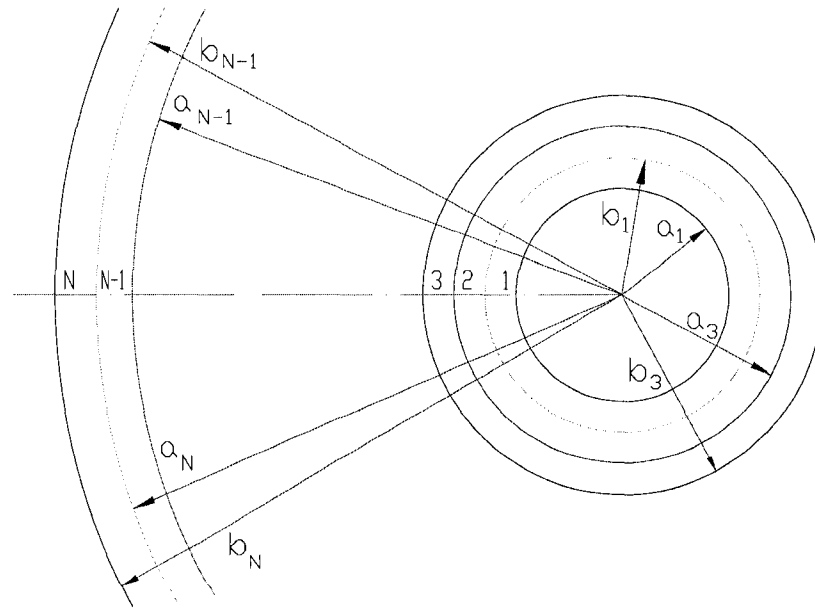
### Boundary conditions

Figure 2-2 shows the cross section of a composite tube having  $N$  layers. The inner and outer radii of layer  $n$  are shown with  $a_n$  and  $b_n$ . The internal and external radii of the tube are  $a_1$  and  $b_N$ . Hereinafter,  $b_n$  shows the interface radius between layer  $n$  and layer  $n+1$ .

Under no slip condition, some stress and displacement components must be identical at the interface of each two adjacent layers to ensure compatibility and avoid interference of the layers

$$[\sigma_r \quad \tau_{r\theta} \quad \tau_{rz} \quad u_r \quad u_\theta \quad u_z]_n = [\sigma_r \quad \tau_{r\theta} \quad \tau_{rz} \quad u_r \quad u_\theta \quad u_z]_{n+1}; \text{ on } r = b_n \text{ for } n = 1, 2, \dots, N-1 \quad (37)$$

where  $N$  is the number of layers and  $b_n$  is the outer radius of cylinder  $n$ . Nonetheless, if there is no friction between layers, longitudinal and tangential slip between cylinders is allowed. As a result, the functions for displacements  $u_\theta$  and  $u_z$  will be discontinuous. Nevertheless, there is still continuity of  $\sigma_r$  and  $u_r$  while the stresses  $\tau_{r\theta}$  and  $\tau_{rz}$  will have a zero value at the interface  $r = b_n$ .



**Figure 2-2: Cross section of a composite tube having  $N$  layers**

### Determination of the constants

Equation (33) includes the following unknown constants:

$$k_1, k_2, k_3, k_4, k_5, k_6, \vartheta, \varepsilon, \kappa_x, \kappa_y$$

Jolicoeur and Cardou (1994) used their logical and engineering judgment to put some of these constants to zero. For example, they set  $k_4=0$  to avoid having a non-periodic function of  $\theta$ , so the possibility of multiple valued displacements vanished. They also assumed that translation components of the rigid body motions to be expressed as follows:

$$u_0' = -C\kappa_y; v_0' = -C\kappa_x \quad (38)$$

where  $C$  is a constant that is to be determined for each cylinder except the first one, where it may be set equal to zero, and indeed it will be seen that this permits one to obtain a solution that ensures compatibility of the bent cylinders. After the above mentioned adjustments, seven unknown constants are left for each cylinder:  $(k_1, k_2, k_3, k_4, k_5, k_6, C)$ . Assuming that the composite tube consists of  $N$  layers,  $7N$  unknowns must be found. Jolicoeur and Cardou (1994) showed that for both no friction and no slip cases there are seven independent equations that must be satisfied at interfaces; this results in  $7(N-1)$  equations for  $7N$  unknown constants. Moreover, stresses  $\sigma_r, \tau_{r\theta}$  and  $\tau_{rz}$  have zero values at both internal and external free surfaces, yielding three equations each, so another six equations are added to the system of equations. Finally, to obtain the last independent equation, they set the value of  $C_1$  equal to zero, which

ensures compatibility of the bent cylinders. This gives a system of  $7N$  equations for the same number of arbitrary unknown constants.

The system of linear equations Jolicoeur and Cardou (1994) obtained may be divided into two distinct subsystems. The first one contains  $5N$  equations and the same number of independent unknowns ( $k_{1,n}, k_{2,n}, k_{3,n}, k_{4,n}, C_n$ ). This system can be directly solved to give the value of aforementioned constants for each cylinder. Nevertheless, the second subsystem, which only contains  $k_1'$  and  $k_2'$ , may only be solved when the global deformations  $\varepsilon$  and  $\mathcal{G}$  are known. They used the following notation to write the second subsystem in the matrix form:

$$K' = M_1^{-1} M_2 \begin{Bmatrix} \varepsilon \\ \mathcal{G} \end{Bmatrix} \quad (39)$$

where

$$K' = \langle K'_{1,1}, K'_{2,1} \cdots K'_{1,N}, K'_{2,N} \rangle^T$$

$M_1$  and  $M_2$  are matrices formed from the terms of the equations of the second subsystem.

In order to find  $k_1'$  and  $k_2'$  the end conditions must be applied to find the global deformation of the tube.

### **Applying boundary conditions**

Most studies found in the open literature assume that the tube is subjected to bending moments,  $M_x$  and  $M_y$ , a twisting torque,  $T$ , and an axial load,  $P$ . Some people also consider internal and external pressures. These boundary conditions can be expressed as follows:

$$\sum_{n=1}^N \int_0^{2\pi} \int_{r_{n-1}}^{r_n} (r\sigma_z) r dr d\theta = P \quad (40)$$

$$\sum_{n=1}^N \int_0^{2\pi} \int_{r_{n-1}}^{r_n} (r\tau_{\theta z}) r dr d\theta = T \quad (41)$$

$$\sum_{n=1}^N \int_0^{2\pi} \int_{r_{n-1}}^{r_n} (r\sigma_z) r \sin \theta dr d\theta = M_x \quad (42)$$

$$\sum_{n=1}^N \int_0^{2\pi} \int_{r_{n-1}}^{r_n} (r\sigma_z) r \cos \theta dr d\theta = M_y \quad (43)$$

where  $n$  is the index of a cylinder and  $N$  is the total number of the layers. Integration of (40) and (41) gives

$$P = \sum_{n=1}^N \frac{2\pi}{C_{33,n}} \left\{ \sum_{i=1}^2 K'_{i,n} [C_{13,n} + C_{23,n} m'_{i,n} - C_{34,n} g'_{i,n}] \frac{a_n^{m'_{i,n}+1} - b_n^{m'_{i,n}+1}}{m'_{i,n} + 1} + [\mu_{3,n} (C_{13,n} + 2C_{23,n}) - \mu_{4,n} C_{34,n}] \mathcal{G} \frac{a_n^3 - b_n^3}{3} + \left[ \mu_{5,n} \left( C_{13,n} + C_{23,n} - C_{34,n} \frac{\beta_{34,n} + \beta_{24,n}}{\beta_{44,n}} \right) - \frac{C_{34,n}^2}{C_{33,n} \beta_{44,n}} - 1 \right] \mathcal{E} \frac{a_n^2 - b_n^2}{2} \right\} \quad (44)$$

$$T = \sum_{n=1}^N 2\pi \left\{ \sum_{i=1}^2 K'_{i,n} g'_{i,n} \frac{a_n^{m'_{i,n}+2} - b_n^{m'_{i,n}+2}}{m'_{i,n} + 2} + \mu_{4,n} \mathcal{G} \frac{a_n^4 - b_n^4}{4} + \left[ \mu_{5,n} \frac{\beta_{14,n} + \beta_{24,n}}{\beta_{44,n}} + \frac{C_{34,n}^2}{C_{33,n} \beta_{44,n}} \right] \mathcal{E} \frac{a_n^3 - b_n^3}{3} \right\} \quad (45)$$

These equations can be written in matrix form

$$\begin{Bmatrix} P \\ T \end{Bmatrix} = M_3 K' + M_4 \begin{Bmatrix} \mathcal{E} \\ \mathcal{G} \end{Bmatrix} = M_3 M_1^{-1} M_2 \begin{Bmatrix} \mathcal{E} \\ \mathcal{G} \end{Bmatrix} + M_4 \begin{Bmatrix} \mathcal{E} \\ \mathcal{G} \end{Bmatrix} = B \begin{Bmatrix} \mathcal{E} \\ \mathcal{G} \end{Bmatrix} \quad (46)$$

$M_3$  and  $M_4$  are matrices formed from the terms of Equations (44) and (45), while  $B$  is the rigidity matrix. For axially symmetric loads (tension and torsion), its terms are:

$$B = M_3 M_1^{-1} M_2 + M_4 = \begin{bmatrix} (EA) & B_{12} \\ B_{12} & (GJ) \end{bmatrix} \quad (47)$$

By integrating (42) and (43), identical equations are obtained that give the flexural rigidity of the assembly of the cylinders:

$$\begin{aligned} M_x &= (EI)\kappa_x \\ M_y &= (EI)\kappa_y \end{aligned} \quad (48)$$

where

$$(EI) = \sum_{n=1}^n \frac{\pi}{C_{33,n}} \left\{ \sum_{i=1}^4 K_{i,n} [C_{13,n} + C_{23,n}(m_{i,n} + 1) - C_{34,n}g_{i,n}m_{i,n}] \frac{a_n^{m_{i,n}+2} - b_n^{m_{i,n}+2}}{m_{i,n} + 2} + [\mu_{1,n}(C_{13,n} + 3C_{23,n}) - 2\mu_{2,n}C_{34,n} - 1] \frac{a_n^4 - b_n^4}{4} \right\} \quad (49)$$

These equations show that there is no coupling between  $M_x$  and  $\kappa_y$ , nor between  $M_y$  and  $\kappa_x$ . More importantly there is no coupling between axially symmetric loads and deformations ( $P, T, \varepsilon, \mathcal{G}$ ) and bending loads and deformations ( $M_x, \kappa_x, M_y, \kappa_y$ ). Global rigidity of a composite tube or an assembly of orthotropic coaxial cylinders is finally can be expressed as

$$\begin{Bmatrix} P \\ T \\ M \end{Bmatrix} = \begin{bmatrix} (EA) & B_{12} & 0 \\ B_{12} & (GJ) & 0 \\ 0 & 0 & (EI) \end{bmatrix} \begin{Bmatrix} \varepsilon \\ \mathcal{G} \\ \kappa \end{Bmatrix} \quad (50)$$

thus global deformations of a composite tube can be obtained once loads are given.

## 2-6 Equilibrium of an anisotropic cantilever beam

Though the above mentioned method to analyze a composite tube is very complex, still it has major inadequacies to be used in the design of a composite landing gear.

First of all, considering the landing gear as a curved cantilever beam, it is obvious that the bending loads are not constant through the length of the tube while shear forces are involved. As the main requirement for derivation of Equation (50) is having constant loads through the length of the beam, it is clear that this prerequisite is violated for the analysis of landing gear. This is also the case for 3-point-bending tests of a straight tube.

As much as it can be found in the open literature, no researcher has approached the problem. The only work, which includes the shear forces in the analysis, is a procedural suggestion by Lekhnitskii (1981). He assumes that if there are planes of elastic symmetry normal to the axis of beam, the elastic equilibrium is of the same type as for an isotropic body, and the deformations qualitatively differ very little from those in an isotropic body.

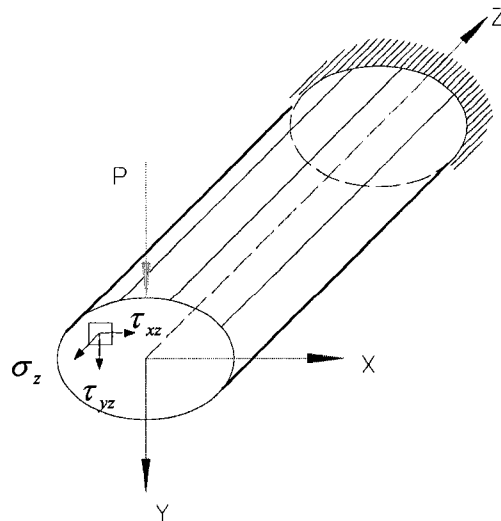


Figure 2-3: A cantilever anisotropic beam

Figure 2-3 shows the state of stress in an isotropic beam loaded at one end by force  $P$  and supported at the other end. The normal stress can be determined by a simple equation,  $-\frac{P}{I}zy$ , and shearing stresses,  $\tau_{xz}$  and  $\tau_{yz}$ , vary across the cross section. It can be shown that if there are planes of elastic symmetry coinciding with the planes of the cross section, the same type of state of stress is developed in an anisotropic body. Nevertheless, when the planes of symmetry do not exist or are not coinciding with the planes of the cross section, the distribution of stresses and strains will not be the same and are affiliated by generalized bending.

For generalized bending of a homogeneous anisotropic cantilever, Lekhnitskii (1981) proposes that the normal stress in the cross sections to be expressed as:

$$\sigma_z = -\frac{P}{I}zy + \sigma_z^0(x, y) \quad (51)$$

He also assumes that all other stress components are not zero but independent of  $z$ . Finally, he shows that under a transverse force  $P$ , a cantilever having general anisotropy develops in-plane stresses  $\sigma_x, \sigma_y$  and  $\tau_{xy}$  characteristics of plane strain beside  $\sigma_z, \tau_{xz}$  and  $\tau_{yz}$  characteristics of bending. Moreover, the cross sections do not remain plane but warped, and finally bending is accompanied by twisting. However, it is noteworthy that even in the general case of anisotropy the deflected axis is a plane curve, and deflection is expressed by the same equation of isotropic beams.

$$y = \frac{Pa_{33}}{6I}(2l^3 - 3l^2z + z^2) \quad (52)$$

where  $\frac{I}{a_{33}} = E_3I$  is flexural rigidity of the beam along  $Z$  axis.

## 2-7 Summary and conclusion

As much as it can be found in the open literature, analysis of composite tubes is confined to the cases that the states of strain and stress are not functions of  $z$ , longitudinal axis of the tube. Most researchers have limited their studies to symmetric extension, torsion and bending of straight constant-cross-section tubes. Moreover, stresses and strains are controlled to be in the elastic limit. No work was found to study the behavior of the body after first ply failure, during delamination or even beyond small strains.

On the other hand, Lekhnitskii (1981) is the only author who includes shear forces in his analysis and presents a method for analysis of anisotropic tubes while loads are not constant through the longitudinal axis of the tube. However, no development of these assumptions has been made to analyze layer-wise composite tubes so far.

As such, unless a new development is made, analytical analysis of composite landing gear is impossible because:

1- Landing gears are subjected to transverse forces; as a result, stresses are not constant through the length of the tube.

2- The landing gear is a curved tube with varying cross section. Even if the loads do not vary through the length of the beam, the stresses will be a function of  $z$  due to the reduced cross section area.

3- What is important in the analysis of a landing gear is the behavior of the structure during crash, where high loads and large deformations are involved and some layers may have already failed in these circumstances.

Considering all above restrictions, it is not hard to see that theoretical analysis of composite landing gears for small strains will not add much practical value in terms of

design and manufacturing. As such, a technique called Strain Controlled Design is presented in this research. Classical laminate theory is also used to analyze the laminate for strength and stiffness requirement. The technique will be able to predict the behavior of the tube beyond first ply failure. The accuracy of the design and the analyses, however, will be verified by experimental results. Meanwhile, progressive failure analysis using ANSYS will be employed for further authentication to minimize the number of experiments and the overall cost of the project.

## **Chapter 3**

### **Characterization of the Mechanical Properties of Carbon AS4/PEKK Composite**

#### **3-1 Introduction**

As discussed in Chapter 1, PEKK (Poly-Ether-Ketone-Ketone) is a relatively new thermoplastic polymer and has certain advantages over PEEK (Poly-Ether-Ether-Ketone). Besides its lower cost in the form of raw material, PEKK is processed at lower temperature than PEEK. Lower processing temperature means less energy consumption during the process and consequently a lower cost for the final products. Other chemical and mechanical properties of PEKK, however, are the same or slightly superior to PEEK. Nevertheless, the main inadequacy of PEKK as a relatively new thermoplastic polymer is the limited database, especially in the form of composites.

Design of a composite landing gear requires simultaneous solutions to contradictory problems. On one side, stress levels must be kept as high as possible to get as much

energy absorption as possible through the plastic deformation while, on the other hand, the stress level must be lowered to avoid fatigue problems. Moreover, the main concern in the design of a landing gear is not the requirement of normal landing, where both stresses and strains are very low and limited to elastic zone. In contrast, the main problems arise during severe conditions of harsh landing. During a crash, the aluminum landing gear go through large deformations and plastic strains to absorb high amounts of energy. As such, the energy transferred to the fuselage of the helicopter would be minimized, and the passengers would remain at lower risk.

Carbon fiber composites, however, are very brittle materials. Even though they may demonstrate high strength and stiffness, their fracture strain and toughness are quite low. This has been the main drawback for CFRP composites to be employed in applications where large deformation is required. Therefore, helicopter manufacturing companies have been reluctant to employ CFRP composites in landing gear. However, the target of this research was to systematically study all potentials of composite laminates and verify how it would be possible to achieve large deformation with these composites.

As such, it was necessary to study the full potential and behavior of composite laminates before any conclusion could be made whether or not carbon fiber thermoplastic composites can be employed in manufacturing of landing gears. Therefore, the mechanical behavior of Carbon AS4/PEKK laminates was extensively studied as a part of this research to find all potential mechanisms of large deformation. The potential outcomes would be used in the design of a deformable composite tube.

## **Background**

Theoretically, having the mechanical properties of a composite lamina in the fiber and transverse directions is enough to analyze the composite laminate consisting different layers at different angles. That is, the strength, stiffness and fracture strain of angle ply laminates can be predicted by transformation of the properties of the unidirectional laminate in the material coordinate system. However, this study showed that while the prediction of stiffness could be to a very high extent accurate, the calculation of fracture strain by theory might be quite off.

During the research, the mechanical properties and behavior of balanced angle ply laminates were examined by tensile tests. It was observed that an angle ply laminate may show large and plastic deformation due to the rotation of the fibers and plastic deformation of the polymer even though this type of behavior is not predicted by any of the classical laminate theories. In fact, the behavior of a laminate or a structure after initial failure is getting too complicated to be predicted by the classical laminate theories, so experiment is the only reliable approach in studying and characterizing composite materials.

In this chapter, after a brief introduction on the manufacturing of the composite laminates by compression molding technique, the process followed to assure the quality of the laminates is explained. Then the results of the tensile tests of different angle ply laminates are presented, and finally the effects of fiber direction on fracture modes of the laminates are analyzed.

### **3-2 Manufacturing and testing of the composite laminates**

The first step in manufacturing composite laminates by the compression molding technique is to cut the pre-impregnated fibers, known as prepreg, at the desired angles and make a pre-form. The material used in this research is Carbon AS4/PEKK thermoplastic prepreg supplied by CYTEC, USA. The material was provided in the form of 12" width unidirectional prepreg to facilitate producing composite plates by compression molding. Figure 3-1 shows a roll of Carbon AS4/PEKK thermoplastic prepreg and the hand cutting of the prepreg at a desired angle.

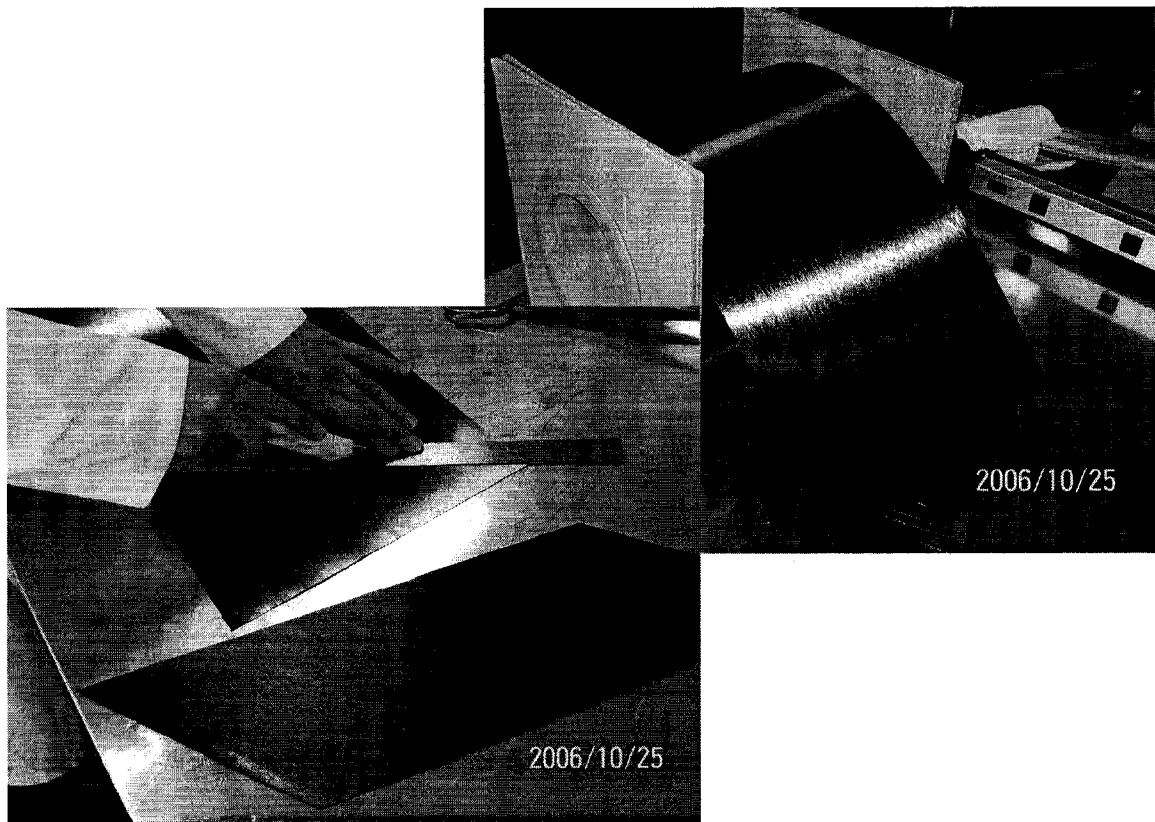


**Figure 3-1: Preform of Carbon/AS4 PEKK for compression molding**

Cutting the plies at the desired angle must be done carefully. A few degrees offset from the preferred angle would result in considerable reduction in stiffness of the laminate. As shown in Figure 3-2, the stiffness of the plies is susceptible to the orientation of the fibers. It can be seen in the graph that 5 degrees offset from zero degree results in 10% reduction in the stiffness. Therefore, it is very important to assure each single ply is exactly cut and laid up in the desired direction.

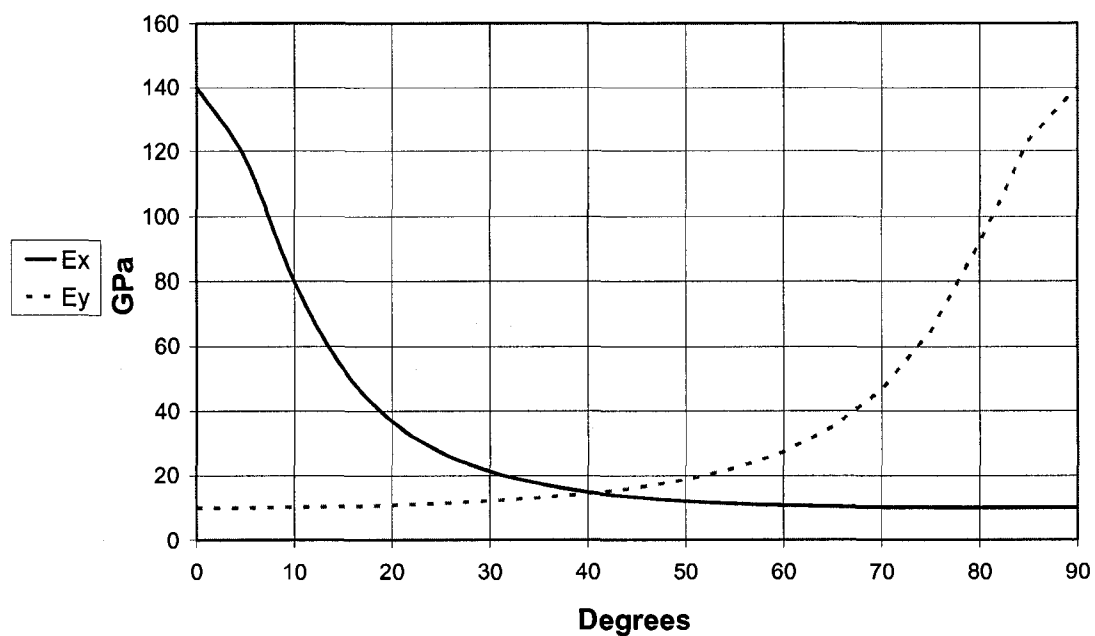


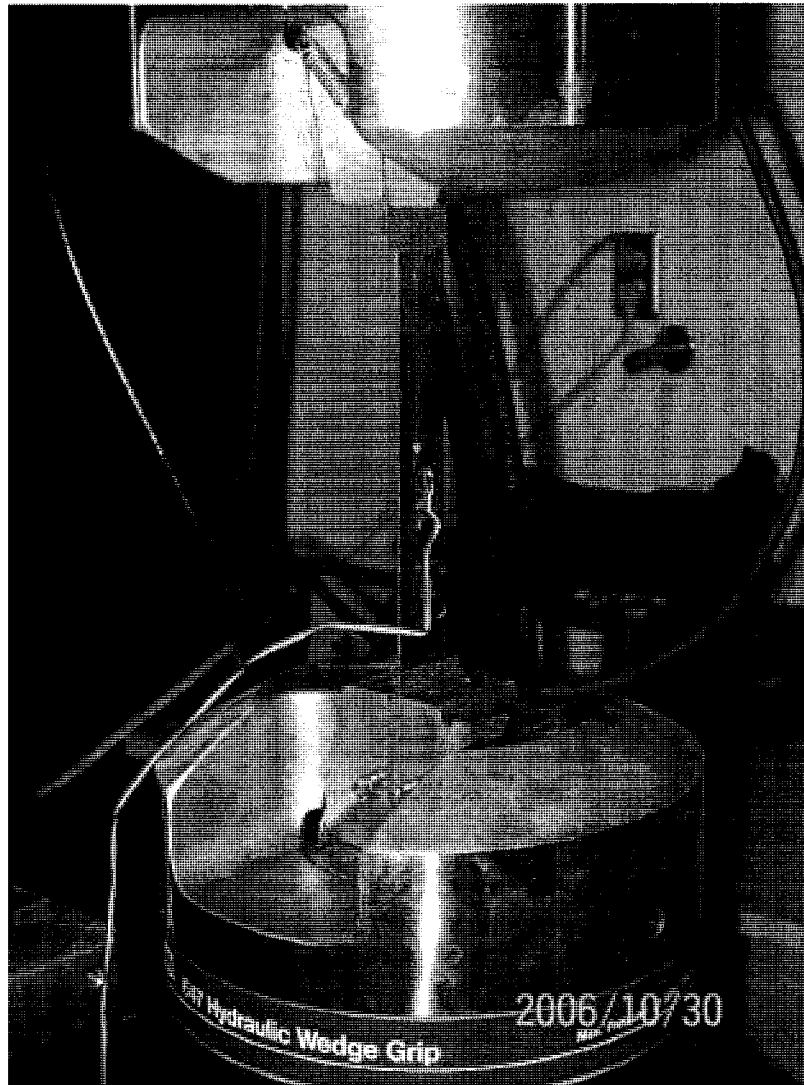
**Figure 3-2: Variation in the ply stiffness by variation in the fiber direction**

The dimensions of the cutting depend on the sizes of the mold and compression molding machine. In this research, it was required to test at least five samples from each laminate to assure repeatability of the results. According to ASTM D3039 Standard, the required size for tensile tests of angle-ply-laminate is 250mm by 25mm (10"×1"). To have five coupons from each plate, a 300mm by 150mm (12"×6") mold (Figure 1-15) was designed and manufactured at Concordia University.

In order to characterize the behavior of the material, different angle ply laminates with  $[\pm \theta / \pm \theta]_n$  layup were made. Each laminate included 8 plies of the prepreg. The thickness of the laminate was about 1mm. The plates were cut into five standard specimens by a diamond cutter. Also from each plate, a few small samples were cut to examine the quality of the laminate and its fiber volume fraction using the micrograph analysis technique.

After cutting the plates, the next step was to install the strain gauges on the coupons to measure the axial strain at the mid-span of the specimen during the tests. Installation of the strain gauges on the thermoplastic composites plates or tubes is an intricate task, and much attention must be paid to the details of the installation procedure. If the strain gauges are not well installed, it would be very probable that during the test, they delaminate from the sample. Appendix B explains the step by step procedure for a proper installation of strain gauges on the composites.

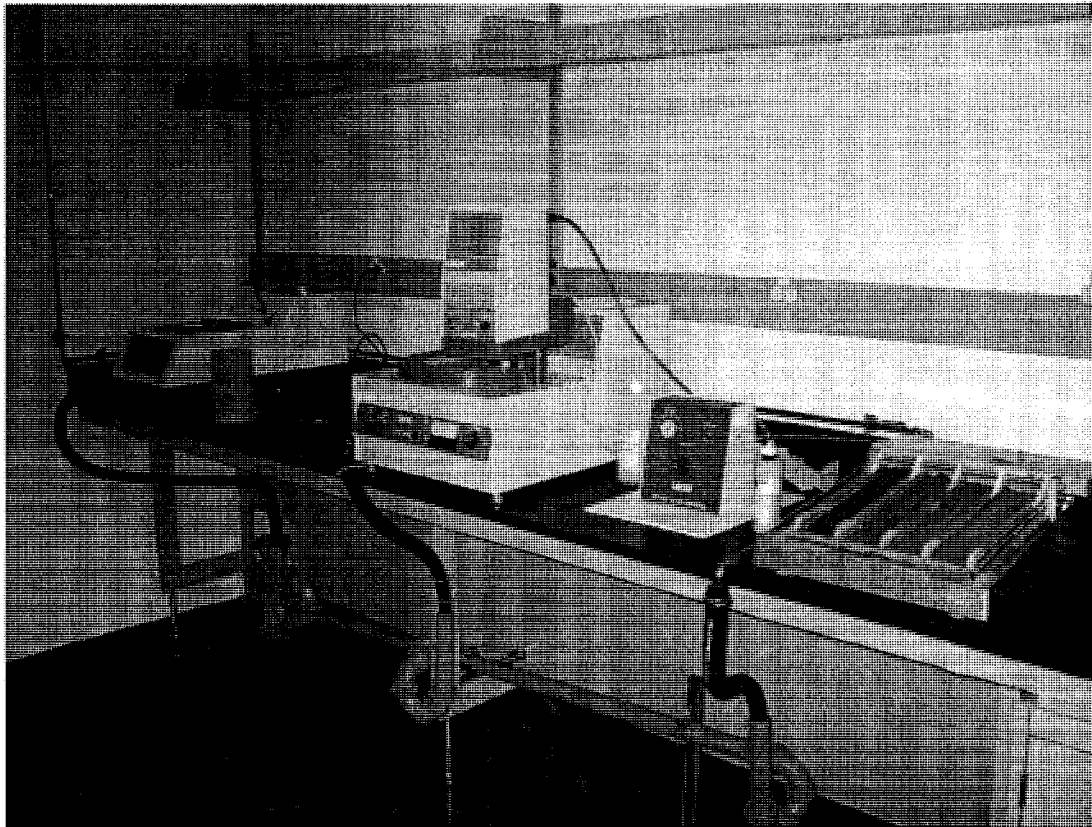
The last step before doing a tensile test is to assure that the sample is well gripped between the jigs of the MTS machine, and no slipping occurs. Nevertheless, if the pressure is too high at the grips, it would be possible that the jigs crush the sample and initiate fracture. As such, it is necessary to reinforce the sample at gripping areas. There are different types of grips for tensile tests based on the material, thickness, etc. For this work, it was observed that Silicon Carbide Coated Abrasive Mesh maintained a very good grip during the test. Moreover, there was less than 5% sample failure or fracture inside the grip area, so the abrasive mesh was adopted as the gripping material for all the tensile tests carried out during this research. Figure 3-3 illustrates a sample installed at the MTS machine ready for the tensile test.



**Figure 3-3: A sample installed at the MTS machine ready for the tensile test.**

### **Quality control of the plates**

After each plate was made, it was necessary to verify the quality of the samples. As such, a few samples, 15mm by 10mm, were cut from each plate. The samples were held by a plastic holder immersed in cup containing epoxy curing system. After the epoxy was cured, the samples were hard enough for polishing. Figure 3-4 shows the machinery used for this purpose.



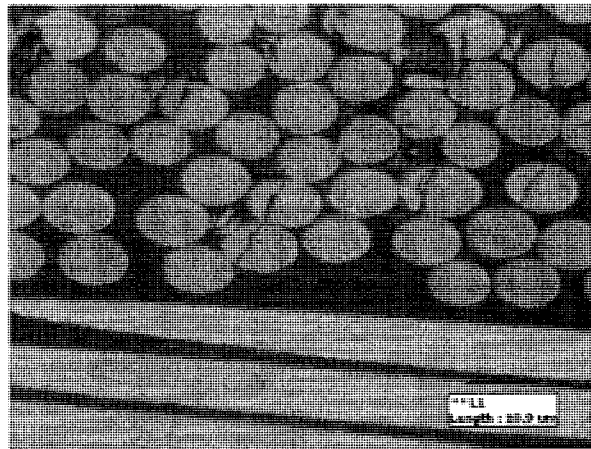
**Figure 3-4: Grinding and polishing equipment**

Table 3-1 suggests a suitable procedure to achieve well polished samples to take micrographs. The quality of micrographs is highly dependent on the quality of the polished surface of the samples. For example, rough grinding breaks the fibers and creates the wrong impression that the processing pressure was high, and that fibers broke due to intimate contact during the process. Also a broken chip of the fibers may be taken off from the samples by rough grinding. Then the micrograph shows a dark area that can be interpreted as a void that is again a wrong quality control impression. A proper procedure for grinding and polishing is obtained through experience, and it may slightly be different from sample to sample; nevertheless, the suggested procedure can always be used as a guideline.

Step	type	Surface	Grit or Particle size	Lubricant	Pressure for 6 samples		Load/specimen		Rotation speed	Time
					psi	KPa	Ibf	N		
1	Grinding	SIC Disc	320	Water	15	103	3	13	250	60
Repeat step 1 until the surface of the samples is flat										
2	Grinding	SIC Disc	600	Water	10	69	3	13	250	30
3	Fine Grinding	SIC Disc	800	Water	15	103	3	13	250	45
4	Polishing	Nylon Artic	3 Micron Diamond suspension	Water based diamond extender	25	172	5	22	150	240
5	Polishing	Nylon Artic	1 Micron Diamond suspension	Water based diamond extender	25	172	6	27	150	240
6	Fine Polishing	Nylon Artic	0.05 Micron Diamond suspension	Water based diamond extender	25	172	6	27	150	240

Table 3-1: Polishing steps to prepare samples for taking micrograph, Lebel (2005)

After the samples were polished and a shiny surface was achieved, an electronic microscope is used to take the micrographs. The microscope has different magnifications, so it would be possible to see the general cross section of the laminate as well as cross section of a fiber. Micrographs are the crucial tools to learn about composites. When a material is built from tiny fibers and polymer resin, small voids, resin rich areas and broken fibers may easily affect the properties of the laminate. As such, great attention must be paid to the microstructure of the material. For example, high processing pressure may result in squeezing out the resin between the fibers so that the fragile fibers touch each other and break. Figure 3-5 illustrates the phenomenon.



**Figure 3-5: Fracture of the fibers due to a high processing pressure**

On the other hand, if the processing pressure is low, extra resin stays in the laminate and creates resin rich areas. Such areas are considered as weak points in the laminate and stress concentration may occur around them. If there are too many resin rich areas in the laminate, the mechanical properties of the laminate including strength and stiffness go down considerably. Figure 3-6 shows a large resin rich area in a  $[+45^{\circ}/0^{\circ}/-45^{\circ}]$  laminate.

The small resin rich areas are inevitable in many cases; however, if the pressure is not enough or uniform on the mold, and there are numerous resin rich areas, the mechanical properties of the composite would descend drastically.

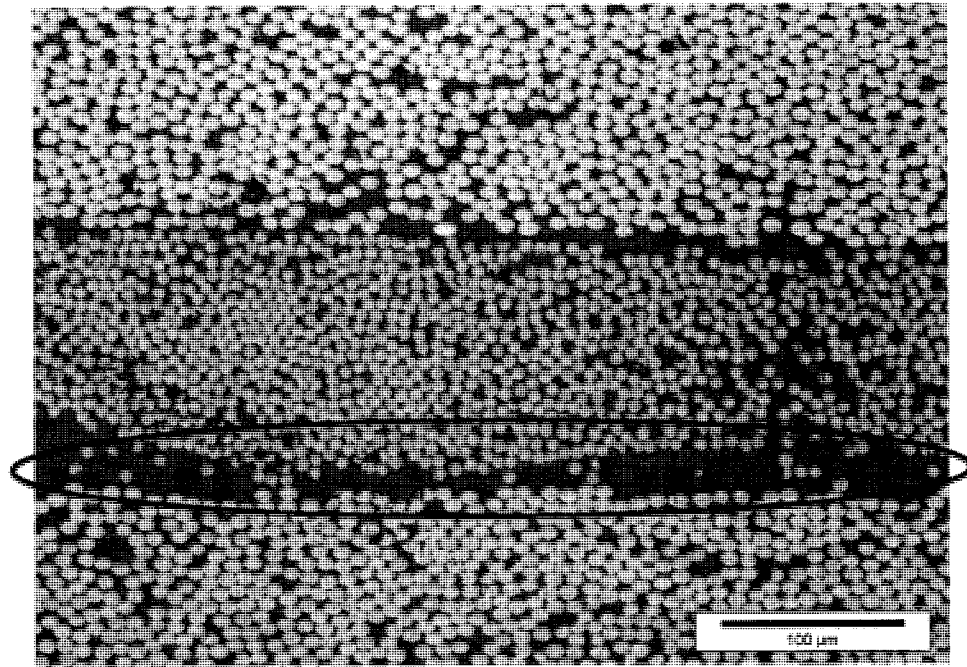


**Figure 3-6: A resin rich area in a Carbon AS4/ PEKK laminate**

Micrographs also give us a clear idea about the fiber volume fraction,  $V_f$ , of the laminate. In general, when fiber content is higher, the laminate would be stronger and stiffer. However, the manufacturing conditions and type of the processing always confine the maximum level of the fiber content. On the other hand, a high performance composite laminate is achieved only if dry fiber zones are avoided. If the fibers are dry and not surrounded by the matrix, they will not be able to transfer loads to one the other and their direct contact may result in the fracture of the fibers. Nevertheless, if the prepreg is used, this concern for manufacturing thermoplastic composite laminates is minimal.

Analyzing the micrographs is a task that must be done with great caution. Figure 3-7-a shows a large area in 90° ply of a quasi isotropic laminate with very low fiber content resembling a resin rich area; however, this type of area is not a resin rich area as slightly below the surface fibers are present. In fact, during the polishing process, fibers laid up parallel to polishing surface have low resistance to high shear forces applied by the machine, and some of the fibers are pulled out. Nevertheless, the area shown in part (b) has higher matrix content than the rest of laminate. These types of resin rich areas could be due to the processing or the quality of the prepreg. Finally, Figure 3-7-c shows a sample with high quality and high fiber content. Through this work, the qualities of the samples were always checked to assure the reliability of the test results.

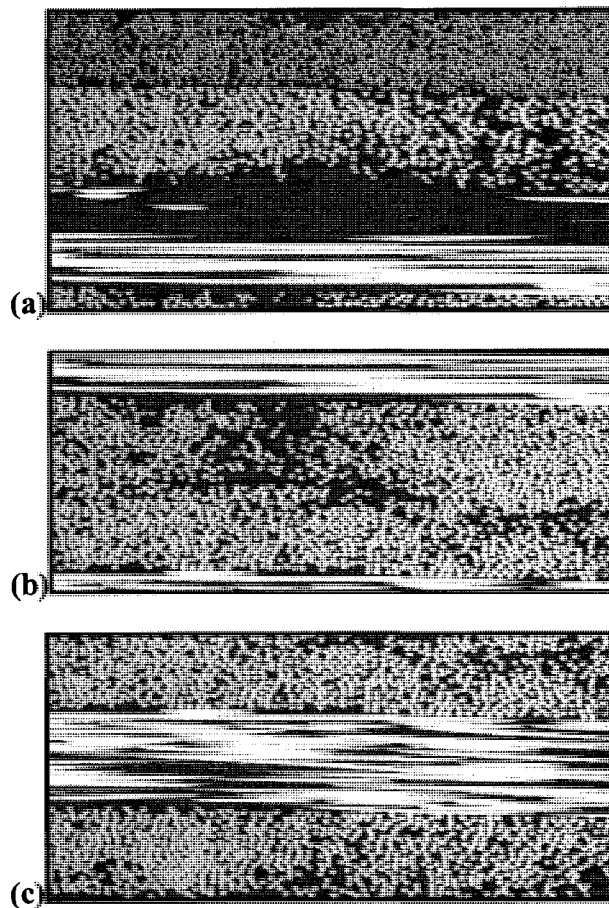


**Figure 3-7: Micrograph of [0/45/90/-45]<sub>s</sub> laminate in 0 direction.**

### **Effects of the mold geometry on the processing parameters**

In the compression molding technique, the geometry of the mold plays an important role in the processing parameters: temperature and pressure. For complex structures, thermal and stress analyses of the mold allow the designer to have an estimate of temperature and pressure distribution across the mold and assure that every corner of the structure falls within the processing window of the material. For the flat plates, however, the temperature distribution inside the mold, to a large extent, follows the temperature distribution on the heating platens of the compression molding machine. In fact, it is very desirable to have a very uniform temperature distribution on the platens to avoid distortion of the laminate after solidification; however, this requirement is hard to achieve. As such, a few degree temperature differences between the edges and the center of the mold are inevitable.

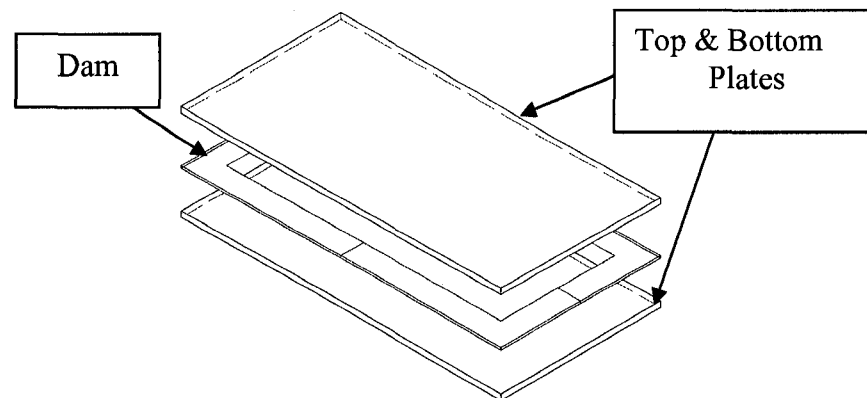


**Figure 3-8: A typical mold for compression molding**

Beside the effect on the temperature distribution, the geometry of the mold plays an important role on the applied processing pressure onto the laminate. Figure 3-8 illustrates a typical mold used in compression molding technique. The mold has three parts: top and bottom plates and a dam. The role of the plates is to apply a uniform pressure on the

laminates and distribute the temperature. The dam keeps the plies and the fibers in the place and prevents the resin from squeezing out the mold. The thickness of the dam is chosen based on the number of the layers in the laminate and the required final plate thickness. There is no exact formula to design the dam thickness based on the number of the layers but in general 20% to 25% reduction in the thickness of the laminate during debulking is considered. The initial thickness of the stack of the plies is more than the designed thickness of the laminate; however, as the pressure is applied and debulking occurs, the thickness reduces to the thickness of the dam.

Figure 3-9 illustrates that during debulking the applied pressure goes directly to the laminate. Nevertheless, when the top plate touches the dam surface, the applied pressure is distributed between the laminate and the dam proportional to their stiffness.

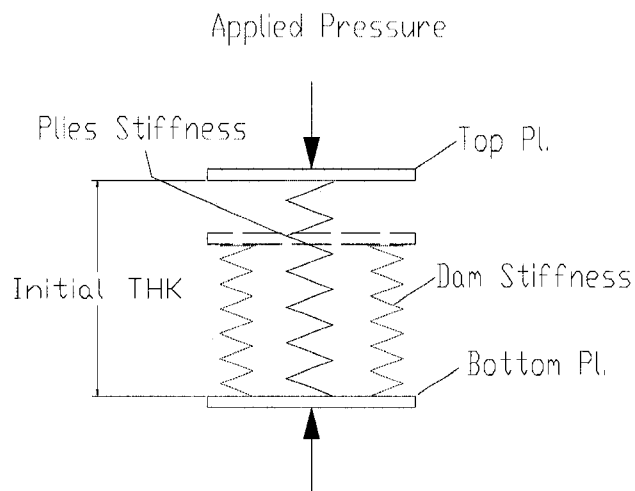


**Figure 3-9: Schematic debulking of a laminate inside a mold**

As such, using a mold like what is shown in Figure 3-8 would increase the required processing pressure. In contrast, a male-female mold like what is shown in Figure 1-15 guarantees that the applied pressure is totally applied on the laminate, so smaller compression molding machines can be used.

### 3-3 Mechanical Properties in the Fiber Direction, 0°

The mechanical properties of Carbon AS4/PEKK thermoplastic composites in zero and ninety degrees have been studied by a few researchers. The experiments were repeated in this research to verify the results and obtain skills for manufacturing and testing of angle plies laminates. Figure 3-10 shows the variation in the strength of different samples in the fiber direction. The maximum strength achieved was about 2400 MPa while a few samples showed less than 2000 MPa fracture strength. Due to the non-uniformity of the Carbon/PEKK prepreg some variation in the results was observed. While this has been observed by other researches as well, Hassan Salek (2005), it was decided to fabricate and test more samples, eliminate off results and focus on the samples with close-to-average properties.

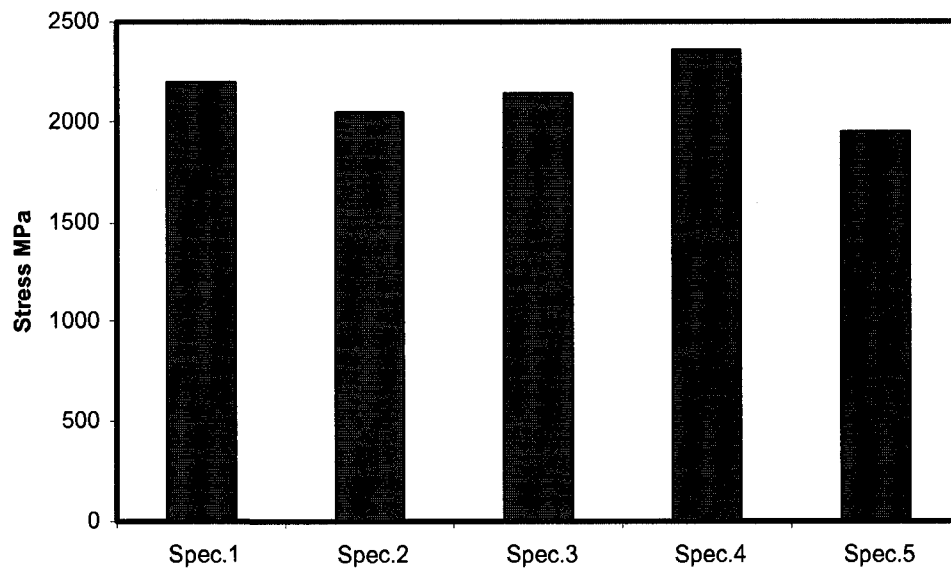


**Figure 3-10: Strength of Carbon AS4/PEKK 0° laminate**

Figure 3-11 shows the stress-strain curves for unidirectional specimens in the fiber direction. As expected, the behavior of the laminate is very brittle, and the fracture is

abrupt. The fracture strain of the laminate is less than 1.5%. Compared to other fibers such as glass fibers, carbon fiber has very low fracture strain, less than 2%, and its direct implication is the brittleness of carbon fiber composites even though they show high strength and stiffness. It can also be extracted from Figure 3-11 that the elastic modulus of the laminate in 0° direction is about 140GPa. Finally, it can be observed that all samples showed the same elastic stiffness, and in terms of stiffness no scatter was observed in the results.

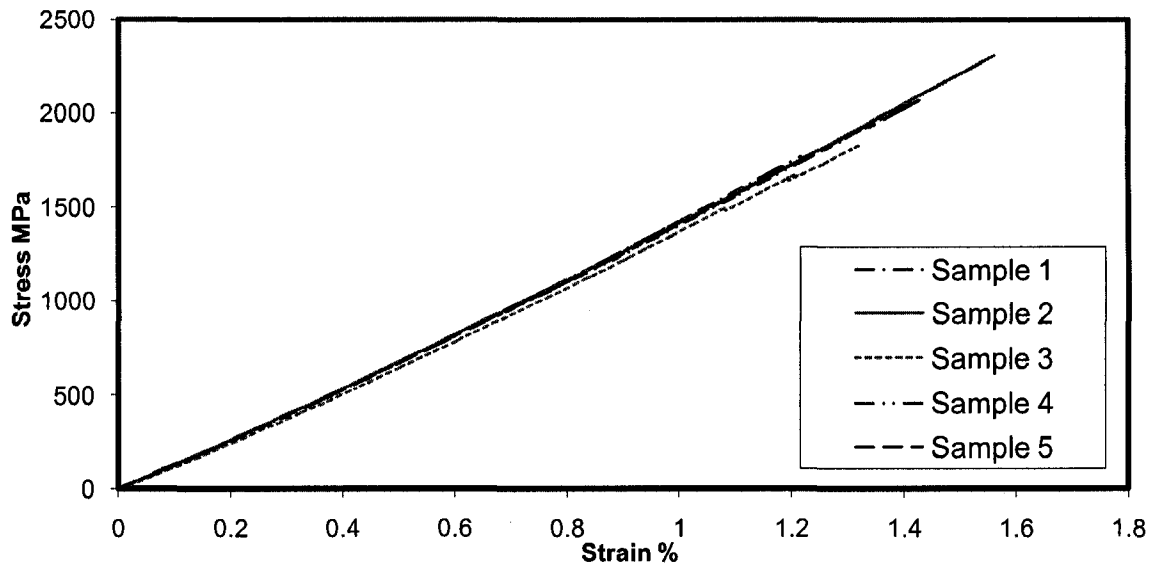


**Figure 3-11: Stress-strain curves of Carbon AS4/PEKK specimens in fiber direction**

### **Fracture modes**

Figure 3-12 shows a sample before tensile test and four samples after fracture. The cracks propagate extensively parallel and normal to the fibers. The whole fracture is too sudden to leave any chance to explain the progress of failure. However, it is conceivable that first

the cracks propagate parallel to fibers and split the specimen into a few narrower elements. At this point fibers are not capable of transferring loads to each other through the matrix, and fracture of the fibers normal to the fiber direction occurs. Nevertheless, it must be mentioned that not all the specimens experienced the same fracture style. Some samples fractured in a random fashion normal to the fiber direction.

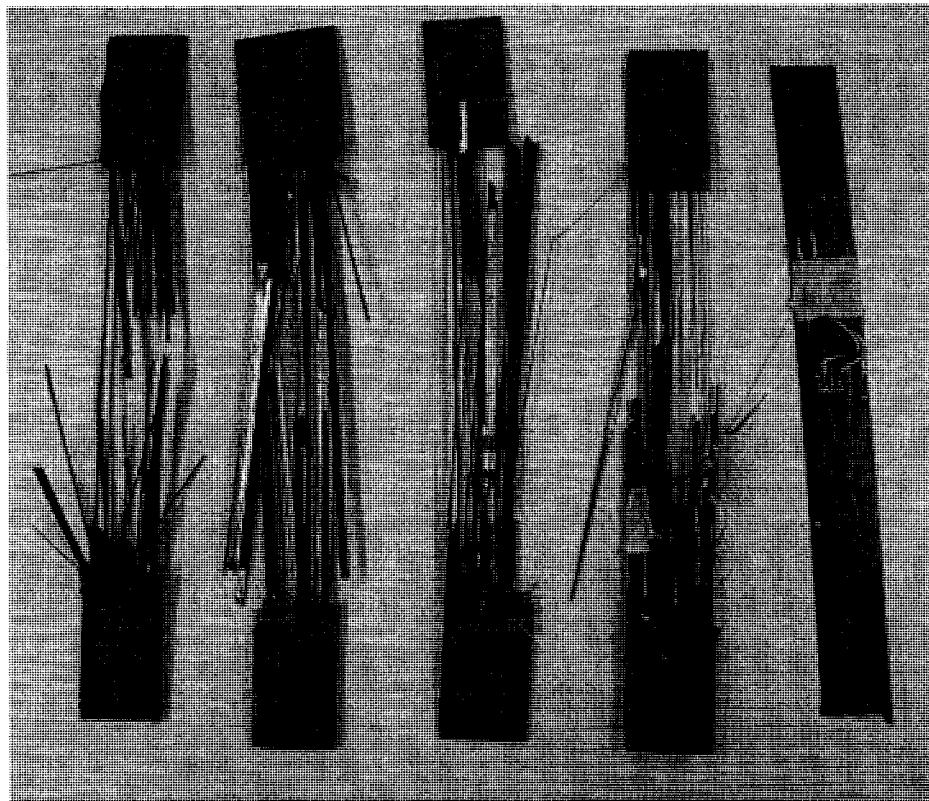


**Figure 3-12: Fractured samples of Carbon AS4/PEKK 0° laminate after tensile tests**

### **Poisson's Ratio**

The Poisson's ratio of the carbon AS4/PEKK composite laminate was measured for a few samples. It was observed that the Poisson's ratio has a value of 0.32 on average, and it is not constant while the laminate is stretched. Figure 3-13 shows the variations in the

Poisson's ratio versus strain. At higher strain values, Poisson's ratio descends to about 0.3, yet the value maybe considered fixed for many typical stress analysis application. For this research the average value of 0.32 was employed in the analyses.

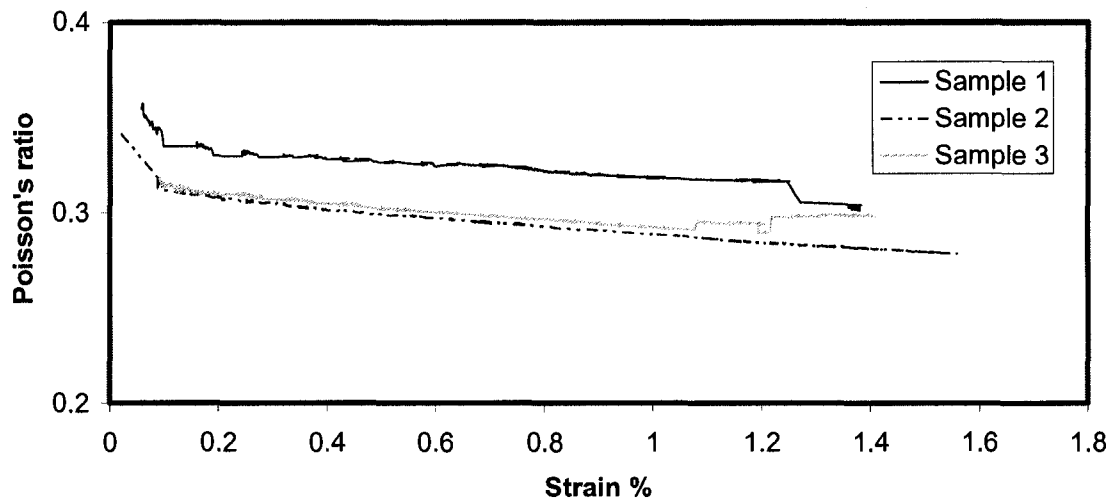


**Figure 3-13: The variation of Poisson's ratio by axial strain**

### **Micrographs**

Figure 3-14 shows the micrographs of unidirectional Carbon AS4/PEKK laminate in the fiber direction. The fiber volume fraction of this laminate is about 67% measured using color threshold technique. The picture shows a very high quality laminate, so it suggests that processing pressure and temperature were suitable. Moreover, no considerable amount of voids is observed.

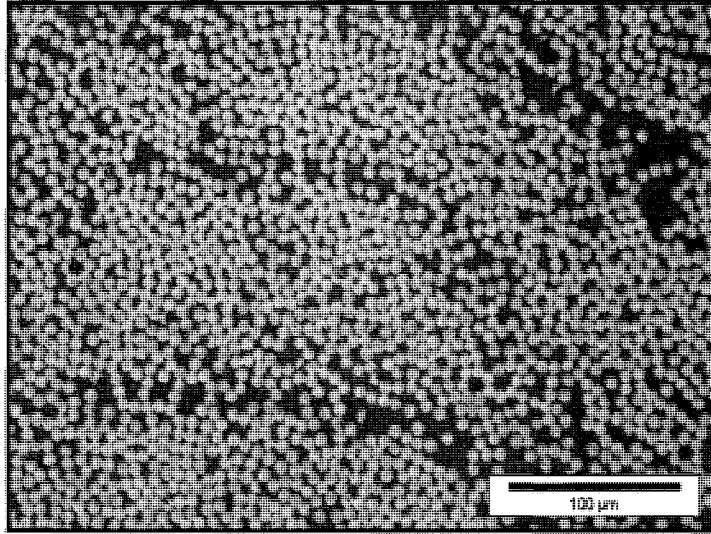
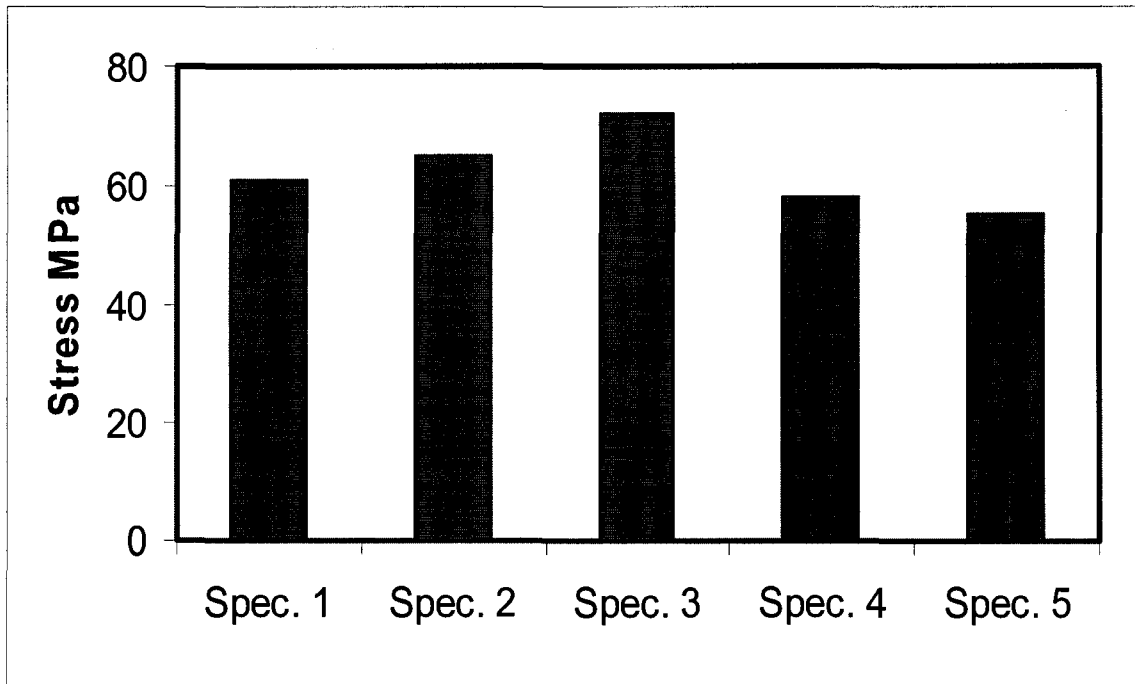


**Figure 3-14: Micrograph of Carbon AS4/PEKK in 0° Direction,  $V_f=67\%$ ,  $V_m=32\%$**

#### **3-4 Mechanical properties in the transverse direction, 90°**

According to the classical laminate theory, properties of a laminate in fiber and transverse directions are essential for stress analysis of the laminate. Following a similar procedure used to study the behavior of 0° laminates, the mechanical properties of Carbon AS4/PEKK laminate in the transverse direction were studied. The stacking sequence was 8 layers of 90° plies. The initial thickness of the plies before debulking was 1.2mm. The average final thickness of the laminate after solidification was 1.055mm. The results show that the average strength of the laminate is about 62 MPa, and the average modulus is about 8 GPa.

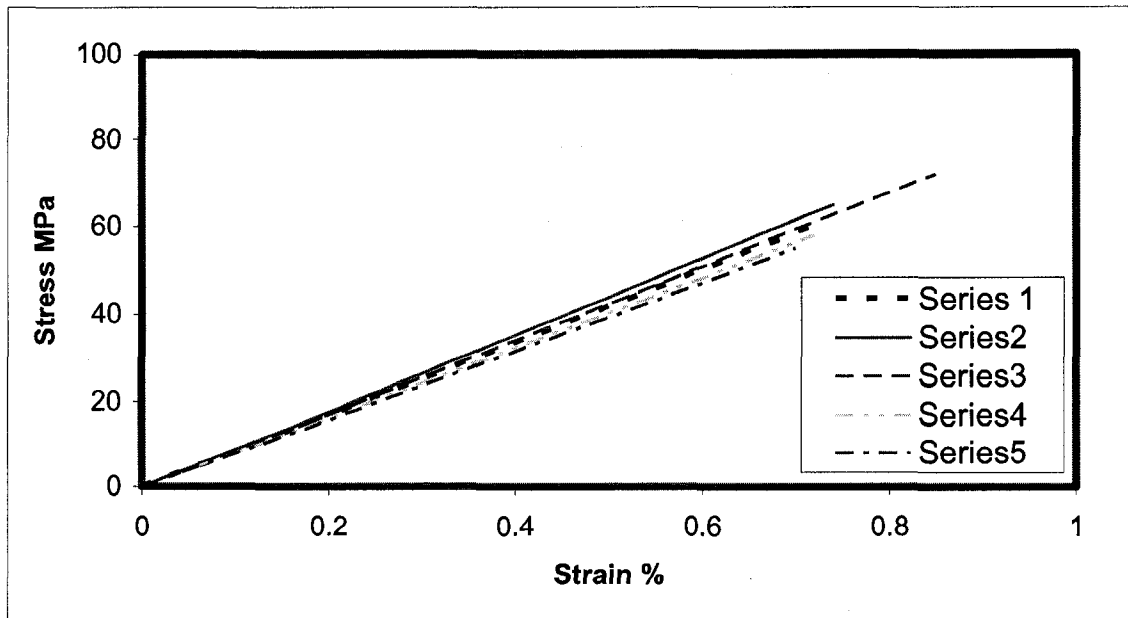
Figure 3-15 illustrates the variation in the tensile strengths of different samples cut from a Carbon AS4/PEKK laminate in the transverse direction. The reason for this variation may again lie in the non-homogeneity of prepreg. However, by fabricating more plates and testing more samples, it was possible to achieve reliable data for this laminate.



**Figure 3-15: Tensile Strength of Carbon AS4/PEKK laminate 90° directions.**

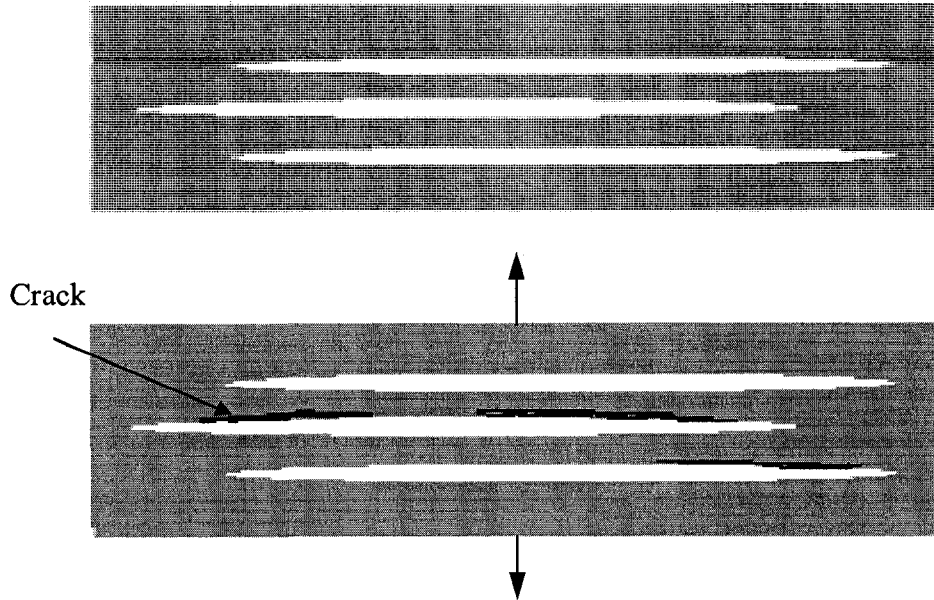
#### **Fracture modes**

Figure 3-16 shows the stress-strain curves for five different samples of Carbon AS4/PEKK laminate in the transverse direction. As can be seen, the fracture strain of all samples is less than 0.85%. A very low fracture strain in the transverse direction where the thermoplastic matrix is dominant is unexpected. In fact, thermoplastic polymers are known for their very high deformability, so it is reasonable to expect high fracture strain to be achieved while the laminate is loaded normal to the fiber direction. However, low fracture strain of 90° laminate can be explained by debonding of fiber and matrix at their interface.



**Figure 3-16: Tensile Strength of Carbon AS4/PEKK laminate in 90° direction.**

The mechanism of the load transfer in the composites between the matrix and the fibers is shear load transfer. The general rule of structure design is that connections joined by bolts, pivots, glues etc. must remain under shear loads during operation. In composites, the matrix acts as the glue to connect single fibers together, and the load is transferred from one fiber to the other through shear forces. So, it is not desirable to load the glued surface by normal forces. In contrary, when a laminate is loaded normal to fiber direction, the joint between the fibers and the matrix is completely under normal stress. It is obvious that the strength of the glued surface in normal to surface direction is not very high. As such, debonding occurs at the fiber-matrix interface. In other words, before the load is increased enough to deform the polymer plastically, the polymer is disconnected from the fibers, and cracks propagate in the laminate parallel to the fiber direction.



**Figure 3-17: Propagation of cracks parallel to the fiber direction and debonding**

Figure 3-17 schematically shows the debonding and gradual propagation of cracks in a laminate loaded in the transverse direction. At low level loads, the matrix and the fibers expand proportionally to their elastic stiffness so the laminate shows a small deformation. As the load increases, cracks initiate at the interface. At some point, the size of the crack is relatively large, so the area that bonds the fibers and matrix becomes small and incapable of resisting the load. A sudden fracture occurs at this time.

Figure 3-18 illustrates a few specimens of Carbon AS4/PEKK laminate composite after tensile tests. The fracture mechanism for all specimens was the same. As explained above, the fracture was due to the debonding of matrix and the fibers. While a crack initiates at some point, it weakens the point and propagates in the same area and most likely in the same line. For all samples tested, the fracture area was almost a straight line, and the fracture zone was very neat. However, as the samples were not in dog-bone shape so the fracture could occur at any point between the grips.

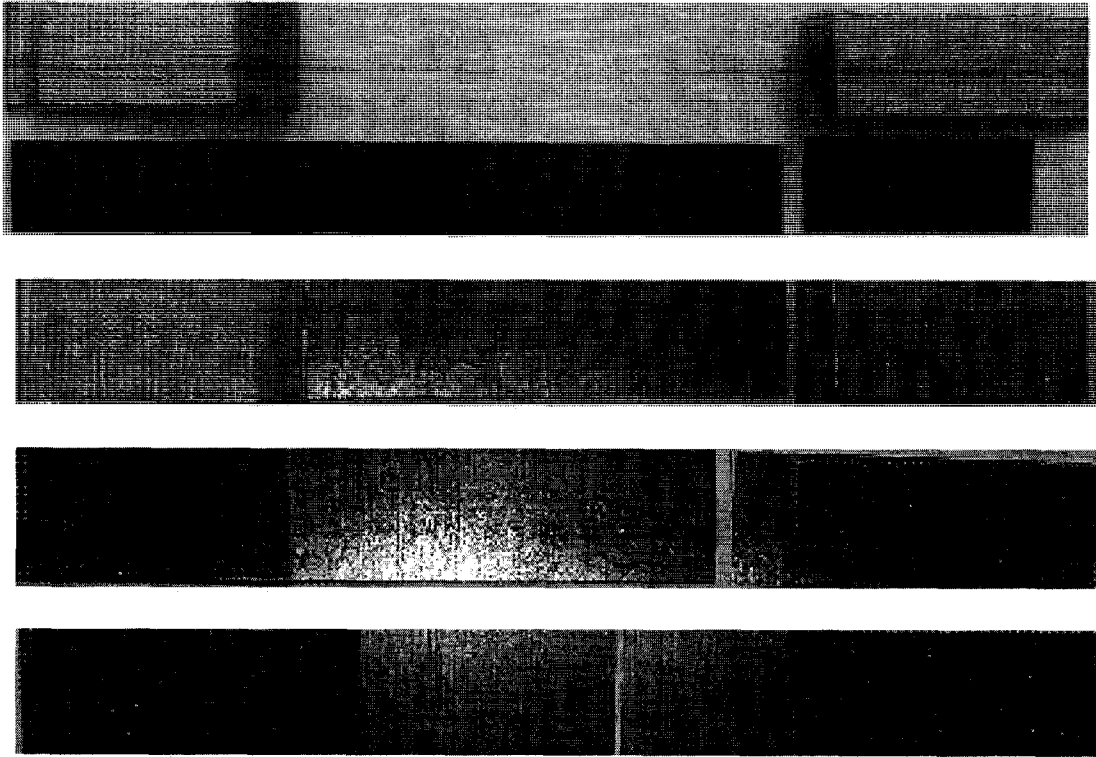


**Figure 3-18: Fracture of 90 degree Carbon AS4/PEKK laminate**

Even though it is expected that the fracture occurs between the grips, it was observed that some samples failed inside the grip. The tests were repeated for more than fifteen times to find a suitable procedure that avoids failure of the sample inside the grips. In the first test, the gripping pressure was 7 MPa. As shown in the Figure 3-18 the image on the top, the fracture occurred inside the gripping area. For the second test, the gripping pressure was reduced to 3 MPa, and it was observed that fracture occurred right outside the grips. For the rest of the tests, the gripping pressure was reduced to 2.5 MPa while all other parameters were kept the same. The fracture then occurred at the mid-span of the specimens. As such, it can be concluded that using emery cloth or sand coated wire mesh to cover the gripping areas (as tabs) and applying 2-3 MPa gripping pressure gives the best results. In all tests flat jigs were used.

## Micrographs

Figure 3-19 shows the micrographs of the 90° Carbon AS4/PEKK composite laminate in the fiber and normal-to-the-fiber directions. The volume fraction of the fiber is about 69%. It can be observed that fibers are uniformly distributed throughout the laminate. No considerable amount of voids is observed. Resin rich areas or dry fibers areas are also not seen. As such, it can be concluded that processing temperature, 340°C (650F), and processing pressure, 1000 KPa (150 psi), are suitable to process 90° laminates.

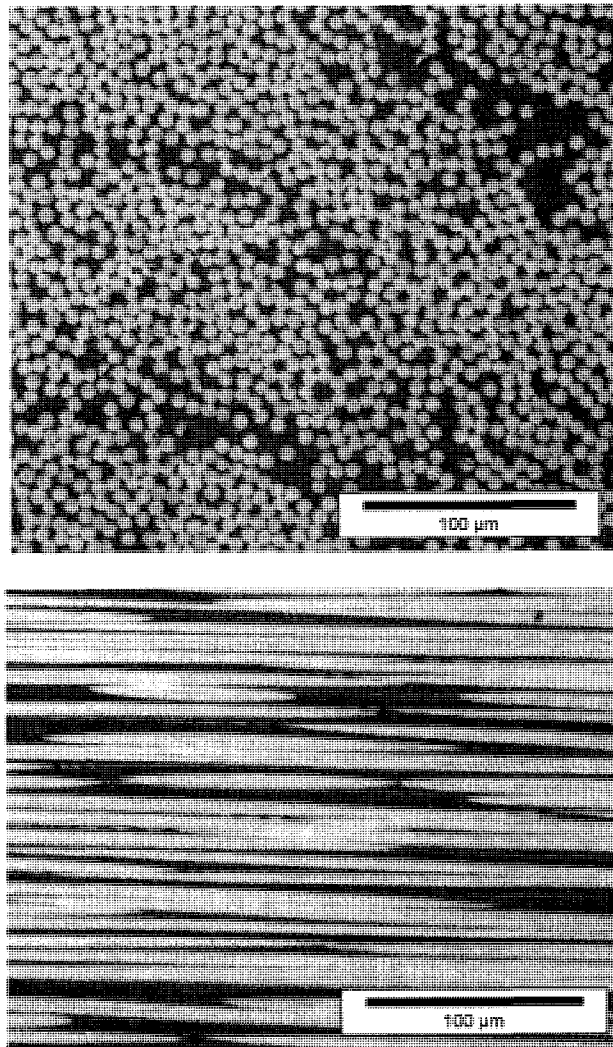


**Figure 3-19: Micrographs in the fiber and transverse directions  
 $V_f = 69\%$ ,  $V_m = 30\%$ , Magnification 200.**

### 3-5 Mechanical properties of quasi isotropic laminates

A laminate built of eight layers with a stacking sequence like  $[\pm 45/0/90]_s$  is called quasi isotropic. Recall from the classical laminate theory that the strains at the mid plane of the laminate are related to the resultant forces through matrix  $A$  as follows:

$$\begin{Bmatrix} N_x \\ N_y \\ N_z \end{Bmatrix} = \begin{bmatrix} A_{11} & A_{12} & A_{13} \\ A_{21} & A_{22} & A_{23} \\ A_{31} & A_{32} & A_{33} \end{bmatrix} \begin{Bmatrix} \varepsilon_x^0 \\ \varepsilon_y^0 \\ \gamma_{xx}^0 \end{Bmatrix}$$

$A$  is called the laminate stiffness matrix, and its terms are computed by integrating the reduced stiffnesses of the layers,  $\bar{Q}_{ij}$ , over the thickness of the laminate,  $H$ , by

$$A_{ij} = \int_{-\frac{H}{2}}^{\frac{H}{2}} \bar{Q}_{ij} dz$$

A very unique property of quasi isotropic laminates is that the components of  $A$  matrix remain constant if the laminate is rotated around an axis normal to the plane of the laminate. As a result, the mechanical properties of the laminate are independent of the angle of rotation. The term quasi, however, is used to distinguish the behavior of the laminate from that of the isotropic plates. For a quasi isotropic laminate, the effective shear modulus,  $\bar{G}_{xy}$ , is not related to the effective extensional modulus,  $\bar{E}_x$ , and effective Poisson's ratio,  $\bar{\nu}_{xy}$ , by the relation

$$\frac{\bar{E}_x}{2(1 + \bar{\nu}_{xy})}$$

as it is for a truly isotropic material. The value of  $\bar{G}_{xy}$  is numerically close to the value computed by this relation, however.

Due to the importance of quasi isotropic laminates and their wide application, the mechanical properties of this type of laminate were also studied in this research. It was also a matter of interest to see if inserting  $\pm 45^\circ$  layers into the laminate changes the brittle behavior of the flat plate laminates or not. As such, an eight-layer laminate with the lay-up  $[\pm 45/0/90]_s$  was manufactured. The total thickness of the plies before processing was 1.2mm while the average final thickness of the laminate was 1.06mm.

It was observed during several tests that the cooling rate- at least for the rates below  $7^\circ \text{C/Sec}$ - did not have a considerable effect on the mechanical properties of angle ply laminates, so the maximum available cooling rate,  $7^\circ \text{C/Sec}$ , was employed in the rest of experiments for this research. Figure 3-20 shows the processing temperature during melting, consolidation and solidification for manufacturing the quasi isotropic laminate.

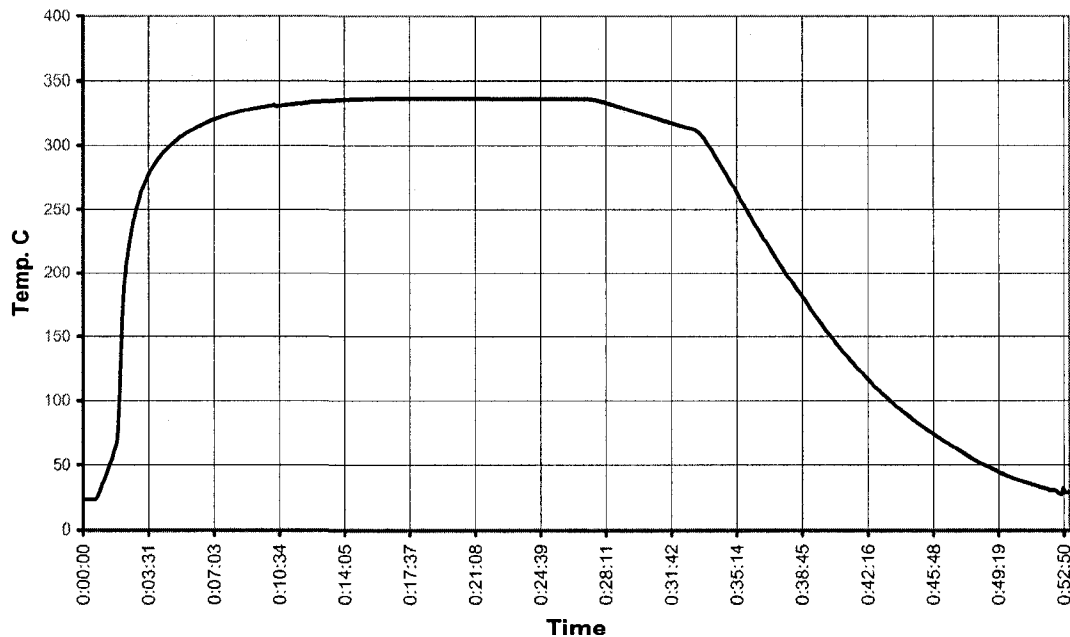


**Figure 3-20: Processing temperatures at different stages of the fabrication**

**Tensile test results**

Table 3-2 shows the data achieved by tensile tests of five quasi isotropic laminate specimens. The samples were all uniform dimension 250mm by 25mm (10" ×1"). The gripping length was 40mm (1.5") at each end. Instead of tabs, silicon carbide coated abrasive mesh was used to cover the specimens inside the jigs of the MTS machine. The average strength and elastic modulus of the laminate are 678MPa and 46GPa. The scatter of the data for the stiffness of the laminate was much less if compared with that of strength. The minimum and maximum tensile modules were 45GPa and 47GPa respectively.

Quasi-Iso	Breaking Force N	Fracture Stress MPa	Average Strength MPa	Tensile Modulus GPa
Spec. 1	17246	630	<b>678</b>	<b>45-47</b>
Spec. 2	17528	660		
Spec. 3	18800	700		
Spec. 4	19086	710		
Spec. 5	18300	690		

**Table 3-2: Tensile test results of carbon AS4/PEKK quasi isotropic laminate**

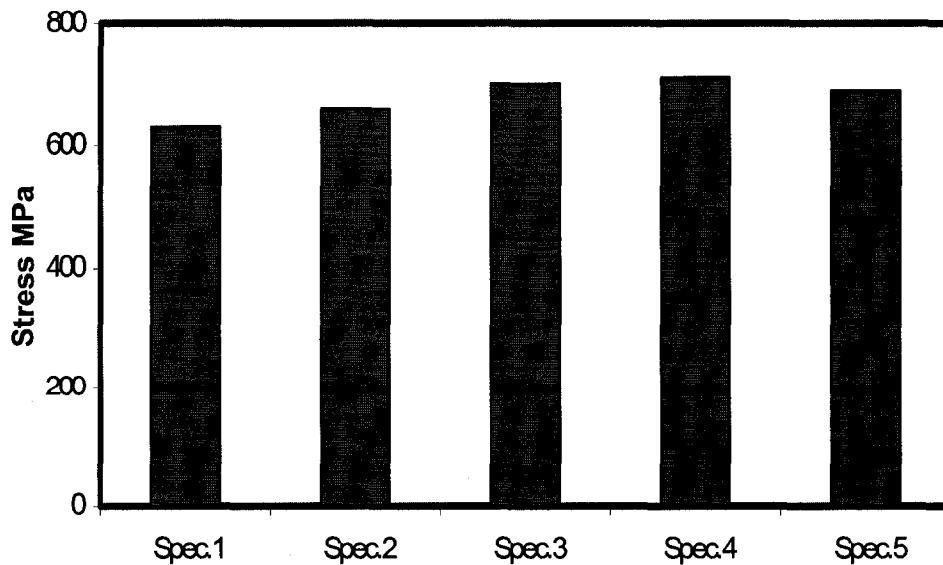


**Figure 3-21: Strength of carbon AS4/PEKK quasi isotropic laminates**

Figure 3-21 illustrates the bar chart presentation of the strength of carbon AS4/PEKK quasi isotropic laminate. As it can be seen, the variation in the data is about 7% that confirms the uniform quality of the laminate and repeatability of the tests. Figure 3-22 shows the fractured samples after tensile tests.

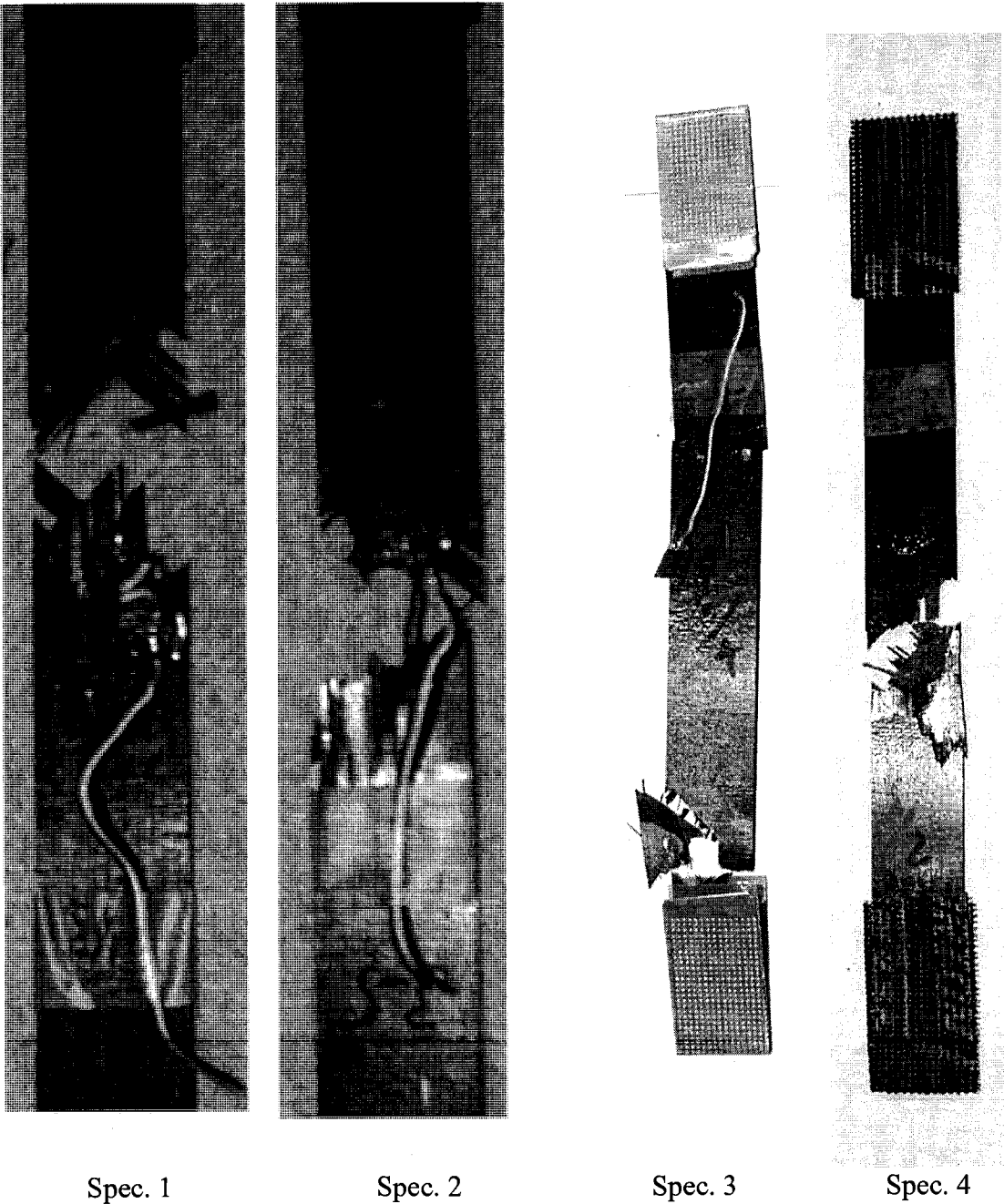


**Figure 3-22: Fractured samples of quasi isotropic laminate after tensile test.**

The fracture modes of  $[\pm 45/0/90]_s$  laminate is quite diverse, and no clear pattern was observed. Some samples broke in normal-to-the-force direction while the others broke at close to 45 degree angles. In contrast to  $90^\circ$  laminates, for quasi isotropic laminates the fracture occurred at multiple locations. However, the common behavior of all samples was the brittle and abrupt final fracture, Figure 3-23. No nonlinear or plastic deformation was observed. It can be concluded that including  $\pm 45^\circ$  layers into the lay-up of the laminate has no effect on changing the general mechanical behavior of the laminate; nevertheless, due to the lower strength and stiffness of the  $\pm 45^\circ$  layers, the strength and stiffness of the laminate is reduced as compared to unidirectional zero degree laminates.

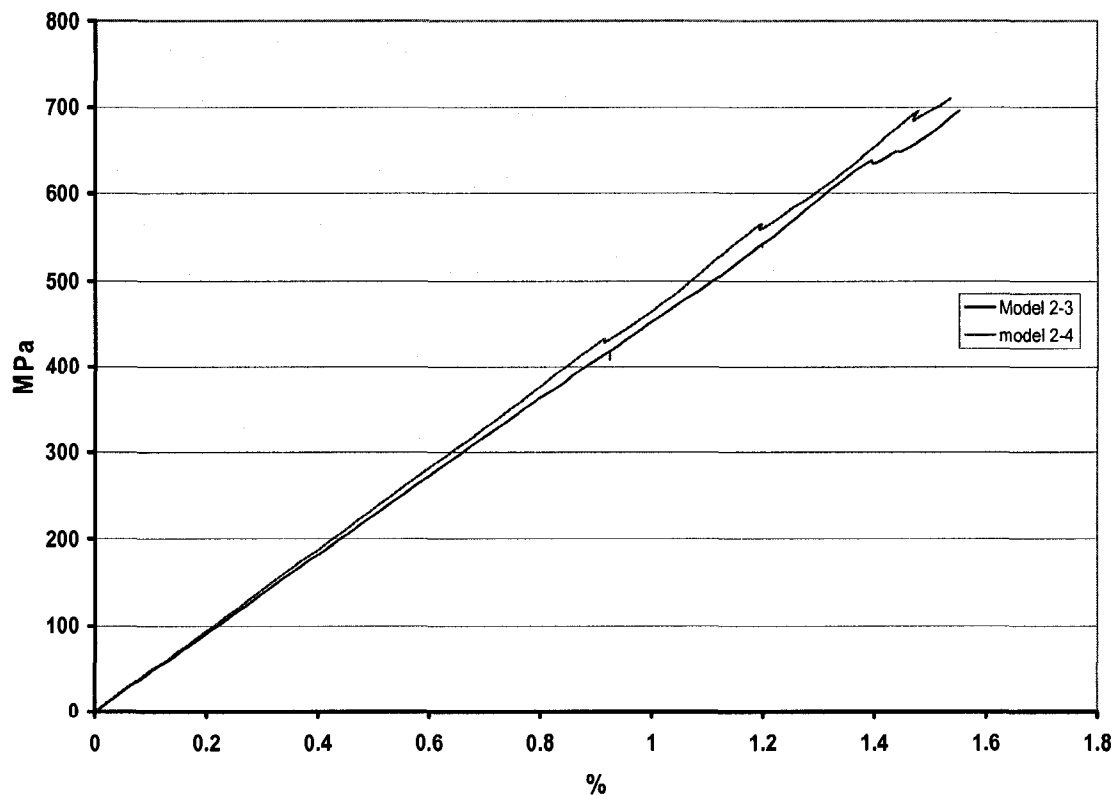
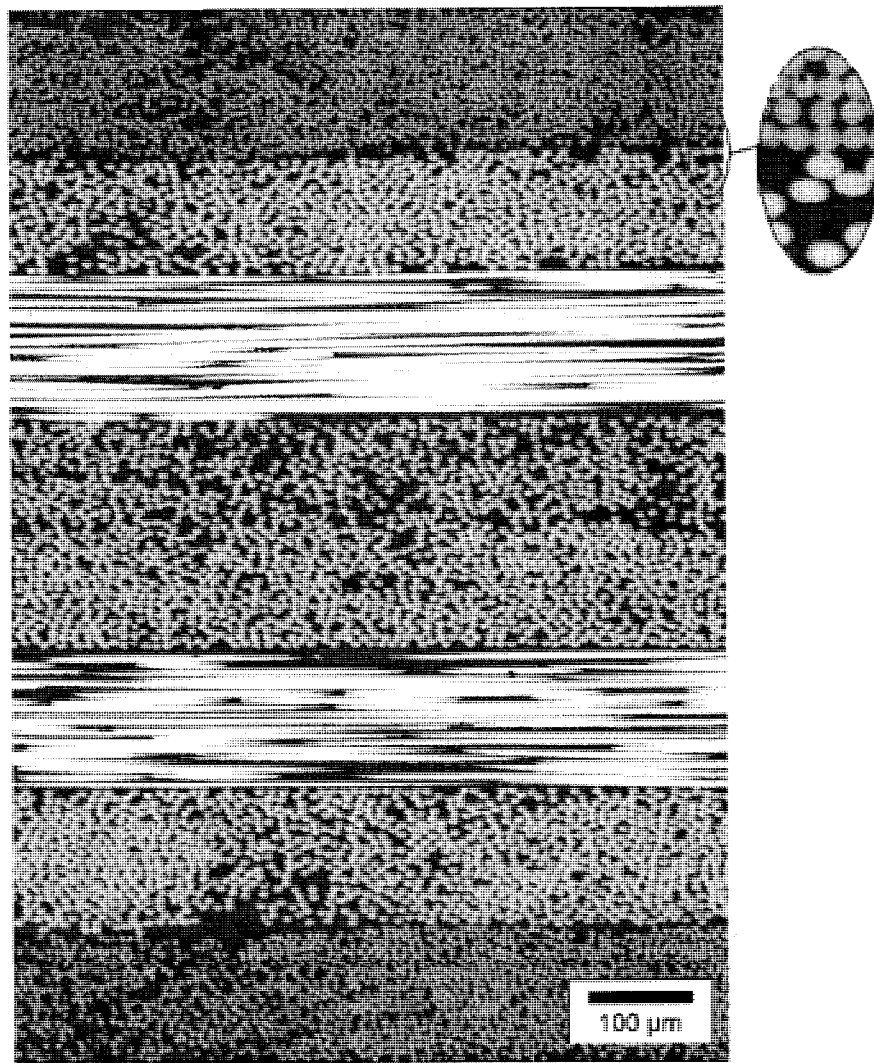


Figure 3-23: Stress-Strain curve of carbon AS4/PEKK quasi isotropic laminate

## Micrographs

Figure 3-24 shows a micrograph of  $[0/45/90/-45]_S$  laminate. The quality of the laminate confirms that the pressure and temperature employed for manufacturing were appropriate. The fiber volume fraction of the sample is 67%. The magnification of the graph is 100 times. A magnified cross section of the fibers has been shown in the right side of the picture. While circular cross sections represent fibers in zero direction, elliptical shapes show fibers oriented in 45 degree respect to the axis of the laminate.



**Figure 3-24: Micrograph of  $[0/45/90/-45]_S$  laminate in  $0^\circ$  direction**

**$V_f=67\%$ ,  $V_m=32\%$ ,  $X=100$**

### 3-6 Mechanical properties of $\pm 45^\circ$ laminates

The main goal of this research is to find a design, a technique or a procedure that introduces nonlinearity into the behavior of composite laminates. The concept then may be used to design a composite tube that is capable of large deformation and high energy absorption before its final failure. In this direction, quasi isotropic laminates were tested to see if some sort of nonlinearity was observed. The results of tensile tests, however, proved that when a laminate includes zero degree plies in its layup, the  $0^\circ$  layers are dominant in the load carrying capacity of the laminate, and when they exceed their strength, the rest of the layers, for example  $90^\circ$  and  $45^\circ$  plies, are not capable of redistributing the load among them due to the high rate of loading. In fact, the fracture of  $0^\circ$  layers is accompanied by the fracture of other layers that were not capable of absorbing the shock. Therefore, the laminate as a plate would show a very brittle and abrupt fracture.

Following the above observations, it was decided to remove  $0^\circ$  plies from the layup of the laminate and test a balanced laminate of  $[\pm 45^\circ]_{2s}$  and see if any nonlinearity can be achieved. As such, eight plies of Carbon AS4/PEKK prepreg were cut and laid up in  $\pm 45^\circ$  in a symmetric balanced fashion. The laminate was set into a MTS machine for tensile test. Figure 3-25 illustrates the stress strain curve for one of the specimens. The result was incredible and promising. The laminate showed more than 5% strain that was beyond the working limit of the strain gauge, so it was delaminated from the specimen at this point. This type of nonlinear behavior will be crucial in the design of deformable structures. The energy absorption and toughness of  $[\pm 45^\circ]_{2s}$  laminate proved to be 2-3 times of quasi isotropic laminates. For applications such as helicopter landing gear, where

shock and energy absorption during harsh landing has great importance, this behavior of  $[\pm 45^\circ]_{2s}$  laminate could be a very crucial design factor.

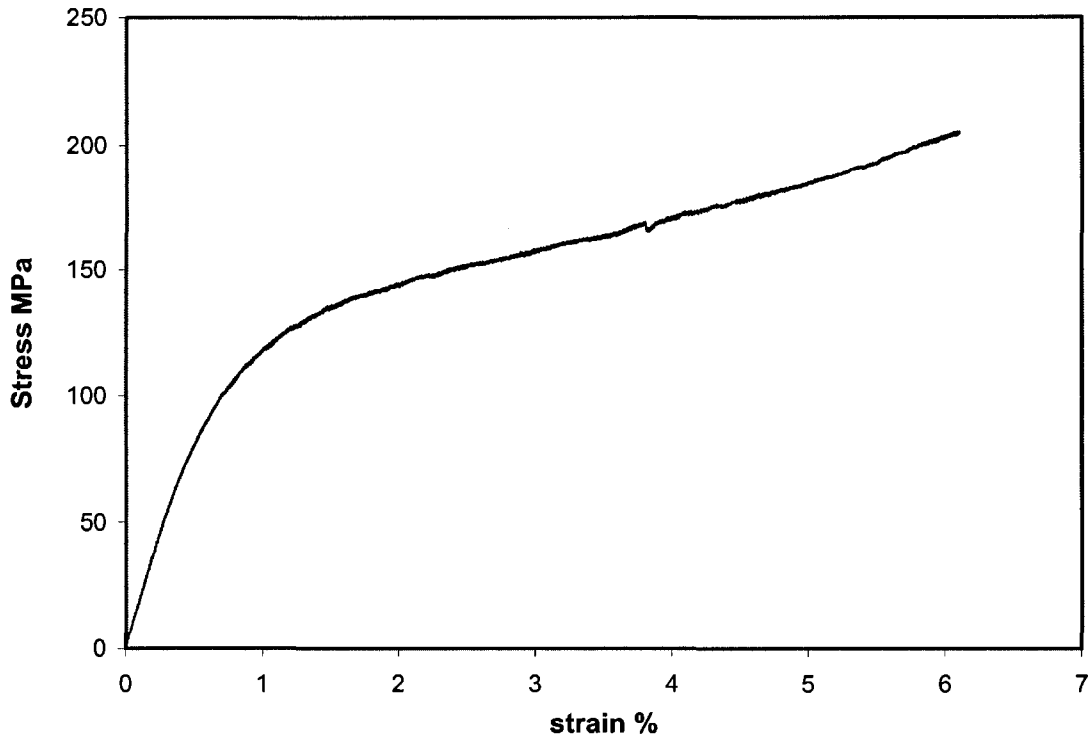


**Figure 3-25: Stress-Strain curve of carbon AS4/PEKK  $[\pm 45^\circ]_{2s}$  laminate**

Even though the strain gauge was delaminated at 5.5% for the first test, the sample continued to carry higher loads before final fracture. As such, it was decided to also use Laser Extension Device, LED, to measure the final fracture strain. Figure 3-26 shows the results of tensile tests for different samples. The graphs obtained by LED are shown by dotted lines to contrast the solid line graphs obtained by strain gauge measurement. For some samples, strain measured by LED exceeded 15%. For the same samples, however, the strain gauge could not measure the strain beyond 5.5%. Nevertheless, the load could be measured by the MTS machine. As such, the solid lines were extended beyond 5.5% strain with the same slope to match with the load level. This approximation was only

done to have an estimate of the final fracture strain of  $\pm 45^\circ$  laminates. Nevertheless, in this research the accuracy of the data below 5% is important, and it can be seen that below this limit both strain gauges and LED measured the same data strain.

The mechanism of large deformation for carbon AS4/PEKK  $[\pm 45^\circ]_{2s}$  laminate is quite complex and different parameters are involved. The observations during the tests and the physical inspection of the samples after the tests are the basis of the following explanations.

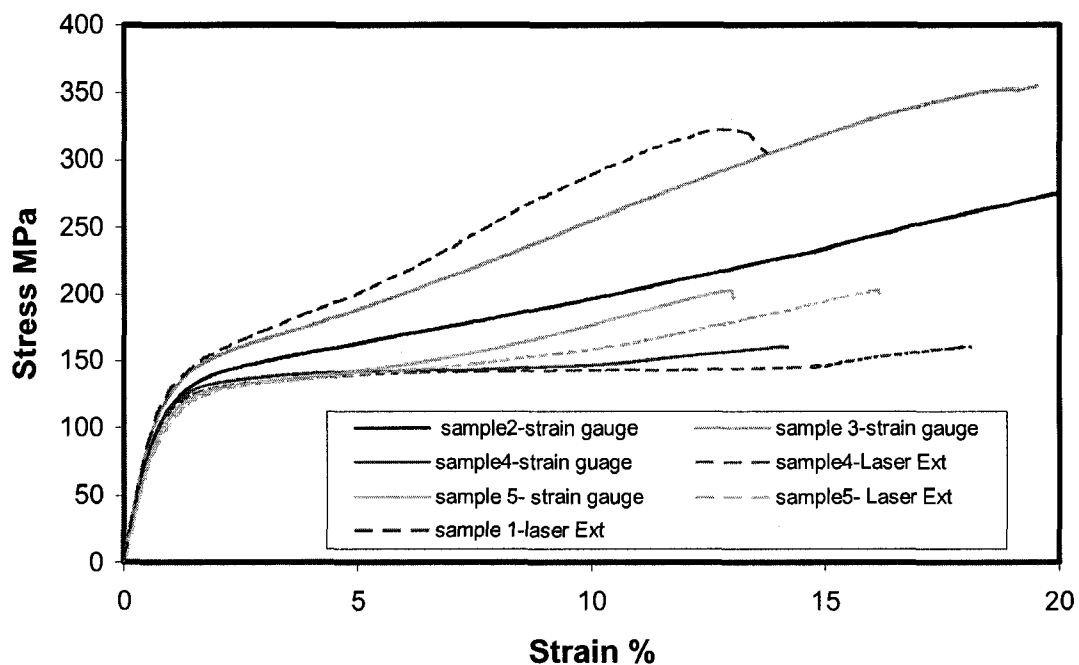


**Figure 3-26: Stress-Strain curve of carbon AS4/PEKK  $[\pm 45^\circ]_{2s}$  laminate**

First, during the tests, no strong sound, which is usually an indicator of large energy release associated with crack propagation, was heard. Not producing a considerable sound during the tests indicates that the fracture of the laminate deviates from the usual abrupt fracture of composites. Second, in the case of  $[\pm 45^\circ]_{2s}$  laminates, these are the shear forces that are dominant, and unlike 90 degree laminates, debonding of the fibers

and matrix does not occur. Also in contrast to unidirectional zero degree laminates, fibers are not dominant in the behavior of  $[\pm 45^\circ]_{2s}$  laminates, so large deformation can be expected.

On the other hand, when the tensile load is transformed to shear loads, fibers are allowed to rotate in the laminate plane while they are stretched or compressed. Rotation of the fibers always occurs toward the load axis, and ultimately if fracture does not occur, fibers will be aligned with the load direction. The consequence of fiber rotation is the large deformation of the specimen. Moreover, as the fibers get aligned in the load direction, the strength of the specimen increases. Similar to the stress hardening phenomenon in metals, the strength of the samples increased at higher strain level, Figure 3-25.

Figure 3-27 shows a carbon AS4/PEKK  $[\pm 45^\circ]_{2s}$  laminate specimen after tensile test. The deformation of the sample was excessive. In some parts of the specimen a behavior similar to necking for ductile metals occurred and the width of the specimen started to narrow locally. As shown below, for some cases the outer layers started to delaminate, and the sample showed some degree of distortion.

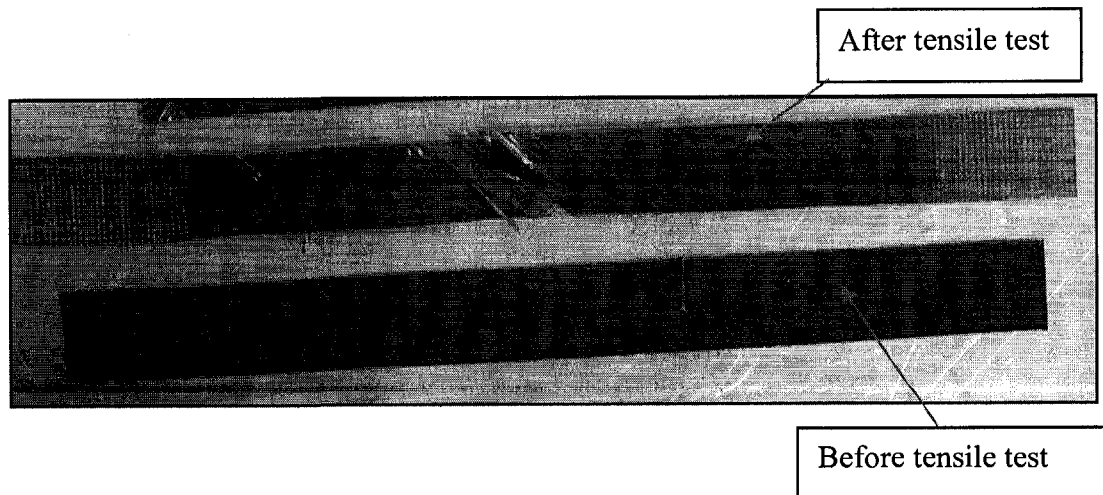


**Figure 3-27: A carbon AS4/PEKK  $[\pm 45^\circ]_{2s}$  laminate specimen after tensile test**

The behavior of  $[\pm 45^\circ]_{2s}$  laminates sheds light into the design of a composite tube with large deformability. Both mechanisms of shear deformation of the matrix and rotation of the fibers must be considered in the design. As such, the behavior of  $[\pm 30^\circ]_{2s}$  and  $[\pm 25^\circ]_{2s}$  laminates will also be studied to find out the similarities and differences of these laminate.

### **3-7 Mechanical properties of $\pm 30^\circ$ laminates**

Mechanical behavior of  $[\pm 45^\circ]_{2s}$  laminates raised hope for designing ductile composite structures; however, the laminate showed very low stiffness and strength in average: 18GPa and 220MPa respectively. If compared with the Young's modulus of aluminum alloys, 72GPa, the stiffness of this laminate is one forth. The density of Carbon PEKK composite, however, is half of that of aluminum. As such, a  $[\pm 45^\circ]_{2s}$  laminate shall have 4 times cross section of an aluminum plate and consequently twice in weight to show the same stiffness. Yet, the strength is much less than that of high grade aluminum alloys.

As such, lower angle ply laminates that show higher strength and stiffness is sought even though they show lower fracture strain than  $\pm 45^\circ$  laminates. From what has been observed so far, it can be concluded that the lower angle ply laminates are more brittle yet stronger as the fibers are more dominant. The maximum ductility is expected to be observed for  $[\pm 45^\circ]$  laminates where shear deformation is enormous. Nevertheless, at least theoretically,  $[\pm 30^\circ]$  Carbon AS4/PEKK laminate is the closest angle ply laminate to  $[\pm 45^\circ]$  laminates that may show higher strength than Aluminum 7075-T6, which is an aerospace grade alloy. Yet, the stiffness of this laminate is not expected to exceed 55GPa, which is still lower than the elastic modulus of aluminum alloys.

Eight layers of  $\pm 30^\circ$  Carbon AS4/PEKK prepreg were stacked up in  $[\pm 30^\circ]_{2s}$  lay-up to manufacture a few composite plates by compression molding technique. The mechanical behavior of the laminates in tension was examined by conducting tensile tests using an MTS machine and according to ASTM 3039 standard. For angle ply laminates, the standard width of the specimens is 25mm (1"), and the length is at least 250mm (10") including 40mm (1.5") at each end for gripping purposes. Figure 3-28 illustrates the strength of carbon AS4/PEKK  $[\pm 30^\circ]_{2s}$  laminates for a few samples. More than ten different samples were tested for this laminate. The variation in strength observed to be between 600 to 1000 MPa. However, most of the specimens showed strength close to the average 750 MPa strength.

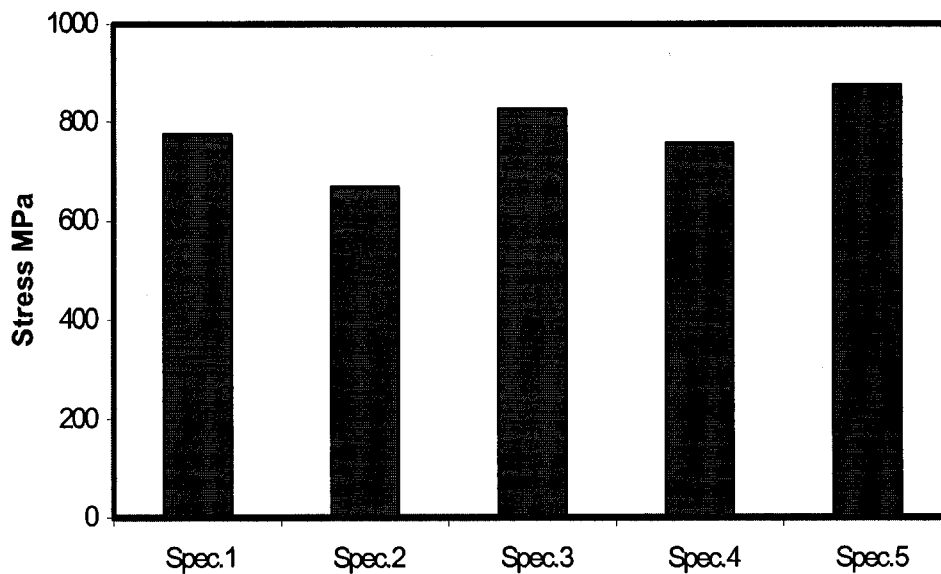


**Figure 3-28: Strength of Carbon AS4/PEKK  $[\pm 30^\circ]_{2s}$  laminates**

Figure 3-29 shows the stress strain curves for different specimens of  $[\pm 30^\circ]_{2s}$  laminates. The stiffness of the samples showed more variation than  $0^\circ$ ,  $90^\circ$ , quasi isotropic and

$[\pm 45^\circ]_{2s}$  laminates. However, the average stiffness of the laminate is around 52 MPa, which agrees with theoretical prediction. The laminate showed less nonlinear deformation in comparison with  $[\pm 45^\circ]_{2s}$  laminates; however, an average fracture strain 2.7% shown by  $[\pm 30^\circ]_{2s}$  laminate is still very promising. It must be considered that carbon fibers are more brittle than many other fibers including glass fibers, which show 3-4% strain to failure. As such, it is very difficult to see ductility and nonlinearity in carbon based composites.

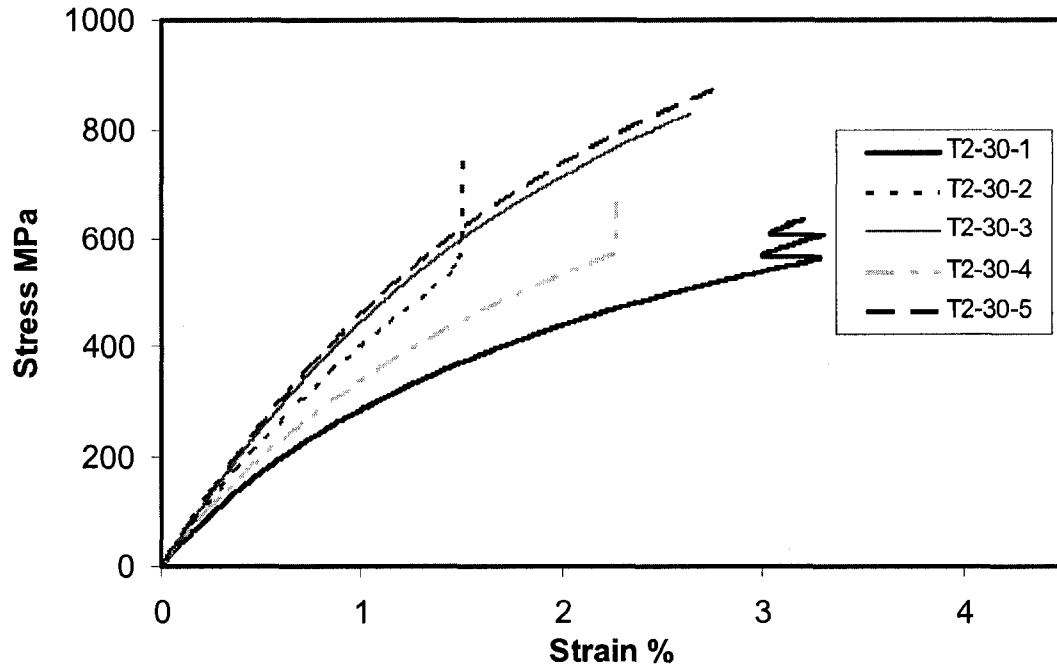


**Figure 3-29: Stress-strain curves of Carbon AS4/PEKK  $[\pm 30^\circ]_{2s}$  specimens**

Figure 3-30 illustrates the Carbon/PEKK  $[\pm 30^\circ]_{2s}$  specimens after tensile tests. The fracture modes of laminates are diverse. Most of the fracture lines are almost parallel to either plus or minus  $30^\circ$ , which is parallel to the fibers. However, there are a few

exceptions that fracture zones are normal to loading direction. The fracture of the laminate, in general, can be considered brittle and abrupt. At the onset of the fracture a huge noise of crack propagation is heard, and then the fracture occurred abruptly. For  $[\pm 30^\circ]_{2s}$  laminates, strength of the fibers was the controlling parameter for fracture. Debonding of the fibers and matrix did not seem to be an important parameter here, and the matrix moderately expanded.

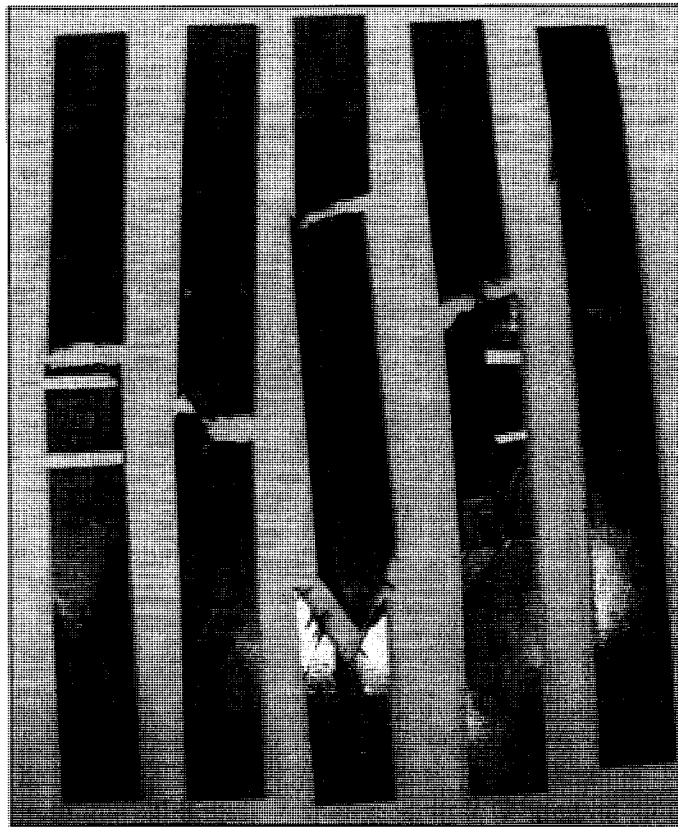


**Figure 3-30: Fracture of Carbon AS4/PEKK  $[\pm 30^\circ]_{2s}$  specimens after tensile test**

One of the most important elements of large deformation of  $[\pm 45^\circ]_{2s}$  laminates was rotation of the fibers. Figure 3-31 shows how this parameter was measured. Before conducting the test, a line was drawn parallel to the fibers at  $30^\circ$  angle. After the test, the

angle of the line was measured again. It was observed that the fibers rotate about 3 to 4 degrees, depending on the fracture strain of the sample.

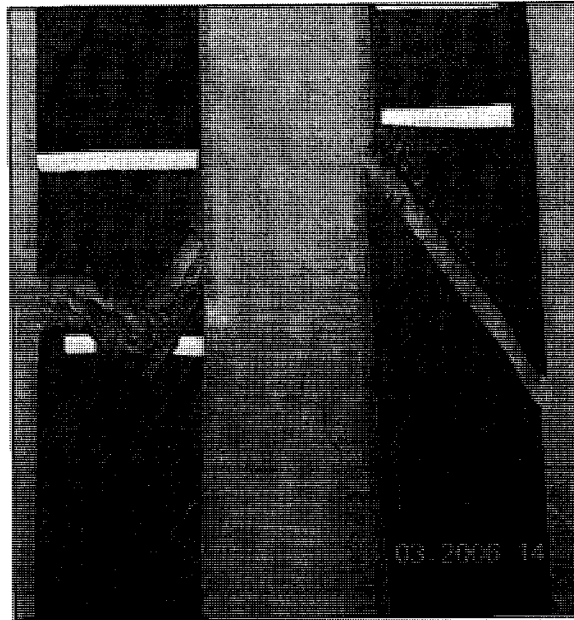


**Figure 3-31: Measuring the rotation of the fibers during the tensile test**

Rotation of the fibers definitely played an important role in achieving 2.7% strain. However, the fibers for this laminate do not have as much chance for rotation. In fact, the low shear strength restricts the potential of the laminate for deformation. Tsai-Hill criteria were used to find out which stresses have higher contribution to failure of the laminate. Accordingly, the fracture is mostly due to the interaction of shear stresses in 1-2 direction and compression stresses in 2-2 direction. While the tensile stresses in 1-1 direction has a minimal effect on the fracture, no important role shall be considered for tensile stresses in 2-2 direction and compression stresses in 1-1 direction. As such, it is obvious that the shear strength limits the shear deformation of the laminate. Consequently, the rotation of the fibers and fracture strain of the laminate is limited to lower values in comparison to those of  $[\pm 45^\circ]_{2s}$  laminates.

### 3-8 Mechanical behavior of $[30^\circ/\text{Resin}/-30^\circ/\text{Resin}]_{2s}$

Achieving the strength and stiffness does not seem to be a real challenge for composites; however, high deformation and high fracture strain is always a challenge. This experiment was set to observe if the isolation of the layers from each other by inserting a layer of ductile resin between each adjacent plus/minus layers helps to increase deformability or not.

Four layers of  $\pm 30^\circ$  prepreg and four layers of pure PEKK film were laid up in  $[30^\circ/\text{Resin}/-30^\circ/\text{Resin}]_{2s}$  sequence. PEKK film is a pure thermoplastic polymer and can show very high ductility, so it was expected that low stiffness low strength PEKK film may not confine the deformation of high strength high stiffness carbon /PEKK plies.

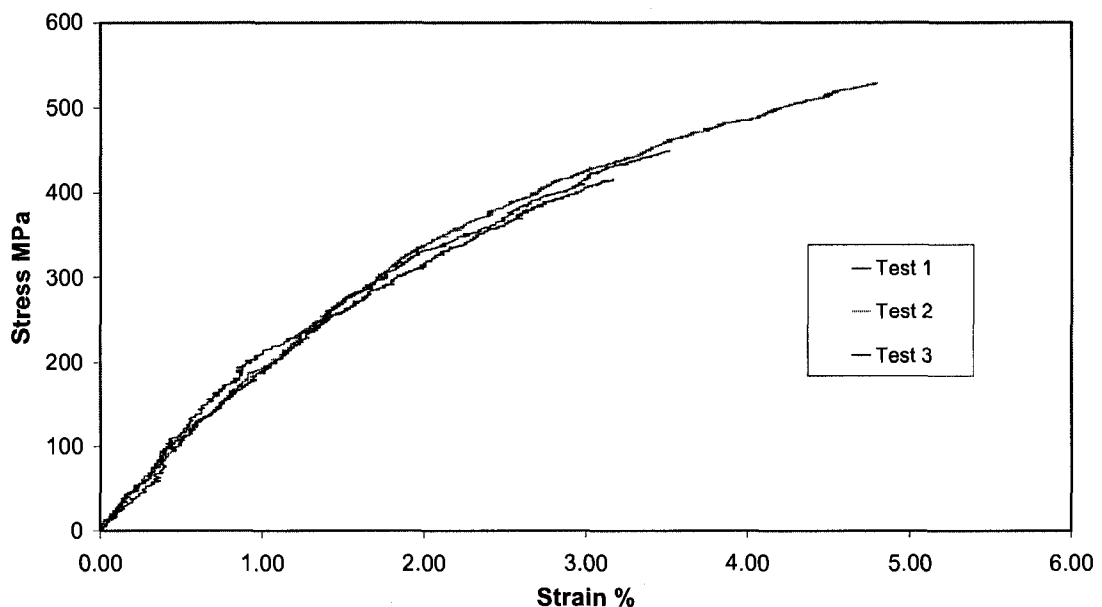


**Figure 3-32: Stress- strain curves for Carbon/PEKK  $[30^\circ/\text{Resin}/-30^\circ/\text{Resin}]_{2s}$  laminate**

Figure 3-32 shows the stress-strain curve for such a laminate. The test results show that the deformation and strain to failure of the laminate increased considerably. At least for

one specimen 5% strain was observed. The rest of the samples showed about 3 to 4 percent fracture strain. The average strength of the laminate is about 450 MPa while the average stiffness is about 25 GPa.

As shown in Figure 3-33, the fracture modes of the samples were not very different from those of  $\pm 30^\circ$  laminates. The lower strength and stiffness of the laminate were also quite predictable. Nevertheless, the goal of this test was only to find a way for increasing the ductility of the laminate. As a result of these tests, it can be claimed that removing restrictions on the plies movement will consequently help to provide high deformation and high fracture strain. When two stiff layers are adjacent, they confine the movements of each other. However, when a low stiffness polymer film isolates the layers, they have a better chance for fiber rotation and longitudinal deformation. This mechanism may not be directly applicable to the design of a composite tube because the strength and stiffness of the tube will be reduced considerably. However, the phenomenon explains why at least different blocks of layers must be somehow isolated from each other. As it will be explained in the next chapter, employing  $90^\circ$  layers at some strategic locations across the cross section of the tube will have the same effect as polymer film while increasing the circumferential strength and stiffness of the tube also.

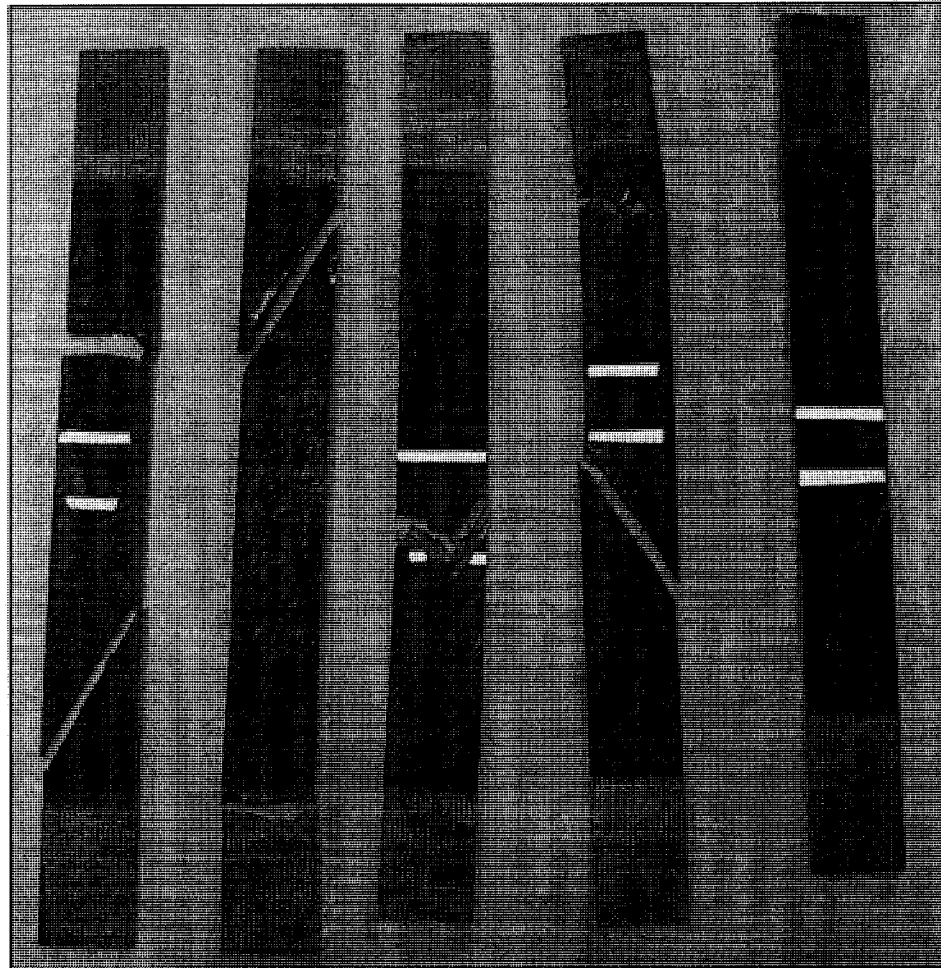


**Figure 3-33: Fracture of carbon AS4/PEKK [30°/Resin/-30°/Resin]<sub>2s</sub> specimens by tensile tests.**

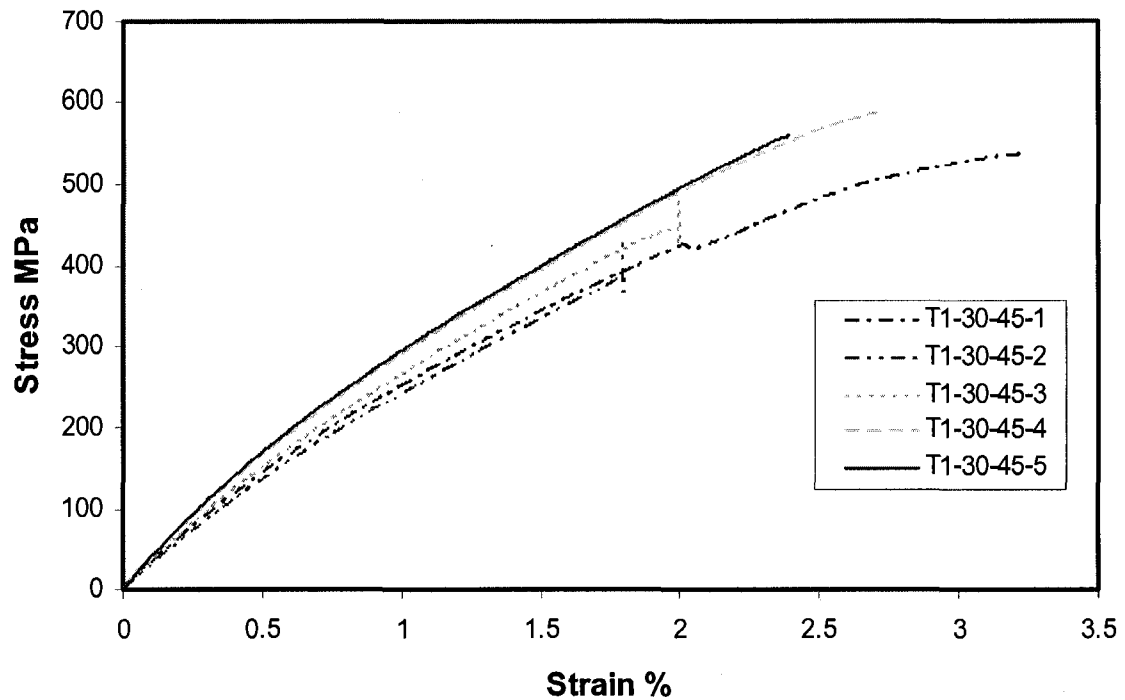
### 3-9 Mechanical behavior of $[\pm 30^\circ/\pm 45^\circ]_s$

After testing  $\pm 30^\circ$  and  $\pm 45^\circ$  laminates, it would be of interest to know how the combination of two laminates behaves. Specifically, an attempt was made to find if beyond 2.7% strain, which is the fracture strain of  $\pm 30^\circ$  laminates, the specimen was capable of carrying some loads even at lower levels or if final fracture would occur. As such, an eight-layer plate with the  $[\pm 30^\circ/\pm 45^\circ]_s$  layup was built. The  $\pm 45^\circ$  plies were set as the inner layers and  $\pm 30^\circ$  plies as the outer layers or skins. The challenge was to see if after fracture of  $\pm 30^\circ$  layers, the inner layer or the core of the sample was capable of redistributing the load.

Figure 3-34 shows the stress-strain curves for five specimens of this laminate. According to CLT such laminate should have the strength and stiffness of 570 MPa and 32GPa respectively. The test results showed that the average strength of the laminate is about 520 MPa. The specimens, however, showed more consistent behavior to  $\pm 30^\circ$  laminates in terms of stiffness. Most specimens showed the elastic modulus about 36GPa that is close to theoretical prediction.

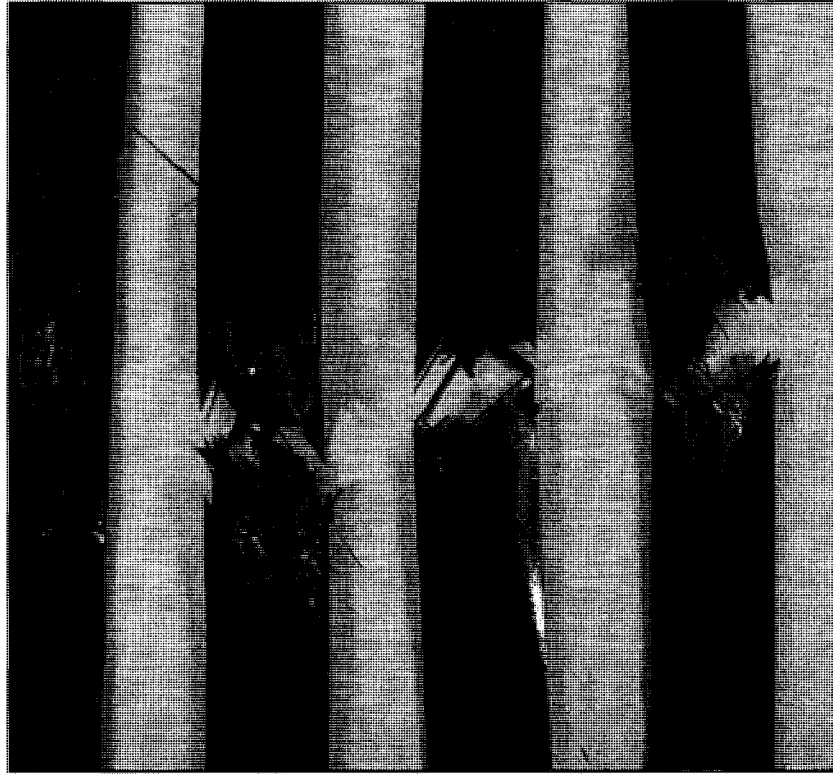
On the other hand, the fracture strain of the laminate did not show considerable improvement in comparison to that of  $\pm 30^\circ$  laminates. In fact, including  $\pm 45^\circ$  plies into the stack of the laminate did not prevent the abrupt fracture of the laminate. When  $\pm 30^\circ$  plies failed, the rest of the layers,  $\pm 45^\circ$  plies, were not capable of resisting the load carried by  $\pm 30^\circ$  plies and failed quickly. This behavior, which may be called “Domino Effect”, was also observed in quasi isotropic laminates. Recall that for quasi isotropic laminates when zero degree layers failed, the rest of the layers were not capable of carrying the load, and the brittle fracture of the laminate was inevitable. This observation

is highly important in the design of composite structures. At this point, it can be claimed that including high angle plies like  $\pm 45^\circ$  does not improve the ductility of the combined laminate.



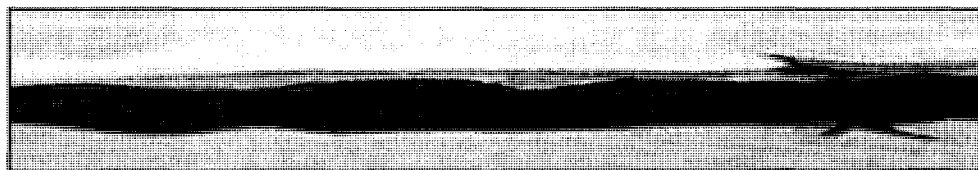
**Figure 3-34: Stress-strain curves of carbon AS4/PEKK  $[\pm 30^\circ/\pm 45^\circ]_s$  specimens**

Figure 3-35 shows a few carbon AS4/PEKK  $[\pm 30^\circ/\pm 45^\circ]_s$  samples after the tensile test. There is no clear pattern in the fracture modes, and the failure was random. The fracture was sudden, and there was not enough time to observe the process of failure. However, again the Tsai-Hill criteria were used to find out which stresses have higher contribution to failure of the laminate. The failure would start in the  $\pm 30^\circ$  plies mostly due to the tensile stresses in the 1-1 direction and compression stresses in the 2-2 direction. While the fracture would occur in the  $\pm 30^\circ$  plies, the  $\pm 45^\circ$  plies would fail mostly due to shear stresses in the 1-2 direction.



**Figure 3-35: Fracture of carbon AS4/PEKK  $[\pm 30^\circ/\pm 45^\circ]_s$  specimens by tensile tests.**

The only interesting phenomenon observed in the fracture of  $[\pm 30^\circ/\pm 45^\circ]_s$  was the delamination of  $\pm 30^\circ$  and  $\pm 45^\circ$  layers before final failure. Figure 3-36 shows a large delaminated area during the tensile test of the specimen. The reason for delamination might be the large Poisson's ratio difference of two layers. For  $\pm 30^\circ$  laminate,  $\nu_{yx}$  is equal to 0.325 while for  $\pm 45^\circ$  layers, it is equal to 0.816. The width of the laminate for a specimen is only 25mm, so the delamination started from the free edges and extended through the whole width.



**Figure 3-36 Delamination areas between the  $\pm 30^\circ$  and  $\pm 45^\circ$  layers.**

### **3-10 Mechanical properties of $\pm 25^\circ$ laminates**

In terms of strength,  $\pm 30^\circ$  Carbon AS4/PEKK laminate supersedes the high strength aluminum alloys; however, its stiffness, 52 GPa, still is lower than that of aluminum, 71GPa. In other words, a plate made of aluminum can be around 35% thinner than a  $\pm 30^\circ$  Carbon AS4/PEKK laminate yet provides the same stiffness. Nevertheless, the density of aluminum,  $2700\text{kg/m}^3$ , is almost twice the density of Carbon/PEKK composite,  $1450\text{kg/m}^3$ . This means that the composite plate is still about 27% lighter than the aluminum plate. Nonetheless, it was attempted to see if lower angle ply laminates, which obviously provide higher stiffness, are capable of high deformation and high strain to failure. As such,  $\pm 25^\circ$  laminates were also made and tested.

Eight layers of  $\pm 25^\circ$  Carbon AS4/PEKK prepregs were laid up together in  $[\pm 25^\circ]_{2s}$  fashion. Five standard coupons were cut from the laminate, and the tests were carried according to ASTM D3039 Standard. Figure 3-37 shows the stress strain curves for different specimens of this laminate. The scatter of the data was considerable. Even though another similar plate was made and tested, the scatter in the results was almost the same. In average the laminate shows strength of 1100 MPa while the average stiffness is about 72 GPa. The laminate was also capable of showing some degree of nonlinear deformation. The maximum fracture strain was observed to be 2.5% while in average the laminate illustrates about 2% fracture strain.

The results of this test will be very beneficial in the design of the composite tube. The laminate has the same stiffness as aluminum yet its strength is higher. On the other hand the deformability of the plate is not very high; nevertheless, it may fulfill the requirements of a helicopter landing gear as it will be explained in the next chapter.

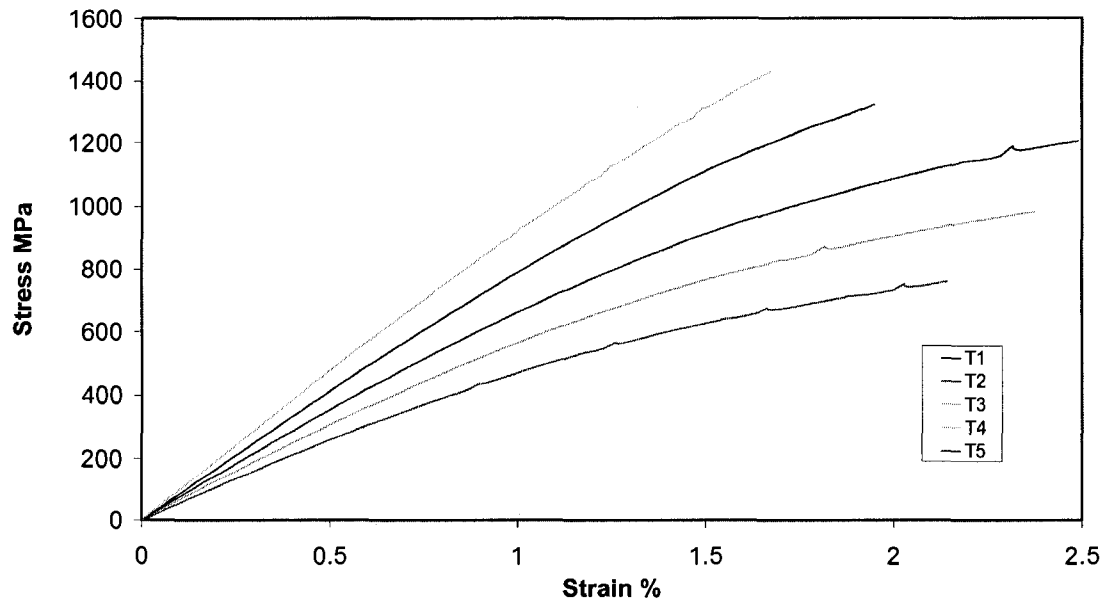


**Figure 3-37: Stress- strain curves for Carbon/PEKK  $[\pm 25^\circ]_{2s}$  laminate**

### 3-11 Mechanical properties of $\pm 20^\circ$ laminates

The behavior of  $[\pm 25^\circ]_{2s}$  laminate raised awareness that the lower angle ply laminates may not show much nonlinear behavior, and the fracture strain of the laminate shall be expected to be low. Nevertheless, the behavior of  $[\pm 20^\circ]_{2s}$  was also studied. The same standard procedure was followed to achieve stress strain curves shown in Figure 3-38. The average strength and stiffness of the laminate are 1200 MPa and 80GPa respectively. The maximum fracture strain of the laminate is 1.86% while the average strain to failure is about 1.6% that is not considerably more than that of unidirectional zero degree laminates. Moreover, the laminate did not show considerable nonlinear behavior. The fracture of the specimens was abrupt. At the fracture point a great amount of sound energy was released.

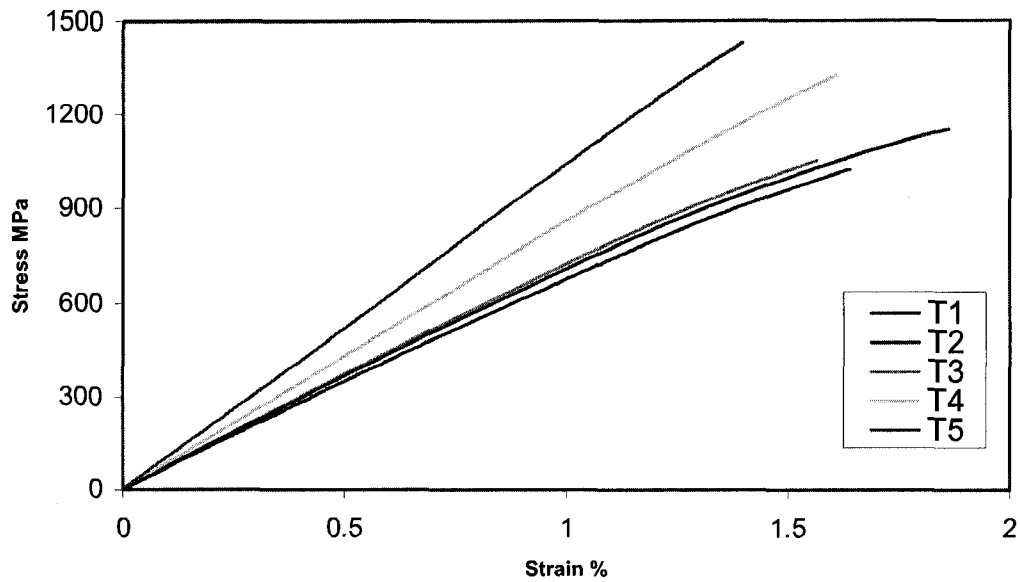


**Figure 3-38: Stress- strain curves for Carbon/PEKK  $[\pm 20^\circ]_{2s}$  laminate**

After the test, it was difficult to find the pieces of the fractured specimens. Most of the fracture lines were parallel to plus or minus twenty degrees; even though, in a few cases fracture occurred in other fashions. Figure 3-39 shows the small pieces of the coupons after fracture.

According to calculations based on CLT,  $\pm 20^\circ$  laminates should have an effective stiffness of 90 GPa. The strength of the laminate is expected to be around 1300 MPa. Also, the fracture strain of the laminate at the first ply failure is about 1.4%. The experimental results agree with the prediction for strength and stiffness; however, slightly more fracture strain can be due to small degree of nonlinear behavior of the laminate. Finally, according to the Tsai-Hill criteria, the fracture is mostly due to the interaction of tensile stresses in 1-1 direction and compression stresses in 2-2 direction. Shear stresses in 1-2 direction are also involved in the overall fracture of the laminate.

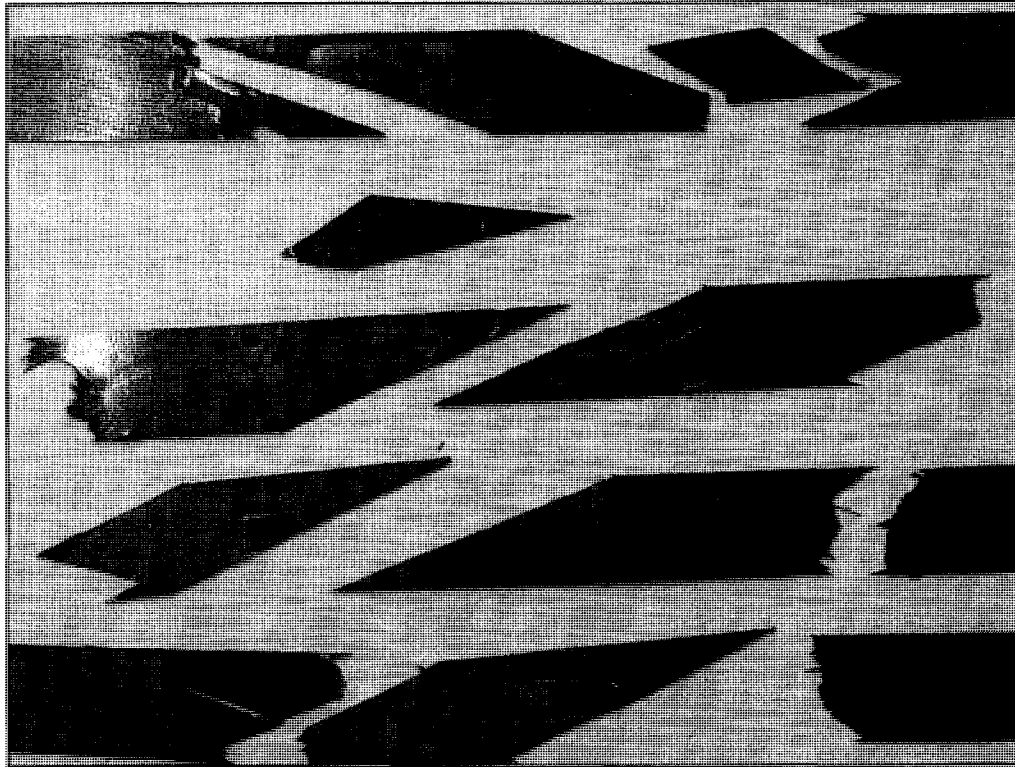


**Figure 3-39: Fractured pieces of  $[\pm 20^\circ]_{2s}$  laminate specimens after tensile test.**

### **3-12 Summary and discussion**

Characterization of Carbon AS4/PEKK was a crucial step in this research. In fact the material is still considered very new in the industry. Even though PEKK has been extensively studied, there is limited database for the material in the form of composite. Analysis of the experimental results shows that the material shall be considered brittle even though the matrix is a thermoplastic polymer.

Despite the brittle nature of the material, a laminate made of Carbon AS4/PEKK may still show some nonlinear behavior and large deformation if certain conditions are fulfilled. For example, debonding between the fibers and the matrix is the primary source of abrupt fracture in  $90^\circ$  laminate, where the ductile matrix is expected to be dominant. By having a proper stacking sequence, this kind of fractures can be avoided. On the other hand,

matrix extension and fiber rotation can be excellent mechanisms for large deformation. In a laminate like  $\pm 45^\circ$ , the matrix is loaded in shear, so the force is transferred between the fibers and the matrix through shear surface, and no debonding occurs. As the matrix deforms, the fibers have a chance to align themselves by the force direction. The two mechanisms together result in large deformation and high fracture strain for  $\pm 45^\circ$  and  $\pm 30^\circ$  laminates.

On the other hand, the domino effect is an undesirable fracture mechanism in the failure of the laminates, and it must be avoided. For instance, consider a laminate such as  $[90^\circ/(\pm 45^\circ)_3/0^\circ]_s$ . For this laminate, the  $0^\circ$  layer carries a considerable portion of the total loads on the laminate. When this layer reaches to its maximum strength, the total strain of the laminate still is below 1.5%. At this point, medium angle plies like  $\pm 45^\circ$  are still far from their fracture strain and must be capable of carrying some loads. However, the rate of loading plays a crucial role and can result in redistributing the loads amongst the layers or abrupt fracture of the laminate upon failure of the  $0^\circ$  layers.

Before first ply failure, it can be expected that the laminate shows a linear behavior until it reaches to its maximum load carrying capacity. At this point, the sudden fracture of  $0^\circ$  plies occurs, and the load carrying capacity of the laminate drops drastically. However, if the high rate of loading and shock due the fracture of  $0^\circ$  layers could be controlled, the laminate should be capable of showing more deformation at lower load level because the majority of the layers are still below their failure strain. The laminate should continue to carry loads even though in lower level of strength and stiffness similar to those of  $\pm 45^\circ$  laminates. Figure 3-40 schematically illustrate the stress-strain curve for such a laminate if the high rate of loading after fracture of  $0^\circ$  layers could be controlled.

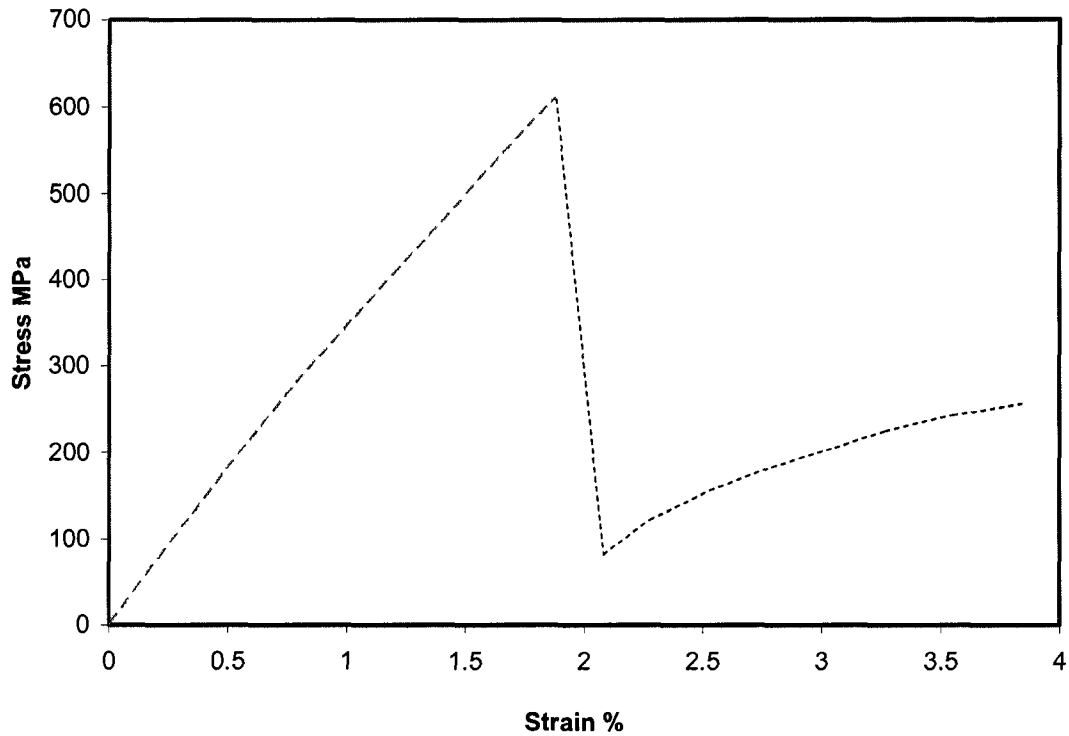


**Figure 3-40: Prediction of stress- strain curves for  $[90/(\pm 45^\circ)_3/0]_{2s}$  laminate.**

However, in practice this behavior was not observed, and the fracture of the laminate was sudden after the fracture of  $0^\circ$  layers. Figure 3-41 shows the experimental results for testing such a laminate. In fact, low angle plies are considerably stiffer than medium angle plies, so they are the main load carrying plies. Upon their failure, the medium angle plies receive a shocking load while they do not have enough time to deform in shear and redistribute the loads, so the fracture occurs.

Interaction between the adjacent layers can also cause domino effect in failure. For instance, by inserting a layer of polymer film between two adjacent layers, it would be possible to decrease their mutual interaction. When the two adjacent blocks of layers are deforming independently, the chance for lateral deformation and subsequently higher

longitudinal deformation increases. In manufacturing composite tubes, it is difficult to insert polymer films; however, by laying up 90° degree layers between adjacent layers, the same results can be achieved: the details will be explained in the next chapters.

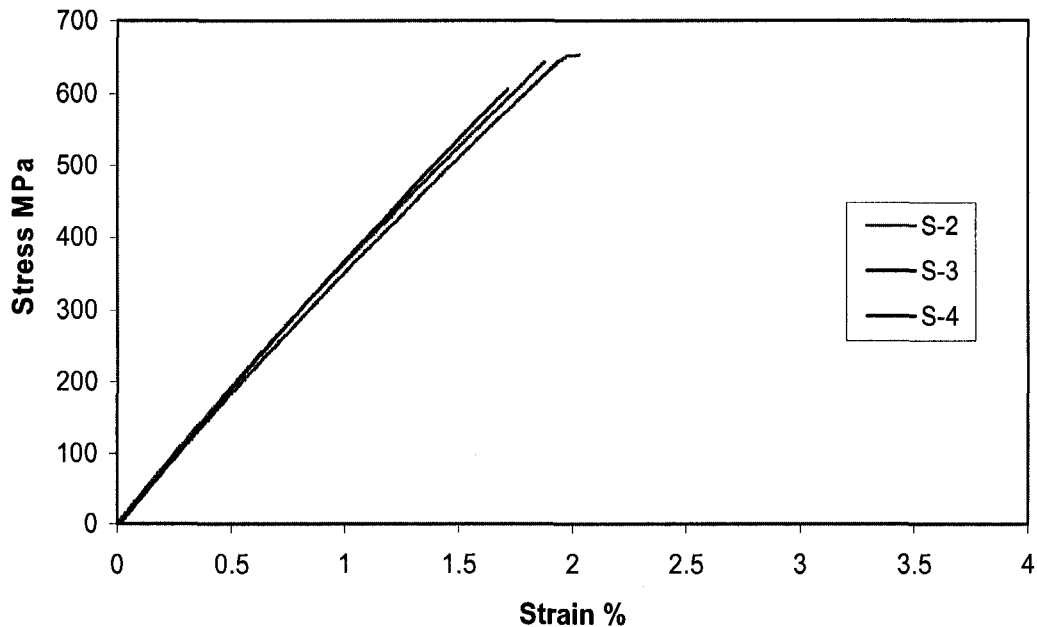


**Figure 3-41: Test results for stress- strain curves of  $[90/(\pm 45)_3/0]_{2s}$  laminate.**

Finally, Figures 3-42 and 3-43 illustrate the comparison of stress-strain curves for different laminates tested in this research with that of Aluminum 7075-T6. Obviously, aluminum is a very ductile metal and shows very high fracture strain. However, for many engineering applications, the structure does not experience strains above 2.5%. As such, the results of the material characterization may shed some light into the design of a composite tube that is capable of large deformation. It can be observed that some of the laminates show more than 5% strain, but they have relatively lower strength and stiffness than aluminum. On the other hand, some low angle ply laminates show relatively lower fracture strain, but they illustrate higher strength and stiffness than aluminum. As such, it

is reasonable to expect that a combination of these layers would satisfy both strength and stiffness as well as fracture strain requirements. In the next chapter, it will be shown how the results achieved from the material characterization would be employed to design a composite tube with large deformation and similar load carrying capacity as its aluminum counterpart.

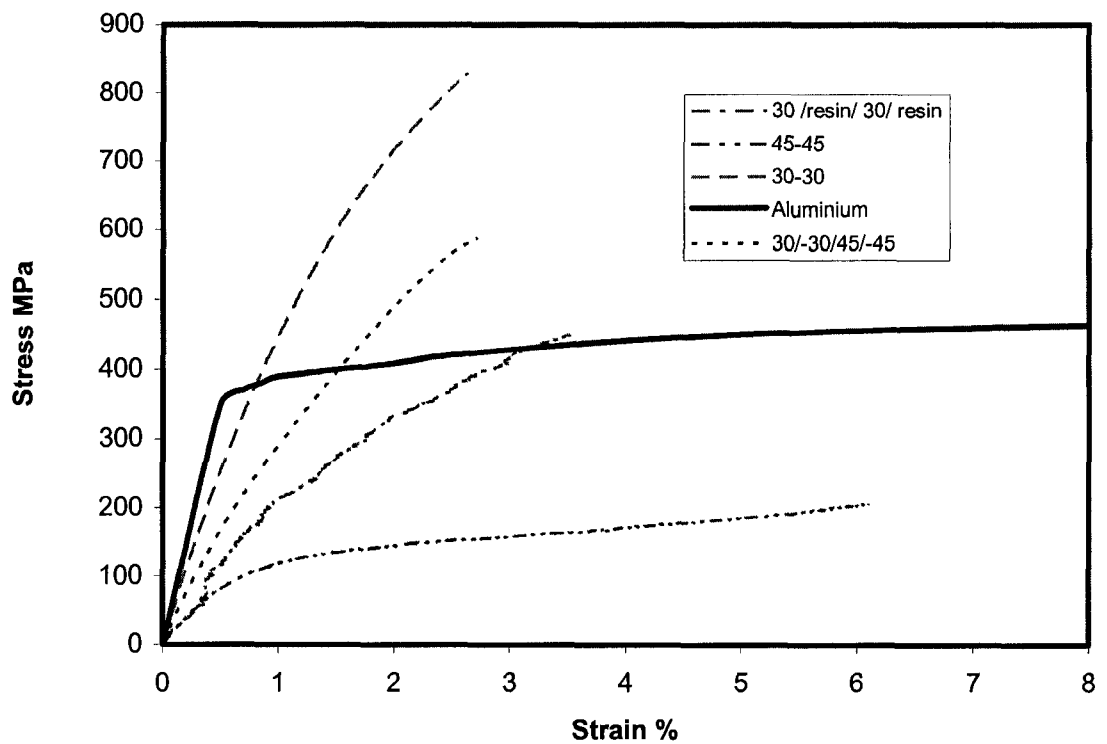


Figure 3-42: Stress-Strain curves of medium angle Carbon/PEKK laminates

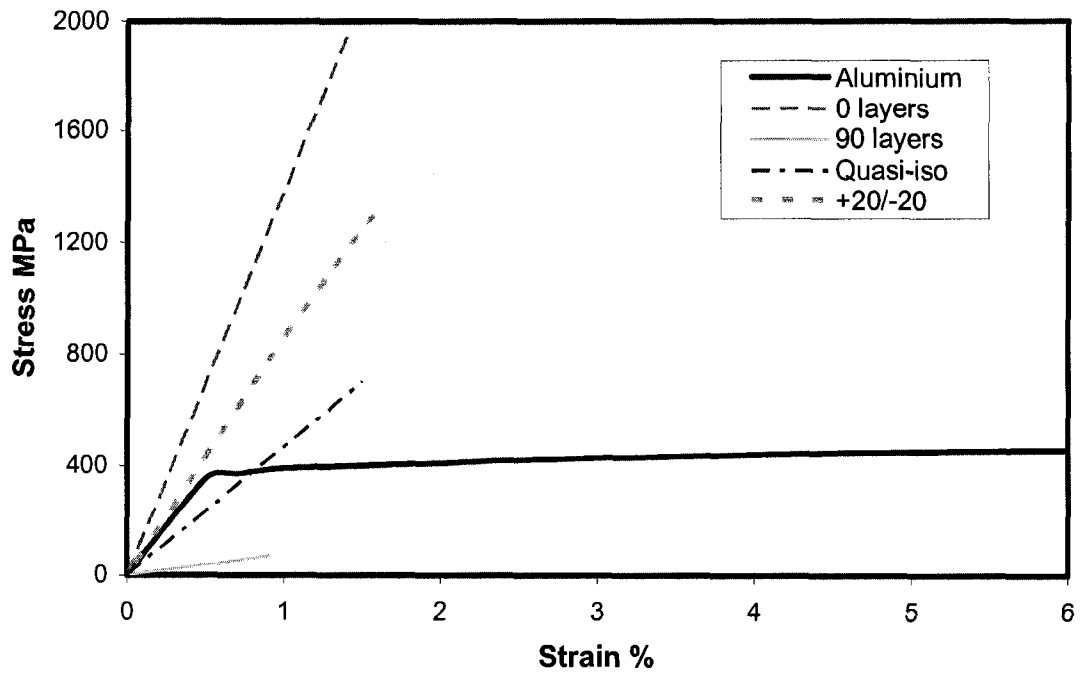


Figure 3-43: Stress-Strain curves of low angle Carbon/PEKK laminate

## **Chapter 4**

### **A Procedure for Bending Test of the Tubes**

#### **4-1 Introduction**

Brittle materials have very low fracture strain. Their fracture is abrupt, and they usually show very linear behavior before their fracture. Despite their polymer matrix, composite materials generally show brittle behavior. A high performance composite usually consists of more than 60% brittle fibers. As such, the brittleness of composites is linked to low fracture strain of the fibers. However, the study of mechanical behavior of Carbon AS4/PEKK composite laminates, reviewed in Chapter 3, raised hope that the substitution of the aluminum landing gear with a composite landing gear might be possible depending on the level of plastic strain in the cross tubes during hard landing. Moreover, the failure of the composite laminate in the tubular form and under bending loads should not follow the same domino pattern observed for the flat plates.

Yield Strength MPa	Ultimate Strength MPa	Modulus of Elasticity GPa	Shear Strength MPa	Modulus of Rigidity GPa	Strain to Failure %	Fracture toughness MPa-m <sup>1/2</sup>
503	572	71.7	330	26.9	11	29

**Table 4-1: Mechanical properties of aluminum 7075- T6, Totten (2003).**

Skid landing gears have been manufactured from elastic-plastic metal alloys which dissipate energy during plastic bending, Shrotri (2008). The aluminum grade 7075-T6 is one the most common materials in manufacturing of rotorcrafts. Table 4-1 shows a few typical properties of this material. The fracture strain of this aluminum alloy is about 11%. However for the case of helicopter landing, even during the severe landings, the maximum strain of the aluminum cross tubes would not exceed 2.5% due to the geometrical constrains, as discussed below.

Bending of curved tubes with variable wall thickness has been studied by numerous researchers among them Cheng et al. (1968 & 1970) and Cherniy (2001& 2003). However, here a simplified method is used to analyze the landing gear cross tubes. Figure 4-1 schematically shows the dimensions of the structure. The main part of the structure is a curved tube with the radius of curvature,  $\rho$ , equal to 1805mm (71.07"). The inner diameter of the tube is constant 56mm while the outer diameter varies from 88mm to 64mm. As such the maximum radius of the tube that presents the maximum distance from the neutral axis is 44mm. During a crash, in the most severe condition, the beam might deform until it becomes almost straight. In this situation, the maximum strain in the

beam by some simplifications can be calculated by a simple equation of mechanics of materials as follows:

$$\varepsilon_{\max} = \frac{r}{\rho} = \frac{44}{1805} = 0.025 = 2.5\%$$

The ANSYS analysis of the aluminum curved tube subjected to a load that made the curved tube straight showed that the maximum strain in the tube is 2.53%, which is in an agreement with the above analysis. This shows that due to the geometrical constrains and rigid body motions, the maximum plastic strain in the structure remains low, and the structure does not require the full capacity of aluminum as a ductile material to absorb the maximum possible energy during harsh landings. As a result, considering the fact that some Carbon AS4/PEKK composite laminates show higher failure strain than 2.5%, there is a possibility that a special layup would exist, through which the composite tube would show the same strength, stiffness and toughness if the failure does not happen in a domino fashion.

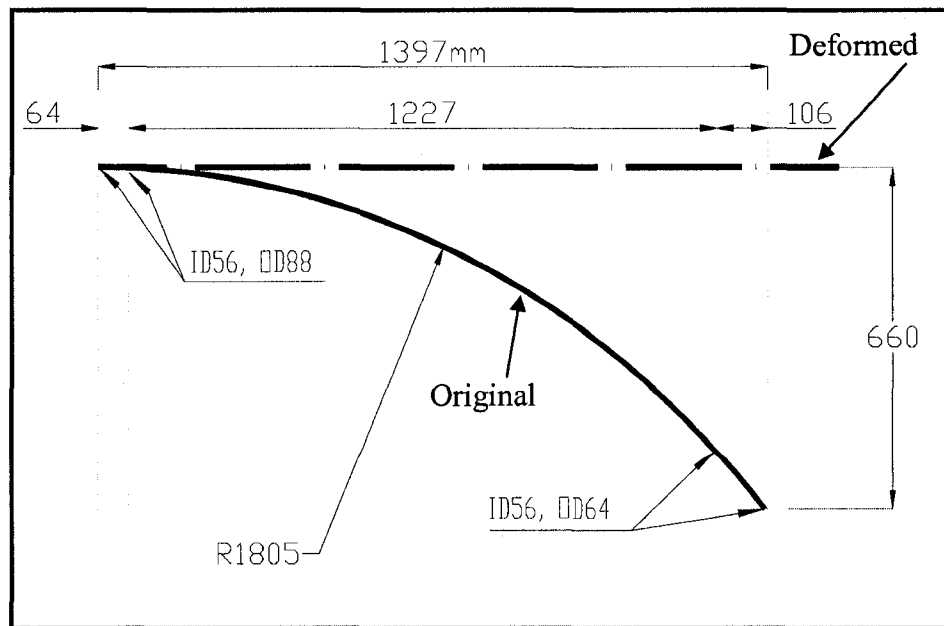


**Figure 4-1: Schematic dimensions of helicopter landing gear: Front Skid Tube**

As such, the first requirement is satisfied. To verify the second condition, bending tests should be carried on composite tubes. As there is no standard procedure for testing the polymer composite tubes, some effort was devoted to finding a proper procedure for testing the aluminum and composite tubes.

When the laminates are subjected to tensile loads, all layers experience the same strain. It was observed that laminates that include zero degree layers would show their final fracture as soon as zero layers fail. This means that the rest of the layers are not able to redistribute and resist the load, so the fracture is inevitable. Nevertheless, when a beam is subjected to bending loads, strain is not the same, and it varies linearly with respect to the distance from neutral axis of the beam. For a composite tube, the inner layers, which are closer to neutral axis of the tube, experience relatively lower strains while the outer layers would experience considerably higher strains. In addition, the stress distribution is not linear due to the fact that different layers have different stiffnesses. In fact, this is a main difference between composite and metal structures. For an aluminum tube, where the properties of the material are isotropic, the strain and stress vary linearly through the section according to the distance of the element from neutral axis. However, in composite tubes, for example, if the zero degree layers are inside and  $\pm 45^\circ$  layers are outside, most of the load is still carried by the inside zero degree layers, and the stress in the  $0^\circ$  layers can be high even though the strain may be low. In contrast, the outer  $\pm 45^\circ$  layers would experience higher strain yet the stress may remain low due to their lower stiffness. These differences may result in observing large deformation for composite tube without domino effect in fracture. As such, it was decided to carry out three point bending tests on aluminum and composite tubes.

However, due to the high cost and intricacy in manufacturing composite tubes, it was necessary to establish a procedure for the tests. The goal was to carry out the tests for large deformation yet localized deformation and premature failures should be avoided. Therefore, several aluminum tubes were tested to observe the behavior of the tubes under bending loads and learn about uncertainties during the tests. The effects of different types of pads at loading nose and supports on the results were studied.

#### **4-2 Design and manufacturing of the fixture**

Though the best way to study the flexural behavior of a material or even a structure is to design a fixture that applies pure bending to the sample, in most cases this is not practical enough. Three and four point bending tests have been standardized for testing the metallic and composite flat coupons. However, no standard procedure was found to carry out bending test on tubes. Nevertheless, the guidelines of bending test of flat specimens was used to set up a methodology that can be used in bending tests of simple structures like tubes and beams providing that the tube or the beam are long enough to fail in bending rather than in shear.

To have an overall idea of the requirements of a fixture for 3-point bending test of composite tubes, a short carbon/epoxy tube was fabricated by hand layup, and it was cured in autoclave. A four point bending fixture available in the composite lab of Concordia University was used to test the tube.

Figure 4-2 shows the test set up on the MTS machine. Though the test was very preliminary, the following results were achieved and used as the guidelines for the design of a three-point bending fixture:

- 1- Although the first ply failure happens at relatively low displacement due to the brittle nature of the composites, the tube might have large deformation due to the local deformation. Therefore, supporting points of the tube must provide sufficient space to let the tube deform without touching the fixture.
- 2- Local fracture at loading nose and at the supports is very possible, so a pad must be designed to avoid pre-mature failure at these locations.
- 3- At high loads, the fixture may distort due to a small eccentricity at the supports. Moreover, a safe arrangement is necessary to assure that the tube stays on the fixture during the test.

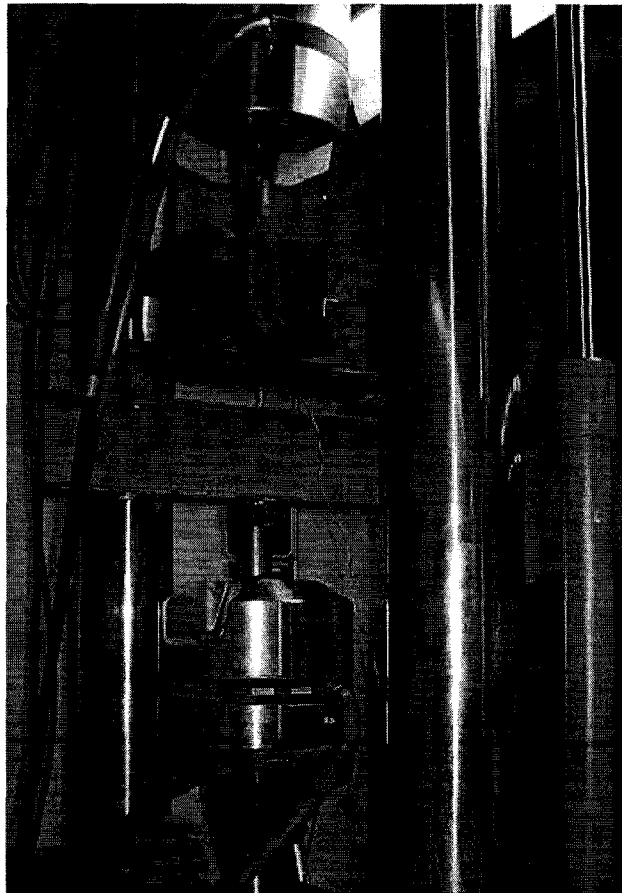


**Figure 4-2: Four point bending test set up on MTS machine**

Besides experiments on a composite tube, ANSYS finite element analysis was employed to determine how much the level of the force could be during the tests for both aluminum and composite tubes. Deformation of the fixture was also considered. If the deformation is high at the supports, the risk of distortion of the fixture is increased. Moreover, the deformation measurement of the tubes due to bending loads becomes erroneous as the MTS machine measures the global displacement of the loading nose rather than the relative displacement between the loading nose and the supports.

In order to evaluate the applied load on the fixture, first the aluminum tube was analyzed to find out how much load was required to achieve 3% strain on the tube. The dimensions of the aluminum tube were selected according to the current aluminum landing gear dimensions. The length of the tube was assumed to be 1m, and the outside and inside diameters of the tube were chosen to be 80mm and 50mm respectively. These arbitrary dimensions are close to the maximum dimensions of the helicopter front skid tube. Figure 4-3 shows the distribution of the total strain in the tube. The tube was loaded until the maximum strain reached to 3%. The corresponding loads and deflections were 60KN and 40mm respectively.



**Figure 4-3: Strain distribution in the aluminum tube**

It was assumed that aluminum has elastic-perfect plastic behavior and hardening effect was not considerable. As such, the load would not increase considerably beyond 60KN as the mid-span of the tube was already in the plastic zone, and the deformation would remain localized at this point.

Figure 4-4 illustrates the deflection of the tube. At this point, the maximum longitudinal strain in the tube is about 2.7%; the deformation is uniform, and no localized deformation is observed. The curvature of the tube varies proportionally to the bending moment throughout the tube. As such, the maximum curvature is observed at the mid-span, where the bending moment is the maximum.



**Figure 4-4: Deflection of the tube**

According to the maximum load values, possible deformation of the tube and the guidelines from testing the composite tube, a fixture for three-point bending tests of the aluminum and composite tubes was designed. The detailed design of the fixture is presented in Appendix C. The design used a factor of safety equal to 2 for stress analysis of the fixture while the maximum deflection of the fixture was kept below 0.5mm to avoid error in measurement of the test data. Moreover, the fixture is adjustable for different tube lengths. Figure 4-5 shows assembly of this fixture. The loading nose has a curvature similar to the outer radius of the tube to assure the load is applied uniformly on

the tube. The supporting points are chamfered to allow deformation of the tube during the test and apply the reaction forces in the radial direction.

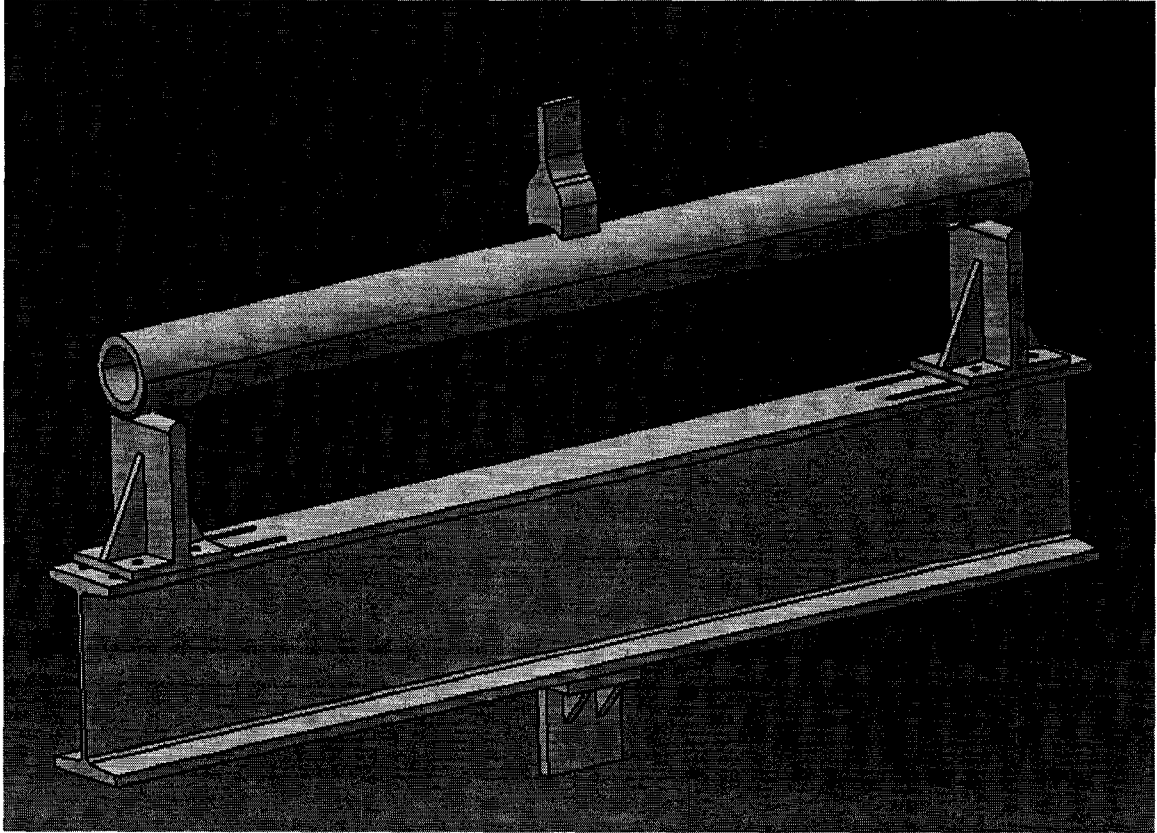


**Figure 4-5: Assembly drawing of the fixture for 3 point bending test**

### 4-3 Three-point bending test of aluminum tubes

Standard procedures exist for different types of tests including characterization of the materials. For example, ASTM D790-00 Standard gives guidelines for three-point bending tests of composite flat panels, ASTM D6272-00 Standard presents directions on how to determine the flexural properties of reinforced plastics by four-point bending. Nevertheless, due to the diversity of the structural forms, it is impossible to set enough standard procedures to cover all possibilities. As such, an attempt was made to test a few aluminum tubes by different procedures and find out a procedure that properly produces reliable data from three-point bending tests of the tubular structures. The guidelines then were used to test and analyze the composite tubes.

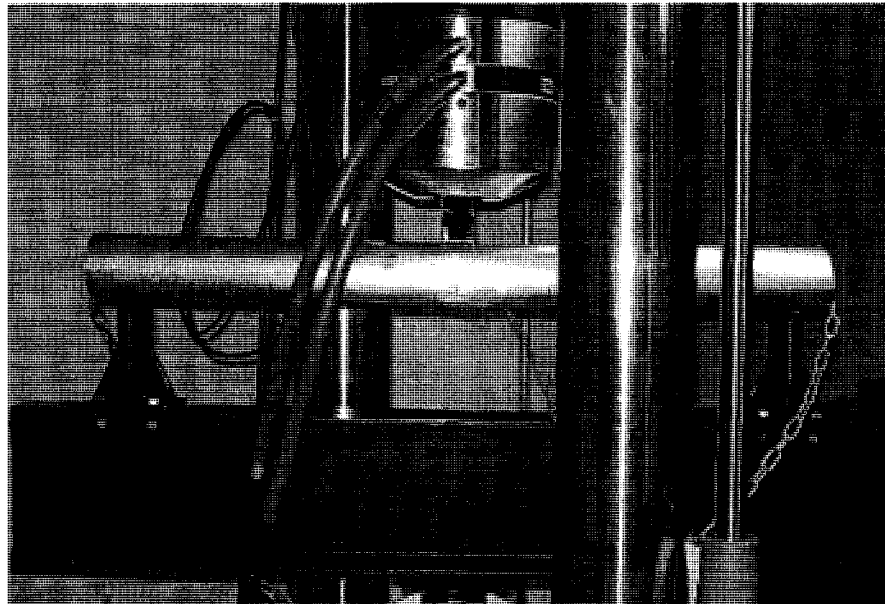
Table 4-2 presents the specifications of standard aluminum 6061-T651, DN 80, SCH 80, tubes, which were used for the bending tests.

Specifications	Aluminum tube DN 80, SCH 80
Inside Diameter, mm	73.66
Outside diameter, mm	88.90
Wall thickness, mm	7.62
Weight of unit length, Kg/m	5.27
Moment of Inertia, mm <sup>4</sup>	1.62E6
Flexural rigidity, EI <sub>xx</sub> , N.mm <sup>2</sup>	11.3E10
Length, m	1.00

**Table 4-2: Specifications of aluminum tube DN 80, SCH 80**

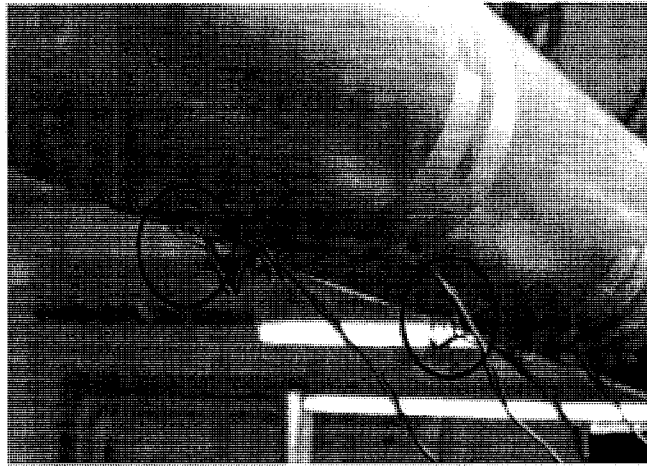
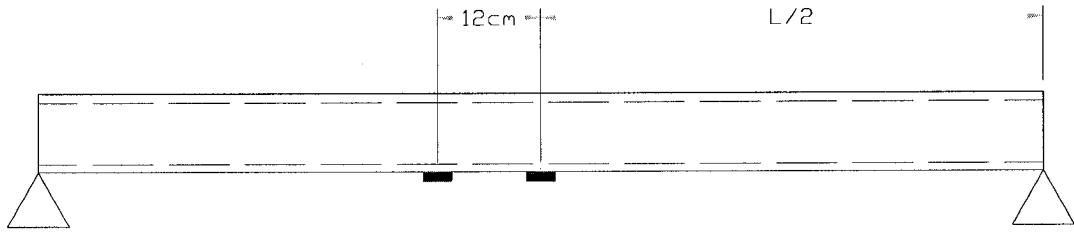
### 4-3.1 Aluminum tubes test 1: No pad

Figure 4-6 shows the bending test set up for the first aluminum tube. For this test, no reinforcement was employed at the supports or at the loading nose. A chain was used to secure the tube on the fixture. The purpose of this test was to observe normal behavior of the tube while no other external parameter was involved. The risk, however, was the localized deformation at loading nose or at the supports. Therefore, the data of large deformation could be inaccurate.



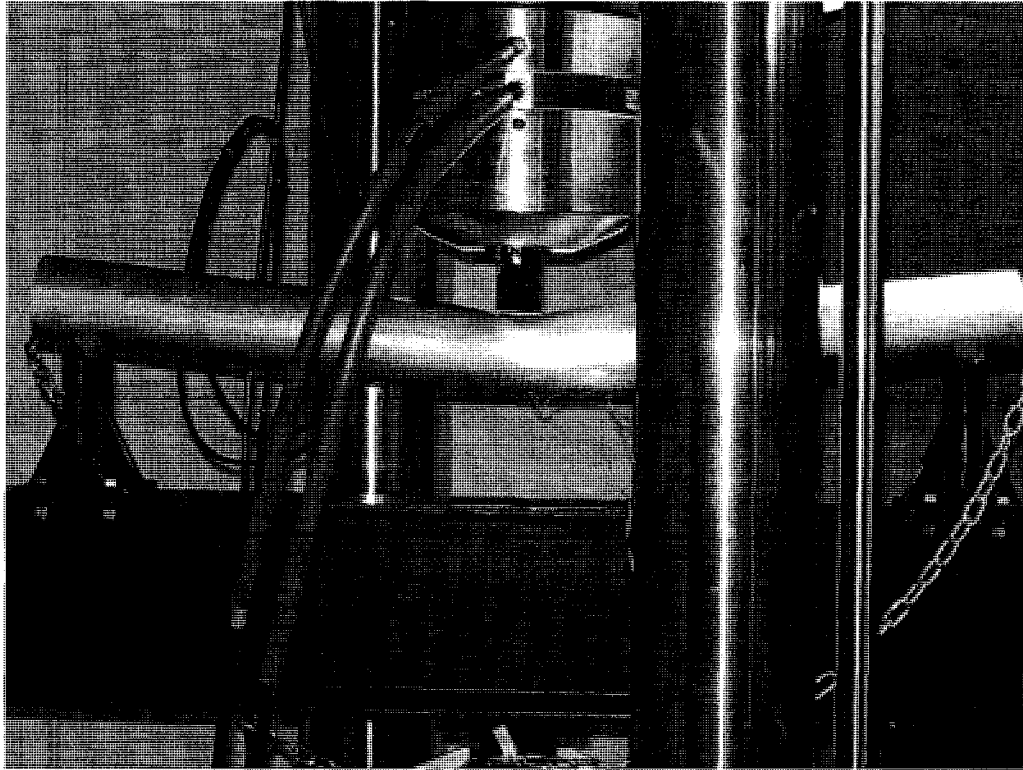
**Figure 4-6: Test set up of aluminum tube: test 1**

Two  $T$  (double) strain gauges were installed on the bottom line of the tube to measure the longitudinal and circumferential strains, as shown in Figure 4-7. The first one was installed at the mid span of the tube while the other one was installed at 12 centimeters offset from the midpoint. The test was carried out in a constant displacement increment of 1mm/min.



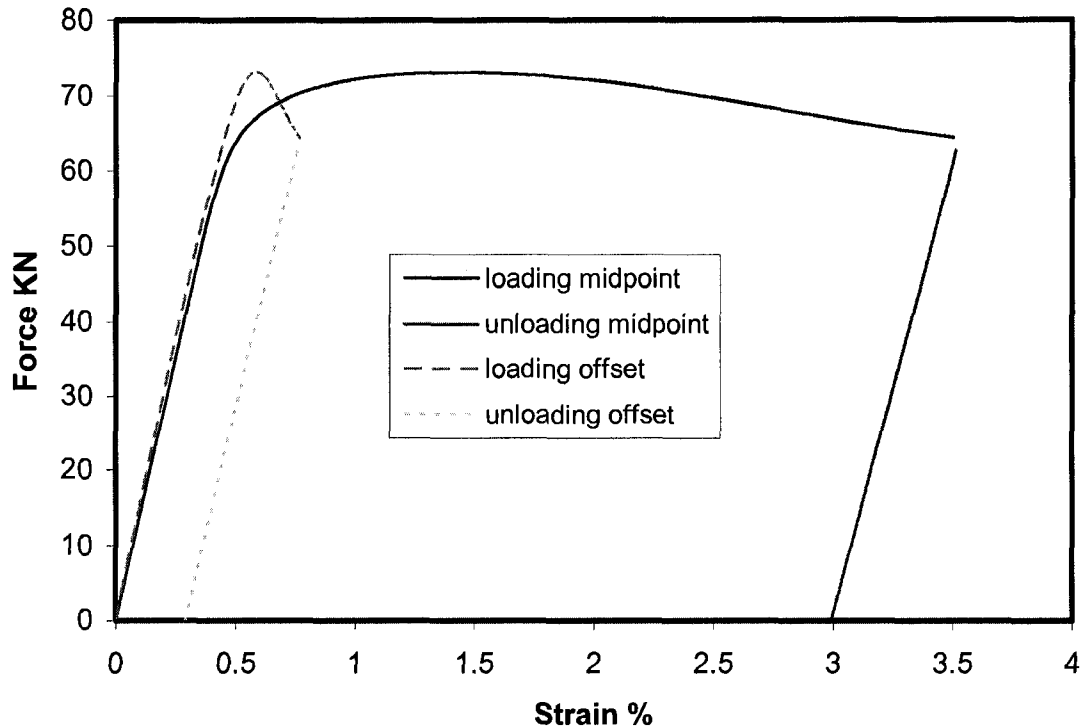
**Figure 4-7: Two double strain gauges installed on the bottom line of the tube**

As the load was increased, the tube was showing more plastic deformation until the maximum strain 3.5% was achieved at the mid-span of the tube. Figure 4-8 shows the aluminum tube at this final stage. As can be observed, some local deformation occurred at the midpoint due to the radial forces applied by the MTS machine. This type of deformation would not be desirable for the composite tube and certainly must be avoided. Upon achieving 3.5% strain, the test was stopped, and the tube was unloaded in a constant negative displacement increment of -1mm/min to see the permanent plastic deformation in the tube.



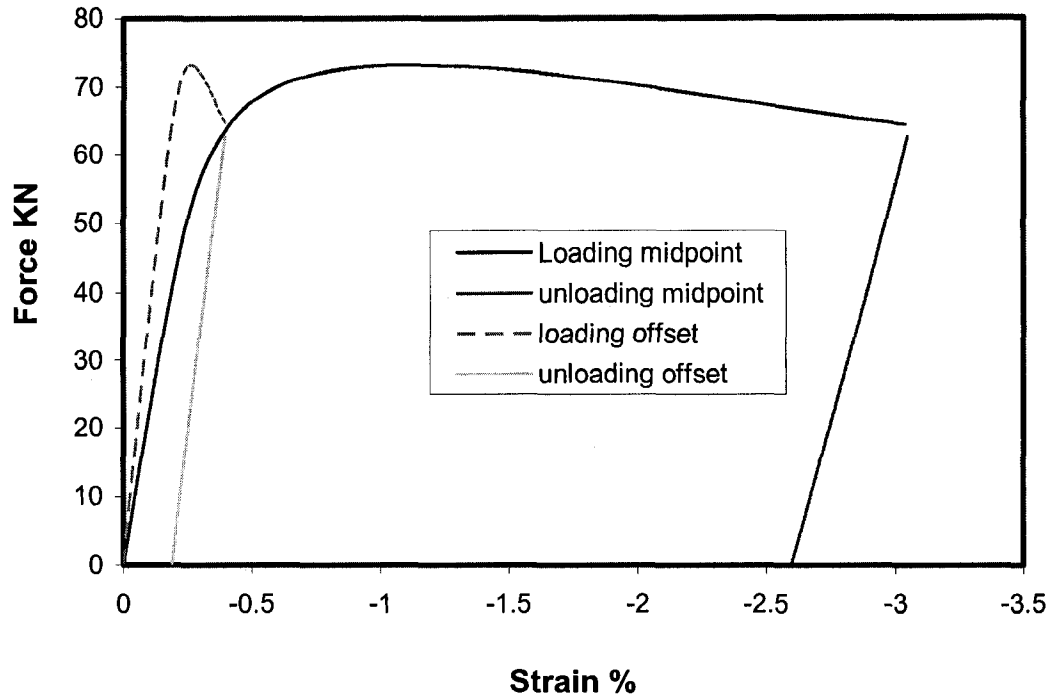
**Figure 4-8: Deformation of aluminum tube during bending test**

Figure 4-9 shows the load-axial strain curves measured at the mid-span and at 12cm offset strain gauges. The loads, time and displacements were directly measured by the MTS machine every half a second. The maximum load carried by the tube was about 75KN. The corresponding maximum displacement was 60mm; nevertheless, part of this displacement was due to local deformation of the tube at the mid span, and it can not be considered as a uniform deformation. On the other hand, the strain measured by the offset strain gauge did not exceed 0.7%. The unloading curve for the midpoint showed that the permanent strain or plastic strain in the tube was 3%. Moreover, as it had been predicted and explained before, beyond plastic deformation of the tube, the load did not increase. Yet, beyond some limit when deformation was more localized than uniform, the load slightly decreased.



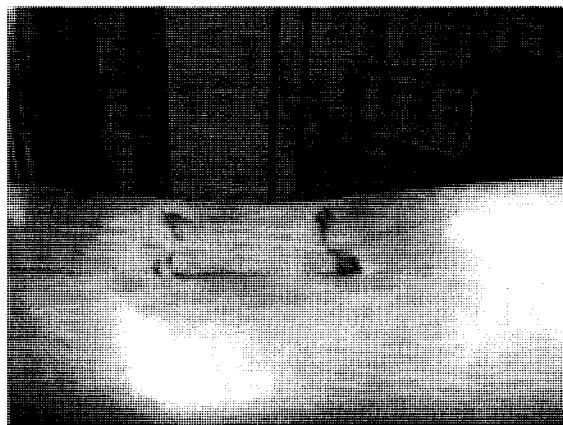
**Figure 4-9: Force-axial strain at mid span and at 12cm offset from midpoint**

Figure 4-10 shows the circumferential strains at the mid-span and at 12 cm offset from the midpoint. As it can be seen the compression strain at the midpoint, -3 %, is very large. The maximum longitudinal strain at the same point was 3.5%, and the Poisson's ratio for the aluminum is about 0.33. As such, it can be assumed that state of stress at the midpoint of the tube and close to loading nose is very complex. At the initial stages of the test and in the elastic zone, the Poisson's ratio was valid between the longitudinal and circumferential strains. However, as the deformation became plastic and more localized, the circular tube deformed to an oval shape, and the circumferential strain increased quickly. For the composite tubes, this complexity will add difficulty to a proper analysis of the fracture modes of the tube.



**Figure 4-10: Force circumferential strain in mid span and 12cm offset**

Finally, Figure 4-11 shows the trace of the loading nose on the tube. Localized deformation at the top of the tube can create serious problems for the composite tubes. Composite laminates are not strong against out-of-plane stresses. Consequently, this type of localized deformation can crush the laminate and decrease the strength of the tube considerably.



**Figure 4-11: Localized deformations at the loading nose**

In contrast to the high local deformation at the loading nose, at the support the tube just slightly deformed. Figure 4-12 illustrates a small dent on the tube after 70KN load had been applied on the tube. This small deformation would not affect the accuracy of the results; hence, the reinforcement of the aluminum tubes at the supports is not required. Nevertheless, at the loading nose, the tube should be certainly protected.



**Figure 4-12: Bearing stress is the only cause of deformation at supporting points**

#### **4-3.2 Aluminum tubes test 2: Rubber pad**

The first test on the aluminum tube proved that there was no real need to protect the tube at the supporting points as no major local deformation was seen there. As a result, for the second test, a piece of wire meshed tire was placed only under the loading nose. The advantage of the tire over other types of the rubber is that the metal mesh could prevent the loading nose from cutting the rubber and contacting directly the top surface of the tube. Moreover, the reduction in the thickness of the wire meshed rubber under large compression loads is less, and less error due to the employment of the pad is created. Figure 4-13 shows the test set up for the second test on the aluminum tube.

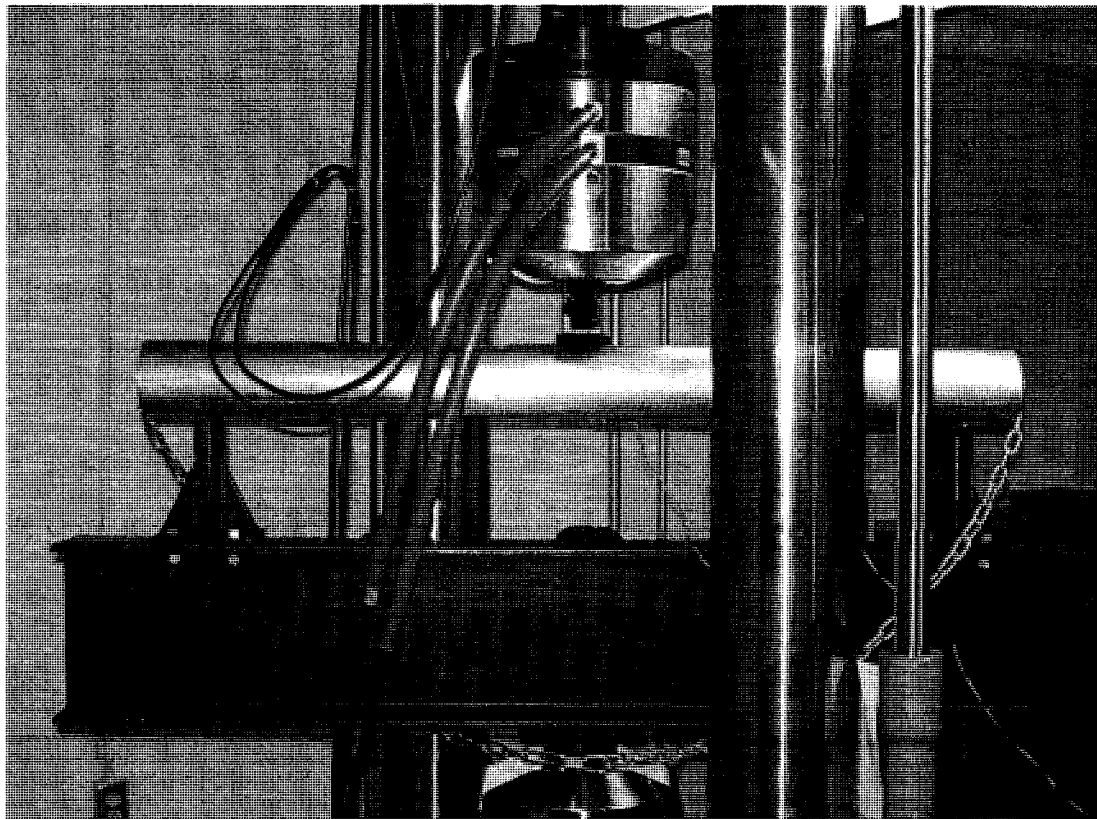


**Figure 4-13: Test set up for second test; wire meshed rubber under loading nose**

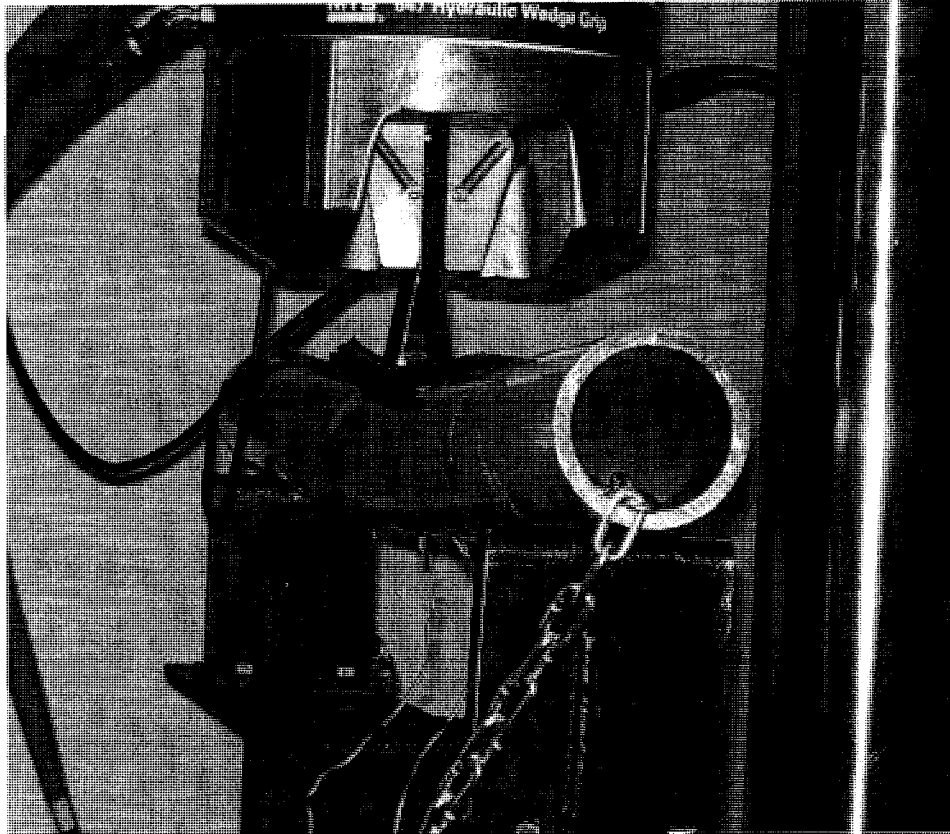


**Figure 4-14: Deformation of the second aluminum tube**

Figure 4-14 demonstrates the deformation of the second aluminum tube subjected to three-point bending test. At this stage the maximum longitudinal strain at the bottom of the tube had reached 2.5%, and the deflection of the tube was 54mm. The maximum load carried by the tube was 65KN.

During the test, the tube showed some lateral deformation. At the first test no pad was used; therefore, the tube adjusted itself with the curvature of the loading nose, and no lateral deformation was observed. At the second test, however, the rubber between the tube and loading nose created a relatively soft medium between them, and the curvature of the loading nose was not felt by the tube; as a result, the tube could show lateral deformation.



**Figure 4-15: Local deformation at the loading nose during the test of second tube**

Figure 4-15 shows the surface of the tube after the test. It can be seen that the employment of the tire helped in reducing local deformation while a better load distribution on the top of the tube was achieved. Nevertheless, still local deformation is considerable, and lateral movement of the tube is a concern. Figure 4-16 shows the load-axial strain for this test at the mid-span and 12cm offset.

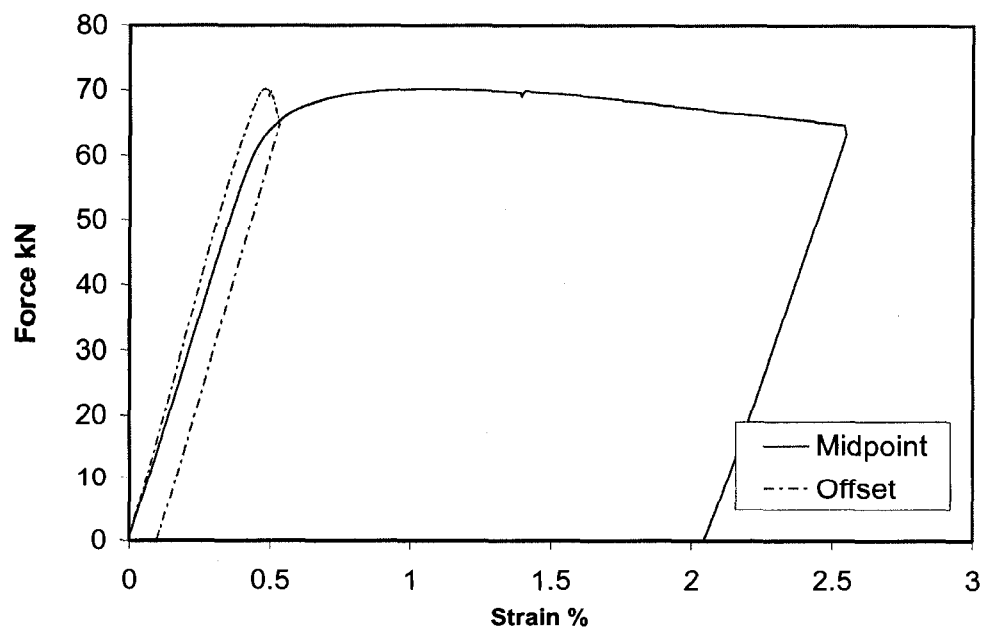


**Figure 4-16: Bending force versus axial strain**

### 4-3.3 Aluminum tubes test 3: Composite pad

For the third test on the aluminum tube, a fiberglass composite pad was placed between the loading nose and the tube. The pad had been laid up on the surface of the tube, so it was perfectly matched with the outer radius. This would help considerably achieve a uniform loading distribution. Laying up a fiberglass pad on the surface of the composite tube would be also possible. The pad can be cured at room temperature, and there is no need to put the tube inside a hot autoclave. Another advantage of the composite pad is that it could be tapered, so as the tube deforms, the pad may bend and follow the curvature of the tube during the test. Figure 4-17 shows the test set up for the third aluminum tube.

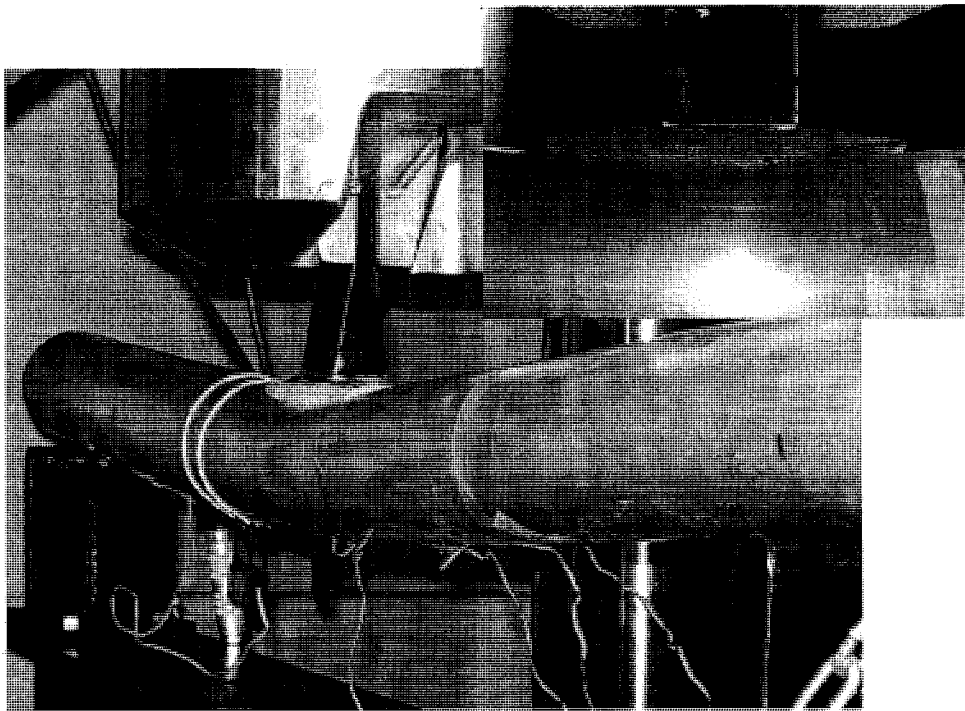
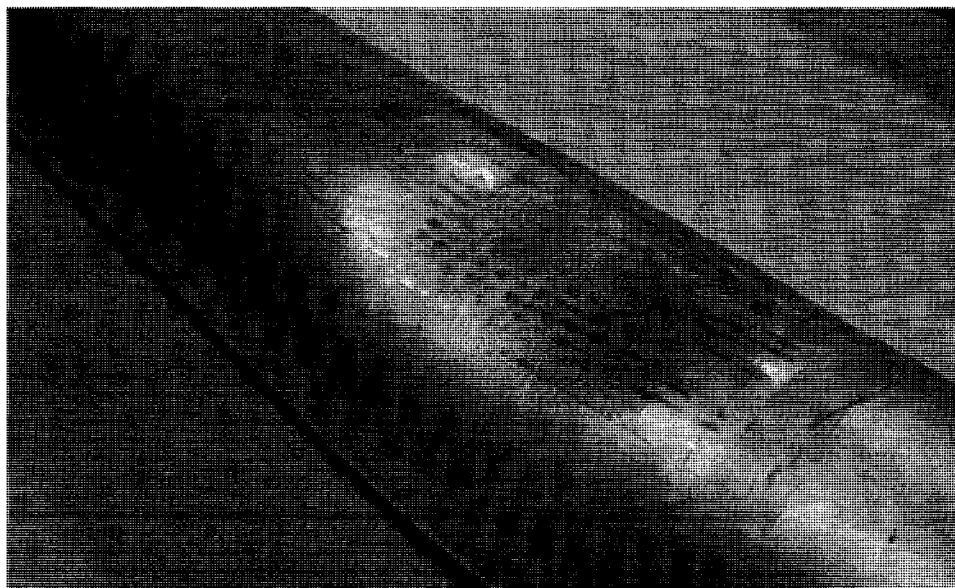
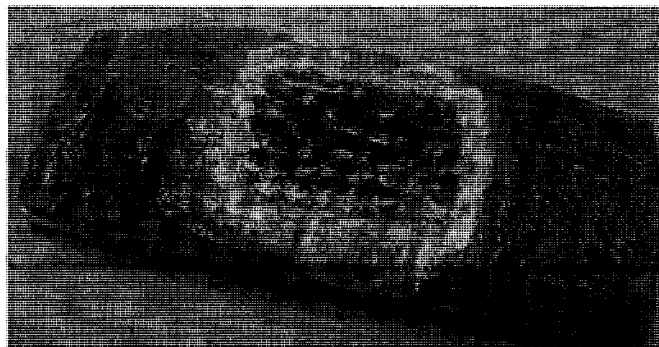


**Figure 4-17: Test set up with composite pad under load applicator**

Two  $T$  (double) strain gauges were installed on the tube to measure axial and circumferential strains at the mid-span and at 12 cm offset from the midpoint. The test results were promising. The tube was deformed uniformly, and no local deformation was observed. Figures 4-18 a & b demonstrate the surface of the tube and the fiberglass pad after the test. The composite pad played a constructive role in distributing the load, and local deformation at the loading nose was insignificant.



(a)



(b)

**Figure 4-18-a, b: Surfaces of the tube and the fiberglass pad after the test**

Figures 4-19 & 20 illustrate the force axial and circumferential strain curves for the bending test of the third aluminum tube. A maximum strain of 3.5% was achieved. The corresponding deflection of the tube was 48mm, which is less than the deflection of the first tube for the same level of strain. In fact, in this test less local deformation was observed, and the curvature of the tube was more uniform. It can be also observed that the circumferential strain shows less value in comparison to the first test. It can be concluded that less localized deformation creates less complexity in the state of the stress and strain at the midpoint. Finally it can be noticed from all tests that the strain at a distance from the midpoint is not very considerable. The maximum strain achieved at 12cm offset from the midpoint was about 0.5% that is very close to the elastic limit.

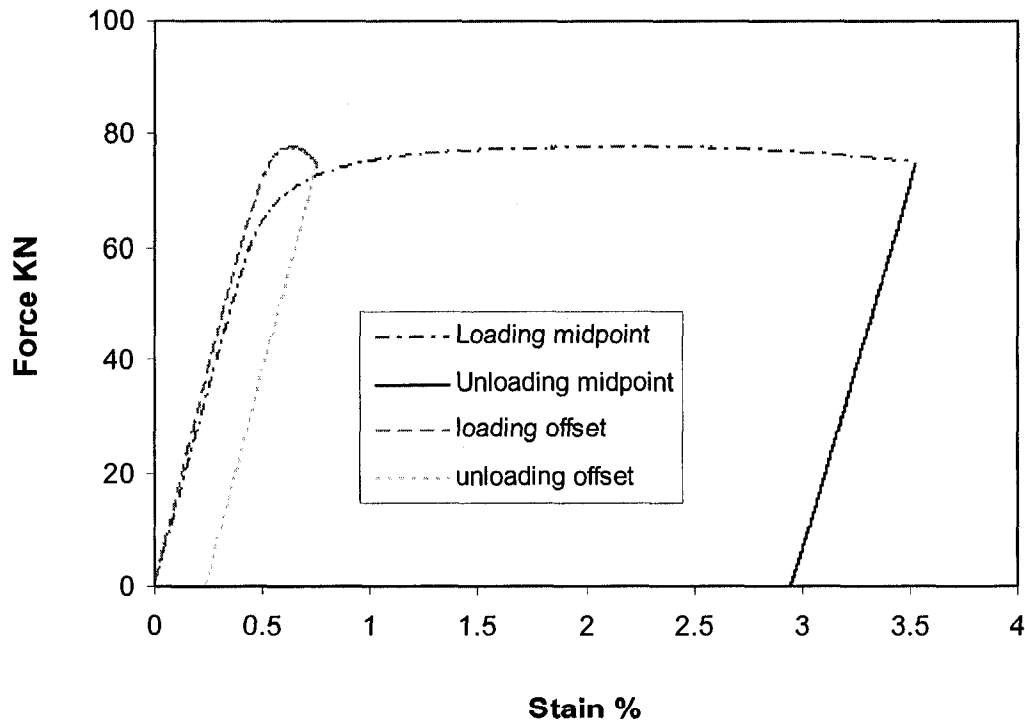


**Figure 4-19: Force-axial strain at the mid span and at 12 cm offset from midpoint**

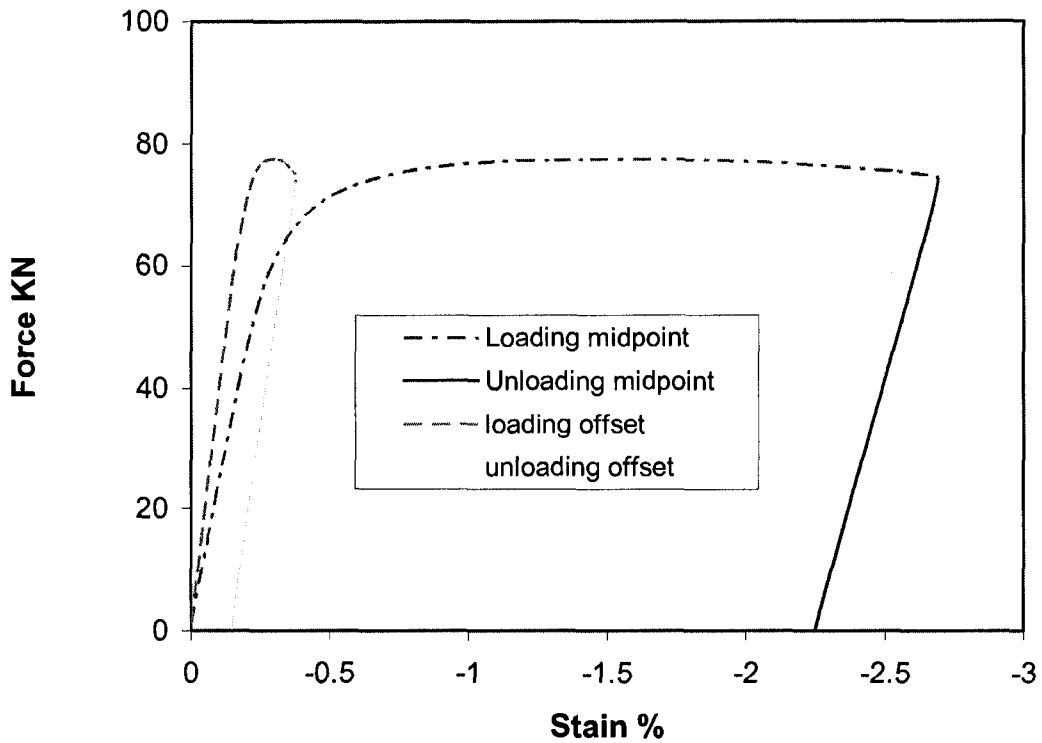


**Figure 4-20: Force-circumferential strain at the mid-span and at 12 cm offset**

#### **4-4 Results from three bending tests on aluminum tubes**

Three point bending tests were carried on a few aluminum tubes to provide guidelines for testing the expensive composite tubes. The major difference between the tests was the type of the pad, which was used at the loading nose. For the first test no reinforcement was employed. For the second and third tests wire meshed rubber and fiberglass composite pads were used.

After the tests on the aluminum tubes the following conclusions were made:

- 1- The bending tests of the aluminum tubes were carried out at 1mm/min displacement increment. The rate might be high for the composite tubes especially

in the elastic range, where the load would increase rapidly. A rate of 0.5mm/min could be suitable for the composite tubes, and the timing would be enough to collect the data.

- 2- The fiberglass pad can assure a uniform load distribution, and it can be employed in testing the composite tubes. Moreover, the chance for the fiberglass pad to cut into the top surface of the composite tube is very low if its edges are rounded appropriately.
- 3- The stress distribution close to the loading nose would be complex. A few strain gauges shall be installed at different locations of the composite tube to provide better understanding of state of stress and strain in the tube.
- 4- The failure of the tube due to the bearing stresses at the supports does not seem probable. Nevertheless, to avoid any uncertainty minor reinforcement by fiberglass is suggested.

Finally, Figure 4-21 compares the force- displacement curves for the three tests carried out on the aluminum tubes. While the curves for the first and third tests are almost matched, the curve for the second test shows deviation. In fact, the stiffness of the wire meshed tire was low, and this created a considerable amount of error in the test results. The slope of the curves at the initial stage should represent the flexural rigidity of the tube; however, when rubber was used, the slope was reduced considerably. In contrast, composite pad was rigid enough not only to provide a good loading distribution on the tube but also to maintain the rigidity of the tube. As a result, employing the composite pad for the future bending tests is recommended.

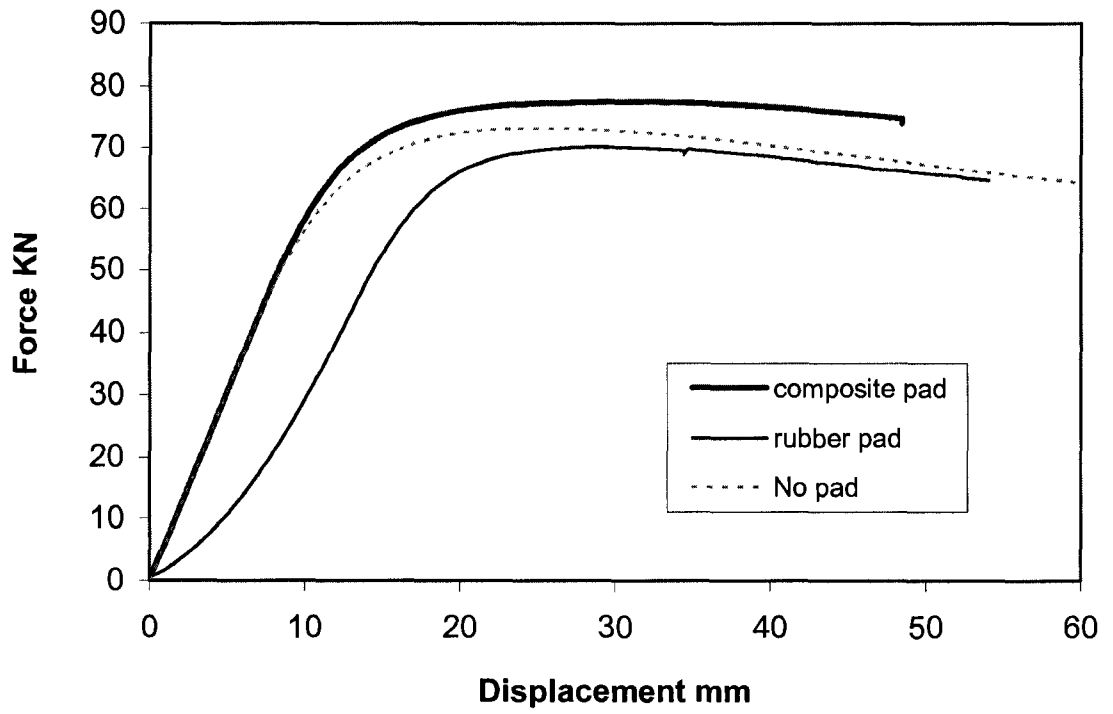


**Figure 4-21: Different pads affect the behavior of the aluminum tubes in bending**

## **Chapter 5**

### **Design and testing of Composite Tubes for Large Deformation**

#### **5-1 Introduction**

In Chapter 3, the behavior of different angle ply laminates was discussed. Some of the laminates such as unidirectional  $90^\circ$  laminate show a very low fracture strain while the medium angle ply laminates such as  $\pm 45^\circ$  may show even more than 10% strain before fracture. While carbon fibers have a fracture strain less than 1.3%, there are other mechanisms such as fiber rotation and extension of ductile thermoplastic matrix to result in nonlinear behavior of the laminate. Nevertheless, due to the domino effect explained in the previous chapter, for the laminates including zero degree layers, the failure of the laminate is sudden right after the failure of zero degree plies. In fact, in a tensile test, all layers are subjected to the same strain. When one layer fails, the load carried by that layer must be transferred to other layers before the tensile load is increased. However, in the laminates including zero degree plies, the portion of the load supported by zero degree

layers is very high. Upon failure of  $0^\circ$  layers, the remaining layers, which were subjected to the same strain but not necessarily high stresses, will be suddenly subjected to a jump in the stress level. Therefore, these layers will not be able to resist this high rate of loading and abrupt fracture would be inevitable.

In contrast to the behavior of the laminates in tension, in bending not all layers are subjected to the same strain. The strain at any point is proportional to its distance to the neutral axis. As such, the farther the layer is from the neutral axis, the strain would be higher. Therefore, low angle plies such as  $\pm 20^\circ$ , which have lower allowable strain, should be laid up as inner layers, and plies with higher allowable strain would be used to construct the outer layers. In this case, the whole structure can experience high strain and show large deformation. Finally, low angle plies would exceed their allowable strain and fail. Beyond this point, different phenomena may occur. One possibility is that the domino effect occurs and the rest of the layers fail quickly. The other possibility is that the layers with intermediate angle would keep the integrity of the tube and deform more. However, because some layers already failed, the load carrying capacity of the laminate would not be the same.

Beyond first ply failure, the behavior of the composite structures becomes more complex, and most analysis techniques are accompanied by considerable assumptions. For example, the common practice when a layer fails is to lower its contribution in overall strength and stiffness of the laminate by some percentage. However, there is no solid ground to which extent this reduction must be done! As such, predictions made by stress analysis of the laminates might be inaccurate, and they should be confirmed by experiments.

## 5-2 Design and testing the first composite tube

As discussed in the previous section, one possibility in behavior of composite tube is that the catastrophic fracture occurs upon fracture of  $0^\circ$  layers. In order to confirm or rule out this possibility, it was decided to manufacture a composite tube with  $[90^\circ_{20}/0^\circ_{20}]$  layup, and test the tube by four point bending test. In this work, the layups presented from left to right indicate the layers of the tube from the innermost layer toward the outermost layer. For example, for this tube,  $90^\circ$  layer is the inner ring and  $0^\circ$  layer is the outer ring of the tube. The subject of this test, however, was not to design a composite tube that shows the same behavior as its aluminum counterpart but simply to study the behavior of the composite tubes under bending, and verify if the domino effect in fracture should be considered. Figure 5-1 illustrates the set up for the four point bending test.

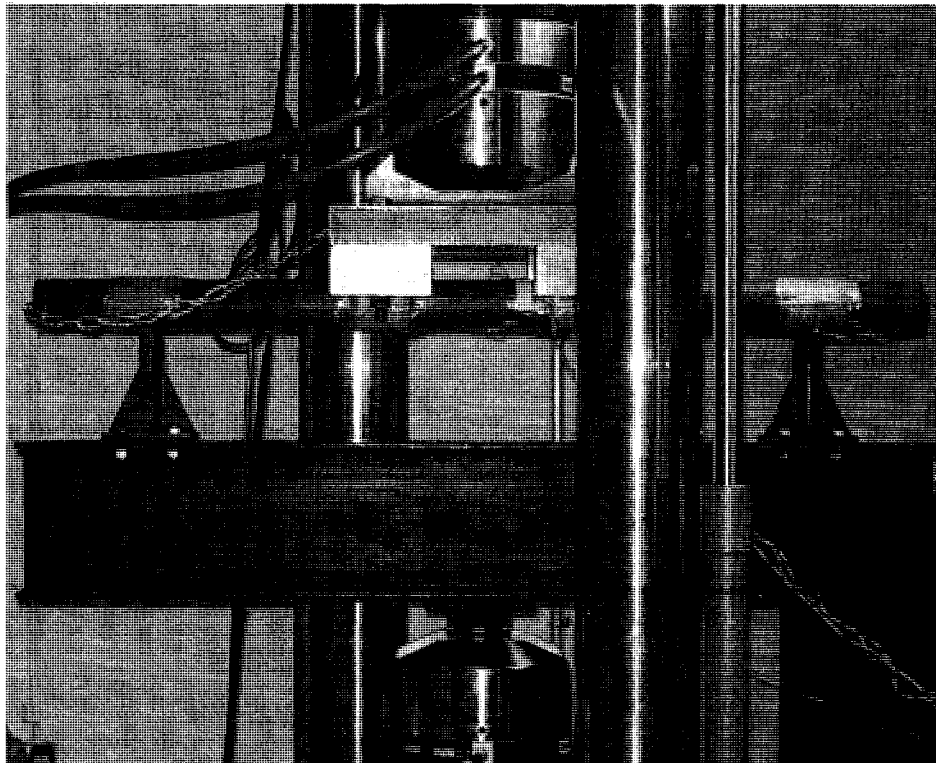


**Figure 5-1: Set up for the four-point bending test**

The tube was made by fiber placement technique. The inner and outer radii were 56mm and 64mm respectively. The tube includes two rings: the inner ring was 90° plies laid up in the hoop direction; the outer ring was 0° plies laid up in longitudinal direction to enhance the stiffness of the tube. The design was done based on the general design criteria of sandwich panels. The outer layer of the tube acts like the skin, so it must be strong and stiff to provide load carrying capacity of the tube. As such, zero degree layers were laid up as the outer ring. In contrast, the inner layers act like the core. Their duty is to keep the distance of the skin from neutral axis and act as a link between tension and compression zones. Core is usually made of foams or honeycombs. For the composite tubes, 90° layers play the same role while enhancing the hoop strength of the tube. Figure 5-2 illustrates the force versus longitudinal strain at the midpoint of the tube.

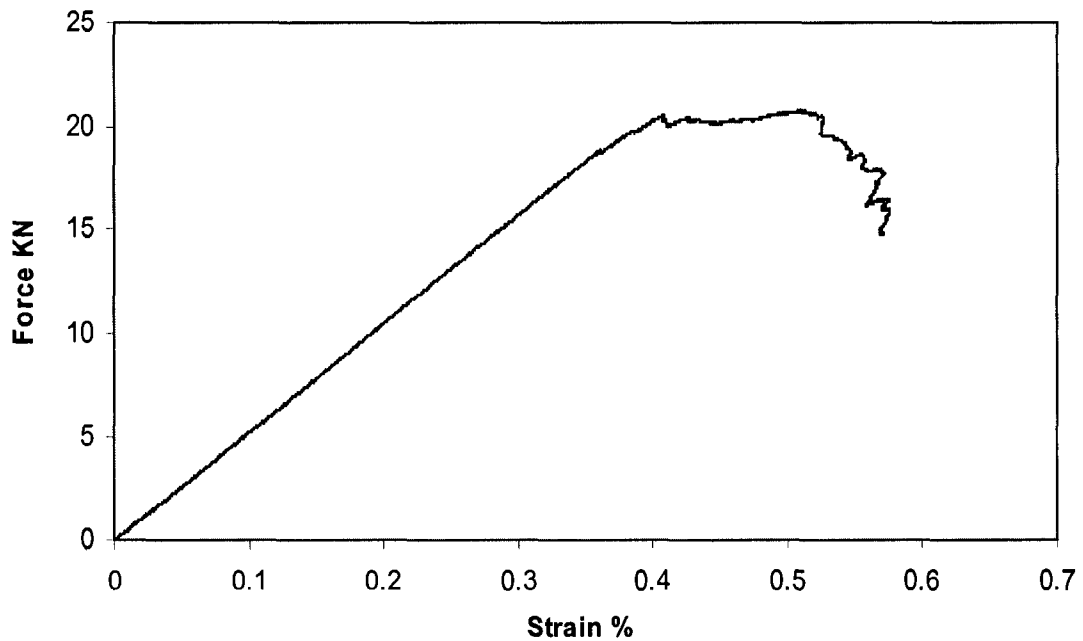


**Figure 5-2: Force- longitudinal strain at the mid-span of [90°<sub>20</sub>/0°<sub>20</sub>] composite tube**

The behavior of the tube was linear until a maximum 20 KN load was achieved. Until this point, the tube almost deformed uniformly, and the strain in tension zone, lower part of the tube, was equal to the strain in compression zone, upper part of the tube. However, the strength of the material in compression, 1500 MPa, is lower than that in tension, 1900MPa. As such, 0° layers failed due to the compression stresses in 1-1 direction. Upon their failure, the final fracture of the tube occurred in a fraction of a second. The graph shows some nonlinear behavior after the first ply failure. However, in terms of time, the period that the tube kept the load level was so short that it can be assumed that abrupt fracture occurred at this point.

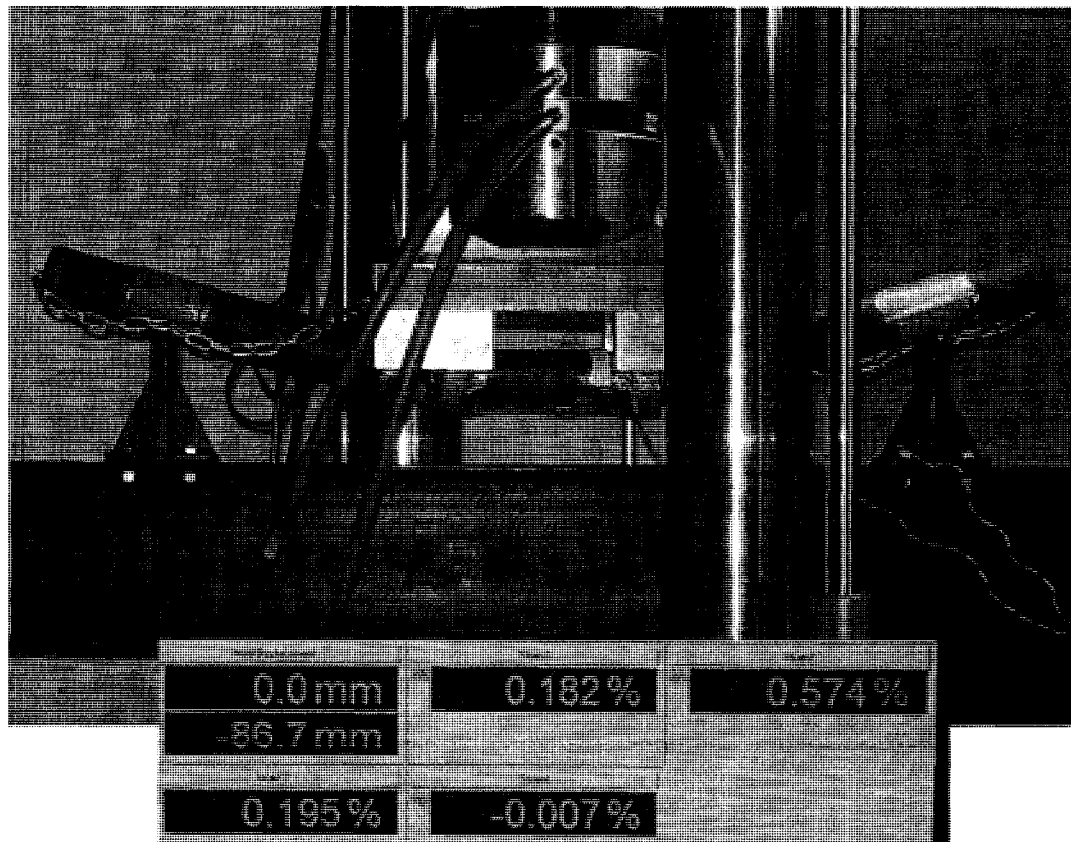


**Figure 5-3: Brittle fracture of the first composite tube**

Figure 5-3 shows the tube in the final stage. Even though the tube had been reinforced by fiber glass pads at the supports and loading noses, fracture occurred at a very low strain, around 0.55%. As it can be seen, the tube is not deformed with the same curvature through the length. In contrast, the tube is deformed into three straight pieces between reinforced points. The displacement of the loading noses at MTS machine was 86.7mm; however, this deformation is mostly due to the rigid body motion of the tube than real deformation due to the bending.

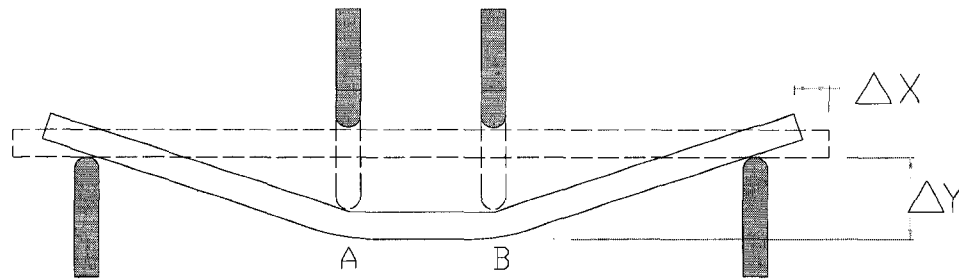


**Figure 5-4: Deformation of the tube is mostly due to the rigid body motion.**

Figure 5-4 schematically illustrates that the deformation of the tube during the four-point-bending test. As it can be seen, the large deformation,  $\Delta Y$ , recorded by the MTS machine is generally due to the rigid body motion of the tube than the flexural deformation. As soon as the fracture occurred at points A and B, the flexural stiffness of the tube is reduced considerably, so on applying a small load a large deformation such as  $\Delta Y$  can be achieved. However, the stress and strain levels in the tube remain very low. Moreover, because there is no restriction in the longitudinal direction, the tube would be displaced as much as  $\Delta X$  from each side to compensate for the vertical displacement. However, this displacement does not produce any kind of extensional stresses inside the tube, and the stress level will remain low.

Figure 5-5 also shows the longitudinal cross section of the tube after the test. The total fracture of the tube occurred within a fraction of second. It can be concluded that the brittle fracture of the zero degree layers was followed by the final abrupt fracture of the tube. In fact, this type of fracture could be predicted, and it was explained as the first fracture mode of composite tubes in the previous sections. The  $0^\circ$  layers are dominant in terms of strength and stiffness. They are also located at the farthest points from the neutral axis of the beam. So, upon their fracture no layer can afford to resist this extra load while the time for redistributing the loads would be very short. Therefore, a phenomenon, which may be called domino effect in fracture of composite laminates, would occur, and the sudden total fracture of the tube would be inevitable.

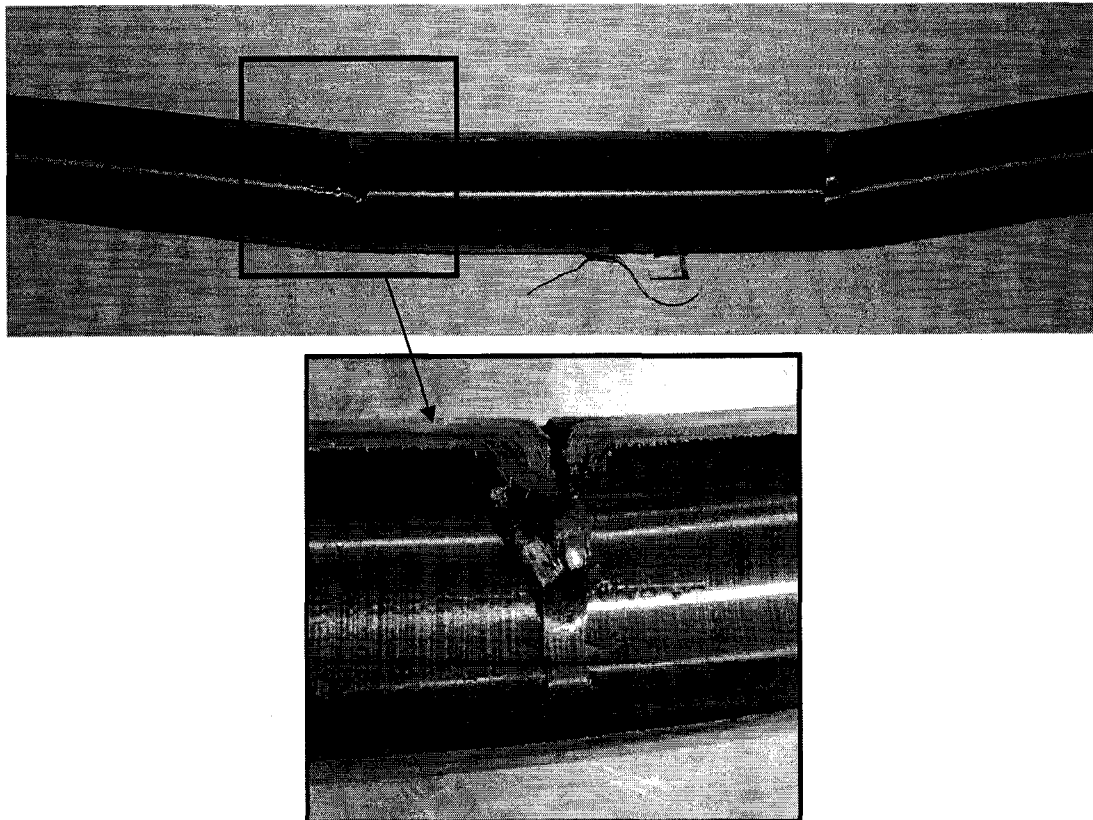


**Figure 5-5: Fracture occurred at the loading noses**

The results of the bending test on the first composite tube had several important lessons to be considered in the design of the next tubes:

- First, domino effect does occur in bending of the laminates as occurred for the laminates in pure tension, and it must be avoided to achieve large deformation.
- Second, designing the tube with similar structure as sandwich panel may provide the required strength and stiffness as the aluminum tube, but the composite tube would not deform in a ductile manner. The fracture strain of the tube would be small, and the energy absorption of the tube would be much lower than the aluminum tube.
- Finally, including low angle plies such as  $0^\circ$  layers, which are considerably stiffer than medium angle plies, into the stacking sequence of the tube is not appropriate. For example, the stiffness of  $0^\circ$  layers is almost three times of that of  $\pm 30^\circ$  layers. So, if there is a combination of these two laminates, upon fracture of  $0^\circ$  layers, the load carrying capacity of the laminate is reduced considerably. This reduction occurs in a fraction of a second, so a shock is produced inside the laminate. The stress lines have to readjust themselves in a very short time in order to transfer the loads to unbroken fibers. The whole process occurs too fast to let such a rearrangement take place. The strain rate is very high, and sudden failure of the tube is inevitable.

### 5-3 Design of a composite tube for large deformation

CFRP composites are brittle materials with small deformability and low fracture strain. For instance, low angle laminates such as  $\pm 20^\circ$  have higher strength and stiffness than many high grade aluminum alloys; however, their fracture strain is lower than that of aluminum. While it was known that laminates with comparable strength and stiffness as high grade aluminum do not show large deformation, an attempt was made to see if in the tubular form and under bending loads the behavior of the laminate could be different.

Design of the first composite tube with  $[90^\circ_{20}/0^\circ_{20}]$  layup was done according to the general design procedure for flexural structures subjected to bending loads. In simple terms, the stiff layers are laid up at maximum distance from the neutral axis to achieve high flexural stiffness and load carrying capacity for the beam. However, test results showed that having the composite plies in the tubular form would not help the composite laminates to show large deformation and high strain to failure if proper design is not made. As such, an innovative approach needed to be developed to systematically consider and include all potential mechanisms for large deformation. If successful, the approach may eventually present an optimum layup that provides the composite tubes with required strength, stiffness and toughness.

In the first step, it is necessary to understand for which strain level the tube is designed. For instance, if the composite tube is designed to be used as a helicopter landing gear, the extreme cases that the aluminum landing gear goes through shall be considered as the design threshold. Figure 5-6 schematically shows the helicopter during harsh landing. In the extreme case, the cross tubes almost deform to a horizontal position. It was shown in Chapter 4 that maximum strain in the aluminum landing gear reaches to 2.5%. The

shaded areas schematically illustrate the sections under plastic deformation. In fact the aluminum landing gear has varying thicknesses and outer diameters. As such, the moment of inertia varies throughout the length of the tube. As such, the maximum stress does not necessarily occur at the section with maximum bending moment. Therefore, stress at different sections may exceed yield stress, so extensive plastic deformation occurs and energy absorption capacity of the tube is increased. While the strain distribution is known, it would be possible to define the design threshold for composite tubes. As such, the goal would be to design a composite tube that illustrates the same strength and stiffness as its aluminum 7075-T6 counterpart. The tube should be capable of large deformation until 2.5% strain is achieved.

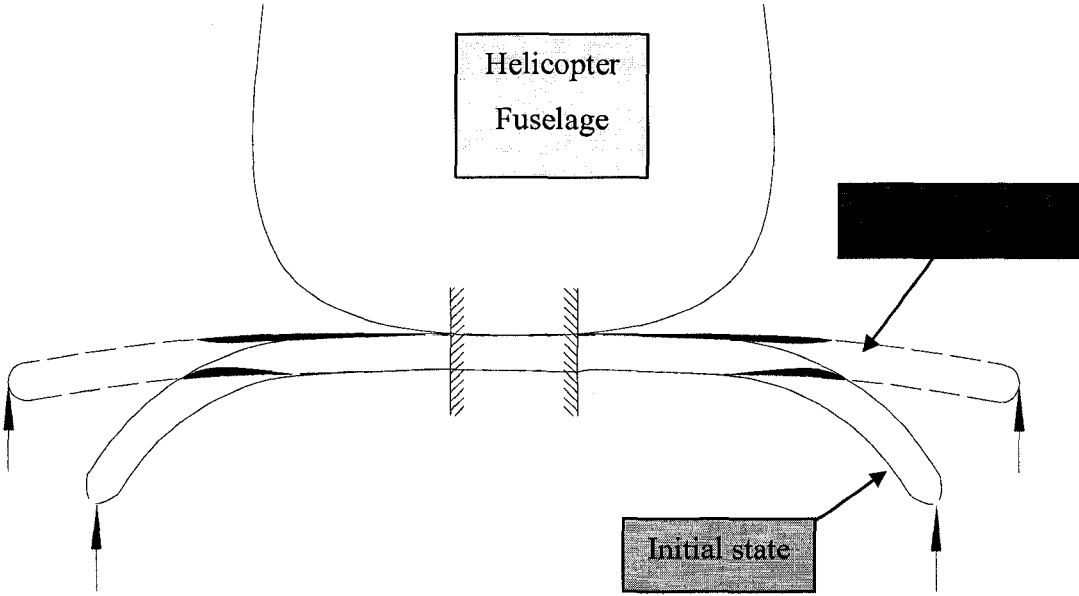


**Figure 5-6: Schematic presentation of harsh landing: Shaded areas represent the plastic deformation of the aluminum landing gear**

### 5-3.1 Strain controlled design

Figure 5-7 shows a cross section of the landing gear front cross tube in its thickest part, where the inner and outer radii of the tube are 56mm (2.25") and 88mm (3.5") respectively. The maximum total strain, 2.5%, occurs during the most severe crash scenario at this cross section. Meanwhile, it is assumed that the strain distribution is linear throughout the section. That is, strain is zero at the neutral axis and increases linearly to a maximum of 2.5% at the outermost point from the centroid.

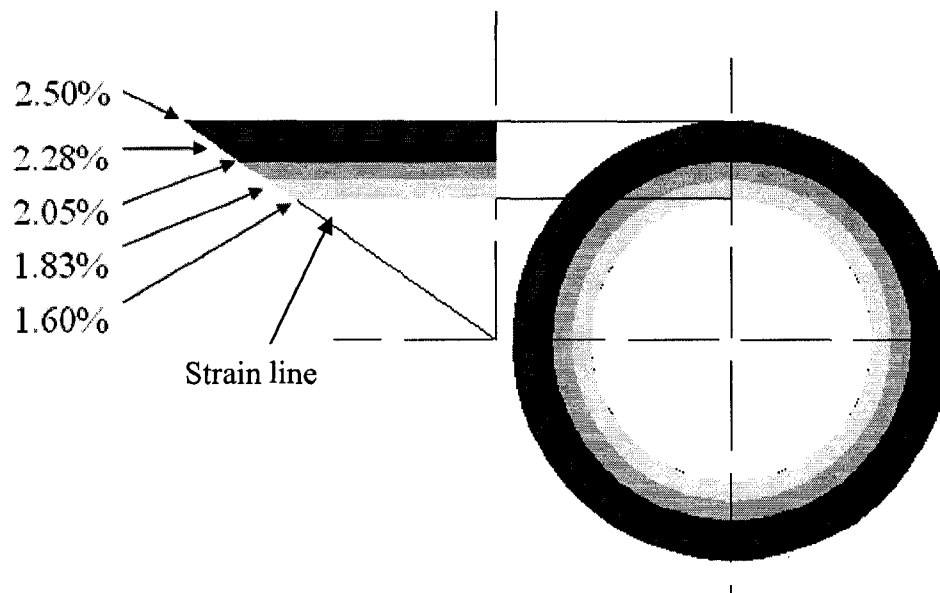


**Figure 5-7: Linear strain distribution at the thickest cross section of the landing gear front cross tube where ID 56mm (2.25") OD 88mm (3.5")**

While the strain distribution throughout the cross section was known, it was assumed that the composite tube would have the same inner and outer radii as the aluminum tube, and it would include only four different angle ply laminates, shown in Figure 5-7 by different

colors. As such, it would be possible to find the required minimum and maximum strains in each laminate. For example, the outermost layer should have a strain to failure more than 2.5%, and the innermost layer should have a failure strain more than 1.83% if this cross section of the tube is required to experience 2.5% strain.

	Aluminum	Carbon AS4/PEKK Composite Laminates					
		90°	0°	±20°	±25°	±30°	±45°
Strength MPa	500	80	2000	1250	1100	760	220
Strain to Failure %	11	0.8	1.5	1.8	2	2.5	10

**Table 5-1: Strength and Failure strain of Carbon AS4/PEKK composite laminates  
(Details of the measurements presented in Chapter 3)**

On the other hand, from Chapter 3, the strains to failure of different balanced laminates are known. Table 5-1 summarizes the strength and failure strain for a few balanced angle ply laminates. As such, according to the required strain for each layer, it would be possible to choose a proper laminate for each layer. For example, for the tube shown in Figure 5-7 according to Table 5-1, the outermost layer might be ±45° laminate while the next layers toward the innermost layer could be ±30°, ±25° and ±20° respectively. As such, a probable layup from inside towards the outside of the tube could be as follows:

$$[\pm 20^{\circ}_{n1} / \pm 25^{\circ}_{n2} / \pm 30^{\circ}_{n3} / \pm 45^{\circ}_{n4}]$$

With such a layup, a composite tube subjected to bending can deform until the maximum axial strain at the outermost layer of the tube reached 2.5% yet no layer has failed. Figure 5-8 schematically shows the strain distribution for such a composite tube.

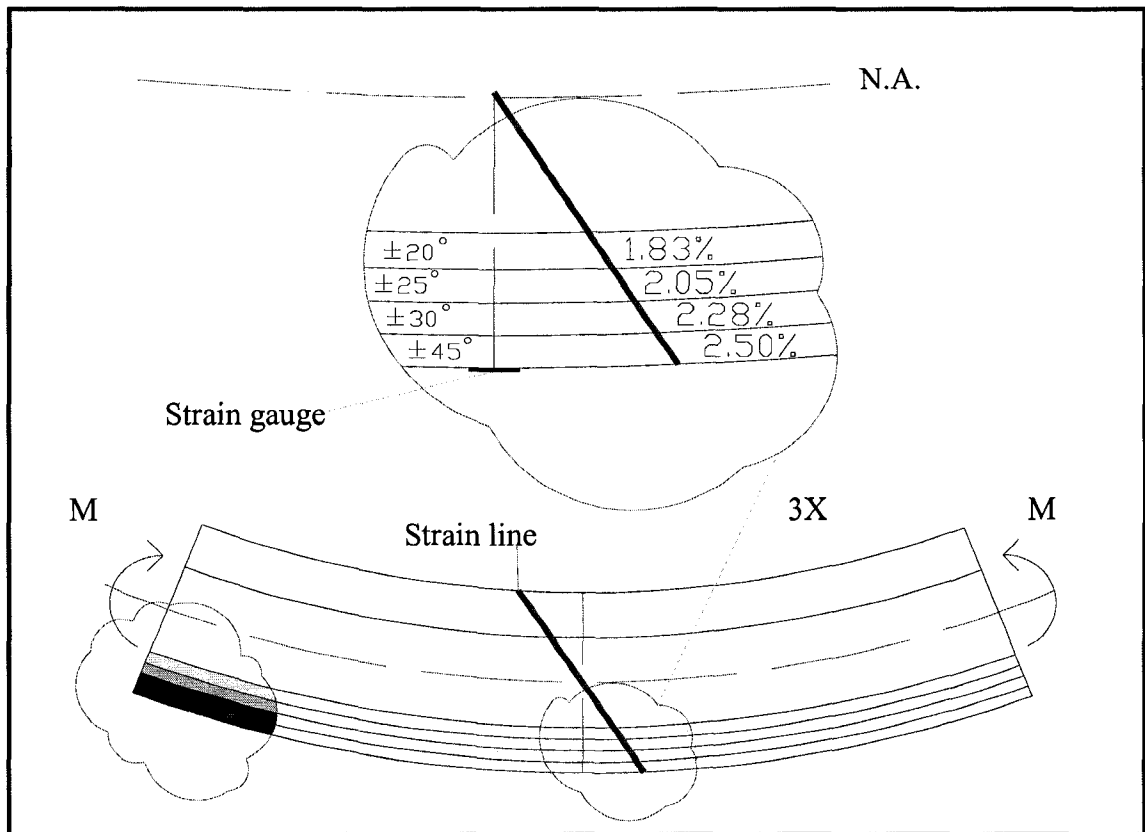


**Figure 5-8: Strain distribution in the composite tube.**

### 5-3.2 Design for strength and stiffness

A design according to the required strain for each layer does not specify the number of plies in each layer and does not guarantee the required strength and stiffness. Moreover, matching the strength and stiffness of the composite tube with those of the aluminum tube may require the composite tube to have different inner and outer diameters. As such,

the position of each layer might be slightly altered, so the required strain for each layer must be rechecked after the stress analysis of the tube is done.

Classical laminate theory was used to analyze the strength and stiffness of the composite tube. Among parameters studied are elastic, shear and flexural moduli, extensional stiffness, weight, strength and dimensions of the tube. The strain to failure and toughness of the tubes were examined experimentally to verify the accuracy of strain controlled design. Figure 5-9 shows a composite tube that is designed to be equivalent to a tube made of aluminum 7075-T6. Dimensions of the composite tube are not necessarily equivalent to those of the aluminum tube; however, in order to reduce the design parameters at this stage, it was assumed that both tubes have the same inner diameter.

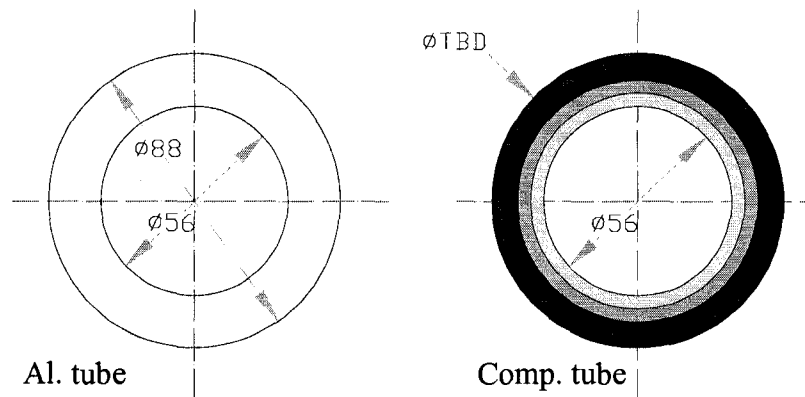


**Figure 5-9: Aluminum and composite tubes cross sections; Dimensions in mm.**

To start with the design, an aluminum tube with the inner diameter 56mm and wall thickness of 16mm is considered. The inner diameter of the composite tube is considered to be the same. For the first attempt, it was assumed that the composite tube also has the same thickness, and it is made of four layers recommended by strain analysis of the tube:

$$[\pm 20^{\circ}_{n1} / \pm 25^{\circ}_{n2} / \pm 30^{\circ}_{n3} / \pm 45^{\circ}_{n4}]$$

Furthermore, it is assumed that  $n_1=n_2=n_3=n_4$ . From the experiments, it was known that each ply after consolidation would have 0.1mm thickness. As such, if the thickness of the composite tube is also 16mm, each layer would have a thickness equal to 4mm. the number of plies in each layer would be 40, accordingly.

The stress analysis of the tube to find the optimum combination of plies is a very intricate task, however. The design parameters including inner and outer radii for each ring or layer, layup angle, weight and so many other parameters make the design task complex. For example, it can be shown that according to CLT, if all layers are laid up at  $\pm 26.5^{\circ}$  angle, the tube would comply with the requirements of stiffness, and manufacturing would be simpler. However, such a tube would not comply with the requirements of large deformation and energy absorption. Moreover, a trial and error method using computer software such as ANSYS would be very time consuming and expensive. As such, a simple approach was used to determine the preliminary design, and then the accuracy of the design would be evaluated using ANSYS analysis.

In order to simplify the analysis, a sandwich panel model is used. Figure 5-10 illustrates cross sections AA' and BB' for the aluminum and composite tubes, respectively. The hatched areas are considered as the skins of the sandwich panels. For the sake of analysis, the cores, which are in fact empty spaces in this case, are modeled to be made of a material with very low strength and stiffness, so that the cores would have no considerable effects on the analysis. As a result, designing a composite tube to match

with an aluminum tube is simplified to the design of a composite sandwich panel that shows the same strength, stiffness and strain to failure as an aluminum panel.

As the layup of the composite tube has already been chosen according to the strain requirements of the landing gear front cross tube, the main challenge at this stage is to find the optimum numbers of plies for each layer so that a light composite tube with similar extensional, flexural and shear stiffness as the aluminum tube.

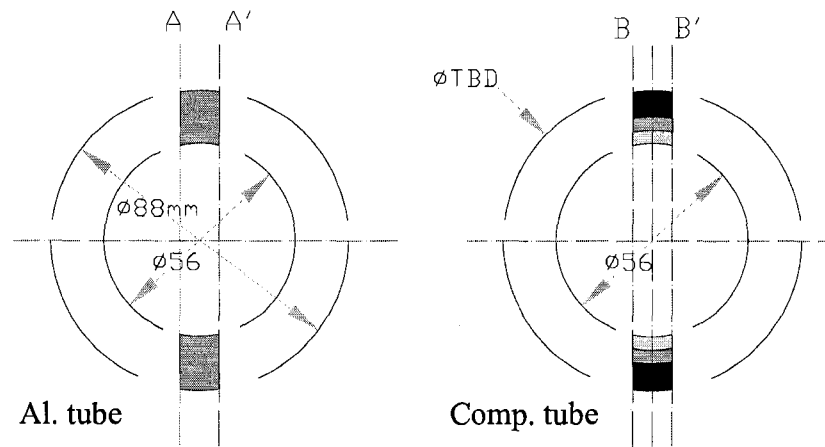


**Figure 5-10: Cross sections AA' and BB' for the aluminum and composite tubes**

### 5-3.3 Stress analysis according to CLT

Figure 5-11 shows two aluminum and composite sandwich panels cut from the tubes shown in Figure 5-10. The small curvatures of the panels are ignored. The skin of the aluminum panel is made of high grade aluminum 7075-T6, and that of the composite panel is made of Carbon AS4/PEKK. The cores of both panels are made of a very low mechanical property material, called foam hereinafter.

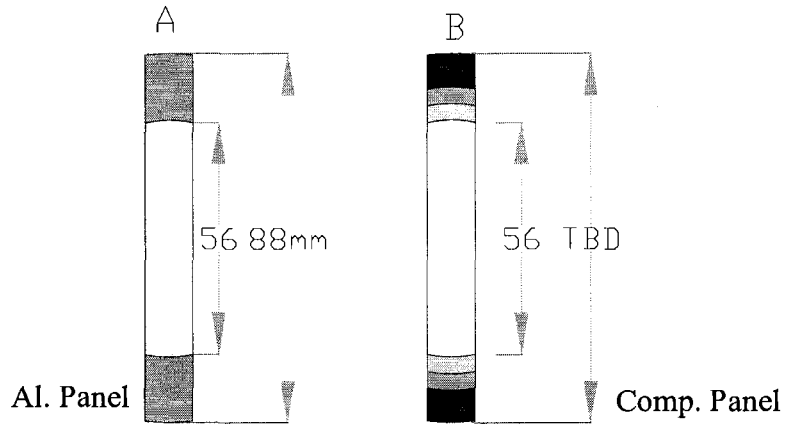


**Figure 5-11: Aluminum and composite sandwich panels**

Table 5-2 shows the mechanical properties of these materials. The properties of aluminum were obtained from Metweb website while those of Carbon AS4/PEKK were provided by Cytec Engineered Materials Ltd. The data for the foam were simply assumed to be very small.

	Aluminum 7075-T6	Carbon AS4/PEKK	Foam
$E_{11}$ , GPa	70	140	5
$E_{22}$ , GPa	70	10	5
$G_{12}$ , GPa	27	4	1
$\nu_{12}$	0.3	0.3	0.3
$S_{11}$ Tension, MPa	500	1900	10
$S_{22}$ Tension, MPa	500	80	10
$S_{12}$ , MPa	300	180	5
$S_{11}$ Compression, MPa	500	1500	10
$S_{22}$ Compression, MPa	500	250	10

**Table 5-2: Materials properties**

A program called Laminate Analysis Program or LAP was used to carry out calculations based on Classical Laminate Theory. The dimensions of the panels are given in Figure 5-11. The calculations are done for the unit of width of the panel, so the widths of the panels are not required. Moreover, at the first attempt, the height of the composite panel, TBD, was assumed to be 88 mm. Table 5-3 compares the extensional, torsional and flexural stiffness of both aluminum and composite sandwich panels. Also, the weights per unit length of both tubes are compared.

As the cross tube of the landing gear has high length to width ratio and no pressure exist inside the tube, the structure can be considered as a long beam. As such, one of the main design parameters is to match the longitudinal flexural stiffness,  $EI_{xx}$ , of the composite tube with that of the aluminum tube. As it can be read from the table, with the current layup, the longitudinal flexural stiffness of the composite tube is less than that of the aluminum tube. So, either the thickness of the composite tube must be increased or stiffer laminates such as  $\pm 30^\circ$  should substitute some of the plies in  $\pm 45^\circ$  layer, which are less stiff. On the other hand, the flexural stiffness in the  $y$ - $y$  direction is quite low for the composite tube. This may be interpreted that some  $90^\circ$  plies must be added to the layup. However, the concern would be the very low fracture strains of  $90^\circ$  laminates. However, the best place to layup the  $90^\circ$  plies is at the innermost points that requires the minimum failure strain. Moreover, the  $90^\circ$  layer can resist the hoop stresses, and other layers can be built upon this ring. With the current layup, extensional stiffness of the composite tube,  $AE_{xx}$ , also needs to be improved to match with the aluminum tube. This might be done by employing more low-angle plies such as  $\pm 30^\circ$  instead of  $\pm 45^\circ$  that improves both flexural and extensional stiffness of the tube at the same time.

	Aluminum 7075-T6	Carbon AS4/PEKK
Lay up	NA	$[\pm 20^{\circ}_{40} / \pm 25^{\circ}_{40} / \pm 30^{\circ}_{40} / \pm 45^{\circ}_{40}]$
Tube Dims, mm	ID 56 OD88	ID 56 OD88
$E_{xx}$ , GPa	70	56
$E_{yy}$ , GPa	70	14
$G_{xy}$ , GPa	27	26
$EI_{xx}$ , N.mm	2.95E+09	2.1E+09
$EI_{yy}$ , N.mm	2.95E+09	0.66E+09
GJ, N.mm	4.55E+09	4.69E+09
Tube Area mm <sup>2</sup>	3619	3619
$AE_{xx}$ , MN	253	202
Weight Kg/m	13.7	7.1

**Table 5-3: General design parameters of the aluminum and composite tubes**

This type of qualitative analysis, even though quite straightforward, is reasonably accurate and sheds light into achieving the final layup. As the final design, the composite tube should have the same strength and stiffness as its aluminum counterpart and show large deformation until the maximum strain 2.5% is achieved. Nevertheless, the outcome of this kind of stress analysis is not necessarily enough to achieve the final design as there are many other parameters involved. For example, after a ply fails, its effect on the total stiffness of the structure must be reduced. However, there is no consensus among

researchers on how this must be done. Most common practice is to reduce the mechanical properties of that ply by 50%; however, there is not enough solid proof to show the legitimacy of this type of approximation. Another parameter, for instance, is the delamination and crack propagation among the layers. It will be shown in the next sections how these two phenomena would be employed in the final design of the composite tube to improve deformability and toughness of the tube. Nevertheless, neither of them can be readily implemented in the analytical work.

In order to discover other parameters affecting the behavior of composite tubes under bending, experiments are necessary. In fact, both stress analysis techniques and experimental work should be used side by side in this research to assure the optimum design would be achieved. While experimental work is involved, restrictions due to the manufacturing and testing must also be considered and addressed. For example, at the early stages of this research, only limited angles, such as  $0^\circ$ ,  $90^\circ$  and  $\pm 45^\circ$ , could be laid up using fiber placement machine available at AMTC-NRC. As such, a procedure consisting design, analysis, manufacturing, testing and modification was set up throughout this research to progressively move toward the final design.

At the first step, a layup is suggested for the composite tube that complies with the requirements of strain controlled design as explained in Section 5-3.1. Then the Laminate Analysis Program is used to modify the layup so that the tube would have the same strength and stiffness as its aluminum counterpart. While the layup is known, ANSYS is employed to recheck the accuracy of the design. The tube is then made using fiber placement technique, and experimental work is carried out by three or four-point bending tests. At the end of each test, the fracture modes and reason of failure are examined. The

force-deflection or force-strain curves are drawn for a point at the mid-span of the tube to check the strength and stiffness of the tube. Finally, all observations are used to carry out necessary modifications, and then the process would be repeated until the optimum design is achieved.

#### **5-4 Design, manufacturing and testing the second composite tube**

As much as it could be verified in the open literature, no experimental result on the behavior of composite tubes subjected to bending is found. As such, it would be necessary to carry out a few tests on composites tubes to collect general data and observe the flexural behavior of this type of brittle material in bending.

The second composite tube was scheduled to be fabricated by NRC-AMTC in summer 2006 using the fiber placement technique. Even though according to the design procedure explained in Section 5-3, different stacking sequences could be proposed, manufacturing problems highly restricted the design. In fact, to lay up the plies at different angles, different head rollers must be installed on the fiber placement machine. The design and manufacturing of these rollers was very time consuming for NRC-AMTC. Moreover, even for one specific angle, different rollers are required to layup the slit prepreg tape as the diameter of the tube increases. As such, the design of the second tube was restricted to the available rollers:  $0^\circ$ ,  $90^\circ$  and  $\pm 45^\circ$  angles.

A composite tube including only these angles may not show the same performance as an aerospace grade aluminum tube; however, the results can be used to learn more about the behavior of the composite tubes under bending in general and verify if there was still the domino effect after  $0^\circ$  layers fail.

#### 5-4.1 Design of the layup

Since the only possible manufacturing angles were limited to  $0^\circ$ ,  $90^\circ$  and  $\pm 45^\circ$ , Step 1 of the design procedure, which is strain controlled design, was skipped. As such, the first objective of the test was set to verify if delamination between adjacent layers occurs or not. If yes, it would be desirable to have controlled delamination at some stage of the test to increase energy absorption and toughness of the tube. As such, the inner layers of the tube can be a combination of  $90^\circ/0^\circ$  in an alternative fashion. Considering the manufacturing concerns, it was decided to alternate between the layers after laying up 10 plies in each round. So a layup such as  $(90^\circ_{10}/0^\circ_{10})_n$  could be suitable to investigate the first objective of the test; however, the number of the layers,  $n$ , would be calculated to match with the strength and stiffness requirements.

The second objective of the test was to observe the behavior of the  $\pm 45^\circ$  laminate in tubular form and adjacent to  $0^\circ$  layers. As explained in Chapter 3,  $\pm 45^\circ$  laminates are capable of large deformation while loaded by in-plane forces. It was observed that some of the tensile samples show more than 10% strain before the failure occurs; however, a combination of  $0^\circ$  and  $\pm 45^\circ$  plies is not useful to improve the failure strain of the unidirectional laminates. As such, it would be important if the  $\pm 45^\circ$  layers deform more and keep the integrity of the tube after other low angle layers fail. Recall from Chapter 3 that some of the low angle laminates, such as  $\pm 20^\circ$ , broke into small pieces after failure. For a structure like the landing gear, this type of behavior would be fatal. In simple terms, it would be crucial for the tube to keep its integrity after failure even though its load carrying capacity reduces considerably. Therefore, it was decided to have a jacket of  $\pm 45^\circ$  plies at the outermost layer of the tube to explore the second objective of the test.

#### 5-4.2 Stress analysis of the layup

According to the above mentioned considerations, the proposed layup for the second composite tube can be as follows:  $[(90^\circ_{10}/0^\circ_{10})_{n1}/\pm 45^\circ_{n2}]$ , yet  $n1$  and  $n2$  are to be determined through the stress analysis of the tube.

It was assumed that the aluminum tube has the inner and outer radii 56mm and 76mm respectively. In order to find the number of layers,  $n1$  and  $n2$ , for the composite tube, Laminate Analysis Program was used. In the same way as the procedure explained in Section 5-3, the comparison was done between two aluminum and composite sandwich panels to determine the proper layup.

After a few modifications, it was observed that a composite tube with  $[(90^\circ_{10}/0^\circ_{10})_3/\pm 45^\circ_{25}]$  layup has the closest design parameters to the aluminum tube. However, as it can be seen in Table 5-4, the outer diameter of the composite tube is slightly larger than that of the aluminum tube. Yet, the flexural stiffness of the composite tube is lower. However, both objectives of the test would be accomplished by this layup, so the dimensions of the composite tube was kept as closest possible to that of aluminum tube.

Another characteristic of this tube is that in contrast to the first tube, the  $0^\circ$  layers were not laid up in the farthest location from the neutral axis of the beam. So, they would carry less loading, and there would be higher chance that upon their failure, the load redistributed among other layers, and a sudden fracture does not occur. Furthermore, the  $0^\circ$  layers were alternated by  $90^\circ$  layers. Through this, two goals might be achieved. First, some sort of delamination may occur between adjacent layers. Second, there is a chance that  $0^\circ$  layers act independently, and less domino effect will be observed.

	Aluminum 7075-T6	Carbon AS4/PEKK
Lay up	NA	[(90° <sub>10</sub> / 0° <sub>10</sub> ) <sub>3</sub> / ± 45° <sub>25</sub> ]
Tube Dims, mm	ID 56 OD76	ID 56 OD78
E <sub>xx</sub> , GPa	70	55.7
E <sub>yy</sub> , GPa	70	55.7
G <sub>xy</sub> , GPa	27	18.6
EI <sub>xx</sub> , N.mm	1.53E+09	1.29E+09
EI <sub>yy</sub> , N.mm	1.53E+09	1.25E+09
GJ, N.mm	2.37E+09	2.11E+09
Tube Area mm <sup>2</sup>	2073	2315
AE <sub>xx</sub> , MN	145	129
Weight Kg/m	5.6	3.4

**Table 5-4: Design parameters of the second aluminum and composite tubes**

The second composite tube has 110 layers in total. The tube was made using the fiber placement machine at NRC-AMTC. The load applied on the roller was about 40 Kg. The manufacturing temperature was about 600° C. This temperature is higher than the processing temperature of the material using compression molding technique. However, it is applied in a short period, so the material does not degrade. The inner diameter of the tube was 56mm while the tube thickness was 10.8mm.

#### 5-4.3 Testing and failure analysis for the second composite tube

Following the procedure recommended in Section 4-4, the composite tube was reinforced by a composite fiber glass pad to avoid local immature failure. Figure 5-12 shows the process of laying up fiberglass pad on the composite tube. Vacuum bagging was used to extract extra epoxy resin and to improve the quality of fiberglass pad. The curing was done at room temperature to avoid any undesirable effect on the composite tube.

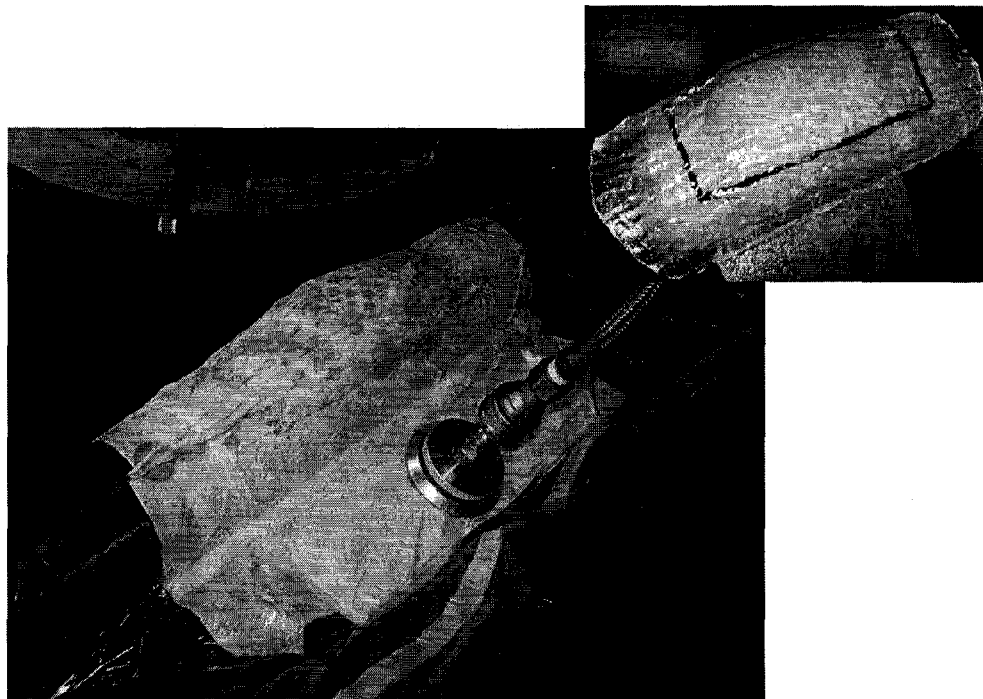


**Figure 5- 12: Laying up a tapered fiber glass pad on the composite tube**

Four double -*T*- strain gauges were installed on the composite tube to measure axial and circumferential strains at the mid span and 12 cm offset from the mid point: two of them at the bottom line and two in 45° circumferentially offset (see Figures 5-13 and 5-14).

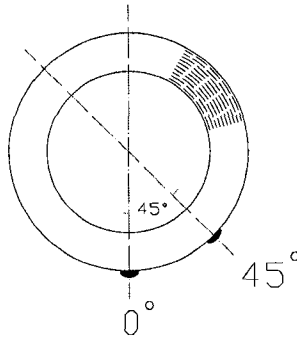


**Figure 5- 13: Location of strain gauges at the bottom line and 45° offset**

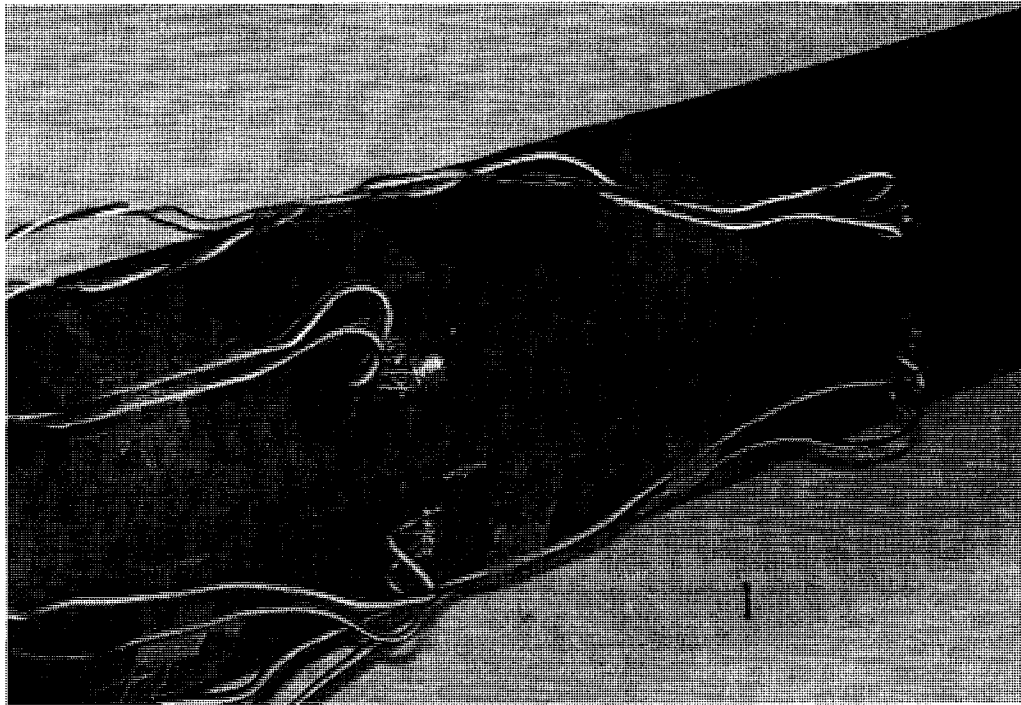


**Figure 5-14: Four *T* strain gauges installed on the second composite tube.**

Though eight strain gauges were installed, the MTS machine in the composite lab of Concordia University is equipped to read a maximum of 4 strain gauges simultaneously. As a result, the test was repeated to measure strains at all locations and directions. Repeating the test was only possible before the first ply failure happens. Beyond this

limit, the behavior of the material and structure would not be the same and the test is not repeatable. Table 5-5 shows the testing procedure. On the first run, the tube was loaded until maximum axial strain at the mid point reached to 0.3%. Strains at the axial and circumferential directions were measured at the mid span and 12cm offset from the mid point by four strain gauges located at zero degree (Figure 5-13). At this low level of strain, it is very unlikely that any serious damage was imposed to the tube, so the test would be repeatable. In the second run, strains at 45° offset were measured. To assure that the maximum strain in the tube does not exceed 0.3% the load level was checked. As it will be observed in the next graphs, for the first and second runs, the maximum applied load was 20KN. For the third and fourth runs the same procedures as first and second runs were followed; however this time, the criteria to stop the test were to achieve 0.6% strain at the mid-span of the beam or hearing a considerable noise indicating onset of the crack propagation, whichever occurs earlier.

The fifth run was the most crucial run. At this stage, the tube was loaded until the maximum axial strain at the mid span of the tube reached to 3.5%. It would be possible that the tube never reached to this strain level, but the test target was set for. However, at any time that a major fracture occurred, and the load carrying capacity of the tube dropped considerably, the test would be halted.

	<b>Axial strain measured</b>	<b>Circumferential strain measured</b>	<b>Criteria to stop the test</b>
<b>First run</b>	Mid span & offset Zero degree	Mid span & offset Zero degree	Max axial strain at mid point < 0.3%
<b>Second run</b>	Mid span & offset at 45 degree	Mid span & offset at 45 degree	To the maximum load reached in the first run
<b>Third run</b>	Mid span & offset Zero degree	Mid span & offset Zero degree	Max axial strain at mid point < 0.6%
<b>Forth run</b>	Mid span & offset at 45 degree	Mid span & offset at 45 degree	To the maximum load reached in the third run
<b>Fifth run</b>	Mid span at Zero degree & 45 degree	Mid span at Zero degree & 45 degree	Up to failure of the tube or Max axial strain at mid point < 3.5 %

\* Zero degree: strains are measured at bottom line of the tube

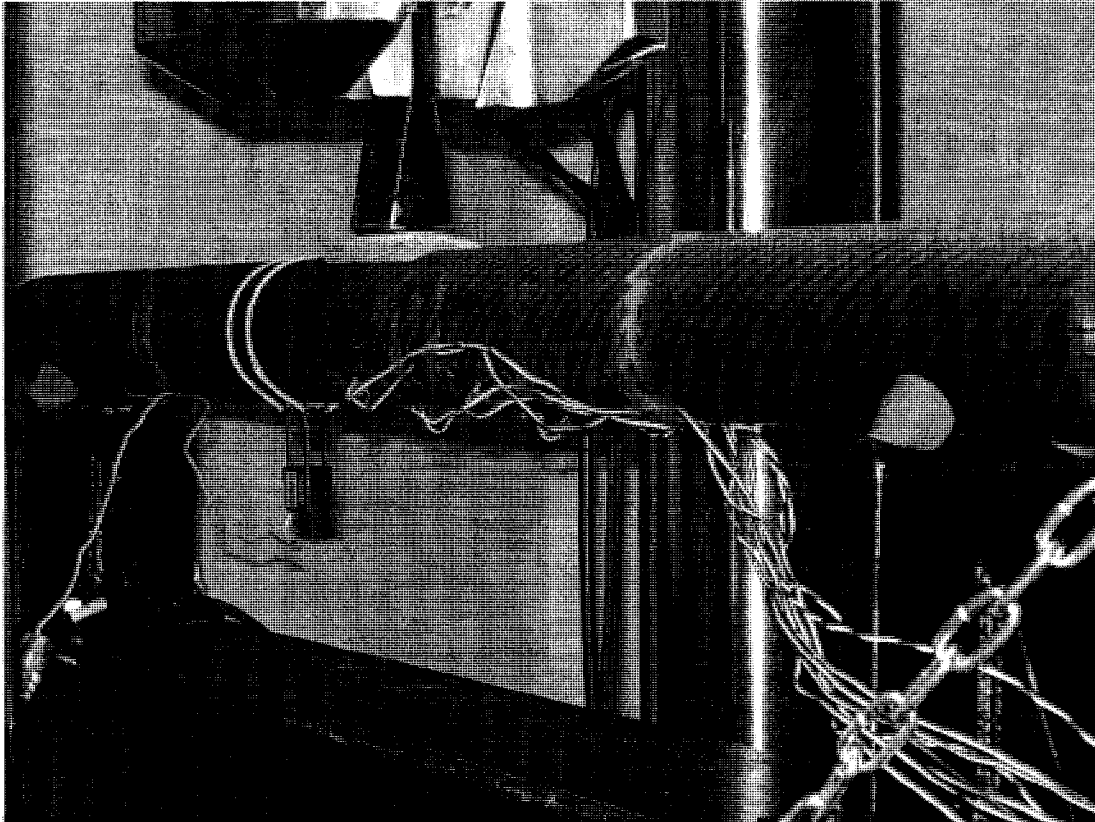
\* 45 degree: strain are measured in 45° circumferentially offset from the bottom line

**Table 5-5: Test plan for the second composite tube**

#### **5-4.4 Testing the second composite tube: first run**

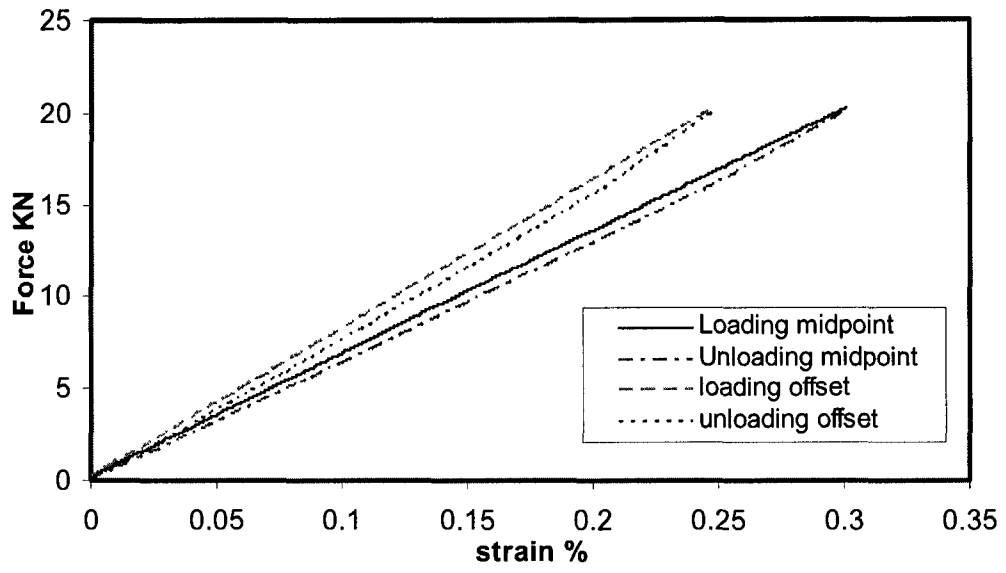
The first test run was limited to the point at which the maximum strain at the bottom line of the tube was about 0.3 %. This limit is well in the elastic zone of all layers, so it was possible to repeat the test and measure the strain at other locations in subsequent runs.

Figure 5-15 shows the test set up for this run.



**Figure 5-15: Testing the second composite tube: first run**

Figures 5-16 & 5-17 show the force variation versus axial and circumferential strains at the mid-span of the tube and at 12 cm axially offset from the midpoint.



**Figure 5-16: Load-axial strain at the midpoint and at 12 cm offset**  
**(At 0° with respect to Figure 5-13)**

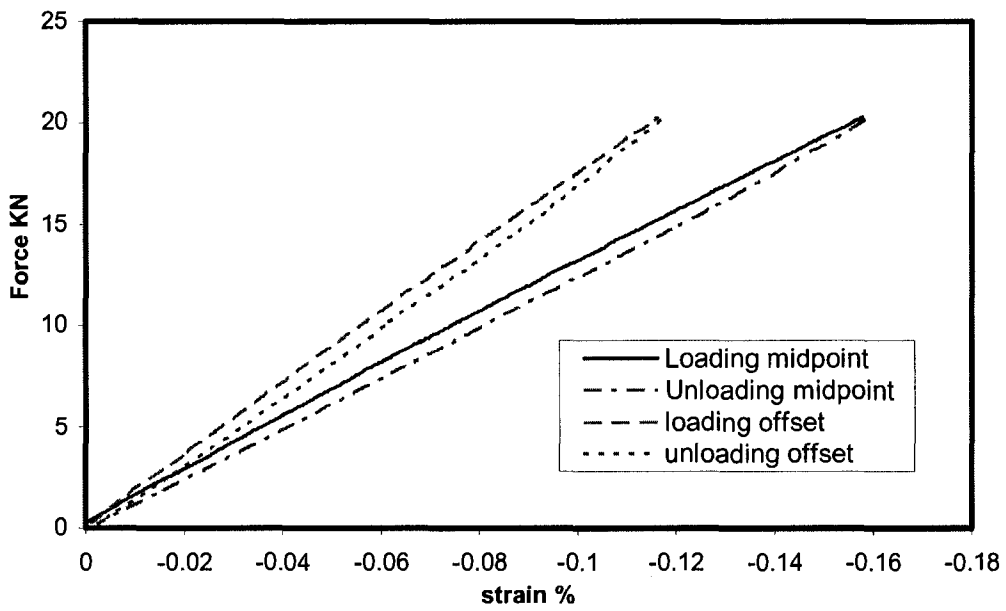


**Figure 5-17: Load-circumferential strain at the mid point and at 12 cm offset**  
**(At 0° with respect to Figure 5-13)**

### 5-4.5 Testing the second composite tube: second run

The second run was planned to measure the strains at 45° angular offset from the bottom point. To assure that the maximum strain at the bottom line does not exceed 0.3% - the limit set at the first run- the load level in the second run was kept to the same level of the first run (20 KN); however, it was obvious that the strain measured at 45° is less than 0.3%. Figures 5-18 & 5-19 show the results at 45° with respect to Figure 5-13.

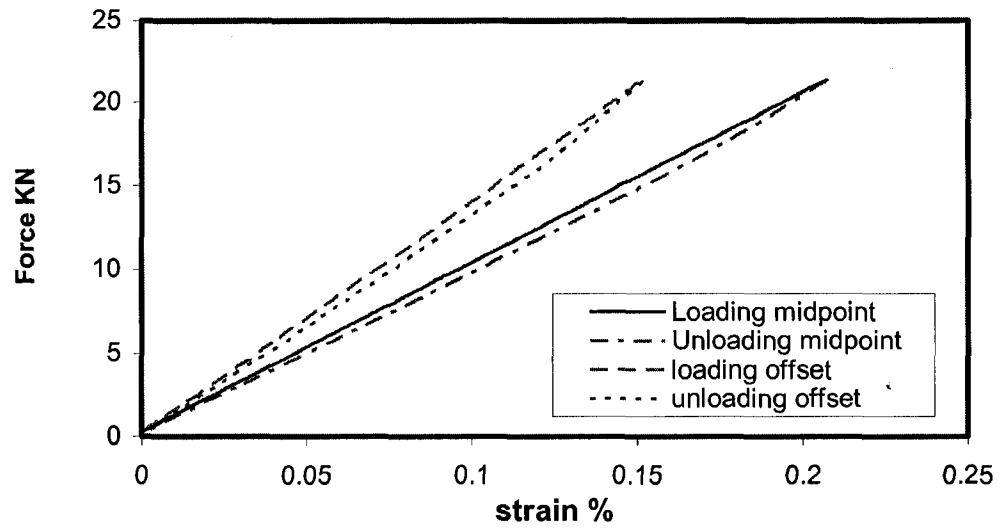


Figure 5-18: Load-Axial strain at the mid point and at 12 cm offset at 45°

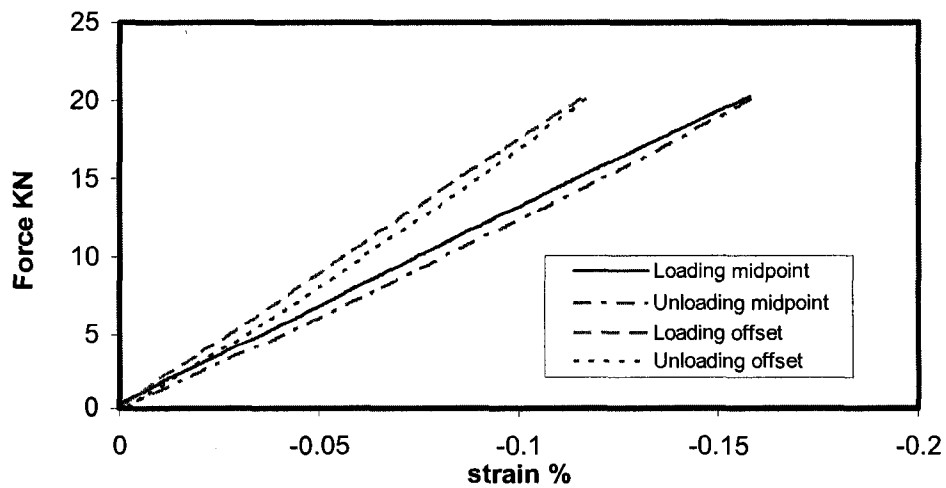


Figure 5-19: Load-Circumferential strain at the mid point and at 12 cm offset in 45°

### 5-4.6 Testing the second composite tube: third run

For the third run, the tube was planned to be loaded until the maximum axial strain at the bottom line of the tube reached to 0.6% or to the point that the first sound of failure was heard. In this test, the latter was the case and test was stopped at 0.55% strain. Figures 5-20 & 5-21 show the results.

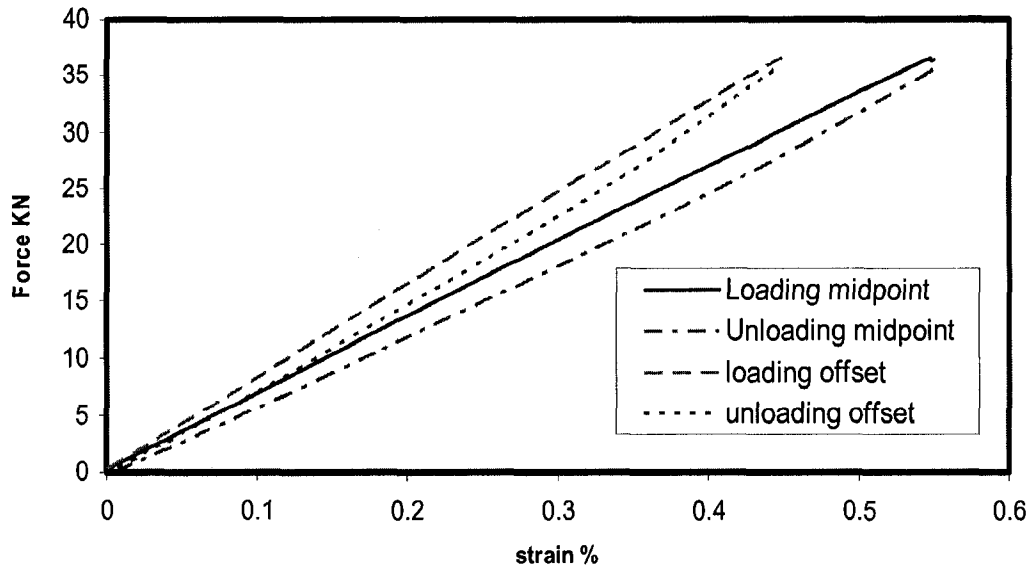


Figure 5-20: Load-Axial strain at the mid point and at 12 cm offset at 0°

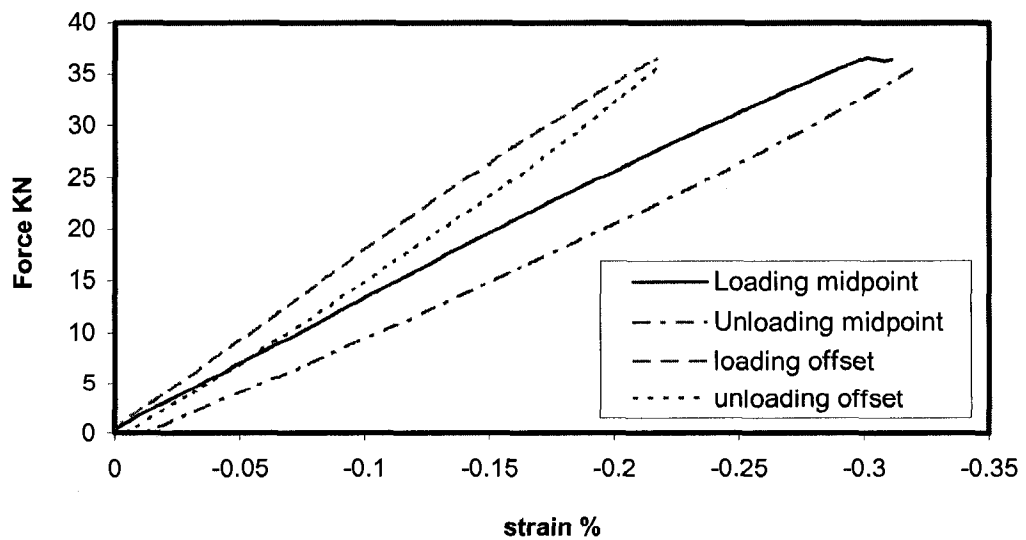


Figure 5-21: Load-Circumferential strain at the mid point and at 12 cm offset at 0°

### 5-4.7 Testing the Second composite tube: fourth run

The fourth test was the last to measure the strains at 45° circumferentially offset from the bottom line. The load level was limited to the same level as the third run to avoid exceeding the maximum strain at the bottom line from 0.55%. Figures 5-22 & 23 show the results.

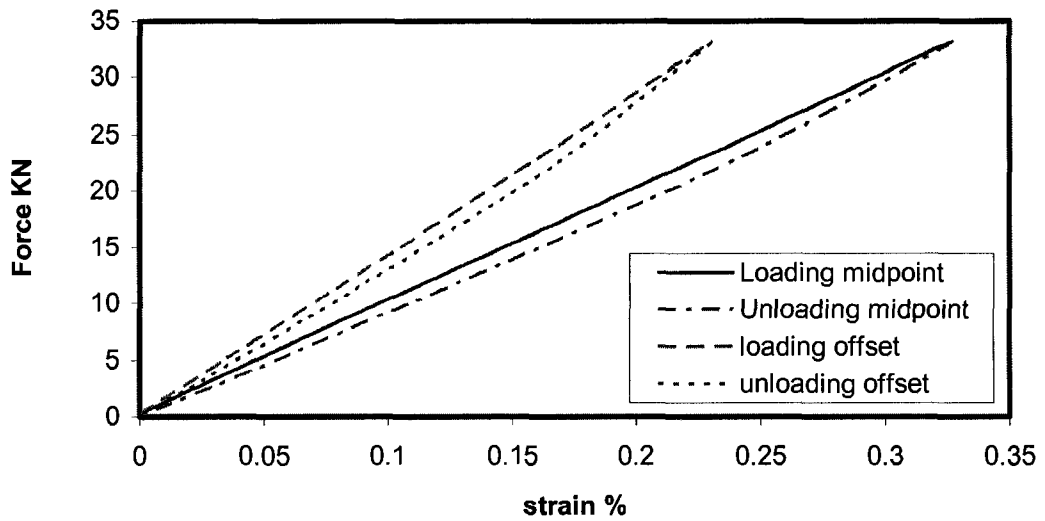


Figure 5-22: Load-Axial strain at the mid point and at 12 cm offset at 45°

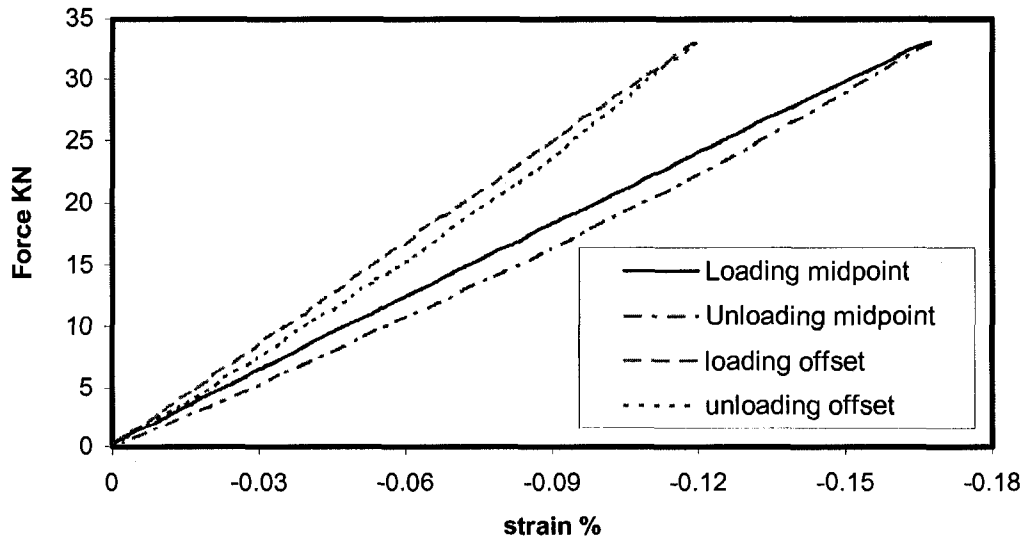
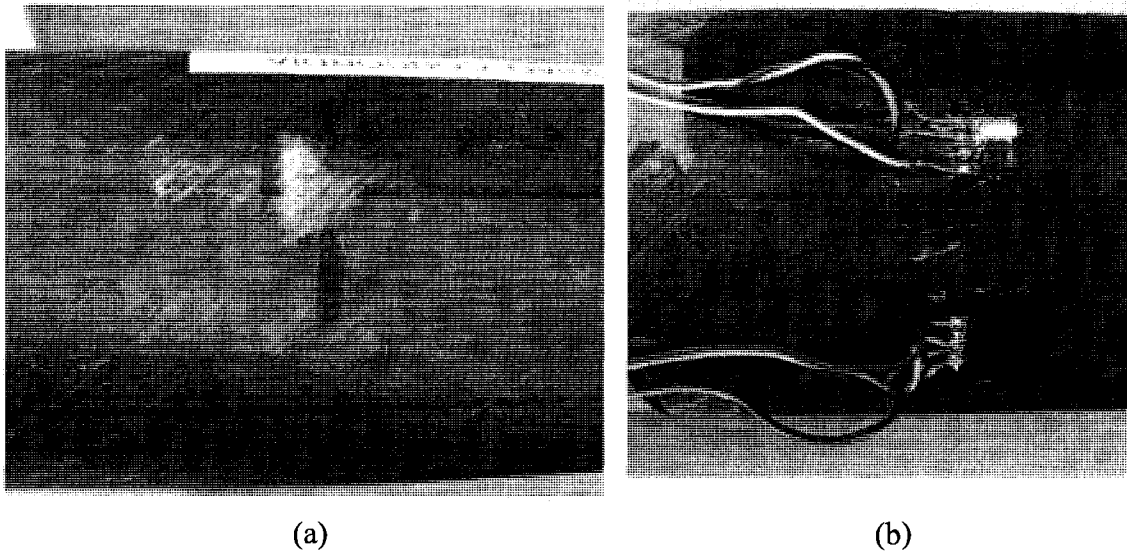


Figure 5-23: Load-Circumferential strain at the mid point and at 12 cm offset at 45°

#### 5-4.8 Final test on the second composite tube

Upon completion of the tests in the elastic zone, the composite tube was examined for any failure or fiber crushing before running the final test. The only minor problem observed was a small dent at the supporting points, Figure 5-24. Though a very similar dent had been observed on the aluminum tube, it was decided to wrap the support points with a few layers of fiber glass to assure that the failure would be due to bending and not due to shear or bearing stresses or any other kind of premature failure. Moreover, strain gauges were examined to see if there was any indication of delamination or failure of the soldered wires. Fortunately, the procedure used for installation of the strain gauges was appropriate and no problem was observed.



**Figure 5-24: (a) Small dent at the support points, (b) No delamination or failure in strain gauges**

After four successful tests in the elastic zone had been accomplished, there was no choice but to select four out of eight strain gauges to measure the local strains during the final run. The strain gauges at the midpoint  $0^\circ$  were essential as it was expected the maximum stresses and strains happen at this point. For another pair of strain gauges, it was decided to focus on stress distribution at the mid-span rather than at the offset along the axial direction. Therefore, for the last run the strain gauges installed at the mid span of the tube in both  $0^\circ$ ,  $45^\circ$  offset locations (see Figure 5-13) were used to measure strain in the axial and circumferential directions. Figures 5-25 a & b and Figures 5-26 a & b illustrate the tube configurations during the test from beginning till failure.

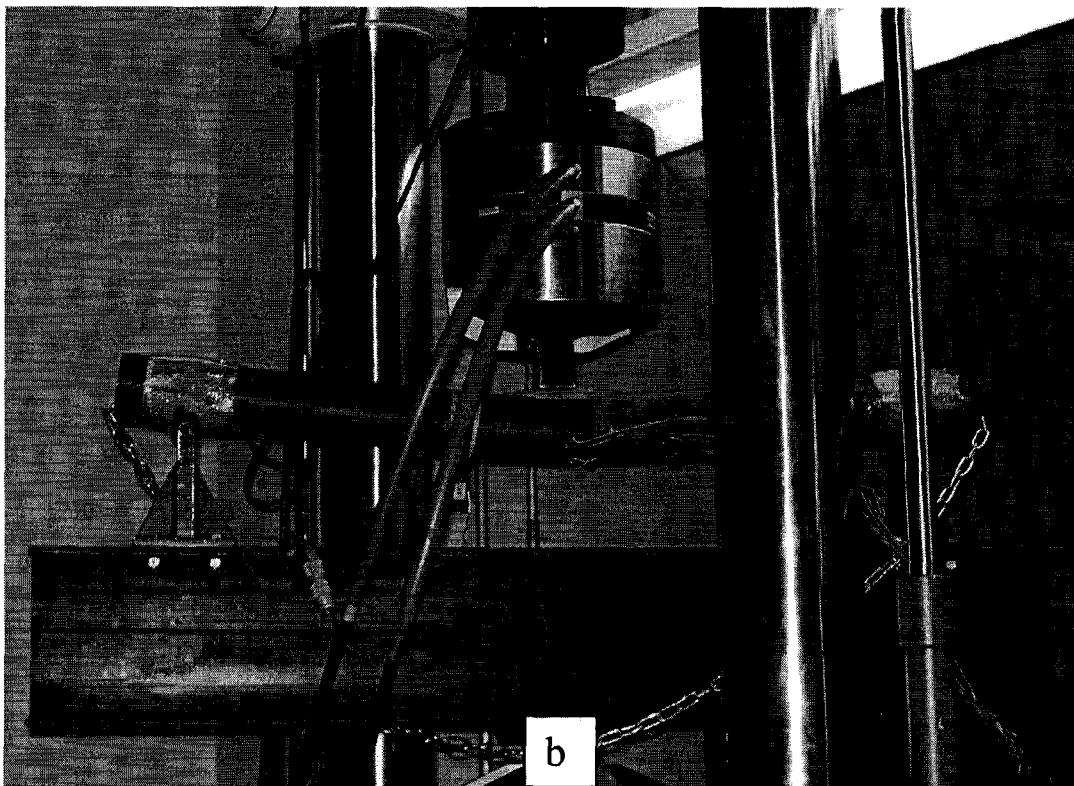
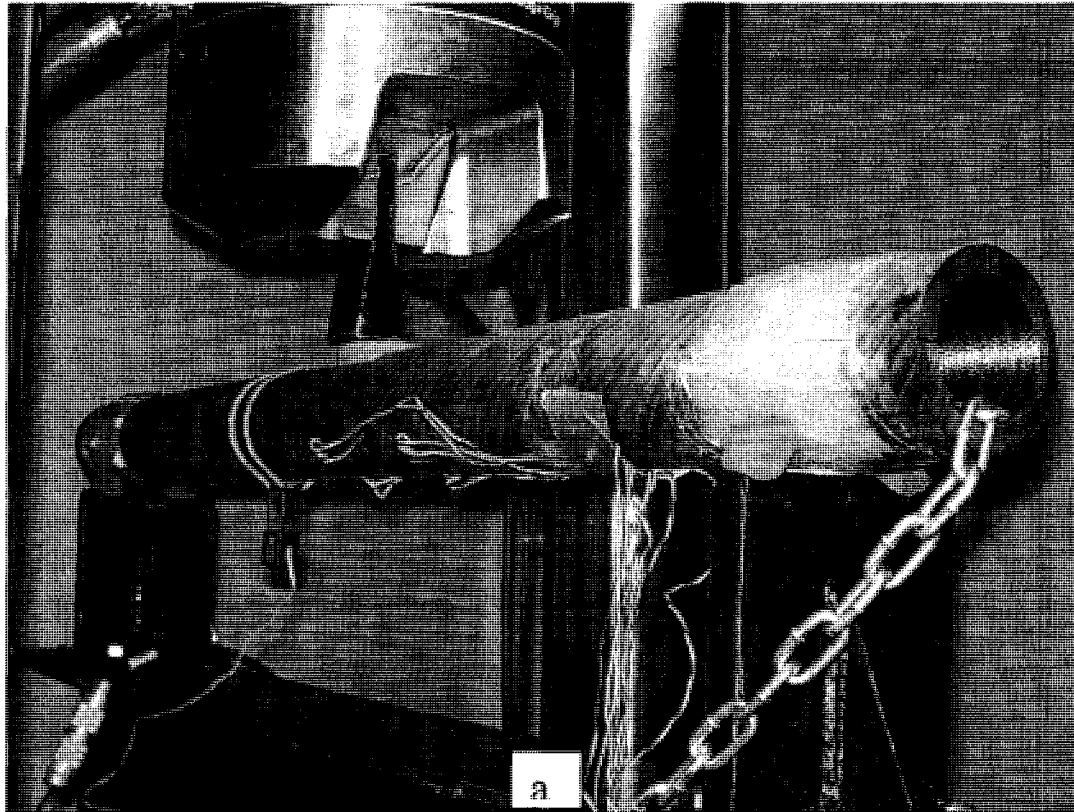


**Figure 5-25: (a) Final test set up, (b) Maximum strain is 1.5% at this stage**

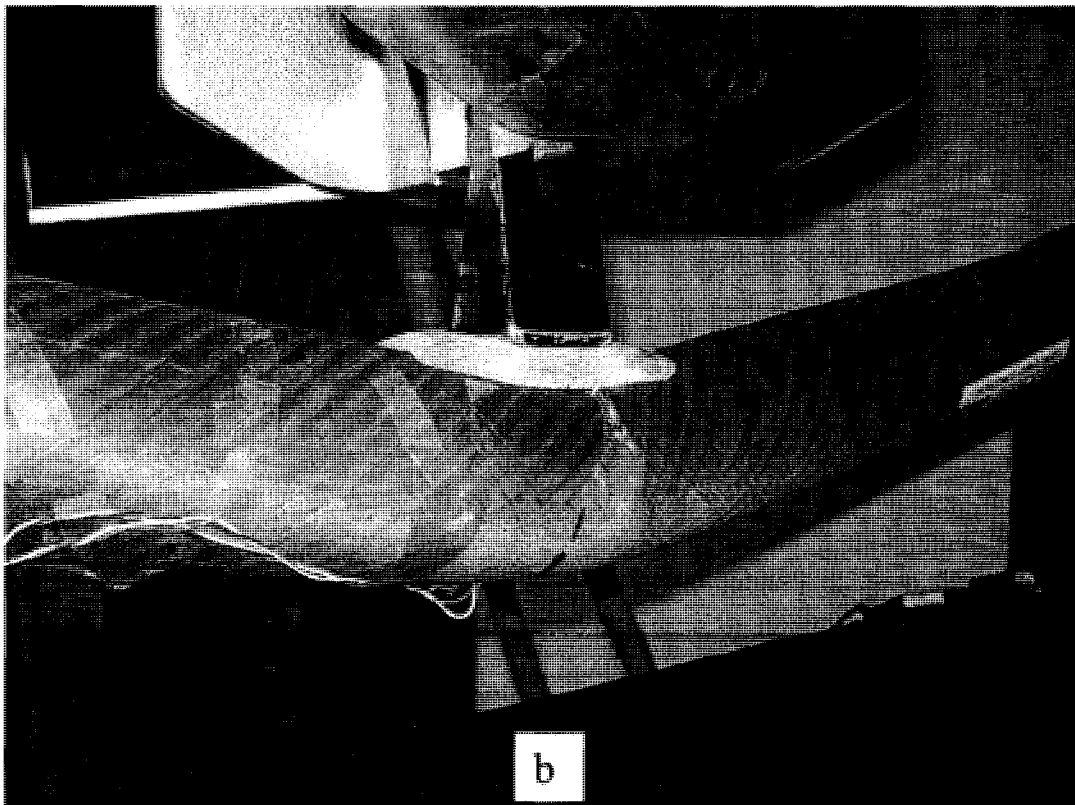
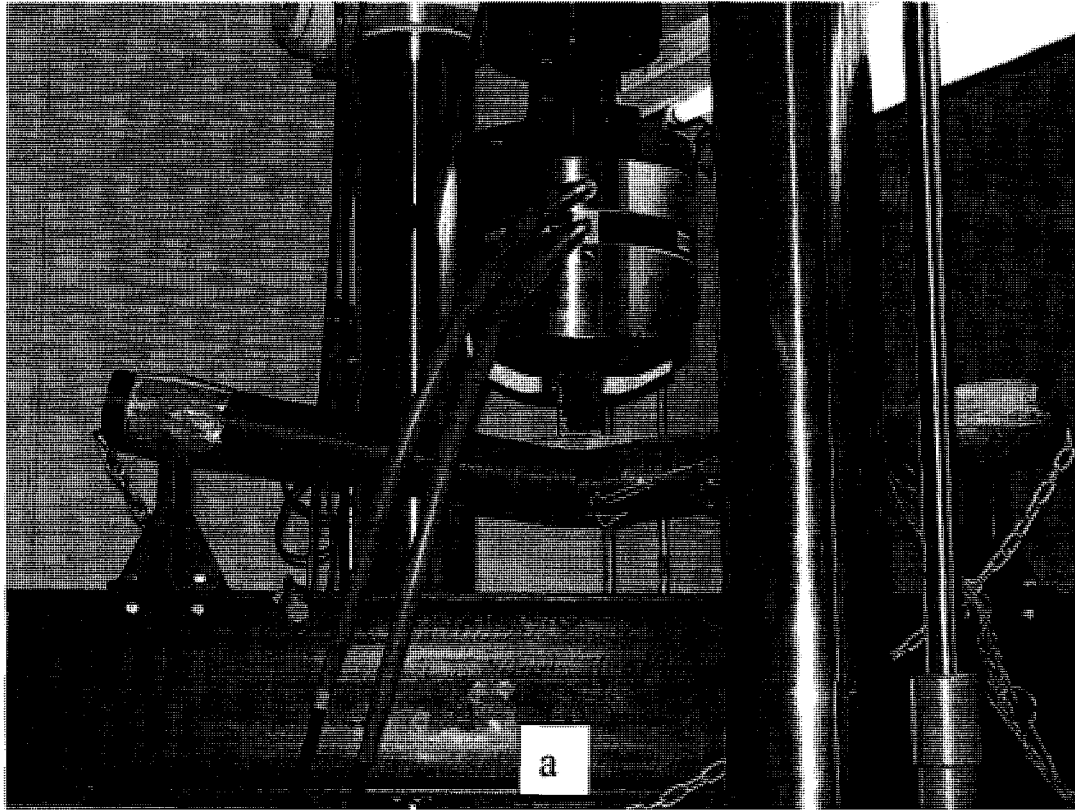


**Figure 5-26: (a) Maximum strain is 3% (b) Maximum strain is 3.5%**

Figures 5-27 to 5-30 show the force-strain curves for the axial and circumferential directions.  $0^\circ$  indicates the bottom line and  $45^\circ$  is angular offset as shown in Figure 5-13.

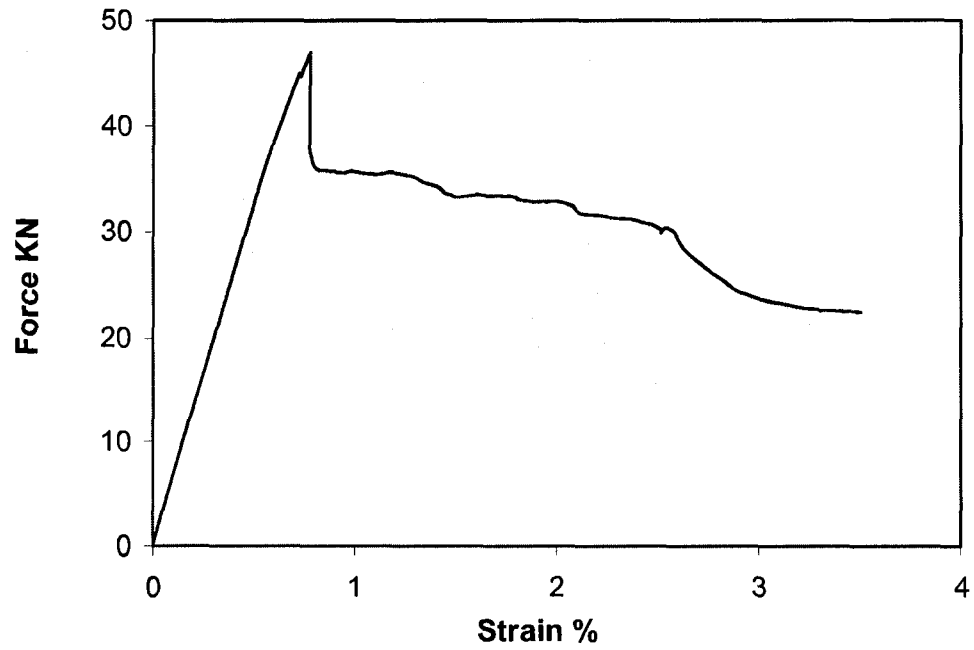


**Figure 5-27: Load-Axial strain at  $0^\circ$   
(with respect to Figure 5-13)**

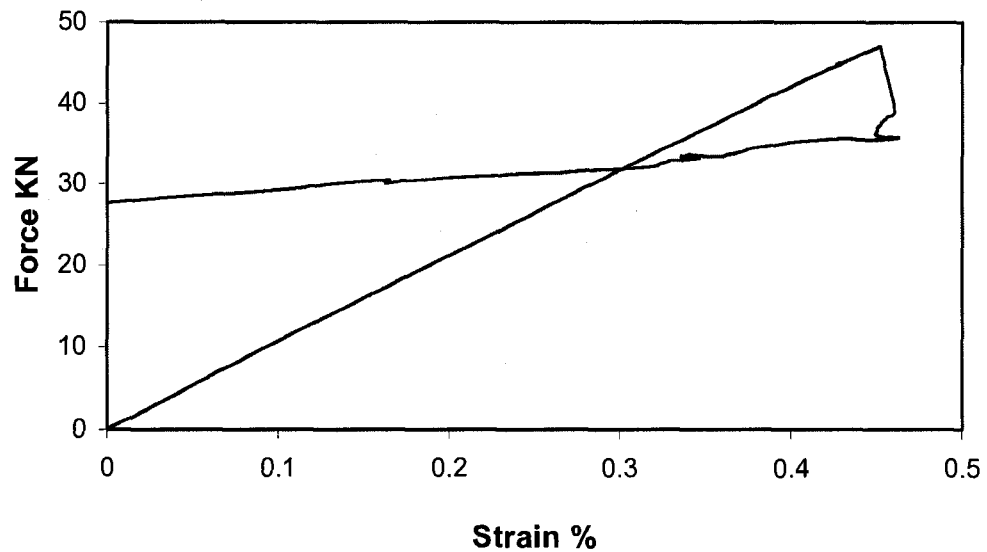


**Figure 5-28: Load-Axial strain at  $45^\circ$   
(with respect to Figure 5-13)**

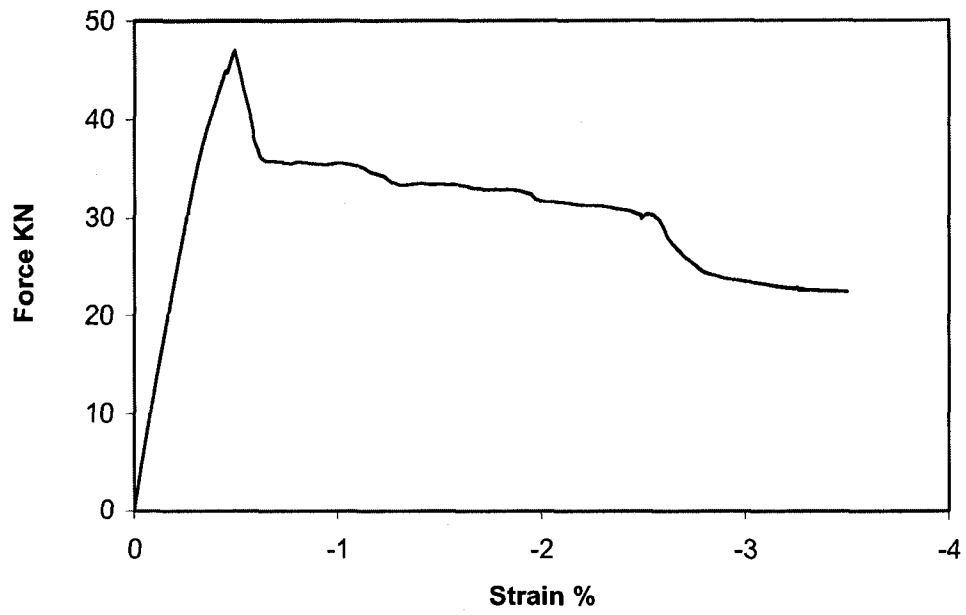


**Figure 5-29: Load-Circumferential strain at 0°  
(with respect to Figure 5-13)**

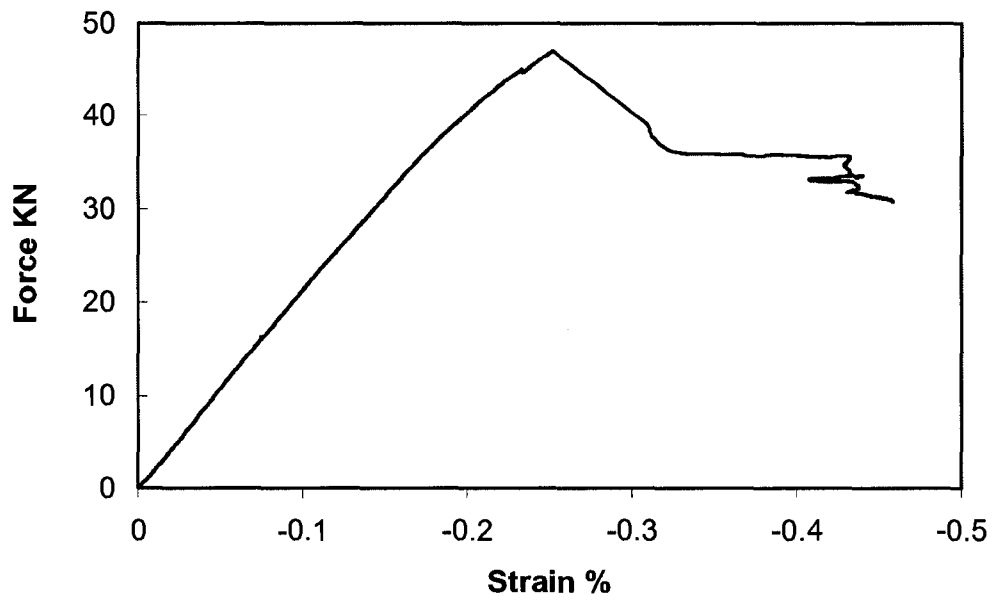


**Figure 5-30: Load-Circumferential strain at 45°  
(with respect to Figure 5-13)**

#### 5-4.9 Analysis of the results

Figure 5-31 schematically shows the tube in different stages of the test. Stages *A*, *B*, *C* and *D* are corresponding to different stages of the test. Stage *A* is the initial state where no strain and stress exist inside the tube, corresponding to Figure 5-25-a. As the load increases, the tube starts to deform. For small loads, the deformation of the tube is quite uniform, and the curvature due to the bending is observed throughout the length of the tube. As it can be seen at state *B*, the deformation is not localized at the loading nose, similar to Figure 5-25-b. To this end, the axial strain at the mid span is about 1.5%.

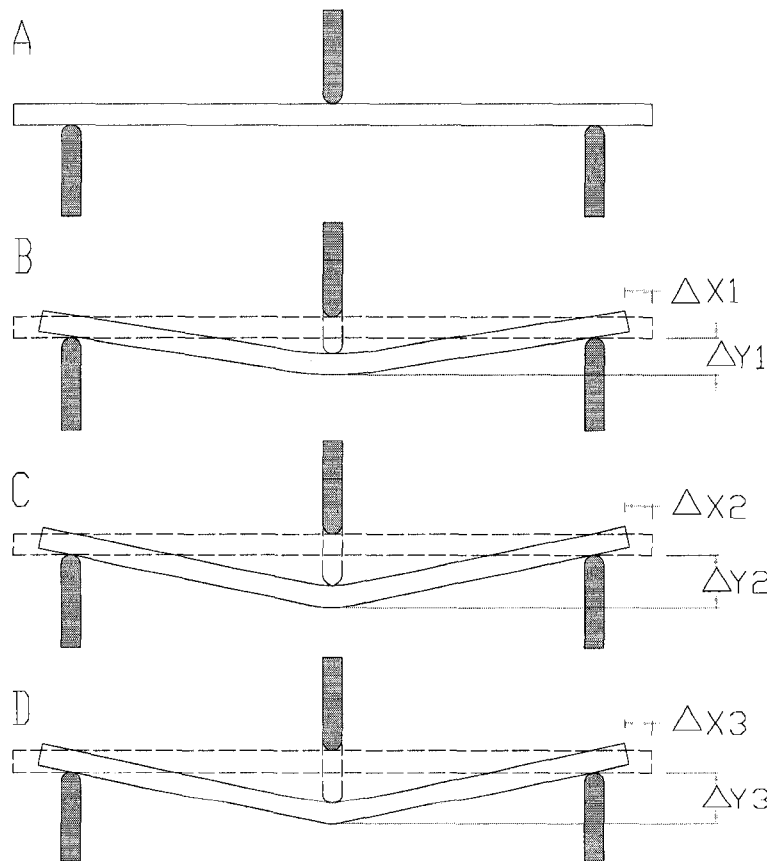


**Figure 5-31: Schematic deformation of the composite beam during the test**

Increasing the load beyond this point is accompanied by fracture of the tube in the compression zone, which is the upper part of the tube. On the other hand, the same zone is subjected to the radial load due to the pressure applied by loading nose. As such, the tube fractures at the mid span, and the deformation becomes highly localized.

Beyond point *C* corresponding to Figure 5-26-a, even though the strain at the mid span increases, at the offset points it is expected to have strain release because the deformation becomes highly localized. The test was continued until point *D* corresponding to Figure 5-26-b, where the maximum strain had reached to 3.5%. To this end, the load carrying capacity of the tube had descended considerably due to the fracture in the compression zone of the tube at the mid span.

#### **Prediction of the failure sequence**

The second composite tube carried a maximum load of 45KN before a major fracture occurred in the tube. The tube then continued to carry the load at lower level and showed high deformation. The maximum strain achieved before stopping the test was 3.5%. The load continued to descend due to failure of the layers in compression zone. In fact during the test, it was observed that fracture started in the top section of the tube. The crack propagated in the compression zone, and some local buckling was observed. Theoretically, it is expected that failure starts in the layers with minimum allocated failure strain. So, 90° layers, which have about 0.8% failure strain, are expected to fail first. Figure 5-32 schematically illustrates the cross section of the tube. The numbers in the small circles illustrate the failure sequence among different layers. Assume that the strain is measured at point *A*, and it varies linearly from the neutral axis of the beam.

Layers 1, 3 and 5 are  $90^\circ$  layers. As the strain increases at point *A*, the strain at the tension zone of layer 5, indicated with point 1, exceeds the failure strain of  $90^\circ$  laminates, and this layer fails. Further increase in the load and subsequently increasing the strain at point *A* will cause the strain in layer 3 and 1 to exceed from the failure strain of  $90^\circ$  laminates. As such, the subsequent fracture points are shown by points 2 and 3.

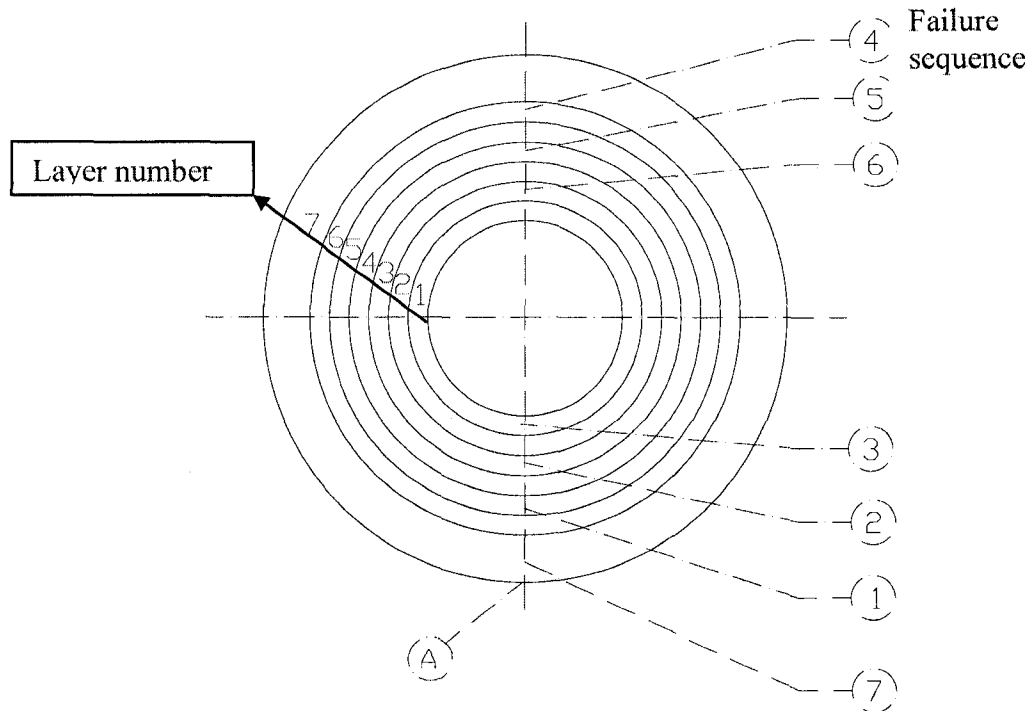


**Figure 5-32: Cross section of the second composite tube and its failure sequence**

At higher load levels, zero degree layers in the upper part of the tube would fail due to their lower strength in compression than in tension. It is obvious that the fracture starts from layer 6 that is at further distance from the centroid and carries higher load. The sequence of the fractures in  $0^\circ$  layers is shown by points 4, 5 and 6. At this point, the flexural stiffness and load carrying capacity of the tube has reduced considerably. Nevertheless,  $\pm 45^\circ$  layers still are safe and capable of keeping the integrity of the tube.

For example, though the fracture has occurred in layer 6, it is confined by layer 5 and 7. So, the layer would crush into itself and still can carry compression loads. Due to this kind of failure a few bumps might be seen on the surface of the tube, and local buckling may occur. As the load increases, finally layer 7 would also fail due to shear and normal stresses in 2-2 direction. At this point, it is expected that the tube would totally fail.

### **Observations of the failure sequence**

Experimentally, it would be difficult to explain the details of the failure as there is no instrument available to observe the progress of the failure inside the tube during the test. As such, the experimental analysis would be limited to what was observed on the surface of the tube as well as examining the cross sections of the tube after the test.

After unloading, the maximum permanent axial strain in the tube was about 2.5% and the permanent deflection was about 35mm. The failure of the tube started and propagated from the compression zone. The first strong sound was heard when the maximum axial strain had reached 0.75%. At this strain level, theoretically no failure is expected neither in tension (bottom half) nor in compression (upper half) zones. However, a careful examination of the tube, while the test was running, revealed the problem. In fact, the primary lay up had a block of 90° as the inner ring, a block of 0° as the middle ring and finally a jacket of ±45° as the outer layer. However, it was decided to have alternating 90° and 0° layers rather than two mass blocks of these layers to increase the chance of delamination and consequently energy absorption of the tube. Nevertheless, during the test, the innermost ring of 90° layers (layer 1 in Figure 5-32) was not able to resist the radial force applied by the loading nose and collapsed toward inside the tube. Figure 5-33 shows the phenomenon.

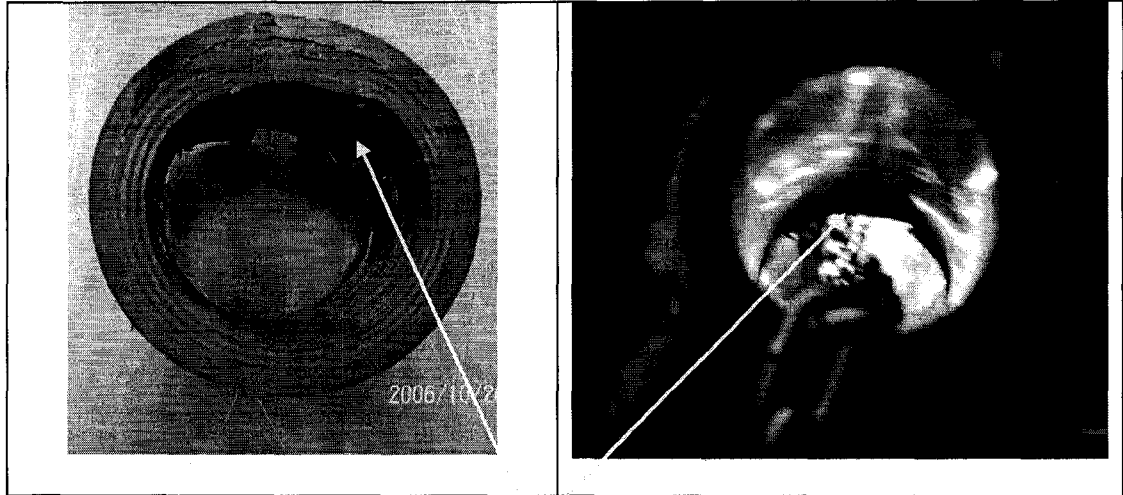


**Figure 5-33: Fracture of the inner ring during the test**

As soon as layer 1 collapsed, delamination occurred between two adjacent layers. As it can be seen in Figure 5-34, the surface of the adjacent 0° layer was very shiny indicating crack propagation at the fracture zone.

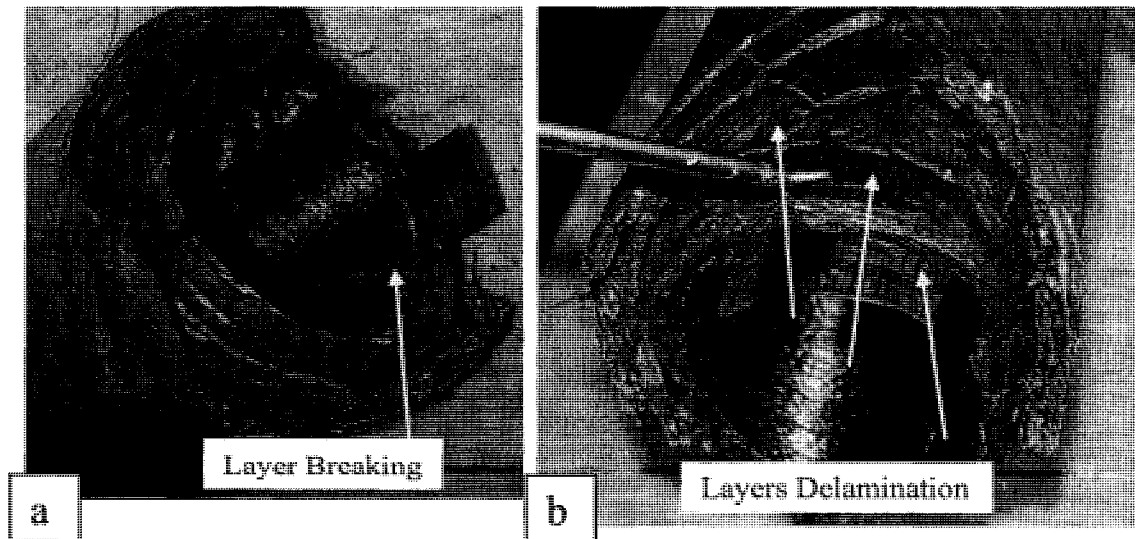


**Figure 5-34: (a) Fracture of the inner ring (b) Delamination of the layers**

After the first collapse, no strong sound indicating another source of failure was heard. This may imply that the rest of failure was gradual and no sudden fracture in any layer happened. As can be seen in Figure 5-35, the starting point of the failure is slightly shifted toward the right and is not symmetric. The reason must be the unsymmetrical geometry of the tube in respect to a plane passing the midpoint of the tube. In fact, in order to facilitate the removal of the mandrel inside the tube during fabrication, the mandrel is slightly tapered. As such, there is no plane of symmetry at the mid span of the tube, so the maximum stress does not necessarily occur at the mid span. Consequently, the failure can not be symmetric.

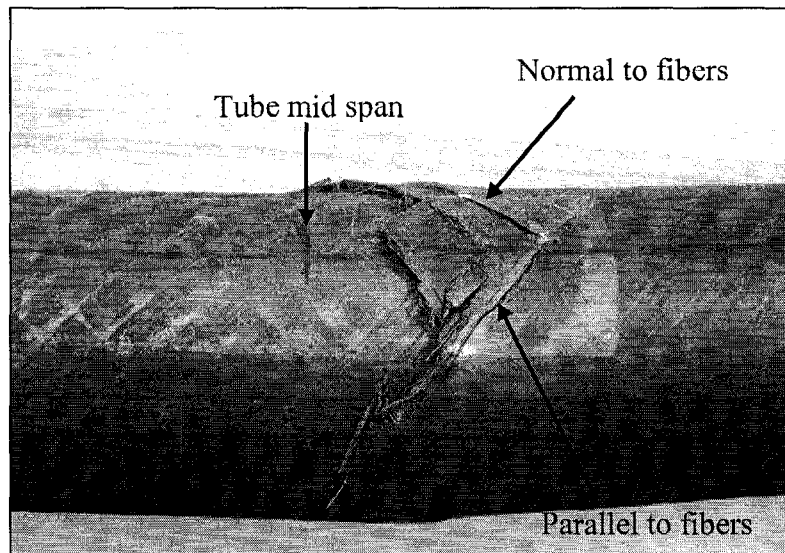


**Figure 5-35: Fracture of the tube in compression zone**

During the test, local buckling was observed on the surface of the tube. Previously in prediction of the failure sequence, it was explained that local buckling could occur due to compression failure of layers underneath. Figure 5-36 shows the local buckling on the front side of the tube. This phenomenon affected the measurement of the axial strain at

45° offset by the strain gauge as seen in the picture. As soon as the cracks propagated in the compression zone and buckling occurred, the axial strain measured by this strain gauge started to decrease while the axial strain at the bottom line was still increasing. As such, it was more difficult to explain the state of stress at the midpoint. Figure 5-37 shows the foot prints of the composite pad on the tube.

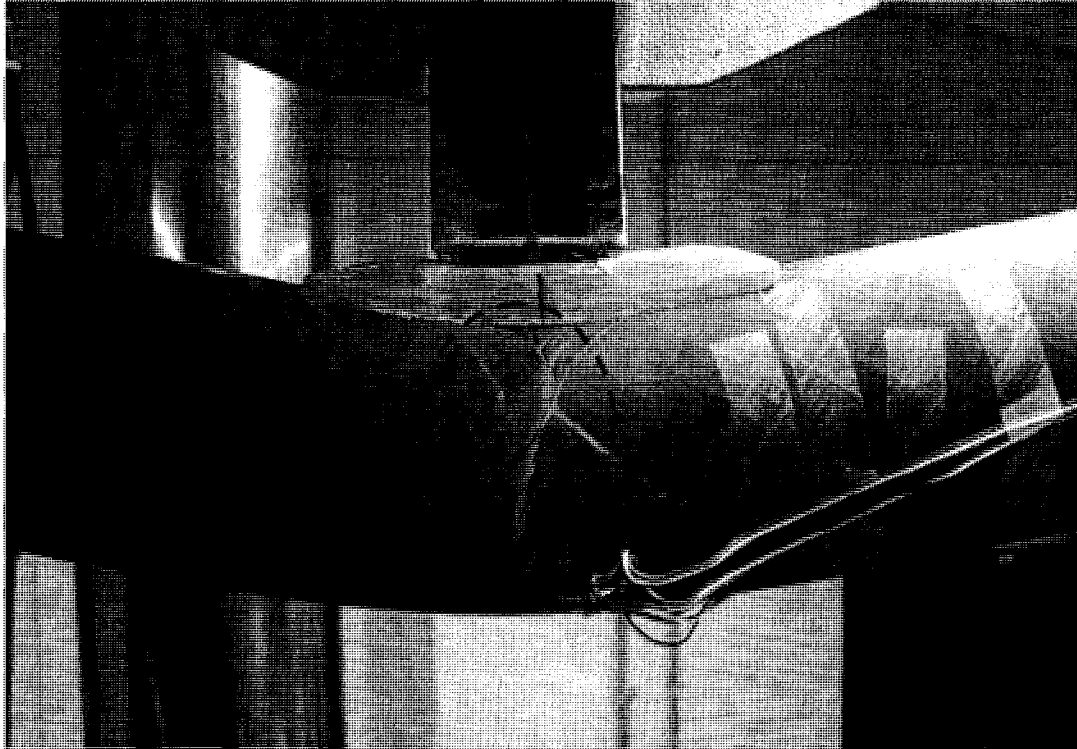


**Figure 5-36: Crack propagation and local buckling at the mid span**

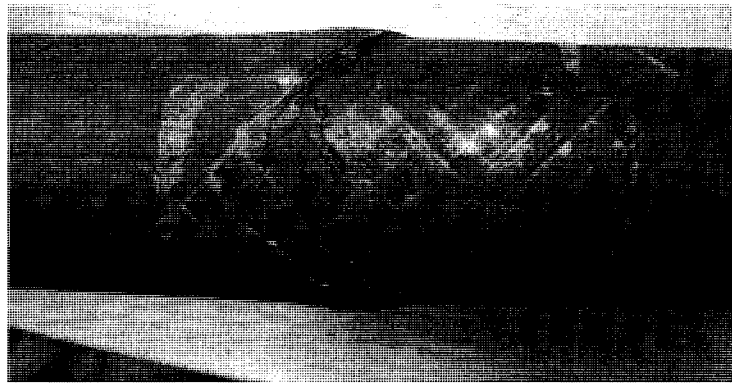


**Figure 5-37: Foot prints of the fiberglass pad on the tube**

#### 5-4.10 Summary and conclusions

A second composite tube was designed, manufactured and tested to study the behavior of composite tubes subjected to bending loads. The objectives of the test were to investigate how a brittle material such as Carbon AS4/PEKK can show large deformation in the tubular form under bending, and it was of interest to observe if delamination can be used as a source for improving the toughness of the tube and for increasing the strain to failure of the laminate. Figure 5-38 compares the force-strain curves for the aluminum tube with its composite counterpart tube.

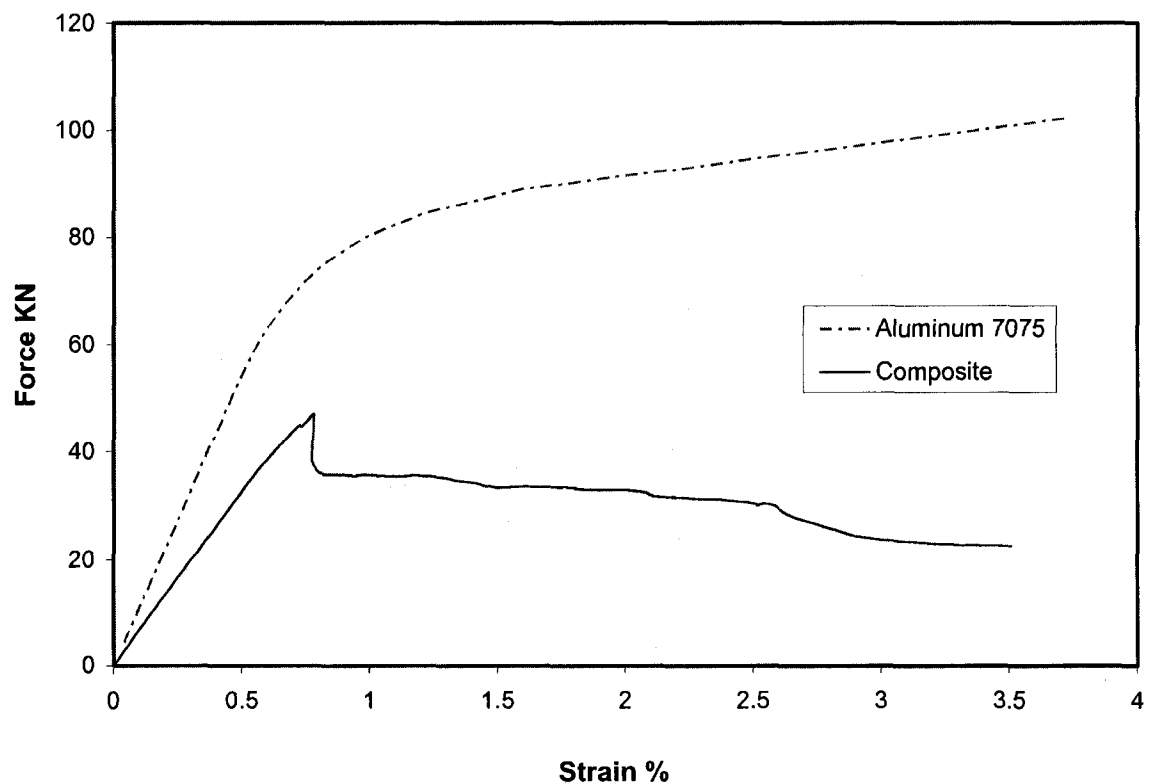


**Figure 5-38: Load– longitudinal strain curves at midpoints of the aluminum and second composite tubes.**

The theoretical and experimental analysis of the tube yields the following conclusions:

- 1- Though nonlinear behavior from brittle composites such as Carbon/PEKK is hardly observed, especially when  $0^\circ$  layers are included in the laminate, in the tubular form, the deformation of the tube might be large.
- 2- After a certain limit, local deformation may affect the accuracy of the measured strains. It is important that the deformation of the tube to be due to overall length curvature rather than due to a local fracture.
- 3- Crack propagation between the layers was minor. Figure 5-39 shows three cross sections of the tube close to failure point. The delamination between layers only occurred in a very small area near the midpoint. Even though a few cracks are observed in sections 1 and 2, in section 3 that is only 25mm away from section 2, there is no indication of crack propagation between the layers. So, it can be assumed that energy absorption due to the delamination is very limited in this case.

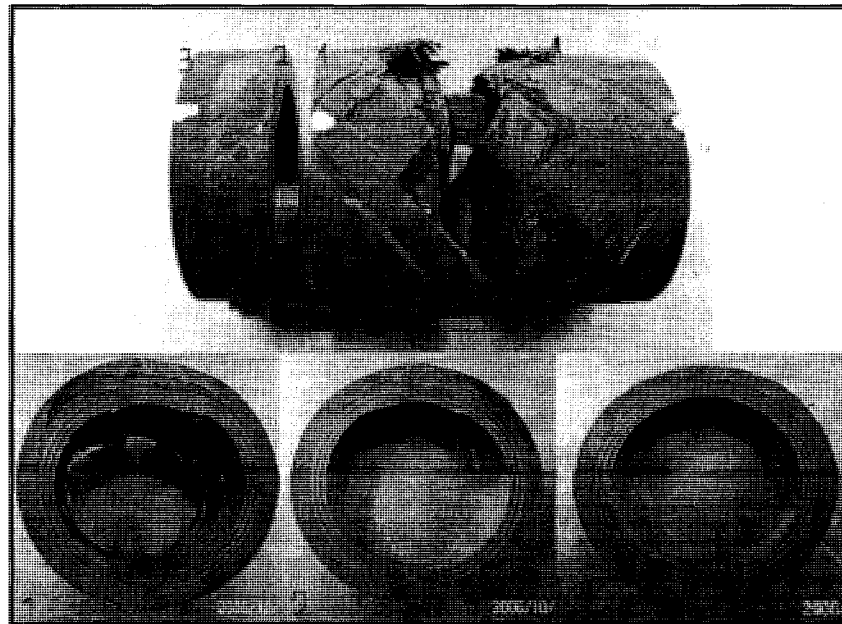


**Figure 5-39: Crack propagation was very limited: No crack in section 3**

### 5-5 Design and manufacturing the third composite tube

As predicted, neither the stiffness nor the strength of the second composite tube was matched with that of the aluminum tube. However, the composite tube showed large deformation and large strain before final fracture. A sharp reduction in load carrying capacity at 0.8% strain is a concern. Moreover, the level of the load carrying capacity of the composite tube was lower than its aluminum counterpart and decreased gradually after first major failure. This affects the energy absorption of the tube, and it must be addressed. The third composite tube is designed to overcome all of these problems.

By the time that the third tube was going to be fabricated, the fiber placement machine at NRC-AMTC has been equipped with the necessary tools to layup the fibers at any desired angles. As such, it was decided to design a composite tube that matches the strength, stiffness and failure strain of an aluminum tube with the following specifications:

Material: AL7075-T6;

Inner Diameter: 56mm;

Thickness of the tube: 16mm;

Weight per unit of length of the tube: 9.7 kg/m.

Moreover, it was decided to assume the same inner diameter for the composite tube to reduce the design parameters. Also, because the slit tape could be laid up at different angles, it was decided to adopt the layup suggested by Section 5-3.1 as the basis of the new design. The layup was as follows:

$$[\pm 20^{\circ}_{n1} / \pm 25^{\circ}_{n2} / \pm 30^{\circ}_{n3} / \pm 45^{\circ}_{n4}]$$

### 5-5.1 Design of the layup

The layup suggested according to the strain controlled criteria does not consider the requirements of strength and stiffness of the tube. As such, the procedure followed the design of the second tube: both aluminum and composites tubes were modeled as sandwich panels to simplify the stress analysis tasks.

Moreover, it was decided to include all experimental observations due to characterization of the material (Chapter 3) and results from testing the second composite tube into the design. More specifically:

- 1- In order to resist hoop stresses and radial forces at the loading nose, it is necessary to have a strong ring of  $90^\circ$  plies as the innermost ring of the tube. The ring would be used as a foundation for laying up the rest of layers.
- 2- A jacket of  $\pm 45^\circ$  plies as the outermost layer of the tube would keep the integrity of the tube, provides large deformation, and restricts the movement of layers that failed due to compression stresses. While these layers are kept in place, they would be able to resist more compression loads, and stiffness of the tube does not diminish drastically.
- 3- Testing the second composite tube proved that delamination does not occur extensively during the bending test. As such, in order to isolate the layers from each other and provide them with more freedom for large deformation another technique is required. On the other hand, in Chapter 3, it was observed that inserting a ply of PEKK polymer between the adjacent  $\pm 30^\circ$  plies improved the flexibility and strain to failure of the laminate. In manufacturing of the tubes, instead of a film of the polymer, a thin  $90^\circ$  layer can be laid up between major

adjacent layers. Figure 5-40 shows that upon fracture of 90° layer, cracks propagate parallel to the fibers. As such, the layer loses its stiffness in longitudinal direction and removes the restrictions on the movement of the adjacent layers. Yet, the fracture has not occurred in the circumferential direction, and the 90° layer can contribute in torsional stiffness of the tube and resist hoop stresses.

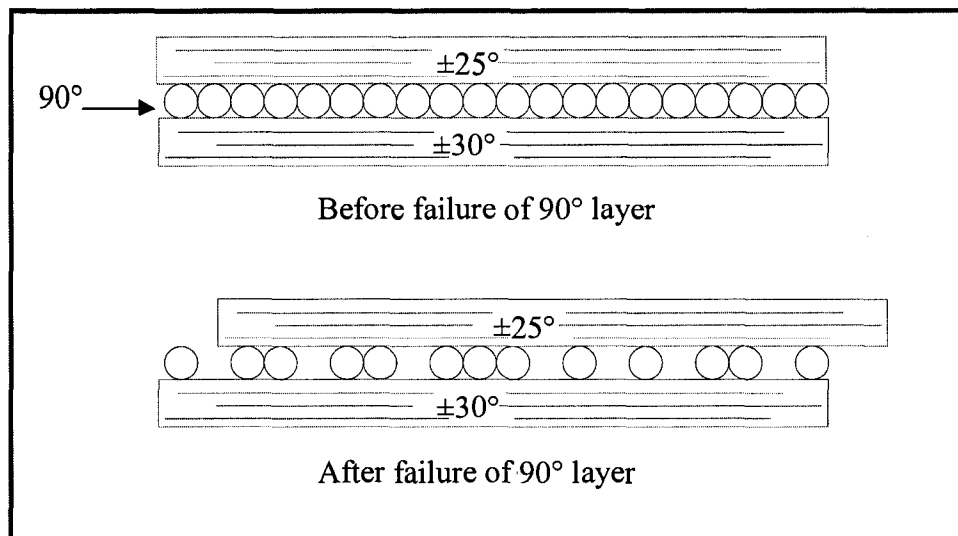


**Figure 5-40: Failure of 90° layer releases the constraint on adjacent layers**

- 4- Finally, zero degree layers are not recommended to be included in the layup of the tube. First, they do not comply with the requirements of strain. The maximum strain to failure of zero degree unidirectional laminates was observed to be less than 1.5% while for a composite tube to show 2.5%, the minimum required strain of a layer is 1.83% (See Figure 5-7). Second, zero degree layers are quite stiffer than other angle ply laminates. As such, they are carrying a considerable amount of loads, so upon their failure a shock is transferred into the structure, and a sharp reduction in the load carrying capacity of the tube occurs.

Considering all the analyses and observations, the following layup is suggested:

$$[90^{\circ}_{n1} / \pm 25^{\circ}_{n2} / 90^{\circ}_5 / \pm 30^{\circ}_{n3} / 90^{\circ}_5 / \pm 45^{\circ}_{n4}]$$

Layer number: [ 1 / 2 / 3 / 4 / 5 / 6 ]

In this design, layer 1 resists the circumferential stresses and radial loads applied by the MTS machine at loading nose. It also prevents ovalization that reduces the flexural stiffness of the tube. Layers 3 and 5 are responsible for isolating their adjacent layers from each other and improving the flexibility of the tube. In fact, when layers 2, 4 and 6 can move independently, the tube would be more flexible. Layers 3 and 5 also have a small contribution in resisting the hoop stresses and circumferential stiffness of the tube. Layers 2 and 4 are the main layers responsible for flexural and extensional stiffness of the tube. The load carrying capacity of the tube would also be highly dependent on these layers. Layer 6 is mainly responsible for keeping the integrity of the tube when inner layers fail. Furthermore, the layer would highly contribute in shear stiffness of the tube. Finally, this layer can show high strain to failure and large deformation.

### **5-5.2 Stress analysis of the layup**

Figure 5-41 shows two aluminum and composite sandwich panels. The layup of the skin for the composite sandwich panel is the same as the proposed layup in the previous section. While the layup was known, the number of plies in each layer was determined by stress analysis of the panels. One more time, LAP was used to carry out the analysis. The same procedure for designing the second composite tube was followed. It was tried to

match as many parameters as possible to assure both panels would have the same behavior while being subjected to bending and axial loads.

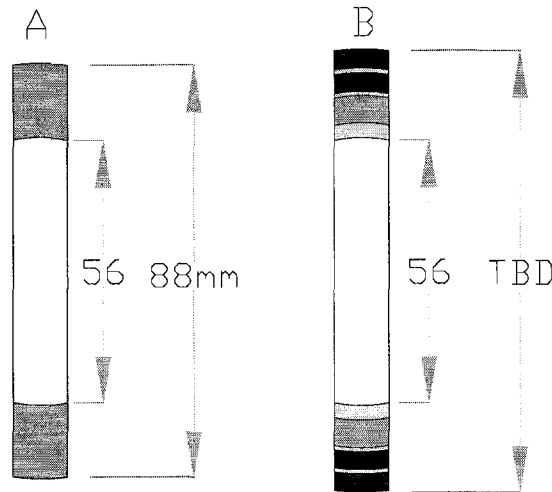


**Figure 5-41: Cross sections of the aluminum and composite panels**

Table 5-6 compares the mechanical properties for both aluminum and composite panels.

The following layup was recommended for the third composite tube:

$$[90^{\circ}_{30} / \pm 25^{\circ}_{45} / 90^{\circ}_5 / \pm 30^{\circ}_{20} / 90^{\circ}_5 / \pm 45^{\circ}_{20}]$$

For a beam mainly subjected to bending loads, the most important parameter is the longitudinal flexural stiffness. This parameter defines the slope of force-deflection or force-strain curves in the elastic limit or before a major failure occurring in the composite tube. For the current layup,  $EI_{xx}$  for the composite panel is about 10% more than that of aluminum panel. Also the extensional and torsional stiffness of the composite panel is more. As such, considering the fact that a beam is mainly subjected to bending, axial and

torsional loads, it was expected that the composite tube would show the same behavior as its aluminum counterpart.

	Aluminum 7075-T6	Carbon AS4/PEKK
Lay up	NA	[90° <sub>30</sub> / ±25° <sub>45</sub> / 90° <sub>5</sub> / ±30° <sub>20</sub> / 90° <sub>5</sub> / ±45° <sub>20</sub> ]
Tube Dims, mm	ID 56 OD88	ID 56 OD98
E <sub>xx</sub> , GPa	70	57.8
E <sub>yy</sub> , GPa	70	37.8
G <sub>xy</sub> , GPa	27	22.8
EI <sub>xx</sub> , N.mm	2.95E+09	3.39E+09
EI <sub>yy</sub> , N.mm	2.95E+09	2.06E+09
GJ, N.mm	4.55E+09	6.39E+09
Tube Area mm <sup>2</sup>	3619	5080
AE <sub>xx</sub> , MN	253	293
Weight Kg/m	9.7	7.6

**Table 5-6: Design parameters of the aluminum and third composite tubes**

The last step in stress analysis is to assure the composite tube has the same or higher strength. Figure 5-42 illustrates the aluminum sandwich panel. To simplify the analysis, it is assumed that the skin is made of four equal thickness layers made of aluminum 7075-T6. It is also assumed that the properties of the material in tension and compression

are the same, and the panel is subjected to pure bending,  $M$ . The Laminate Analysis Program was used to find out at which load the panel starts plastic deformation, and finally what could be the maximum load that the panel might resist.

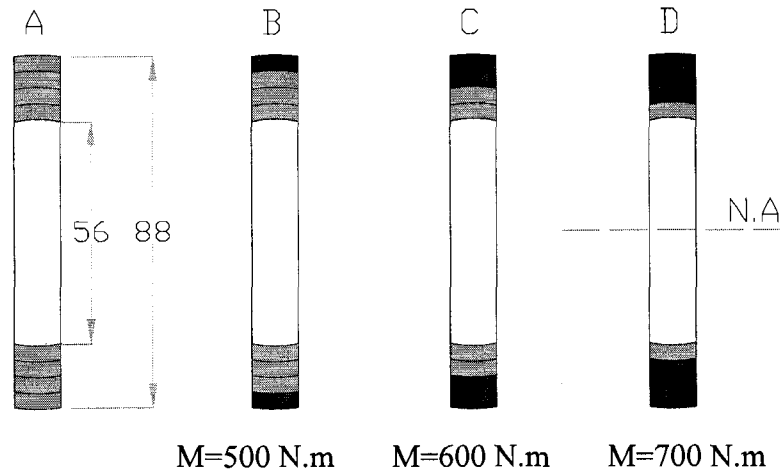


**Figure 5-42: Failure process of the aluminum panel  
(Shaded areas show the failed region)**

As the material is the same for all layers, and the strain varies linearly from the neutral axis, N.A., the first layer to exceed the yield stress would be the layer furthest from the centroid. As shown in part B of the figure, a bending moment equal to 500 N.m would be required. Increasing the bending moment to 600N.m and next to 700N.m would cause the second and third layers to fail as shown in parts C and D of the figure. At this point, most of the beam is in the plastic zone, and the load can not be increased considerably if the effect of strain hardening is ignored.

Similarly, Figure 5-43 shows the composite sandwich panel. The red zones (dark gray in black and white prints) show the failed layers as the bending moment was increased. The first layers to fail are 90° layers in tension zones, shown by B, C and D in the figure. It can be seen that bending moment required to have the first ply failure, 550 N.m, is more

than the bending moment that causes the outermost layer of the aluminum to fail. Moreover, as it can be seen in parts *F* or *G* of the figure, the bending moment required to produce considerable failure in different layers is much larger than the bending moment required to deform the aluminum panel into the plastic zone.

In these analyses, the effect of strain hardening for aluminum panel is not considered. Moreover, the stiffness of the failed composite layers in tension and compression is reduced by 50% and 30% respectively. Even though these assumptions may not be accurate, it is clear that the strength of the composite panel is not less than that of the aluminum panel.

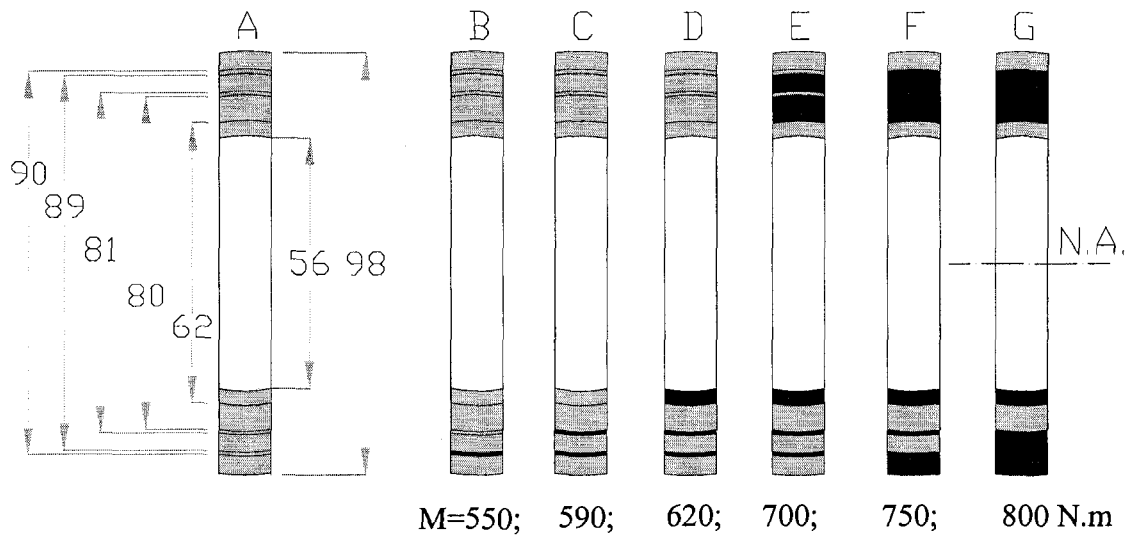


**Figure 5-43: Failure process of the third composite panel  
(Shaded areas show the failed region)**

Stress analysis of both aluminum and composite panels shows that the composite tube should be superior to the aluminum tube in terms of strength and stiffness. However, during the bending test of the second composite tube, it was observed that the innermost 90° layer broke inside at the loading nose. This changed the behavior of the tube, and the

deformation of the tube transferred from global to local. As such, the load carried by the composite tube is reduced drastically. To avoid similar phenomenon, in the design of the third composite tube, the thickness of the innermost 90° layer was increased from 1mm to 3mm to cause higher resistance to radial loads and circumferential stresses.

Figure 5-44 schematically illustrates the cross section of the third composite tube. The sequence of failure in different layers based on the above analysis is shown by the numbers in the small circles. The points referred to on the figure are the most probable locations of the failure. It can be seen that failure starts in the lower part of the tube that is under tension and then jumps to the upper part of the tube that is subjected to compression. This is a crucial parameter for large deformation of the composite tubes to have fracture in weaker layers occur first. Here, it can be seen that fracture at  $\pm 30^\circ$  layers occurs before fracture at  $\pm 25^\circ$  layer, so the latter can resist the extra load after fracture of  $\pm 30^\circ$  layer in compression. Finally layers 6 and 4 fail in the tension zone. By this end, it is expected that the tube would fail totally.

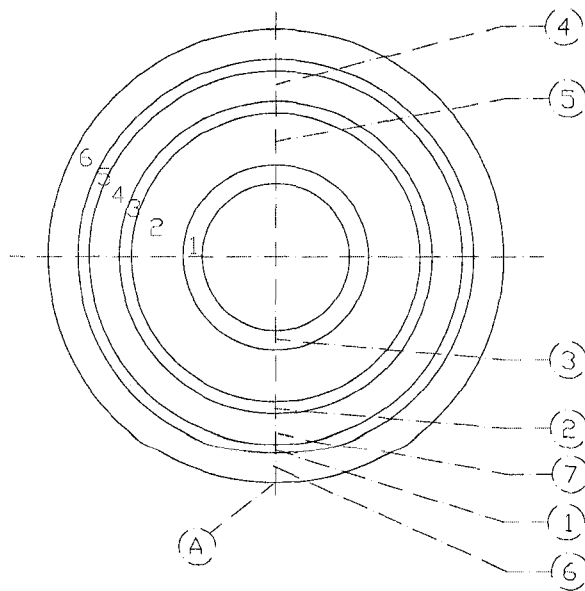


**Figure 5-44: Sequence of failure for the third composite tube.**

### 5-5.3 Testing the third composite tube

The third composite tube has the inner and outer diameters 56mm and 98mm, respectively. Figure 5-45 shows the test set up. Four strain gauges were installed at the mid-span of the tube to measure axial and circumferential stresses. One  $T$  strain gauge was installed at bottom line of the tube, at  $0^\circ$  position as shown in Figure 5-13. The other  $T$  strain gauge was installed at  $45^\circ$  offset position, referring to the same figure.

The tube was reinforced by a few layers of fiberglass at the supports to prevent local damages on the tube. Also, a fiberglass pad was used at loading nose to redistribute the applied load on the tube and reduce the likelihood of local deformation.

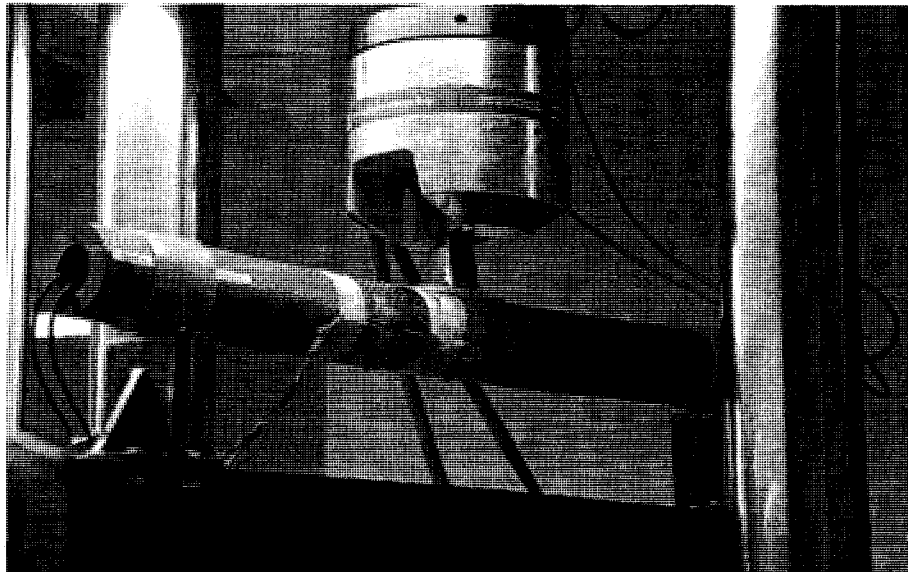


**Figure 5-45: Test set up for the third composite tube**

Figures 5-46 a & b show the configuration of the tube in the intermediate and final stages of the test. The tube carried a maximum load of 165 KN, and the maximum strain reached to 2.6%. The tube kept its load carrying capacity around 130 KN during the test.

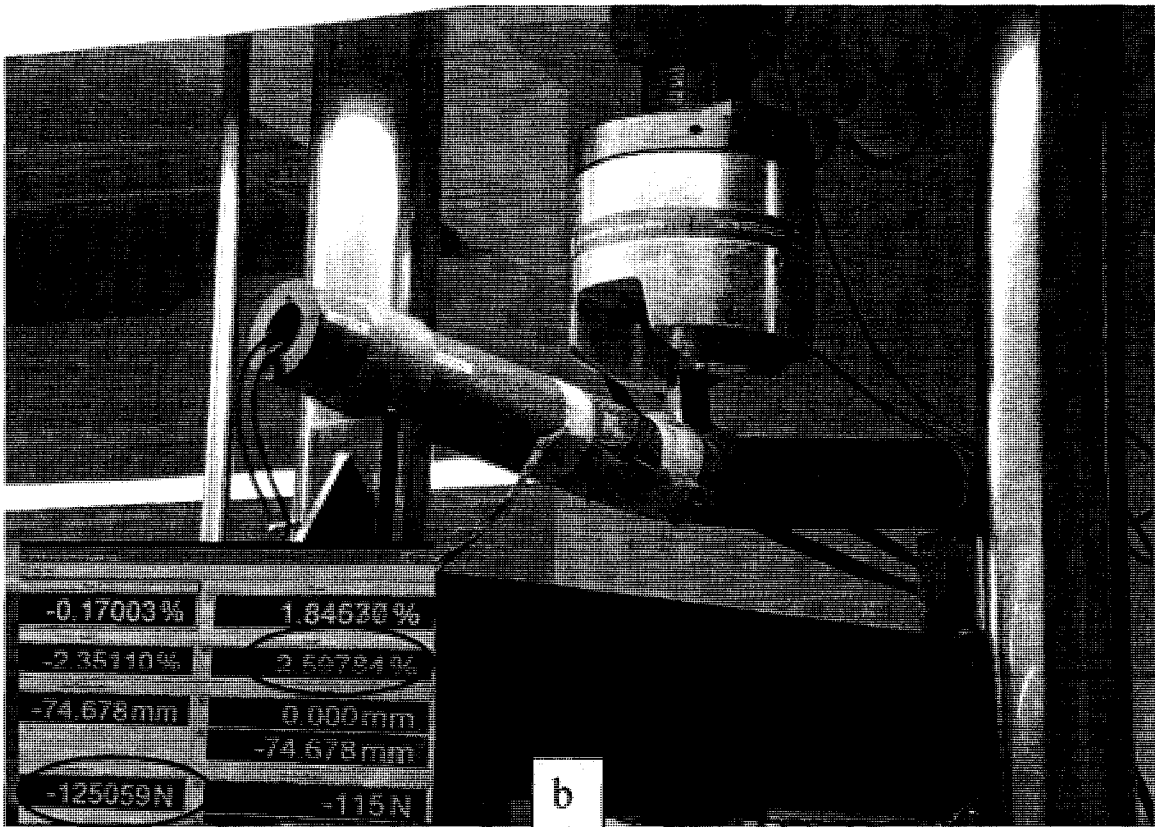
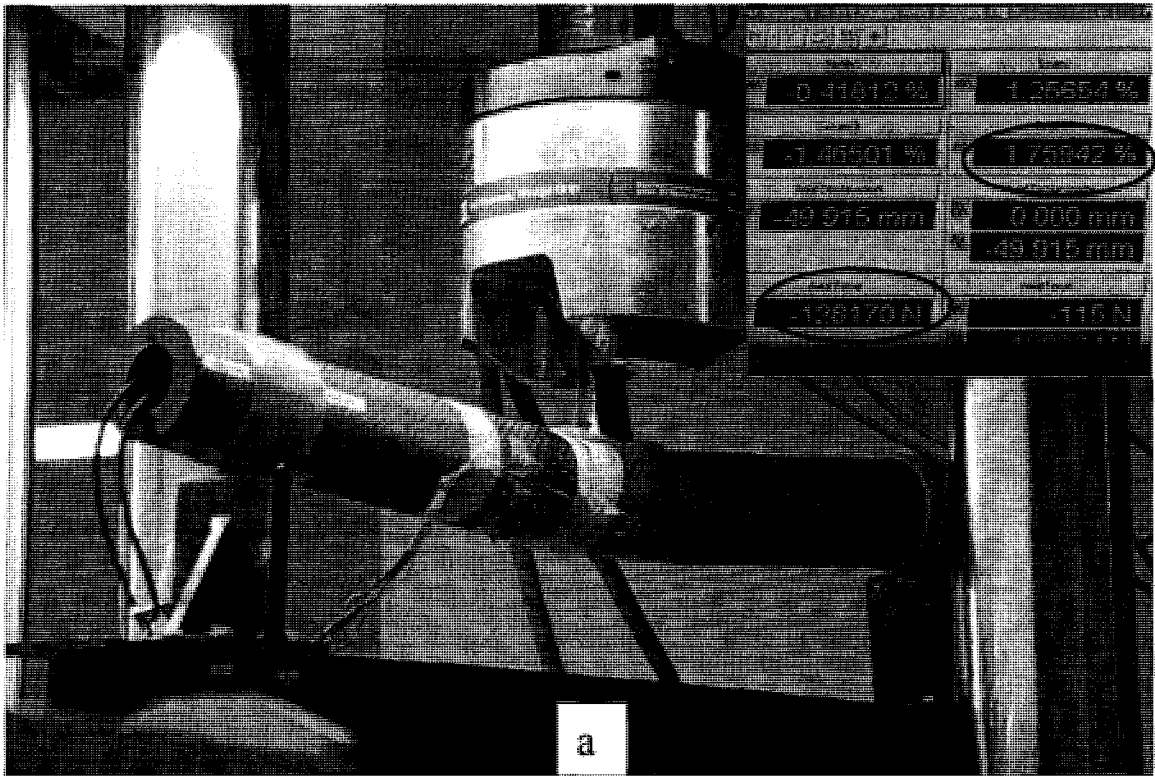


Figure 5-46: a & b Bending test of third composite tube

Figure 5-47 shows the force-deflection curve for the third composite tube in comparison with those of two aluminum tubes with 7075-T6 and 6061-T651 grades. For small deformation and in the elastic zone, the three curves are totally matched. This confirms that the flexural stiffnesses of the tubes are the same. As such, the accuracy of the simplified sandwich panel model used to design the layup of the composite tube is proven.

Beyond 100 KN, the tube made of aluminum 6061-T651 started to deviate from the rest as this grade of aluminum has lower strength, and plastic deformation of the tube started at this point. However, both composite and AL7075-T6 tube continued to carry more load to about 160 KN. At this level, a failure occurred in the composite tube and the two curves started to deviate. At slightly higher load, around 165KN, a strong sound was heard from the composite tube, and the tube failed to carry more loads.

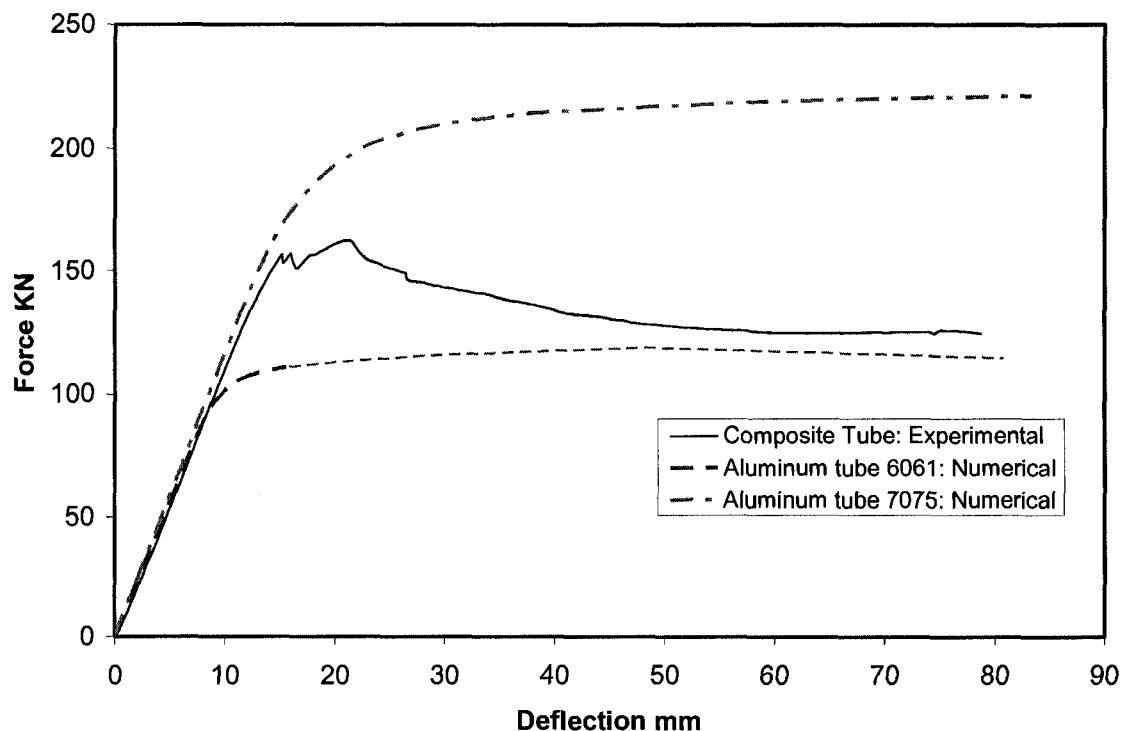
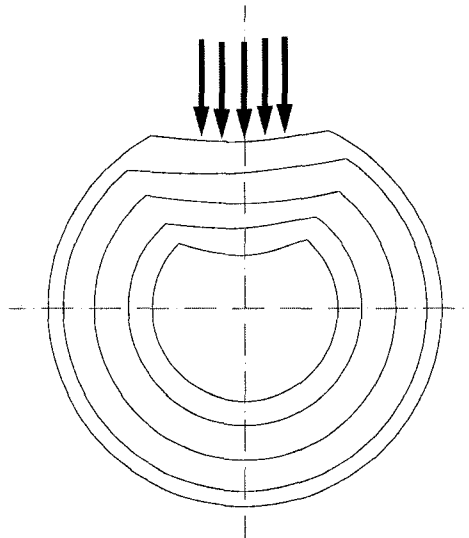


Figure 5-47: Force deflection curves for aluminum and third composite tubes

#### 5-5.4 Failure analysis of the third tube

In comparison to the second tube, the thickness of the innermost 90° ring had been increased in the design of the third tube to resist the radial loads applied at the loading nose by the MTS machine. As the radial load increases, the layers under loading nose first become flat to some extent. Then the innermost layer collapses toward inside the tube as shown in Figure 5-48. As such, the intermediate layers lose their foundation and obtain more freedom for deformation. So those layers deform while subjected to less load. As such, the stiffness and load carrying capacity of the tube decreases considerably.



**Figure 5-48: Failure of the innermost layer due to the radial load.**

Figure 5-49 shows the fracture of innermost 90° ring toward the inside of the tube. Similar phenomenon happened during the test of the second composite tube. This shows that increasing the thickness of the innermost 90° ring from 1mm to 3mm was not effective enough to prevent the fracture. As such, the adjacent  $\pm 25^\circ$  layer had more room to deform, and the flexural stiffness of the tube was reduced. So, the composite tube did

not carry more loads while the aluminum tube did until 220 KN, where the aluminum tube also started plastic deformation.

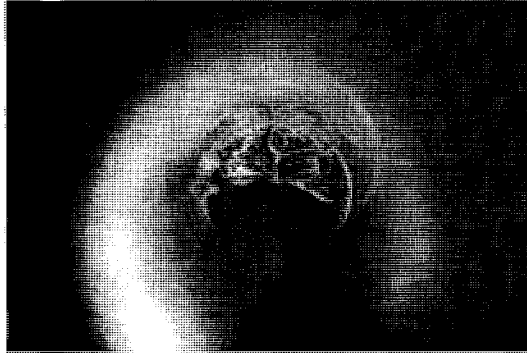


**Figure 5-49: Fracture of 90° layer due to radial and circumferential stresses**

Finally, Figure 5-50 shows the surface of the tube after the test. It can be easily observed that the fiberglass pad was not strong enough to distribute the force on a large surface area of the tube. As such, the load applied by the MTS machine concentrated on a small area and caused the fracture of the innermost layer of the tube.

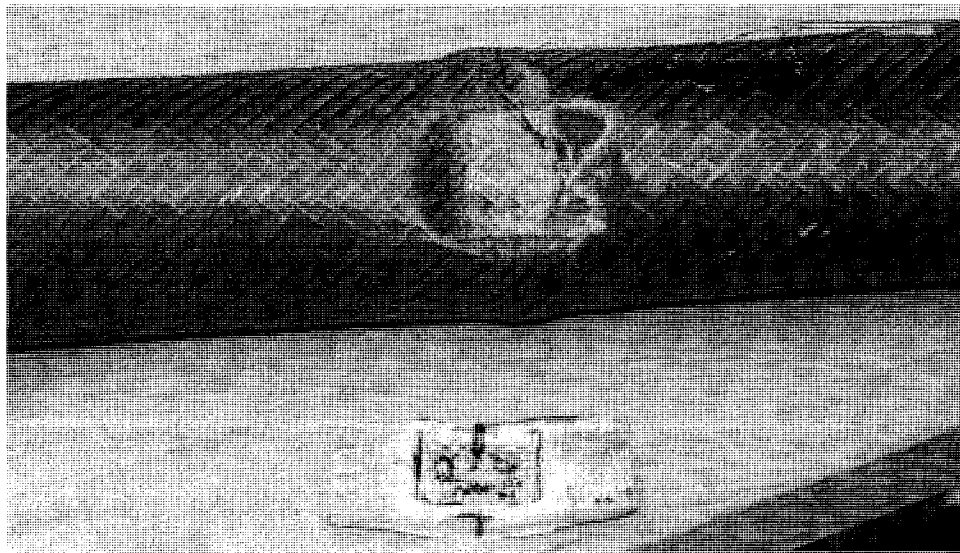


**Figure 5-50: Damage at loading nose for third composite tube**

Nevertheless, the design of third composite tube had several advantages over the previous tubes.

- First, the stiffness of the tube complied with the requirements of the design and matched with that of the aluminum tube.
- Second, the maximum load carried by the composite tube was about 75% that of the aluminum 7075-T6 tube while it was around 50% for the second tube.
- Third, no sharp reduction in carried load was observed. In other words, no considerable shock was transferred to the tube due to the first ply failure. As such, the rest of the layers managed to redistribute the load. As a result, the tube kept its load carrying capacity at a very high level- more than 80% of the maximum carried load- during the test.
- Fourth, the tube showed very high fracture strain. In fact, even beyond 2% strain, the deformation was not local, and the curvature due to bending could be seen throughout the length of the tube.

Figure 5-51 compares the force-strain curve of the third composite tube with that of Aluminum 7075-T6 tube. Both tubes are matched in terms of stiffness and failure strain. The only concern left to be addressed is to match the load carrying capacity of the tubes. The stress analysis of the third composite tube, Section 5-5.2, showed that the composite tube should have superior strength and stiffness to the aluminum tube. As such, the testing procedure can be the only reason that does not allow the composite tube to show its maximum load carrying capacity, and this concern should be addressed in the next design.

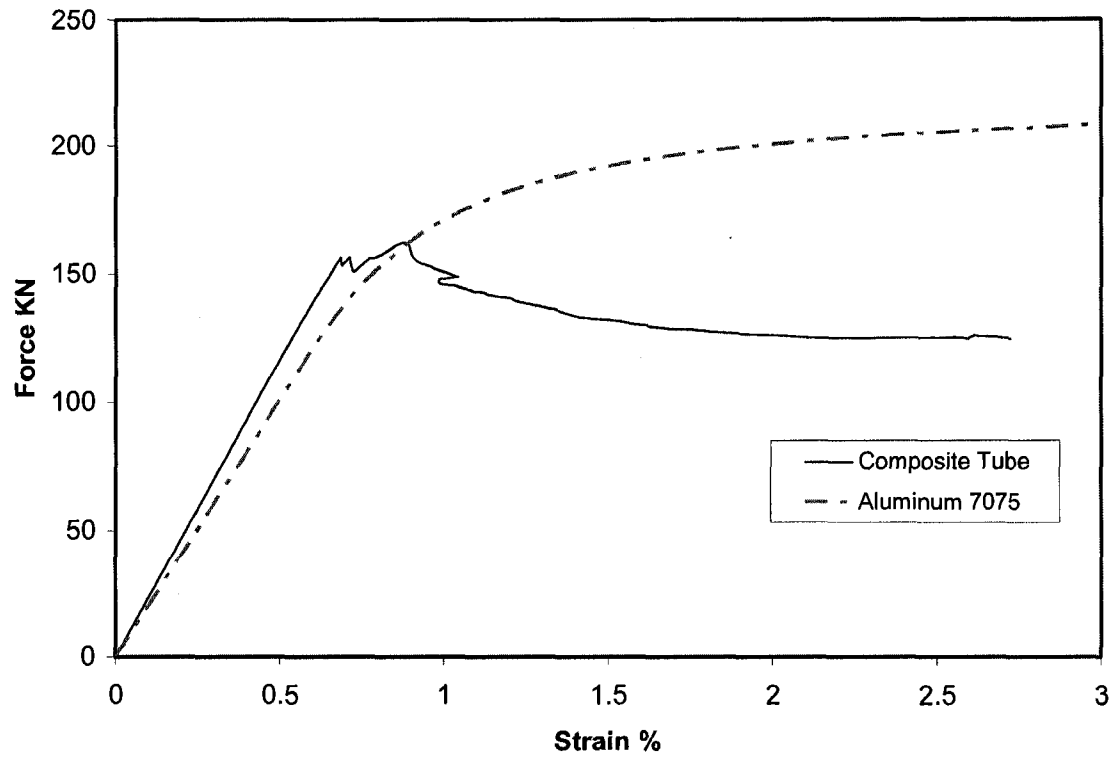


**Figure 5-51: Force-strain curves of aluminum and third composite tubes**

### 5-6 Design and testing the fourth composite tube

The results of testing the third composite tube showed that the load carrying capacity of the tube was about 30% less than that of its aluminum counterpart. However, careful examination of all calculations and analysis left no doubt that the third composite tube had higher flexural stiffness and strength than the aluminum tube (Section 5-5.2) and therefore must carry more load than its aluminum counterpart. As a result, the only reason for the lower load carried during the test should be sought in the testing procedure. As explained in the previous section, fracture analysis of the tube revealed that the fracture of the innermost 90° layer could be the reason. As such, it was decided to design the fourth composite tube with similar layup sequence as the third tube and reinforce the tube at the loading nose by a very thin aluminum liner. While the aluminum liner should be strong enough to prevent the undesirable fracture of the 90° layer, it must be thin and flexible also to allow natural deformation of the composite tube. As such, according to the predicted load level for the fourth composite tube, a liner made of aluminum 6061 was designed as shown in Figure 5-52.

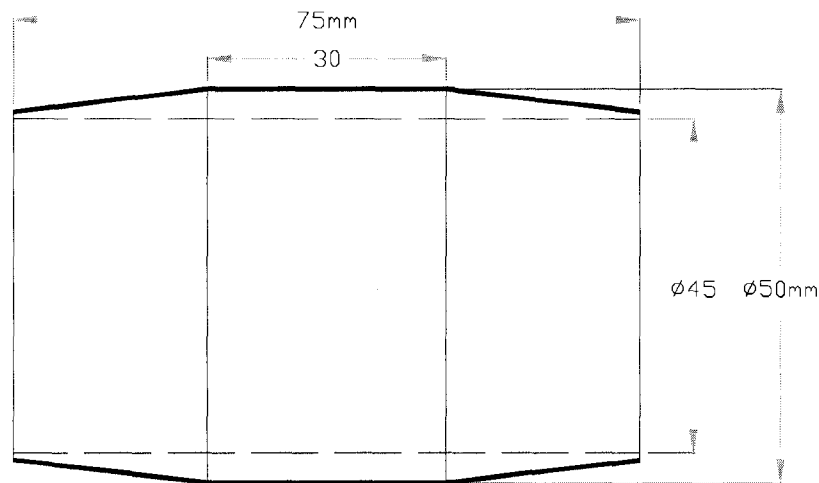


**Figure 5-52: Aluminum liner to reinforce the fourth composite tube**

### 5-6.1 Layup of the tube

While it was certain that the third composite tube had all potentials to match with its aluminum counterpart, it was decided to manufacture a similar tube and repeat the test using the aluminum liner. However, due to the shortage of Carbon AS4/PEKK slit tape, it was decided to use only the general layup presented in Section 5-5.1

$$[90^{\circ}_{n1} / \pm 25^{\circ}_{n2} / 90^{\circ}_5 / \pm 30^{\circ}_{n3} / 90^{\circ}_5 / \pm 45^{\circ}_{n4}]$$

Layer number: [ 1 / 2 / 3 / 4 / 5 / 6 ]

and design a composite tube that matches a thinner aluminum tube. The dimensions of the aluminum tube were assumed as follows:

Material: AL7075-T6;

Inner Diameter: 56mm;

Thickness of the tube: 10mm;

Weight per unit of length of the tube: 5.6 kg/m.

From previous designs, it was known that the outer diameter of the composite tube would be larger than that of the aluminum tube if the same stiffness needs to be achieved. On the other hand, for many applications including the helicopter landing gear, it is preferred if the outer diameters of the composite and aluminum tubes are the same or very close to each other. As such, it was decided to reduce the inner diameter of the fourth composite tube to 50mm. This would help in keeping the outer diameter of the composite tube closer to that of its aluminum counterpart tube. Moreover, the innermost 90° ring would be more capable of resisting the radial loads when its inner diameter is smaller.

### 5-6.2 Stress analysis of the layup

The same stress analysis procedure as before was used to design the fourth composite tube. Table 5-7 illustrates the results of calculations. Comparison of the flexural, torsional and extensional stiffness of the tubes shows that the composite tube is superior. Furthermore, the weight per unit of length of the composite tube is lower, and this secures 30% weight saving that would be very valuable for aerospace applications.

	Aluminum 7075-T6	Carbon AS4/PEKK
Lay up	NA	[90° <sub>20</sub> / ±25° <sub>20</sub> / 90° <sub>5</sub> / ±30° <sub>25</sub> / 90° <sub>5</sub> / ±45° <sub>10</sub> ]
Tube Dims, mm	ID 56 OD76	ID 50 OD78
E <sub>xx</sub> , GPa	70	56.7
E <sub>yy</sub> , GPa	70	40.1
G <sub>xy</sub> , GPa	27	22.6
EI <sub>xx</sub> , N.mm	1.53E+09	1.57E+09
EI <sub>yy</sub> , N.mm	1.53E+09	1.03E+09
GJ, N.mm	2.37E+09	2.83E+09
Tube Area mm <sup>2</sup>	2073	2814
AE <sub>xx</sub> , MN	145	293
Weight Kg/m	5.6	3.9

**Table 5-7: Design parameters of the aluminum and fourth composite tubes**

The next step is to assure that the composite tube would have the same or higher strength. Figure 5-53 illustrates the aluminum sandwich panel. To simplify the analysis, it is assumed that the skin is made of four equal thickness layers made of aluminum 7075-T6. It is also assumed that the properties of the material in tension and compression are the same, and the panel is subjected to pure bending,  $M$ . The Laminate Analysis Program was used to find out at which load the panel starts plastic deformation, and finally what could be the maximum load that the panel might resist.

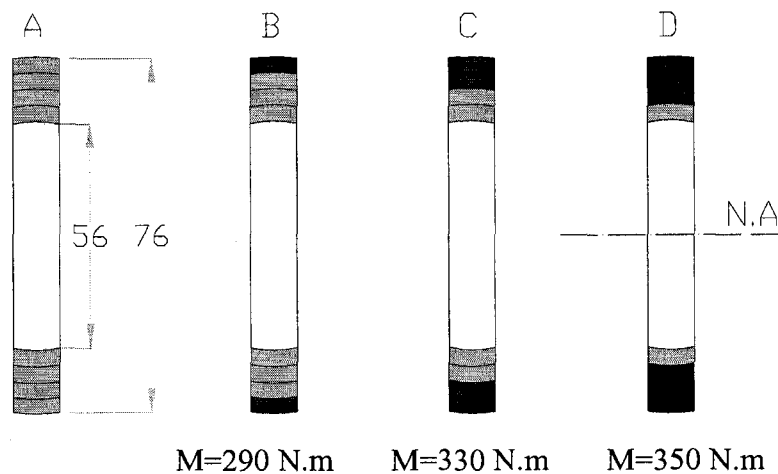


**Figure 5-53: Failure process of the aluminum panel  
(Shaded areas show the failed region)**

As the material is the same for all layers, and the strain varies linearly from the neutral axis, N.A., the first layer to exceed the yield stress would be the layer furthest from the neutral axis. As shown in part B of the figure, a bending moment equal to 290 N.m would be required. Increasing the bending moment to 330N.m and next to 350N.m would cause the second and third layers to fail as shown in parts C and D of the figure. At this point, the most part of the beam is in the plastic zone, and the load can not be increased considerably.

Similarly, Figure 5-54 shows the composite sandwich panel. The red zones (dark gray in black and white prints) show the failed layers as the bending moment was increased. The first layers to fail are 90° layers in tension zones, shown by *B*, *C* and *D* in the figure. It can be seen that bending moment required to have the first ply failure, 400 N.m, is more than the bending moment that causes the outermost layer of the aluminum to fail. Moreover, as it can be seen in parts *F* or *G* of the figure, the bending moment required to produce considerable failure in different layers is much larger than the bending moment required to deform the aluminum panel into the plastic zone.

In these analyses, the effect of strain hardening for aluminum panel is not considered. Moreover, the stiffness of the failed composite layers in tension and compression is reduced by 50% and 30% respectively. Even though these assumptions may not be precise, it is clear that the strength of the composite panel is not less than that of the aluminum panel.

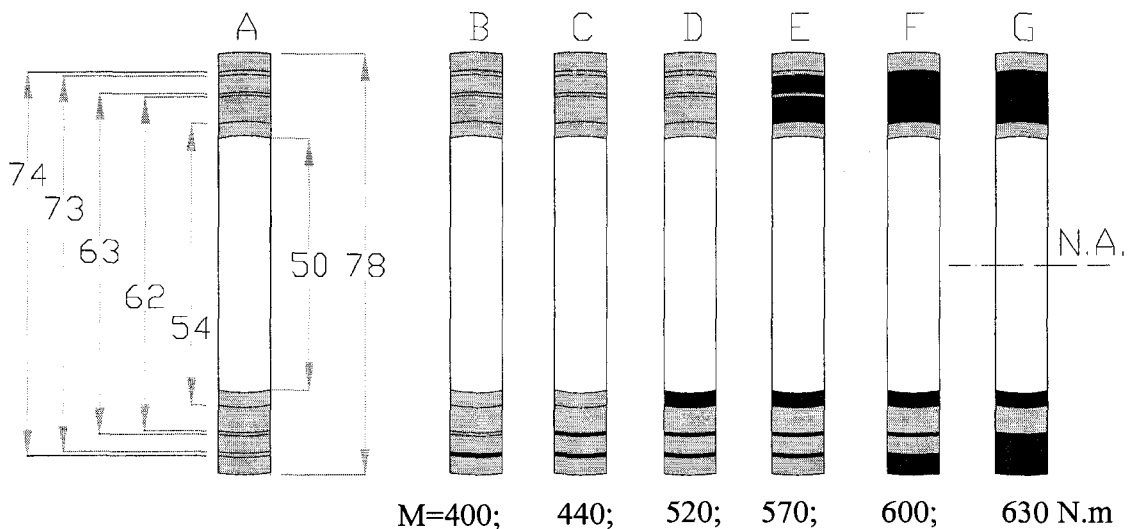


**Figure 5-54: Failure process of the fourth composite panel  
(Shaded areas show the failed region)**

Figure 5-55 schematically illustrates the cross section of the fourth composite tube. The sequence of failure in different layers based on the above analysis is shown by the numbers in the small circles. The points on the figure refer to the most probable locations of failure. It can be seen that failure should start in the lower part of the tube that is under tension and then jump to the upper part of the tube that is subjected to compression. Finally layers 6 and 4 fail in tension zone. By this time, it is expected that the tube would fail totally, and the analysis shows that the strain at point *A* would be around 2.2%. It is noteworthy that the failure sequence is exactly the same as that predicted for the third composite tube even though the dimensions of the tubes were different.

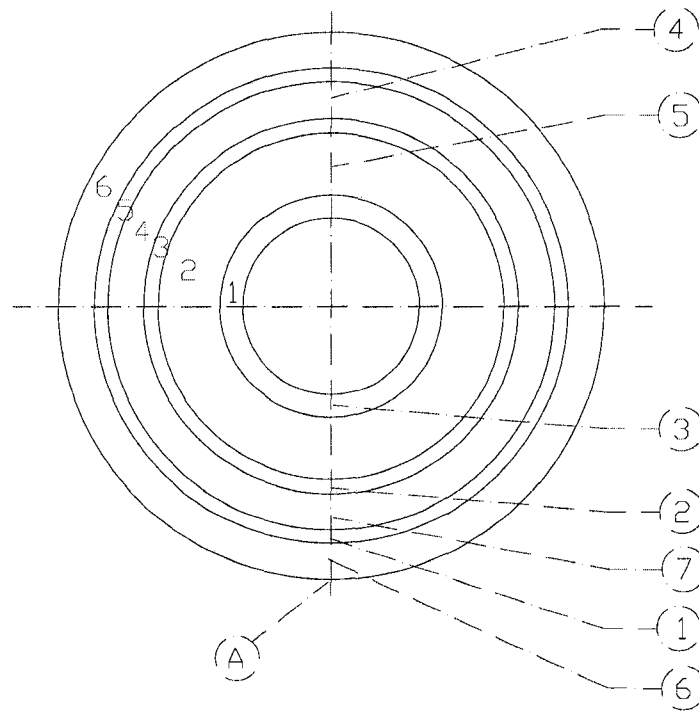


**Figure 5-55: Sequence of failure for the fourth composite tube.**

### 5-6.3 Testing and the results

Figure 5-56 illustrates the test set up for the fourth composite tube. As it can be seen in the figure, a new fixture with double curvatures was used as loading nose to assure that the load would be applied on the tube properly, and no local damage would be imposed on the tube. The design of the fixture is presented in Appendix D.

A double or  $T$  strain gauge was installed at the bottom line of the tube at the mid-span to measure the longitudinal and circumferential strains.

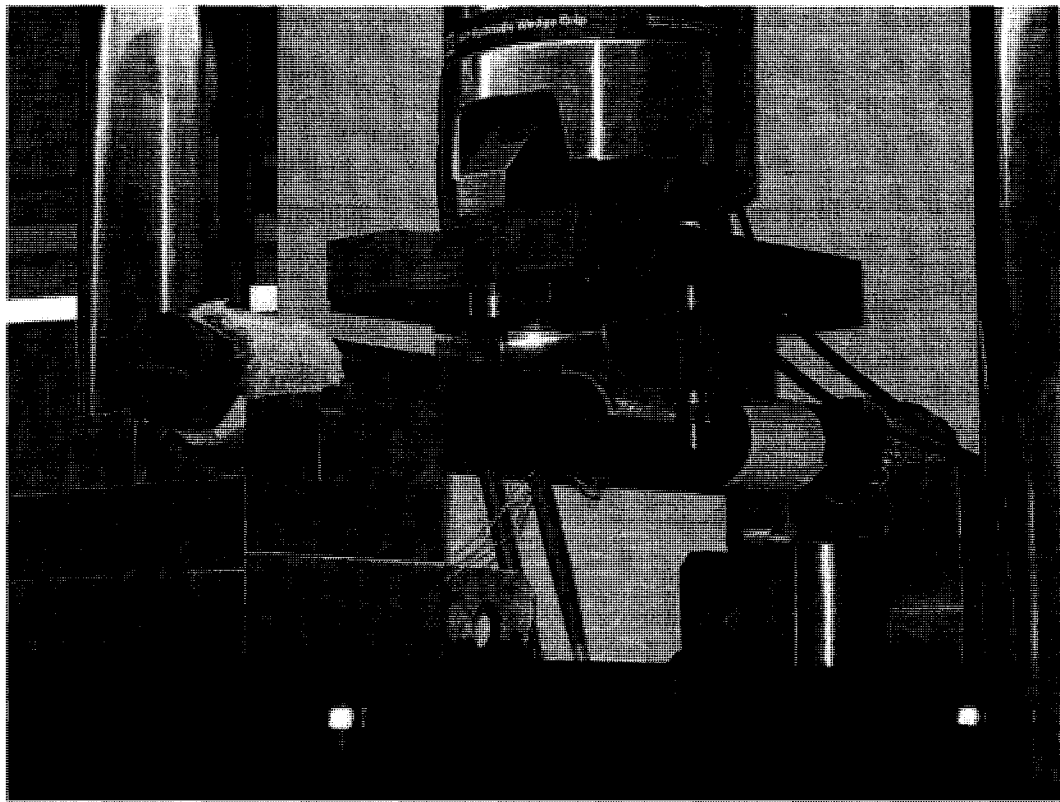


**Figure 5-56: Test set up for the fourth composite tube**

Figures 5-57 a & b show the tube configurations during the test and at the final stage, when the test was stopped deliberately for further study. The tube showed 2% strain while the load stayed at about 90% of its maximum during the test.

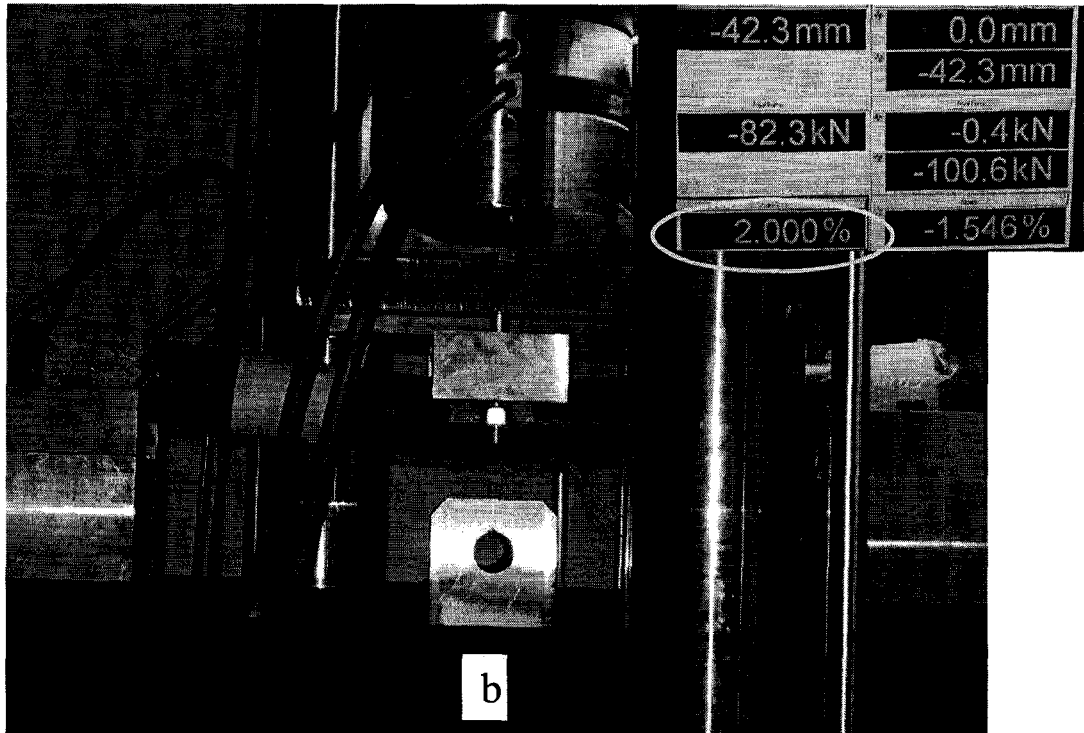
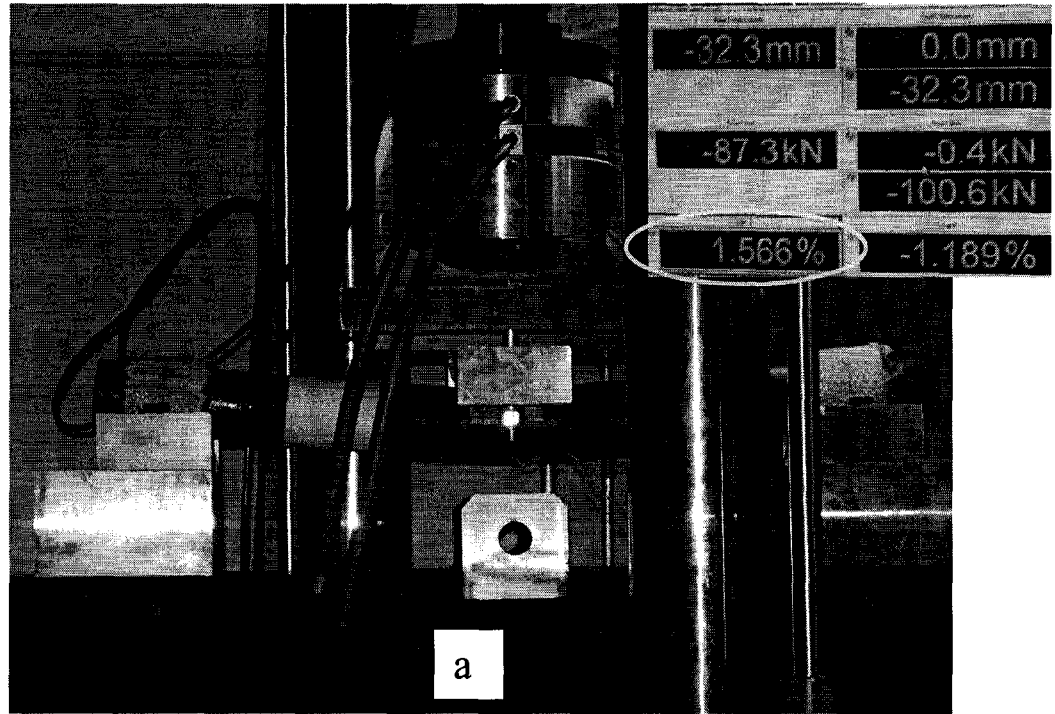
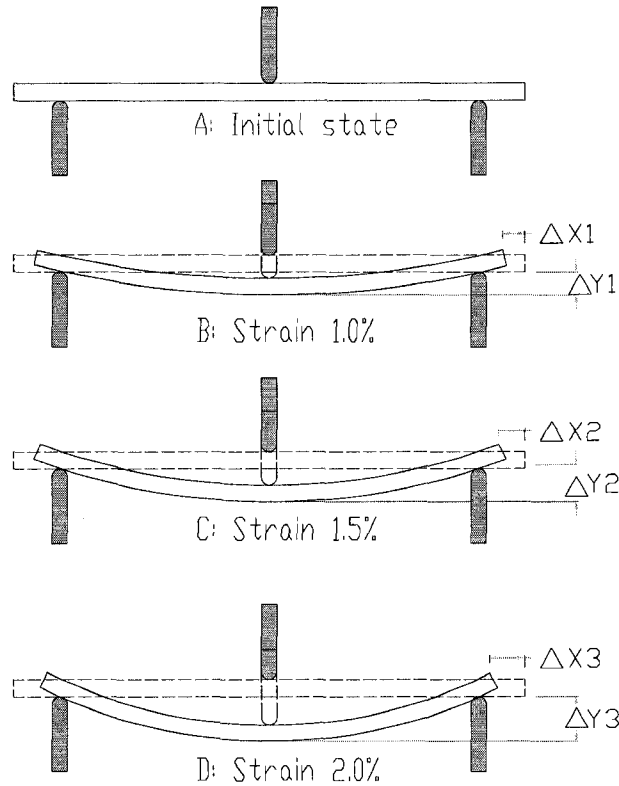


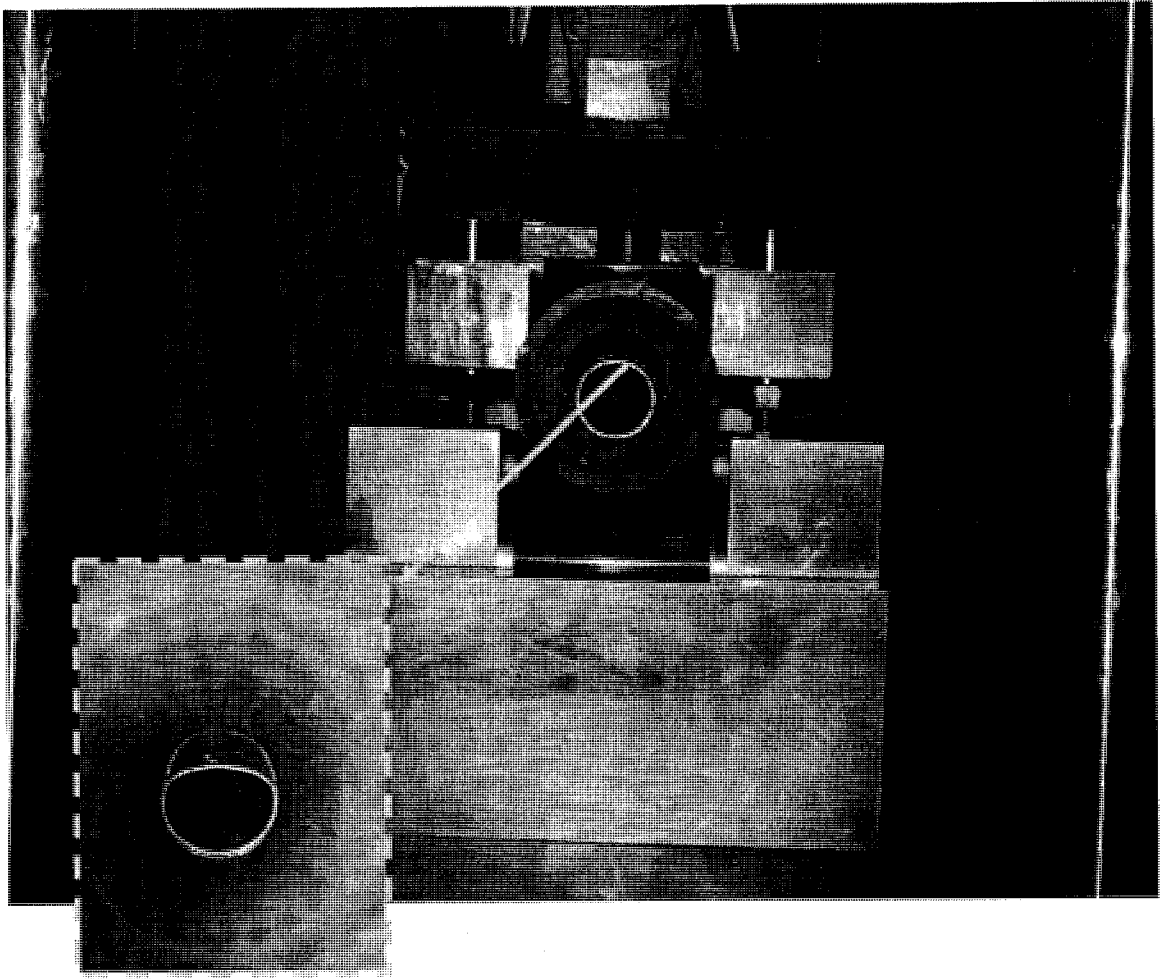
Figure 5-57-a, b: Bending test of the fourth composite tube

Figure 5-58 schematically illustrates the fourth composite tube at different stages during the bending test. Based on Figure 5-57 and these sketches, the tube deformed uniformly throughout the test. The curvature of the tube varied consistently according to the variation of bending moment across the beam, and no local deformation was observed.



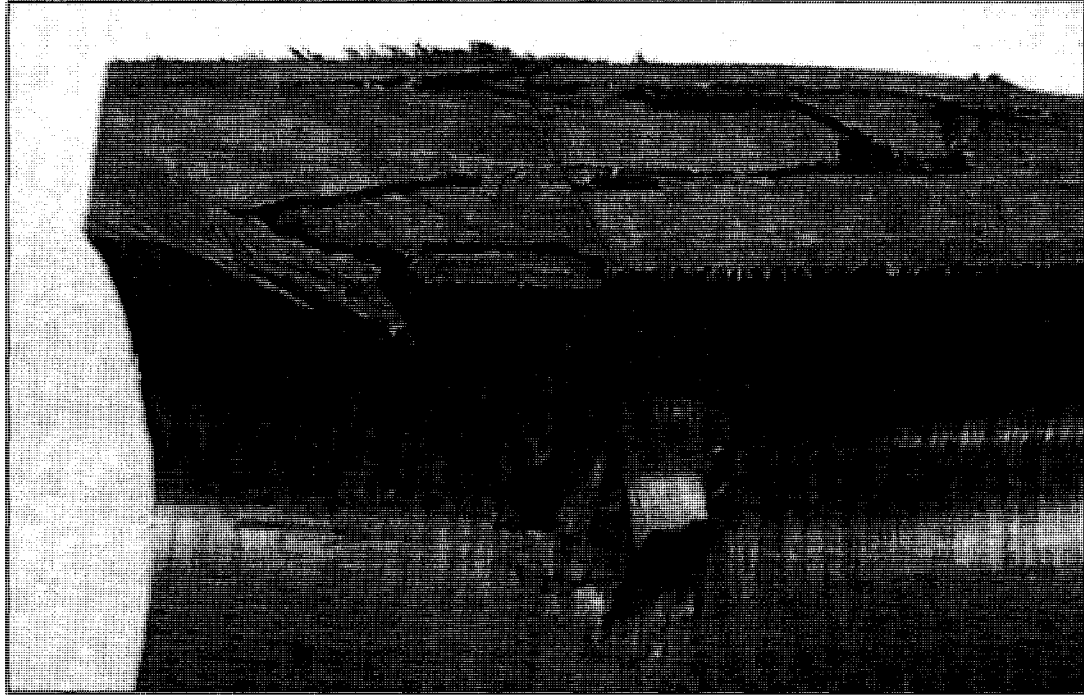
**Figure 5-58: Schematic representation of the bending of the fourth composite tube**

Figure 5-59 shows the aluminum liner inside the fourth composite tube. It can be seen that the thin aluminum ring deformed plastically as the radial load was increased on the tube. The ring had been pressed fit inside the tube and stayed fit until the end of the test. On the other hand, it was not very stiff to prevent the natural deformation of the tube. The aluminum liner kept the 90° innermost layer in place, and no collapsing occurred during the test.



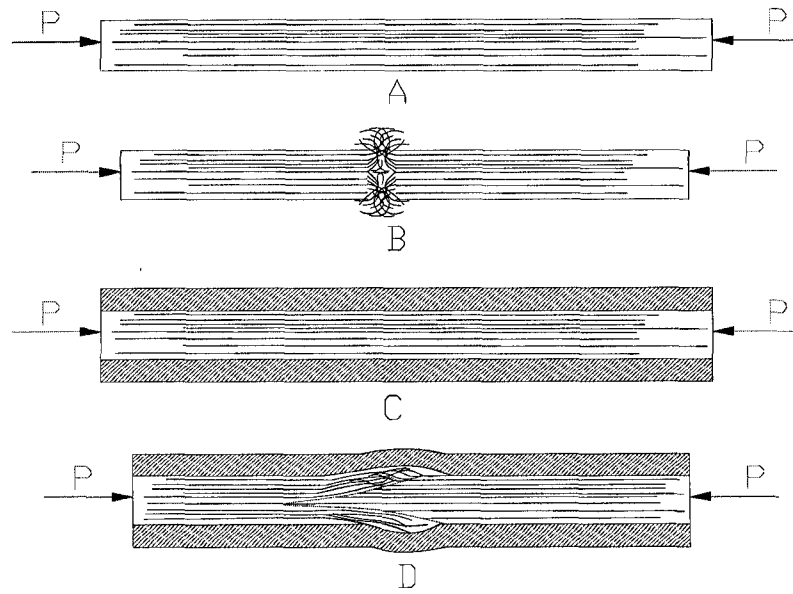
**Figure 5-59: The aluminum liner inside the fourth composite tube**

Figure 5-60 shows fracture and delamination of the layers at mid span of the fourth composite tube. Referring to Figure 5-55, layers 2 and 4 fail due to the compression stresses.



**Figure 5-60: Delamination and fracture of the layers at the mid span of the fourth composite tube**

Nevertheless, when a layer fails due to the compression, it would like to deform as the sketch shown in Figure 5-61 (B). However, in the current design, layer 4, which is  $\pm 30^\circ$ , is confined with layer 6, which is  $\pm 45^\circ$  laminate and capable of large deformation. As such the broken fibers would crush into each other and push their adjacent layers out. If the adjacent layers are brittle, like  $90^\circ$  layer, they collapse and break as it was observed for the innermost  $90^\circ$  layer during the test of third composite tube. In contrast, when the adjacent layer can absorb large deformation, a little bump may be produced under the surface as shown in Figure 5-61 (D). In this situation, the flexural stiffness of the tube is not reduced considerably because the layers that failed in compression are still capable of carrying more loads. As such, the load carrying capacity of the tube would remain at a high percentage of its maximum.



**Figure 5-61: A, B, C & D Failure due to compression stresses**

Figure 5-62 shows the variation of the force versus time during the test. For brittle composite materials where their fracture is always abrupt, this type of behavior is very unique. The force was kept at a constant high level; the deformation and strain increased; and the time was ongoing. This kind of behavior is characteristic of ductile structures. While all evidences during the test were indicating a successful design, the outcome was better understood when the force-strain curves for the fourth composite tube was matched with that of the aluminum 7075-T6 tube. As it can be seen in Figure 5-63, the fourth composite tube showed the same flexural stiffness as its aluminum counterpart. Moreover, as it had been theoretically predicted, the composite tube demonstrated higher strength and load carrying capacity than the aluminum tube. More importantly, the composite tube kept its load carrying capacity at the same level as the aluminum tube until 2% strain was achieved. The energy absorption of the composite tube was also slightly more than that of the aluminum tube.

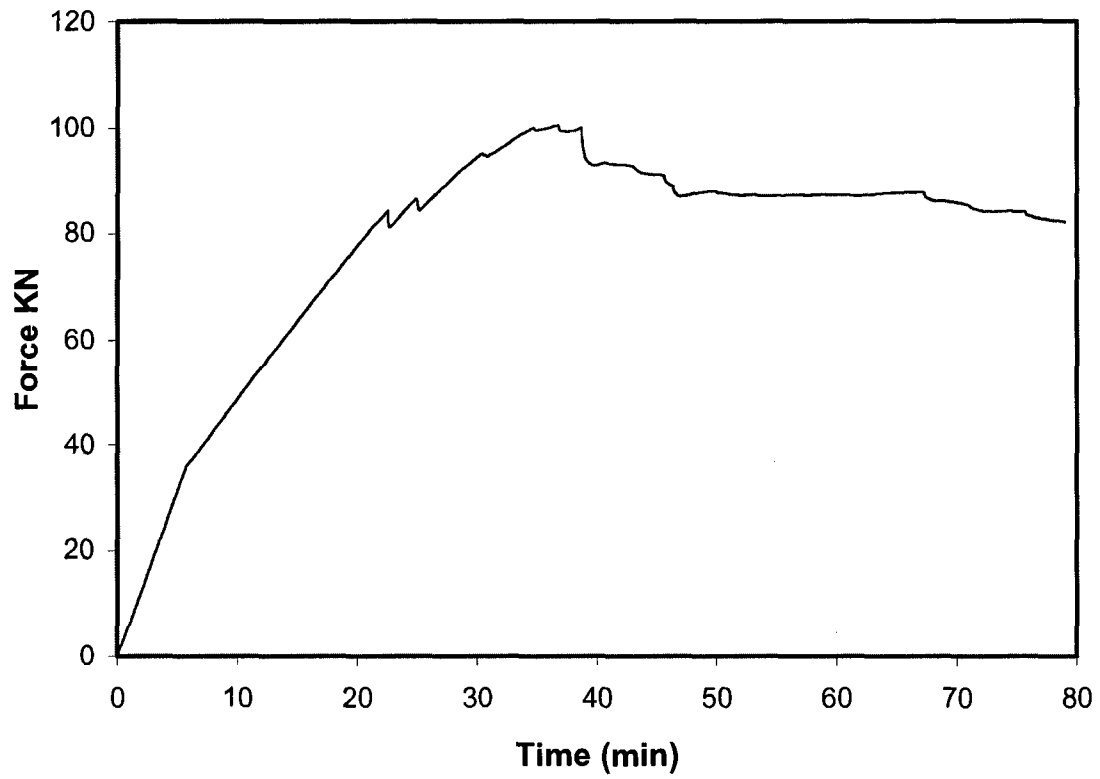


Figure 5-62: The fourth composite tube kept the load level during the test

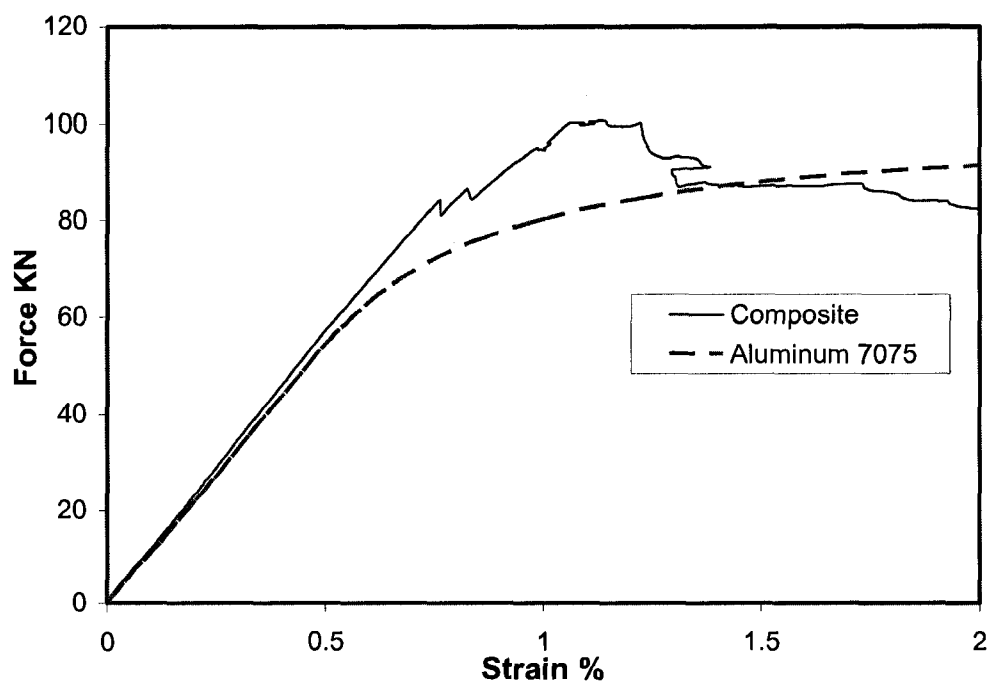
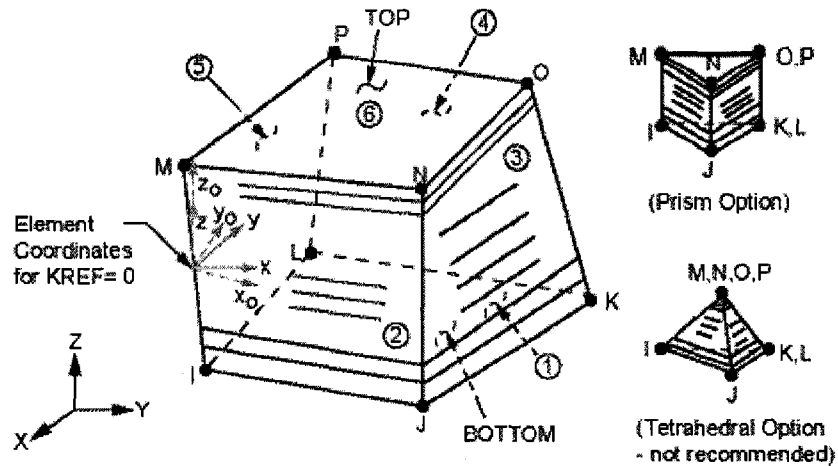


Figure 5-63: Force-strain curves of aluminum and fourth composite tubes

## 5-7 ANSYS results

The plastic deformation in isotropic tubes subjected to bending loads starts at the outermost skin of a critical section, where the stresses are maximum, and may proceed through the length or through the section of the tube in a uniform fashion depending on the state of stress. Composite tubes, however, illustrate geometrically random failure through the section due to the difference in the strengths and stiffnesses of the layers. The first ply failure may occur at a point where interaction of stresses indicates breakdown of a layer according to one of stress failure criteria such as Tsai-Hill. This layer is not necessarily located at the furthest point from the neutral axis of the tube. The first failure may occur at any point through the thickness depending on the material properties, ply sequence and fiber orientation. After first ply failure, even though the whole structure may not collapse, the flexural stiffness and load carrying capacity of the tube may be reduced. Some load may be released but the structure continues to deform at a lower load level until another ply fails. A similar procedure is continued until a considerable number of layers fail. At this point, the structure may not be capable of carrying more loads and final fracture may occur.

In this research, the progressive failure analysis of the layered composite tubes using commercial software ANSYS was performed by Xu (2008). The element used to perform the analysis is a layered solid element, SOLID46, as shown in Figure 5-64. The tube is meshed by 70 elements in longitudinal, 32 elements in circumferential and 7 elements through the thickness, as shown in Figure 5-65, so the total number elements are 15680. Load is applied at the midpoint of the tube on the top surface over an area that is approximately the same as that of the load application pad for the experiment.



**Figure 5-64: Geometry of layered element SOLID46  
(Adopted from ANSYS Instruction Manual)**

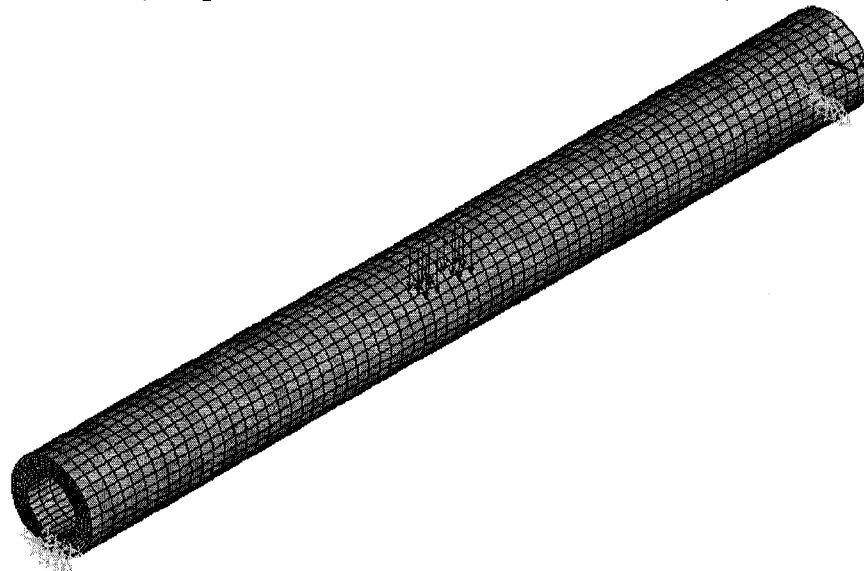


**Figure 5-65: ANSYS model of the Fourth composite tube, Xu (2008)**

Progressive failure analysis was used. For any layer in any element whose stress has reached the limit, the elastic constants of the layer are degraded before the analysis is resumed. If the event is along the fiber direction, then the Young modulus  $E_1$  along the fiber direction and the in-plane shear modulus  $G_{12}$  are degraded to 0.01% of their initial values. If the event is transverse to the fiber direction, then the modulus  $E_2$  is degraded to a value that is 0.01% of its initial value.

Figure 5-66 compares the force-axial strain curves for the Fourth composite tube achieved by ANSYS analysis and experiment with that of an aluminum tube. The prediction of stiffness and maximum load carrying capacity of the tube by ANSYS illustrates good agreement with experimental results. However, the results for ANSYS analysis are only available until 1.2% axial strain is achieved.

The agreement between ANSYS analysis and experiment is very important since this has the potential to save efforts in manufacturing and testing of composite tubes which is very time consuming and expensive. From this agreement it can be claimed that the ANSYS model and the deployed analysis technique are valid, and they can be used to predict the strength, flexural stiffness and failure modes of composite tubes.

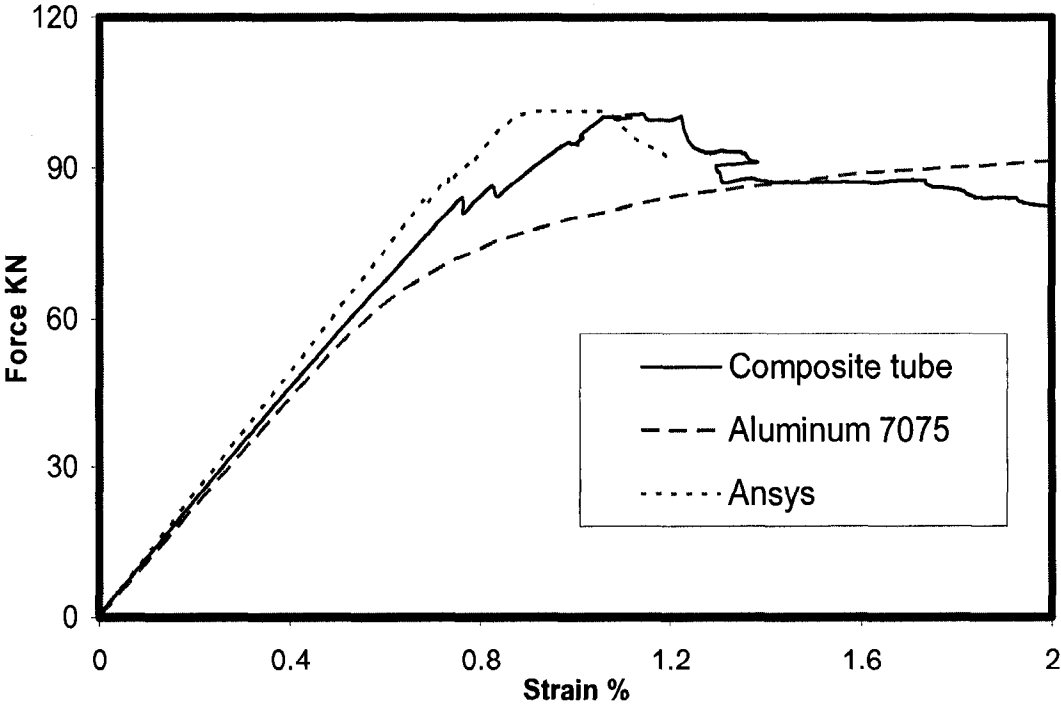


**Figure 5-66: Force-axial strain of the Fourth composite tube in comparison to that of aluminum tube.**

## 5-8 Extraction of design procedure

CFRP composites are typically brittle materials with very low fracture strain. Their fracture is abrupt, and they usually show very linear behavior before first ply failure. A high performance composite usually consists of more than 60% brittle fibers. As such, the brittleness of composites is associated with the low fracture strain of the fibers.

Despite the brittle nature of the material, a composite laminate may still show some nonlinear behavior and large deformation if certain conditions are fulfilled. For example, debonding between the fibers and the matrix is the primary source of brittle fracture in  $90^\circ$  laminate, where the ductile matrix is expected to be dominant. As such, in a design for large deformation, enough attention must be paid on how the structure is loaded, so the layup of the laminate can be tailored to avoid this type of failure.

On the other hand, matrix extension and fiber rotation can be excellent mechanisms for large deformation. In a laminate like  $\pm 45^\circ$ , the matrix is more probably loaded in shear. Therefore no major debonding occurs, and the matrix has more chance to deform. Meanwhile fibers can align themselves along the force direction. The two mechanisms together result in large deformation and high fracture strain for  $\pm 45^\circ$  and  $\pm 30^\circ$  laminates.

In contrast, the domino effect is an undesirable fracture mechanism in the failure of the laminates, and it must be avoided. When the layup of the laminate includes very low angle plies, a shock is imposed onto the laminate upon failure of these layers. As such, the rate of loading would be very high, and the time would not be sufficient to redistribute the loads among safe layers. Accordingly, fracture of low angle plies is accompanied by abrupt fracture of the laminate. If the structure requires large

deformation and large strain to failure, including low angle plies in the layup must be avoided.

Composite laminates may show higher failure strain as the angle of the laminate is increased up to  $45^\circ$ . In other words, strain-to-failure of  $\pm 20^\circ$  laminate is less than that of  $\pm 30^\circ$  laminate. The maximum failure strain belongs to  $\pm 45^\circ$  laminate. Such laminate can show more than 15% strain yet the fracture may not occur. Moreover, if the adjacent layers are isolated from each other, for instance by inserting a film of polymer between the layers, their mutual restriction is reduced, and more deformation can be achieved.

### **Design of composite tubes**

Composite materials are orthotropic, and their mechanical properties are highly directional. Hence, the first step in the design of a composite structure is a thorough understanding of the nature of the loads. For example, beams, tubes, the cabin of trains and even the fuselage of airplanes are mainly subjected to longitudinal stresses due to bending rather than transverse or shear stresses. In other words, even though the strength of the composites is lower in one direction as compared to the other, there are numerous applications where stresses are also the same, and this is the point that composites can be deployed to produce a lighter structure.

In design of the composite tube, the first step is to determine the required strain level. In fact, large deformation of a structure is not necessarily accompanied by large strains. In contrast, due to rigid body motions and geometrical constraints, plastic strain can be relatively low. In these cases, using the explained mechanisms of large deformation for composite laminates, it would be possible to design a composite tube with potential of

large deformation and high strain to failure. For Carbon AS4/PEKK composite, this threshold is 2.5% strain. As such, it would be possible to design a composite landing gear because the aluminum cross tube does not require more than 2.5% strain during a severe landing.

When the strain level is known, a linear strain distribution throughout the cross section is considered. At this point, it can be assumed that the composite tube has the same inner and outer radii as its aluminum counterpart. The thickness of the tube is divided into a few layers. The required strain of each layer is calculated based on the available strain distribution. On the other hand, if the mechanical behavior of the composite is characterized, as it was done in this work for Carbon AS4/PEKK, the strains to failure of different balanced laminates are known. As such, according to the required strain for each layer, it would be possible to choose a proper laminate for each layer. For example, if at a distance from the neutral axis of the tube only 1.8% strain is required,  $\pm 20^\circ$  laminate can be laid up at that location, Table 5-1. Similarly, if at the outer layer more than 4% strain is required,  $\pm 45^\circ$  laminate is the only option.

As can be seen, this type of design, which is called strain-controlled design, is totally different from the traditional design procedure for beams or sandwich panels subjected to flexural loading. In a normal design, strong and stiff layers are laid up at the furthest points from the neutral axis to have the maximum contribution in the moment of inertia of the section. For example, in the design of sandwich panels, the skins are usually made of strong and stiff materials while the core is made of a light material with high shear strength. In contrast, in the design of a composite tube, the strong and stiff laminates are laid up as the inner layers to fulfill the requirements of strain while  $\pm 45^\circ$  laminate with

low strength and stiffness is laid up as the outer jacket to keep the integrity of the tube and provide large deformation.

Following this procedure, usually a layup such as

$$[\pm 20^{\circ}_{n1} / \pm 25^{\circ}_{n2} / \pm 30^{\circ}_{n3} / \pm 45^{\circ}_{n4}]$$

is achieved, yet the number of plies,  $n$ , should be determined according to the requirements of strength and stiffness of the tube. The stress analysis of the tube to find the optimum combination of plies is a very intricate task, however. The design parameters include determining the inner and outer radii for each ring or layer, layup angle, reducing weight, maximizing the strength and stiffness of the tube while keeping the layup recommended by strain controlled design to assure large deformation. These parameters are very often contradictory, so the design task would remain complex. A simplified method is presented in this work for the purpose of stress analysis of composite tubes.

### **Stress analysis technique**

A strain controlled design does not specify the number of plies in each layer and does not guarantee the required strength and stiffness. Moreover, matching the strength and stiffness of the composite tube with those of the aluminum tube may require the composite tube to have different inner and outer diameters. As such, the position of each layer might be slightly altered, so the required strain for each layer must be rechecked after the stress analysis of the tube is done.

In order to simplify the analysis, a sandwich panel model as shown in Figure 5-10 is used. The main challenge is to find the optimum numbers of plies for each layer so that a

light composite tube with similar extensional, flexural and shear stiffness as the aluminum tube is achieved. Computer programs such as Laminate Analysis Program or LAP may be used to carry out calculations based on Classical Laminate Theory. The extensional, torsional and flexural stiffness of aluminum and composite sandwich panels should be matched while weight saving must always be considered.

Due to the high number of design parameters and some unknown behaviors of the composite tubes, through this research a systematic iteration procedure was set. Four composite tubes were designed, fabricated, tested and analyzed. The observations of each test were used to improve the design of the next tube. The target was set to present a layup and design a composite tube that matches the strength and stiffness of its aluminum counterpart while capable of large deformation and high strain to failure. Through this progressive design procedure, a tube was finally designed that its behavior under bending loads is far from the brittle behavior of the traditional composite tubes with abrupt fracture. Some observations that improved the design are as follows:

- 1- The innermost ring of the tube should be a strong ring of  $90^\circ$  plies to resist hoop stresses and radial forces at the loading nose.
- 2- A jacket of  $\pm 45^\circ$  plies as the outermost layer of the tube would keep the integrity of the tube, provides large deformation, and restricts the movement of layers that failed due to compression stresses.
- 3- If a thin  $90^\circ$  layer is laid up between the adjacent layers, the layers would have more flexibility and freedom of movement. This would contribute in large deformation of the tube.

- 4- Low angle plies such as  $0^\circ$  layers are not recommended to be included in the layup of the tube. First,  $0^\circ$  layers have very low fracture strain. Second, upon their failure a shock is transferred into the structure, and the rest of layers would not be capable to absorb this high rate of loading, so the laminate fails abruptly.
- 5- The compression strength of the composite laminates might be less than tensile strength. As such, the movement of the fractured layers might be restricted by adjacent layers, so the load carrying capacity of the tube does not reduce considerably.
- 6- A metal liner is required inside the composite tube to prevent collapse of the innermost ring at the loading points. This liner keeps the layers failed due to compression stress in place, so the tube can carry more loads until the point that fracture occurs in tension zone of the tube.

Considering all above mentioned analyses and observations, the following layup is suggested:

$$[90^{\circ}_{n1} / \pm 25^{\circ}_{n2} / 90^{\circ}_5 / \pm 30^{\circ}_{n3} / 90^{\circ}_5 / \pm 45^{\circ}_{n4}]$$

Layer number: [ 1 / 2 / 3 / 4 / 5 / 6 ]

Layer 1 is the innermost ring of the tube. This layup can provide any composite tube with the requirements of large deformation and avoids abrupt fracture. The numbers of the plies for each layer, however, should be determined using computer programs such as ANSYS or by using the simplified method presented in this work. In order to match the strength and stiffness of the composite tube with those of its aluminum counterpart, the thickness of the composite tube might be slightly higher. However, it was shown in this

research that the composite tube can be still 30% lighter than high grade aluminum 7075-T6 tube. Matching the properties of lower grade aluminum tubes will remain more convenient, and more weight saving can be achieved. Figure 5-67 illustrates the design procedure.

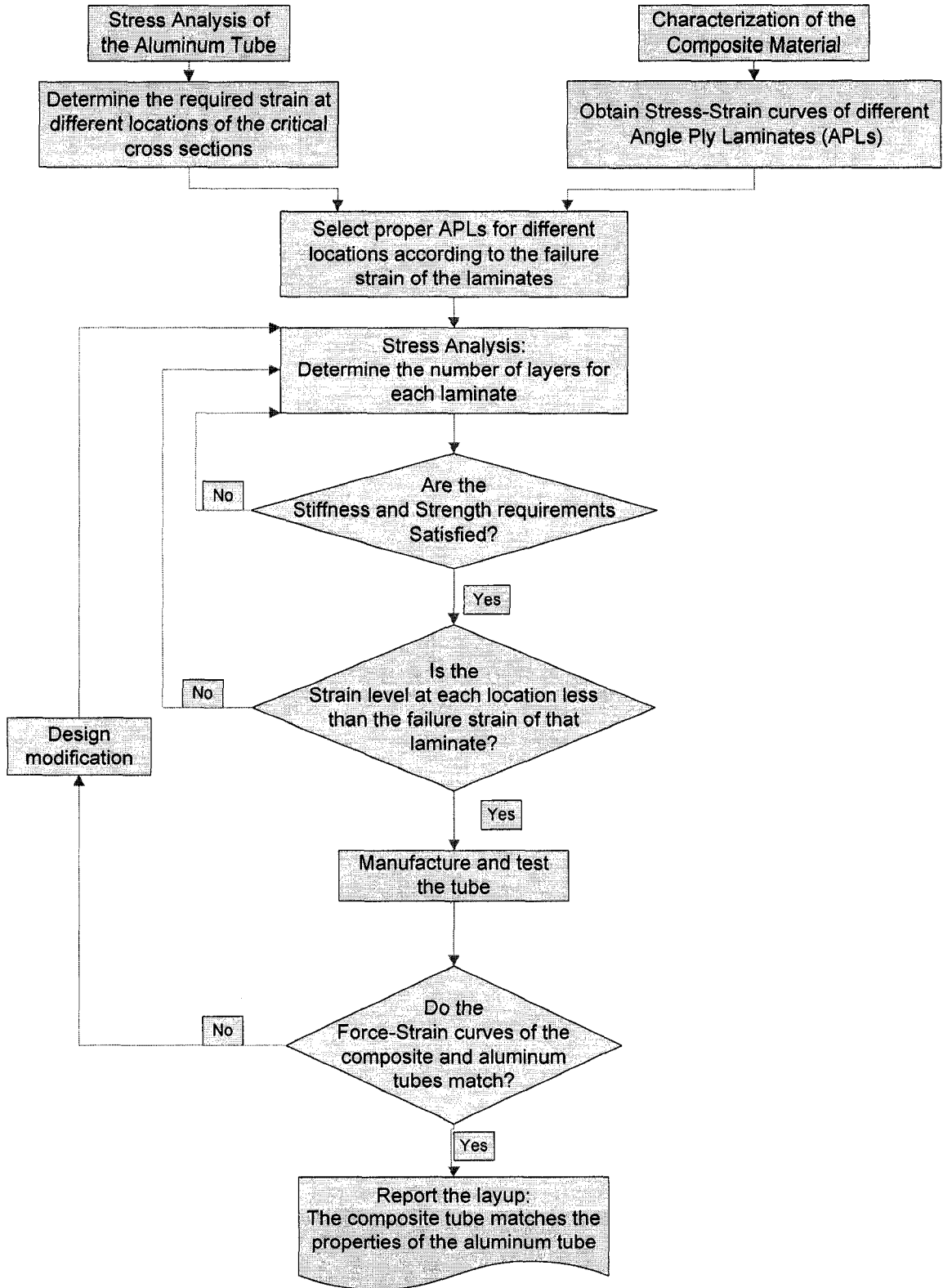


**Figure 5-67: Design flowchart for deformable composite tubes.**

# **Chapter 6**

## **Summary and Conclusions**

### **6-1 Summary**

CFRP composites have proved their great potentials for many aerospace applications, where the high performance can justify the high cost. However, the brittleness of the composites has been a main drawback for many applications that require large deformation, high failure strain and extensive energy absorption before final fracture occurs. The objective of this research was to present a solution to the brittleness of the composites in tubular form and to introduce a composite tube that shows the same strength, stiffness and failure strain as its high grade Aluminum 7075-T6 counterpart tube.

One application of this research can be in the development of composite landing gear for helicopters. Up to date, almost all helicopter landing gears are made of high strength aluminum, and despite their major problems in maintenance and fabrication, aluminum landing gears have remained the only choice for helicopter manufacturing industry. Still,

composites are not considered as a reliable source to substitute high grade aluminum alloys for such a heavy duty application. Nevertheless, the outcome of this research can open a new window for the aerospace industry to seek a solution for brittleness of their composite tubes through the design presented here.

The research was conducted in two major sections. As the first step, the mechanical behavior of flat plate Carbon AS4/PEKK was characterized. Carbon fiber has been the major reinforcement for aerospace applications. Different combinations of carbon fiber and thermosetting polymers have been available in the market for relatively long time. However, thermoplastic composites are new, and no extensive database is available for these materials even though they have very high potentials due to their inexpensive and fast manufacturing process. Besides seeking the general mechanical properties of Carbon AS4/PEKK laminates, special attention was made to find different mechanisms that may improve deformability of the composite laminates. It was learned that the laminates must be loaded in angles between 25 to 45 degrees if large deformation is required. Fiber rotation, matrix extension and isolation of the adjacent layers are other mechanisms that improve the ductility of the laminate.

The second major focus of the research was to design a composite tube that shows the same strength, stiffness and energy absorption as its high grade aluminum counterpart. First, a proper three-point bending test procedure was established to meet the requirements of testing the composite tubes. Second, after discovering that the traditional stress analysis approach does not meet the design targets, an innovative approach called Strain Controlled Design was presented instead of conventional strength and stiffness controlled designs. Then, a methodology was presented to design the composite tubes by

simulating a cross section of the tube by sandwich panels. The accuracy of the method was confirmed when the test results exactly matched the theoretical predictions. In a parallel work to some parts of this research, ANSYS was employed to verify the accuracy of the methodology presented here for design purposes. The ANSYS results were always confirmative.

Four composite tubes were designed, manufactured and tested during this research. The acquired information of each test was adopted and implemented in the next design. Final achievement of this research is to introduce a simplified design procedure for composite tubes and present a general layup for tubular structures that require large deformation.

## **6-2 Conclusion**

The following conclusions can be made from this research:

- Composite laminates can show relatively large strains and deformations when loaded off-axis due to the fiber rotation and matrix extension. Isolating the adjacent layers from each other by soft layers such as polymer films can increase flexibility and freedom of movement for the layers. This mechanism can be used to improve strain to failure of the composite laminates in the form of plates or tubes.
- It is possible to design a composite tube that demonstrates similar behavior as its aluminum counterpart tube under bending. The test results of the fourth composite tube showed that the tube had the same flexural stiffness, slightly higher strength and load carrying capacity and large strain to failure. The tube was capable of redistributing the loads upon failure of an arbitrary weak layer. No sharp

reduction in the load level was observed after failure of any layer. The tube kept its load carrying capacity throughout the test period. While the natural behavior of brittle composite structures is to have abrupt fracture, the behavior of the fourth composite tube was closer to elastic-plastic behavior than brittleness. This is a unique outcome of this research.

- At high level loads, aluminum tubes deform plastically to show large strain to failure. Composite tubes go through progressive failure, delamination and rotation of the fibers to comply with the requirements of large deformation.
- Testing procedure is quite important in properly characterizing the behavior of composite tubes. Composites are not usually designed to resist out-of-plane stresses. During the bending test, an enormous load is applied in radial direction, which is normal to the plane for the laminate. This might cause premature failure in a local area and prevents the tube from demonstrating its natural behavior. In such cases, the tube should be reinforced at loading noses and supporting points.
- Design of a composite landing gear is feasible. However, the structure may not be the same as the current aluminum landing gear.

### **6-3 Contributions**

The main contributions of this effort are to break the belief of CFRP composites brittleness and to open a new window for numerous applications. For many years, composites have been known for their high specific strength and stiffness; however, they never disposed of their brittleness.

Carbon AS4/PEKK was a new high performance material in the market, and no open database was available for this material. Through extensive studies, the performance of this composite was studied, and an open reference for the material was created. However, the outcomes of these studies were far beyond characterization of the material. In fact the core of this research was maintained on how to overcome the brittleness of CFRP composites. To achieve this goal, all possible mechanisms for large deformation of composite laminates were sought.

It was discovered that through three mechanisms the deformability of composite laminates can be improved. First, debonding between the fibers and matrix is a major cause of crack propagation inside the laminate, and it must be prevented. Second, the matrix can only contribute in the deformation of the laminate by shear extension. In the fiber direction, fibers are dominant, and in the transverse direction debonding is the concern. In neither case, the matrix has a chance for extension. In contrast, for angle laminates high failure strain can be achieved as the angle approaches  $\pm 45^\circ$ . Third, fiber rotation can improve the ductility of the laminate. The maximum fiber rotation is achieved when the restriction of the adjacent layers on top of each other is removed. In the laminate form, film plies of the same matrix can be inserted between the layers. In the tubular form, inserting a few  $90^\circ$  plies would show the same performance.

The second achievement of this research is introduction of a simple semi analytical method for stress analysis of composite tubes. The system of analytical equations derived according to the fundamentals of stress analysis of anisotropic media includes many unknown variables. The solution to this system is cumbersome. The method presented in

this study is very simple and straightforward. The results, however, were confirmed by ANSYS analysis and experiments while a great confirmation was achieved.

Finally, all above mentioned discoveries and analysis techniques were used to design a composite tube with same mechanical properties as its aluminum counterpart. According to the general layup presented here, for any aluminum tube with any thickness, a counterpart composite tube can be designed that shows the same strength and stiffness as the aluminum tube. The composite tube would be capable of large deformation until 2.5% strain. This amount of strain requires very large deformation, and for many practical cases the required failure strain does not exceed this threshold due to the geometrical constrains and rigid body motions of the structure. The last advantage of this layup is that it can be used to match with different thicknesses of aluminum tube. As such, if the aluminum tube has varying thickness, as it is the case for helicopter landing gear, still the layup can be deployed.

#### **6-4 Process for design**

CFRP composites are brittle materials with very low fracture strain. Their fracture is abrupt, and they usually show very linear behavior before first ply failure. Despite the brittle nature of the material, a composite laminate may still show some nonlinear behavior and large deformation if debonding between the fibers and the matrix is avoided. The domino effect in fracture is another undesirable fracture mechanism. In contrast matrix extension and fiber rotation are excellent mechanisms for large deformation, and they must be highly employed in the design of composite structures for large deformation

In design of a composite tube, the first step is to determine the required strain level. In fact, large deformation of a structure does not necessarily accompanied with large strains. In contrast, due to rigid body motions and geometrical constraints, plastic strain can be relatively low, so the explained mechanisms of large deformation for composite laminates can be used to design a composite tube with potential of large deformation and high strain to failure.

While the strain level is known, a linear strain distribution throughout the cross section may be considered. The required strain of each layer is calculated based on the available strain distribution. On the other hand, the strains to failure of different balanced laminates can be determined by experiments. As such, according to the required strain for each layer, it would be possible to choose a proper laminate for each layer.

As it can be seen, this type of design, which is called strain-controlled design, is totally different from the traditional design procedure for beams or sandwich panels subjected to flexural loading. In a normal design, strong and stiff layers are laid up at the furthest points from the neutral axis to have the maximum contribution in the moment of inertia of the section. In contrast, in the design of a composite tube, the strong and stiff laminates are laid up as the inner layers to fulfill the requirements of strain while  $\pm 45^\circ$  laminate with low strength and stiffness is laid up as the outer jacket to keep the integrity of the tube and provide large deformation.

A strain-controlled design, however, does not specify the number of plies in each layer and does not guarantee the required strength and stiffness. As such, stress analysis of the tube is required to find the optimum numbers of plies for each layer so that a light composite tube with similar extensional, flexural and shear stiffness as the aluminum

tube is achieved. Classical Laminate Theory can be used for this purpose. The following guidelines can improve the design and result in a layup that provides the composite tube with high strength, stiffness and large deformation potentials:

- 1- The innermost ring of the tube should be a strong ring of  $90^\circ$  plies to resist hoop stresses and radial forces at the loading points.
- 2- A jacket of  $\pm 45^\circ$  plies as the outermost layer of the tube would keep the integrity of the tube, provides large deformation, and restricts the movement of layers that failed due to compression stresses.
- 3- If a thin  $90^\circ$  layer is laid up between the adjacent layers, the layers would have more flexibility and freedom of movement. This would contribute in large deformation of the tube.
- 4- Low angle plies such as  $0^\circ$  layers are not recommended to be included in the layup of the tube. First,  $0^\circ$  layers have very low fracture strain. Second, upon their failure a shock is transferred into the structure, and the rest of layers would not be capable to absorb this high rate of loading, so the laminate fails abruptly.
- 5- The compression strength of the composite laminates might be less than tensile strength. As such, the movement of the fractured layers might be restricted by adjacent layers, so the load carrying capacity of the tube does not reduce considerably.
- 6- A metal liner is required inside the composite tube to prevent collapse of the innermost ring at the loading nose. This liner keeps the layers failed due to compression stress in place, so the tube can carry more loads until the point that fracture occurs in tension zone of the tube.

Considering all above mentioned analyses and observations, the following layup is suggested:

$$[90^{\circ}_{n1} / \pm 25^{\circ}_{n2} / 90^{\circ}_5 / \pm 30^{\circ}_{n3} / 90^{\circ}_5 / \pm 45^{\circ}_{n4}]$$

Layer number: [ 1 / 2 / 3 / 4 / 5 / 6 ]

Layer 1 is the innermost ring of the tube. This layup can provide any composite tube with the requirements of large deformation and avoids abrupt fracture. The numbers of the plies for each layer, however, should be determined using computer programs such as ANSYS or by using the simplified method presented in this work. In order to match the strength and stiffness of the composite tube with those of its aluminum counterpart, the thickness of the composite tube might be slightly higher. However, it was shown in this research that the composite tube can be still 30% lighter than high grade aluminum 7075-T6 tube. Matching the properties of lower grade aluminum tubes will remain more convenient, and more weight saving can be achieved.

#### **6-5 Future work**

The specific continuation of this project is to design, manufacture and test the composite curved tube. If successful, the outcomes can be used to design a helicopter composite landing gear.

However, in general, the knowledge produced can be applied into many applications. For example, offshore oil industry can benefit from a more reliable tool in their drilling, where riser tubes which hold the fluids and the drill string extend from the platform to the

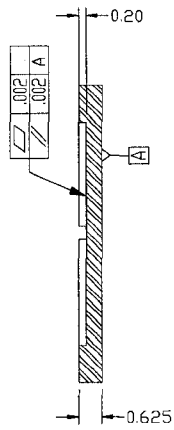
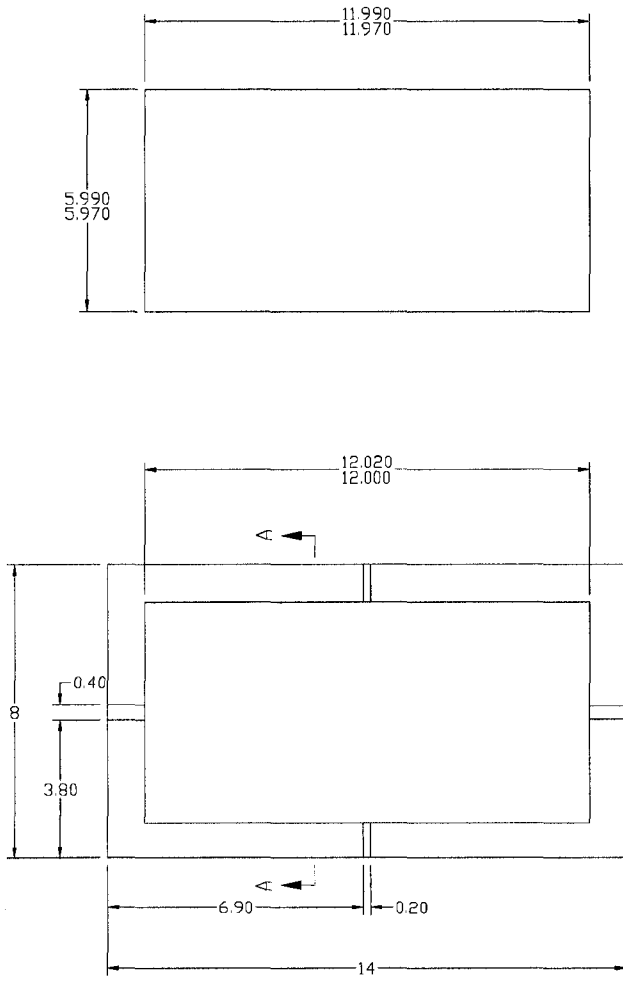
well head at the ocean floor and go through a complex procedure. The torsional stresses are very high at the tube, and the relative rotation of the tube from one end to the other is large. A brittle failure presents not only financial losses for the drilling company in terms of rig down time, but also could be catastrophic to the environment. The design presented in this research can be a reliable solution.

Another application can be in sandwich panels. Aircrafts, ships, fighters, hovercrafts, containers and many other vessels are using sandwich panels as their deck, fuselage, rudder etc. The sandwich panels are usually stiff structure with high load capacity and low tolerance to deformation. Brittle fracture of the panels is sometimes fatal for a hovercraft and always costly to repair. The layup presented here can be employed to produce a deformable sandwich panel with high strength and stiffness. The product would have many applications in the industry.

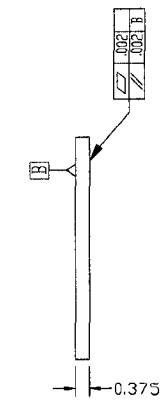
Appendix A:  
Compression Mold Drawings

ITEM	DESCRIPTION	NUM.	WEIGHT Kg.	MATERIAL
1	Bottom Plate	1	6.5	4140 Ht
2	Top Plate	1	3.5	4140 Ht

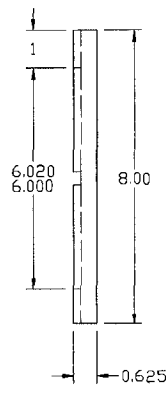
Notes:  
 1- Dimensions are in Inches.  
 2- Mating surfaces to be ground  
 3- Curvatures in the corners can be up to .1"



Sec. A-A



Part 2



Part 1

Concordia University CONCOM	Drawn by: B. Deris	Drawing No: Ther-CP-001
	Approved by: Dr. Hoo	Drawing Title: Mold for Flat Plate laminates
		Date: 23/08/2005
		Rev: 0

## Appendix B:

### Installation of Strain Gauges on Thermoplastic Composites

## INTRODUCTION

Installation of strain gauges on polymer matrix composites is more difficult than on metals. If the proper procedure is not followed, it would be very possible that the strain gauge delaminates from the surface of the specimen or the tube during the test. Figure B-1 compares a good and poor strain gauge installation on flat coupons.

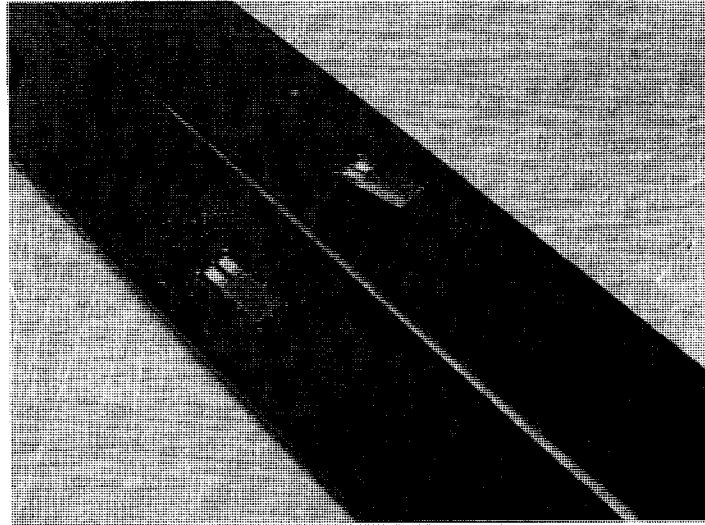


**Figure B-1: Comparison between poor and good adhesion**

The strain gauge was used during this research is of CEA-06-125UT-350 type that can measure up to 5.5% strain. However, during the tests, it was observed that at 1.5% strain, sometimes the strain gauges were delaminated due to the poor adhesion to the surface of specimens. Therefore, the following steps adopted from instruction bulletin by Vishay are recommended to minimize the risk and assure good adhesion between the surfaces of the strain gauge and composite specimens.

Figure B-2 shows the required chemicals for installation of strain gauges on the surface of polymer matrix composite. From left to right, *M-Prep Conditioner A* is used to clean the surface of the specimen; *M-Prep Neutralizer 5A* is used to neutralize the acidity of *Conditioner A*; *M-Bond 200* is an epoxy polymer acts as glue and *Catalyst C* initiate cross linking.



**Figure B-2: Required chemicals for installation of strain gauges**

M-Bond 200 is an excellent general-purpose laboratory adhesive because of its fast room-temperature cure and ease of application. When properly handled and used with the appropriate strain gage, M-Bond 200 can be used for high elongation tests in excess of 6% strain, for fatigue studies. The normal operating temperature range is  $-30^{\circ}$  to  $+65^{\circ}\text{C}$  [ $-25^{\circ}$  to  $+150^{\circ}\text{F}$ ]. For best reliability, it should be applied to surfaces between the temperatures of  $+20^{\circ}$  to  $+30^{\circ}\text{C}$  [ $+70^{\circ}$  and  $+85^{\circ}\text{F}$ ], and in a relative humidity environment of 30% to 65%. M-Bond 200 catalyst has been specially formulated to control the reactivity rate of this adhesive. The catalyst should be used sparingly for best results. Excessive catalyst can contribute many problems including poor bond strength.

---

*Note: The installation procedure presented here is the properties of Vishay and somewhat abbreviated. The details of the procedure can be found in a bulletin presented by Vishay listed in the References.*

### **Step 1**

Thoroughly degrease the gaging area with solvent, such as CSM Degreaser or GC-6 Isopropyl Alcohol. All degreasing should be done with uncontaminated solvents thus the use of “one-way” containers, such as aerosol cans, is highly advisable.

### **Step 2**

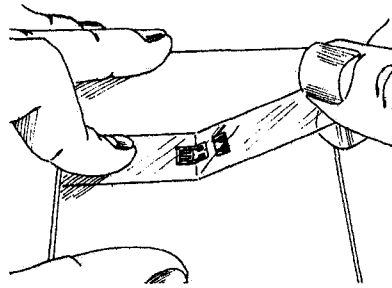
Preliminary dry abrading with 220- or 320-grit silicon- carbide paper is generally required if there is any surface scale or oxide. For composites flat coupons this step is not necessary; however, for composite tubes made by fiber placement technique it is a must. Final abrading is done by using 320-grit silicon-carbide paper on surfaces thoroughly wetted with M-Prep Conditioner A. This is followed by wiping dry with a gauze sponge. Repeat this wet abrading process with 400-grit silicon-carbide paper then dry by slowly wiping through with a gauze sponge. Never allow any solution to dry on the surface because this invariably leaves a contaminating film and reduces chances of a good bond.

### **Step 3**

Now apply a liberal amount of *M-Prep Neutralizer 5A* and scrub with a cotton-tipped applicator. With a single, slow wiping motion of a gauze sponge, carefully dry this surface. Do not wipe back and forth because this may allow contaminants to be redeposited.

### **Step 4**

Place the gage (bonding side down) on a chemically clean glass plate or gage box surface. Place a 100mm piece of Vishay Micro-Measurements PCT-2M gage installation tape over the gage and terminal. Take care to center the gage on the tape. Carefully lift the tape at a shallow angle (about 45 degrees to specimen surface), bringing the gage up with the tape as illustrated above.



### **Step 5**

Position the gage/tape assembly so that the triangle alignment marks on the gage are over the layout lines on the specimen. If the assembly appears to be misaligned, lift one end of the tape at a shallow angle until the assembly is free of the specimen. Realign properly, and firmly anchor at least one end of the tape to the specimen. Realignment can be done without fear of contamination by the tape mastic if Vishay Micro-Measurements PCT-2M gage installation tape is used, because this tape will retain its mastic when removed.

### **Step 6**

M-Bond 200 catalyst can now be applied to the bonding surface of the gage and terminal. M-Bond 200 adhesive will harden without the catalyst, but less quickly and reliably. Very little catalyst is needed, and it should be applied in a thin, uniform coat. Lift the brush-cap out of the catalyst bottle and wipe the brush approximately 10 strokes against the inside of the neck of the bottle to wring out most of the catalyst. Set the brush down on the gage and swab the gage backing. Do not stroke the brush in a painting style, but slide the brush over the entire gage surface and then the terminal. Allow the catalyst to dry at least one minute under normal ambient conditions.

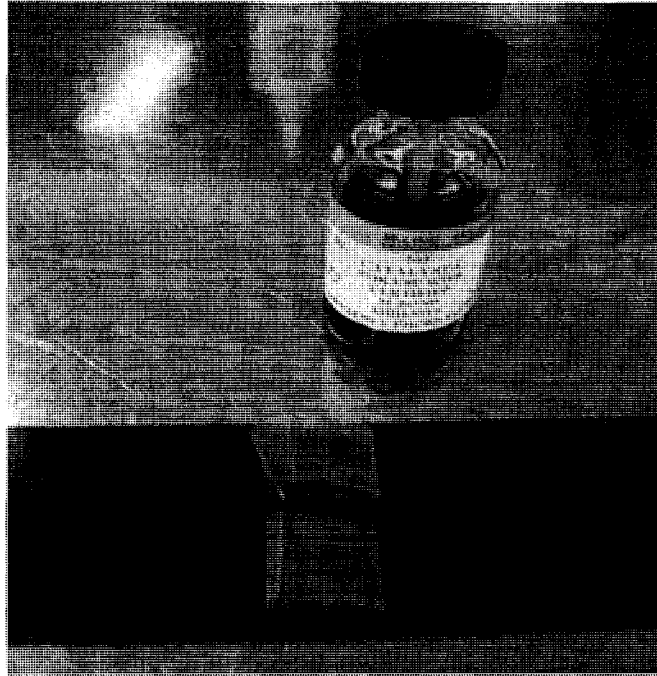
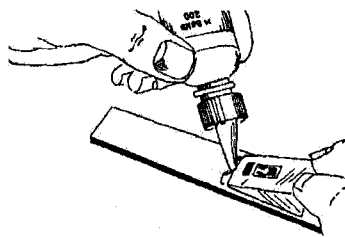


**Figure B-3: Apply catalyst only on the surface of the strain gauges**

**Note:** The next three steps must be completed within 3 to 5 seconds.

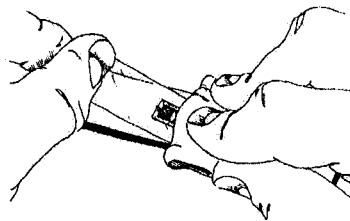
### **Step 7**

Apply one or two drops of M-Bond 200 adhesive at the fold formed by the junction of the tape and specimen surface. This adhesive application should be approximately 13mm outside the actual gage installation area. This will insure that local polymerization that takes place when the adhesive comes in contact with the specimen surface will not cause unevenness in the gage glue line.



### **Step 8**

Immediately rotate the tape to approximately a 30-degree angle so that the gage is bridged over the installation area. While holding the tape slightly taut, slowly and firmly make a single wiping stroke over the gage/tape assembly with a piece of gauze bringing the gage back down over the alignment marks on the specimen. Use a firm pressure with your fingers when wiping over the gage. A very thin, uniform layer of adhesive is desired for optimum bond performance.



### **Step 9**

Immediately upon completion of wipe-out of the adhesive, firm thumb pressure must be applied to the gage and terminal area. This pressure should be held for at least one minute.

### **Step 10**

The gage and terminal strip are now solidly bonded in place. It is not necessary to remove the tape immediately after gage installation. The tape will offer mechanical protection for the grid surface, and it may be left in place until removed for gage wiring. To remove the tape, pull it back directly over itself, peeling it slowly and steadily off the surface. This technique will prevent possible lifting of the foil on open-faced gages or other damage to the installation.

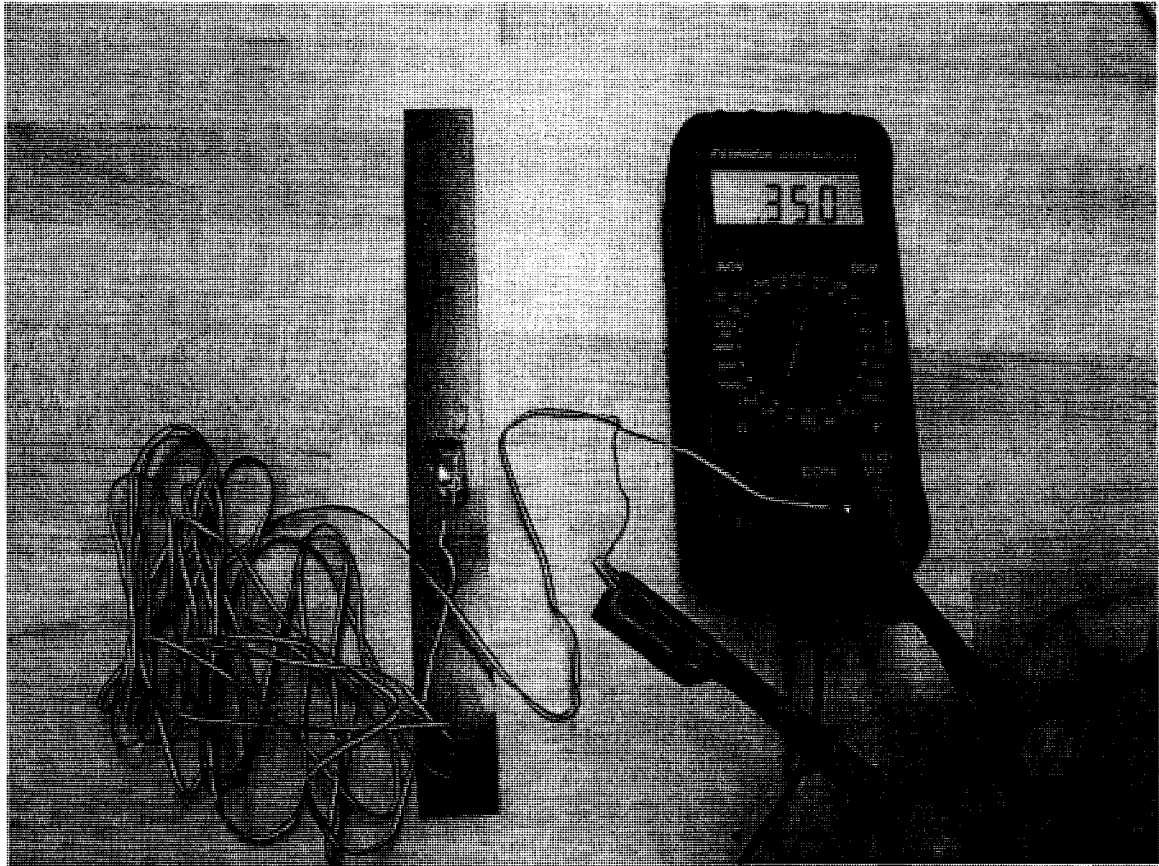


**Figure B-4: Wiring the strain gauge before tensile test**

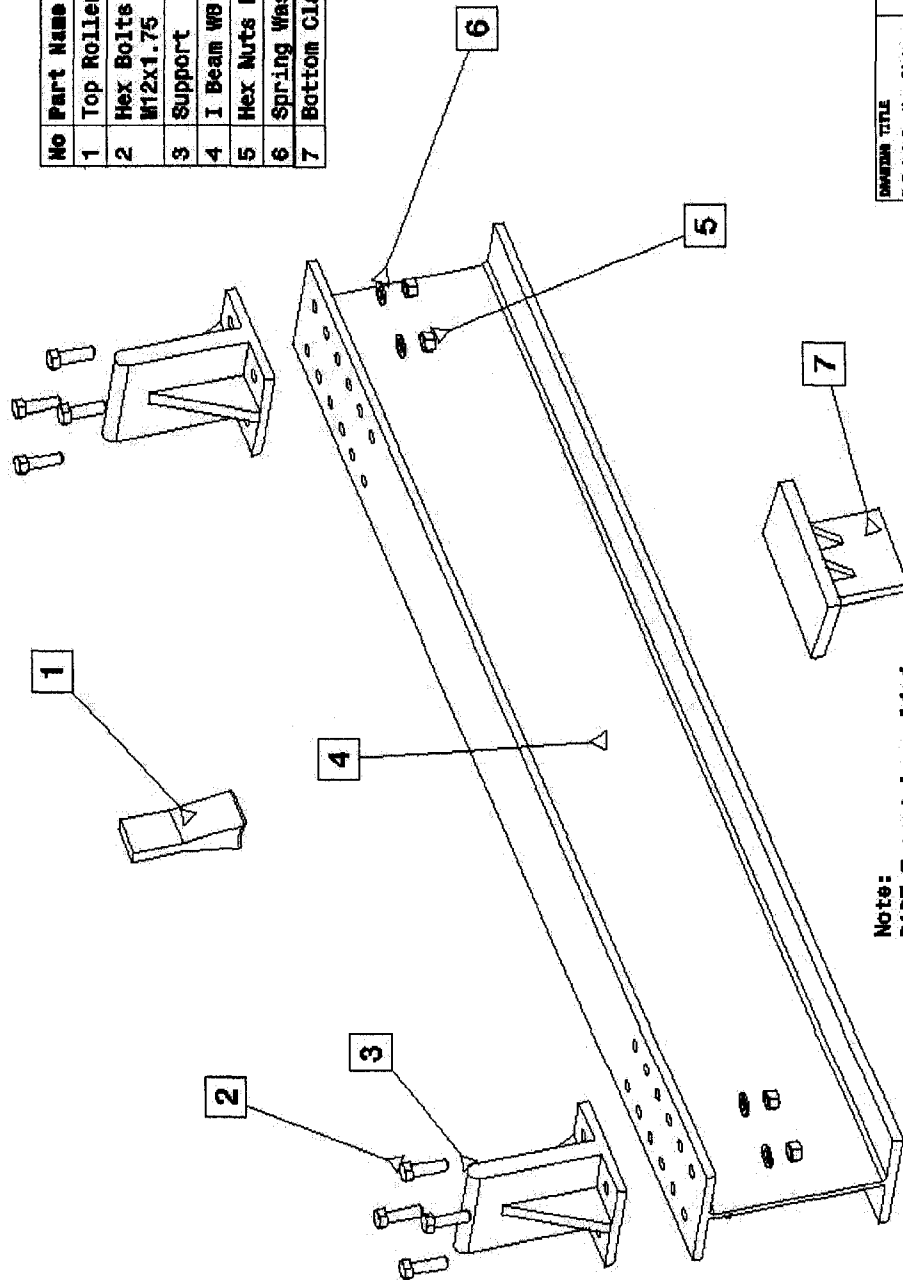
The last step is to wire the strain gauge by soldering. If the wires and the strain gauge are not damaged and properly installed, a resistance of  $0.350\Omega$  should be measured between the two terminals of the strain gauge when the scaling bottom is set on 2K.

## Appendix C:

### Three-Point Bending Fixture Drawings



No	Part Name	Qty.	Matl.
1	Top Roller 30deg	1	Steel
2	Hex Bolts M12x1.75	8	Steel
3	Support	2	Steel
4	I Beam WB x 21	1	Steel
5	Hex Nuts M12x1.75	8	Steel
6	Spring Washers	8	Steel
7	Bottom Clamp	1	Steel



Note:  
PART 7 must be welded  
to the center of PART  
5. Leg of welding 5mm

**ISSUING TITLE**  
3 Point Bending Fixture  
Exploded Assembly

**CONSTRUCTION ENGINEERING CENTER RESEARCH CENTER**  
The center of research in the field of mechanical engineering.  
1000 University Blvd/Box 1000  
Champaign, Illinois 61820  
Tel: 217/244-3200  
Fax: 217/244-3200

DESIGNED BY	DATE	REVISION	DATE
CHECKED BY	DATE	SIZE (NO. OF PARTS)	
APPROVED BY	DATE	SCALE	1/1

MATERIAL: Steel

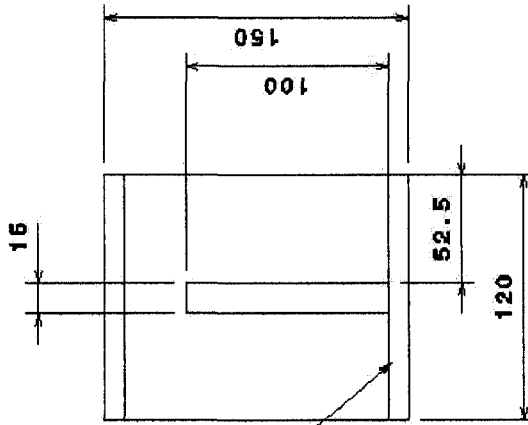
SCALE: Millimeter

SHEET 1/1

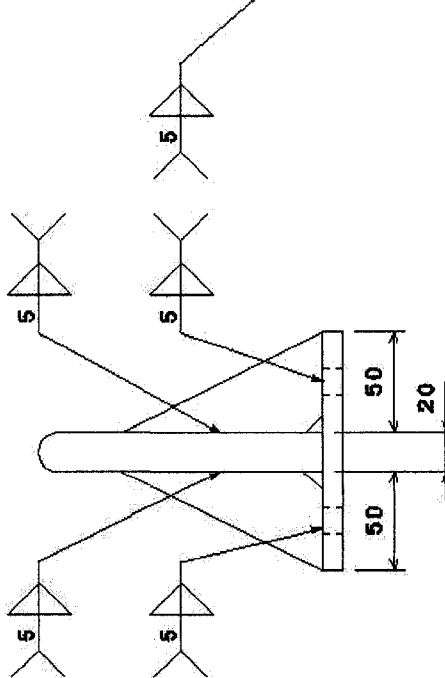


No	Part Name	Qty.
1	Support PART 1	1
2	Support PART 2	1
3	Support PART 3	2

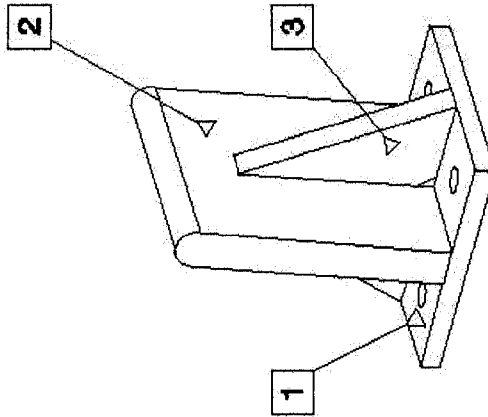
Note:  
Weld all the T joints with double fillet.



Side View



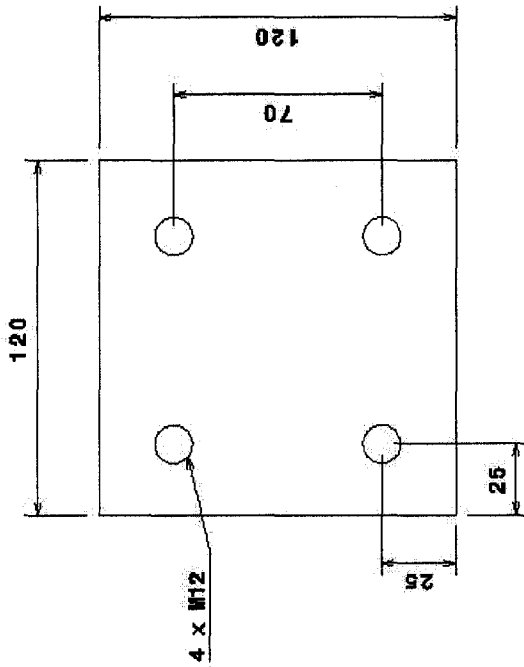
Front View



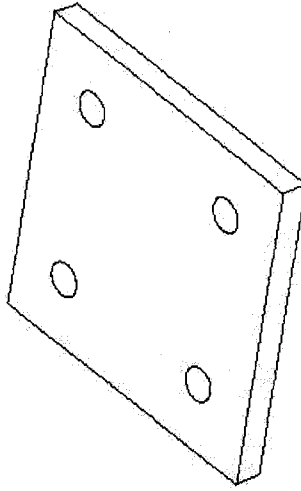
Isometric View

<b>CONCORDIA UNIVERSITY</b> CENTRE FOR INFINITE CONCORDIA AN INTERNATIONAL COLLEGE FOR INFINITE CONCORDIA	
<b>DESIGN TITLE</b> 3 Point Bending Fixture Support Assembly	
<b>DESIGNED BY</b> MOUNT M. CHECKED BY BLJAO D. DESIGNED BY DATE	<b>DATE</b> DATE DATE DATE
<b>SCALE</b> Units: Millimeters	
<b>INTERVALS</b> Total	
<b>SHEET</b> 1/4	

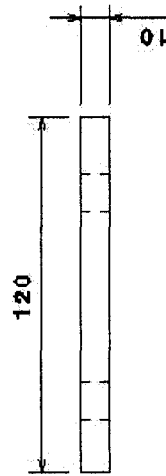
Note:  
Assure alignment of the  
holes with the I Beam



Bottom view

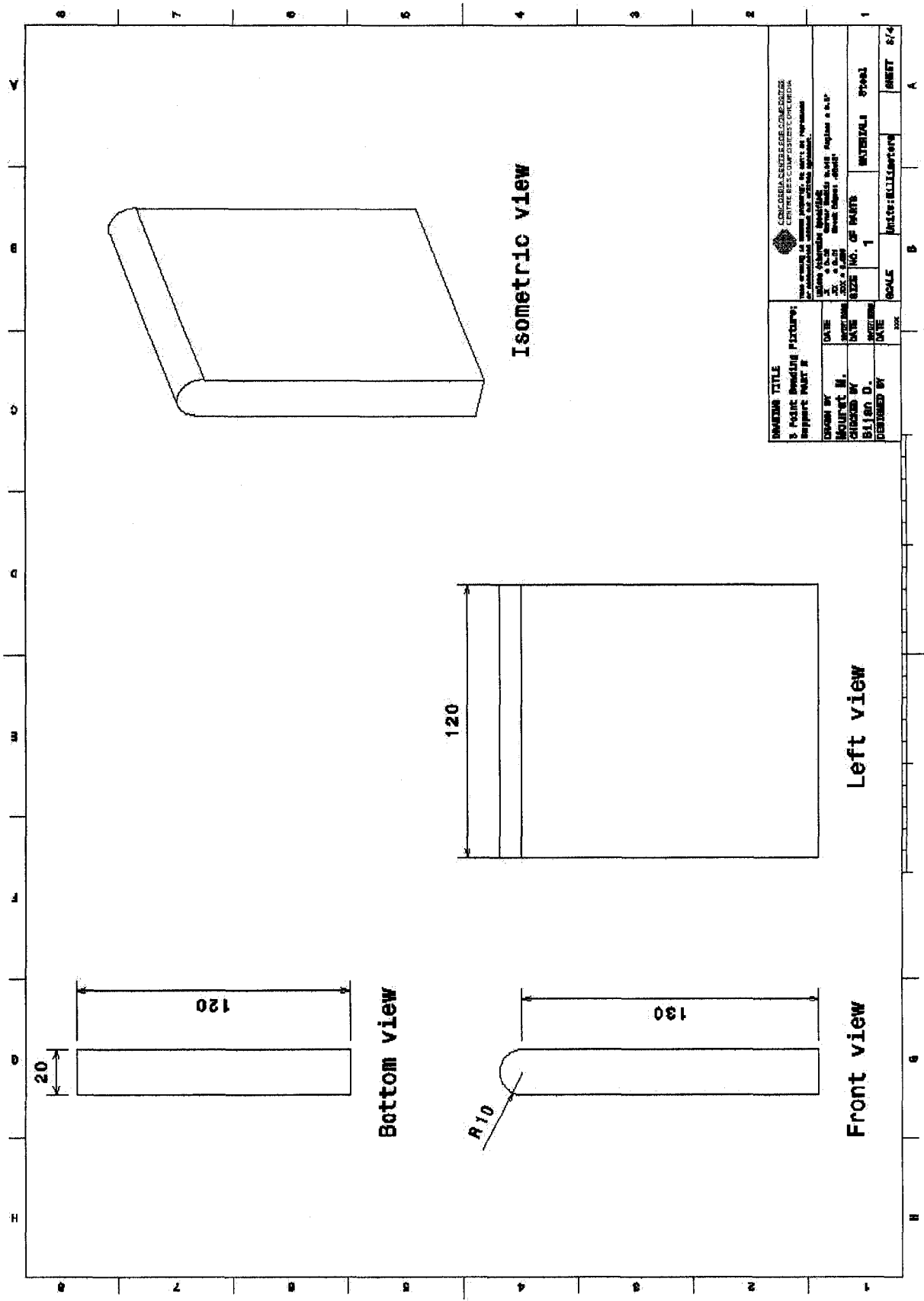


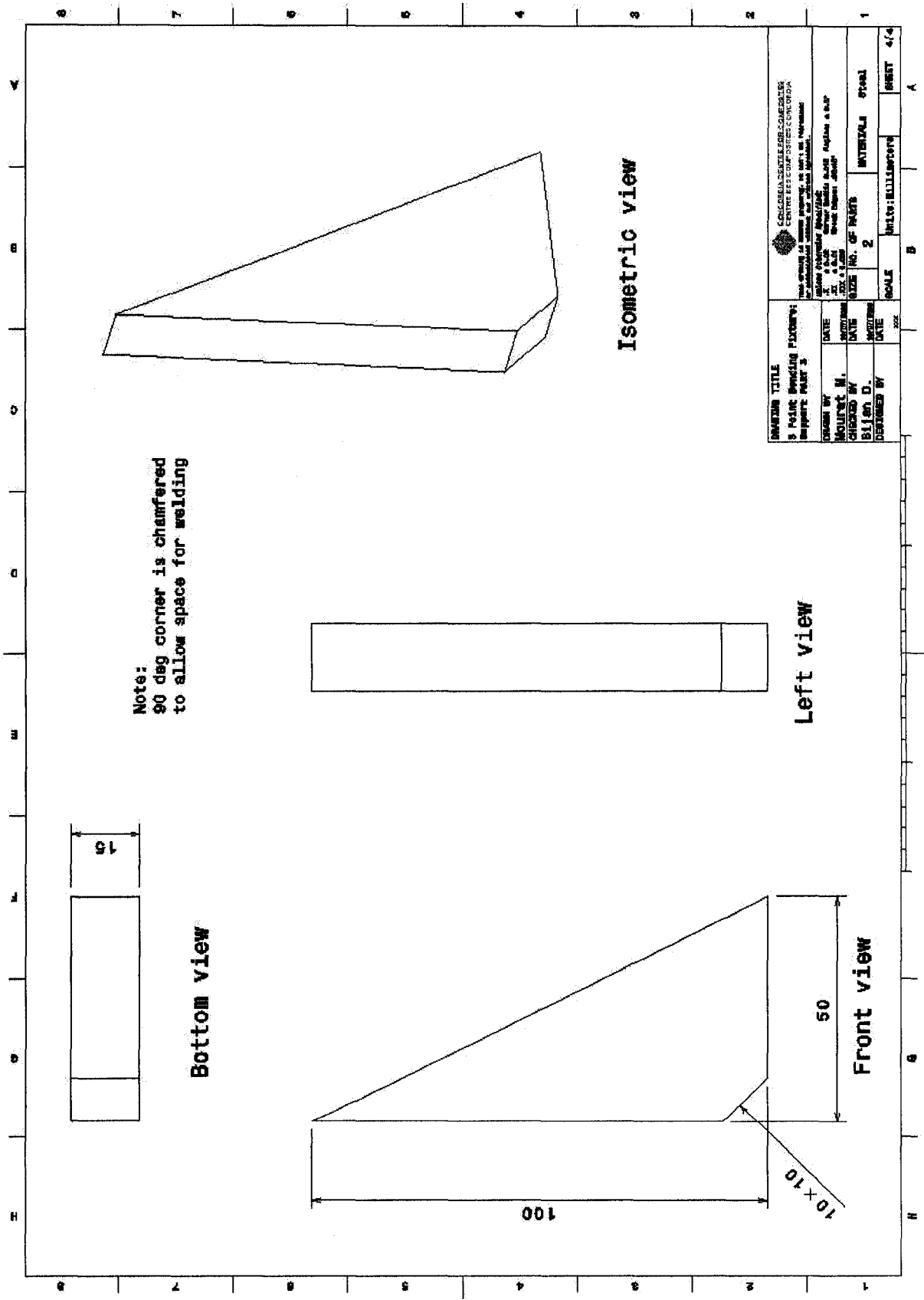
Isometric view

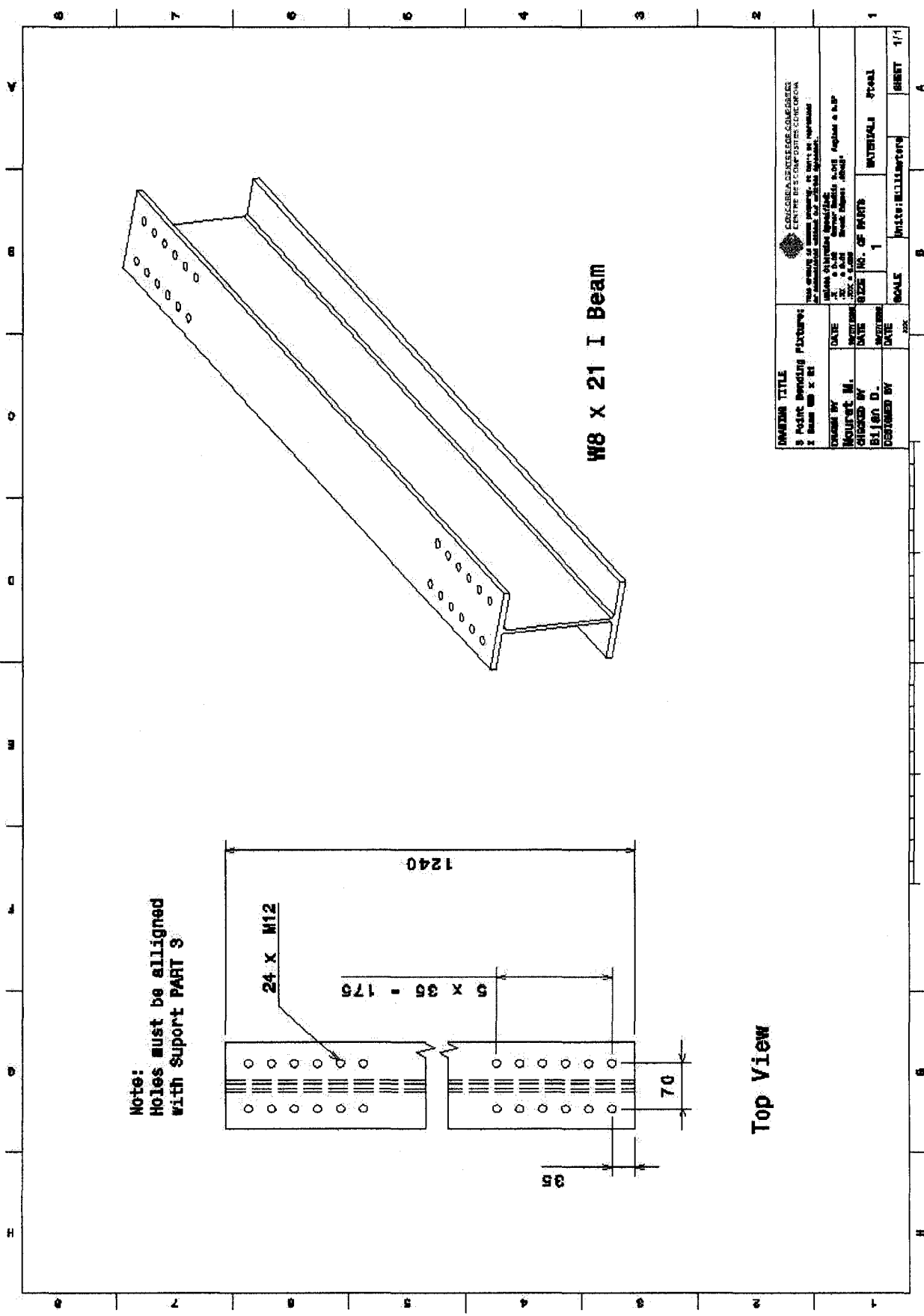


Front view

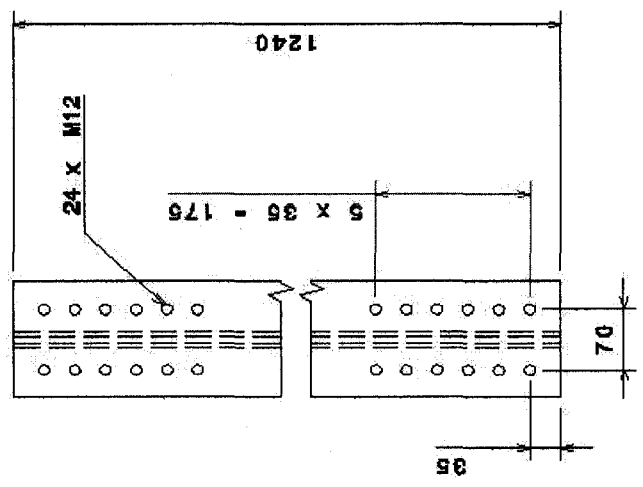
<b>INDUSTRIAL TITLE</b> 2 HOUR DRESSING PATTERN Support Part 1		CALIFORNIA STATE DEPARTMENT OF LABOR EMPLOYMENT AND INDUSTRIAL RELATIONS INDUSTRIAL TRAINING CENTER 1201 N. COLLE AVENUE, SACRAMENTO, CALIF. 95811	
<b>DESIGNED BY</b> MOLLINET M. DATE 10/1/88	<b>CHECKED BY</b> B. J. ROY D. DATE 10/1/88	<b>NO. OF PARTS</b> 1	<b>MATERIALS</b> Steel
<b>SCALE</b> 1:1		<b>UNIT</b> MILLIMETERS	<b>SHEET</b> 2/4







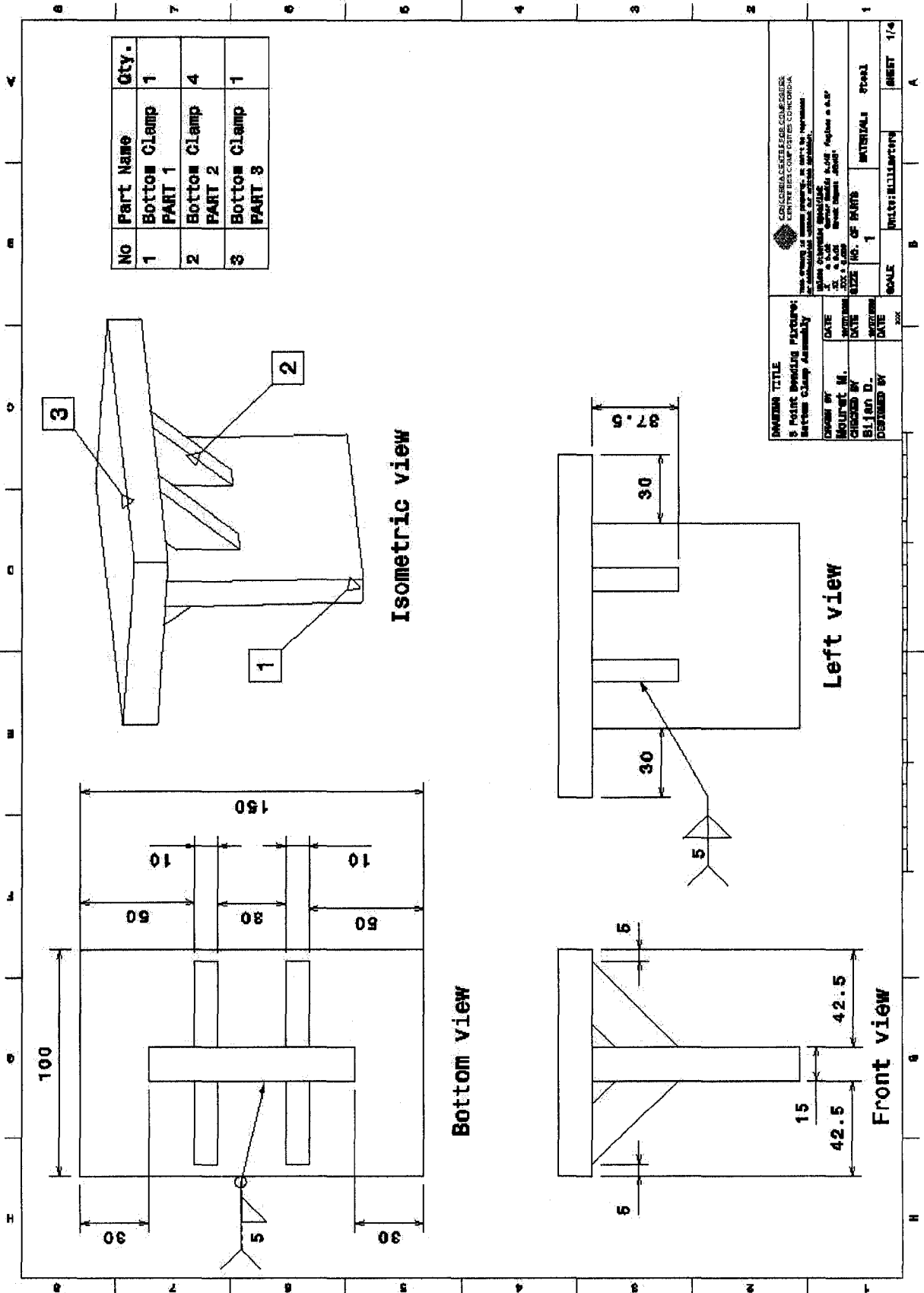
Note:  
Holes must be alligned  
with Support PART 3

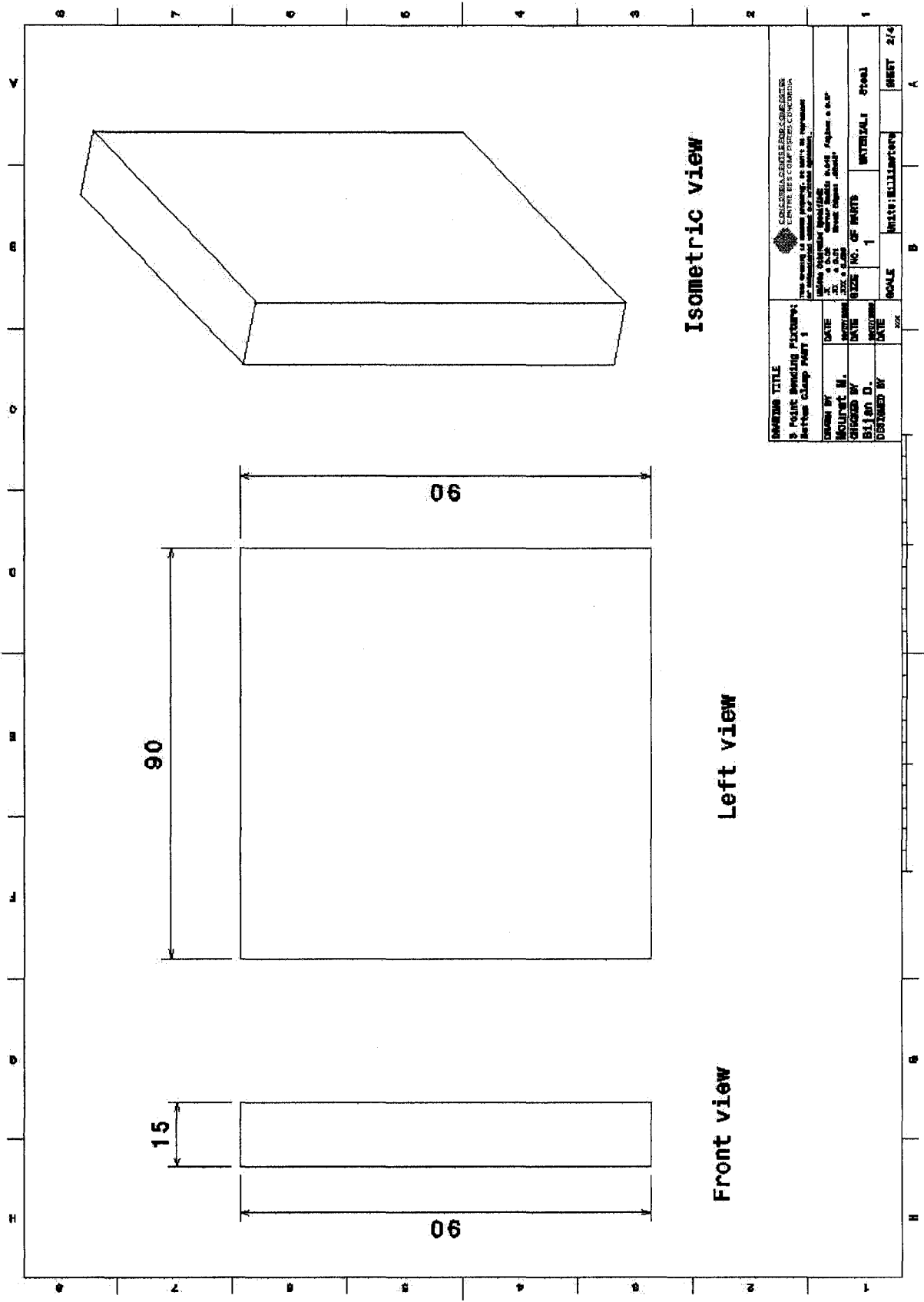


W8 X 21 I Beam

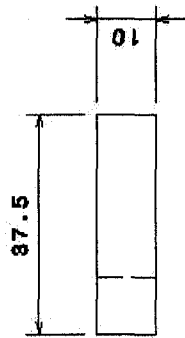
Top View

<b>DRAWING TITLE</b> 3 Point Bending Fixture 2 Beam 80 x 81		CONCRETE REINFORCING STEEL CENTRE BEL CONSTRUCTION	
DRAWN BY CHECKED BY DESIGNED BY		DATE DATE DATE	
SIZE (NO. OF PARTS) 1		MATERIALS Steel	
SCALE 1:1		SHEET 1/1	

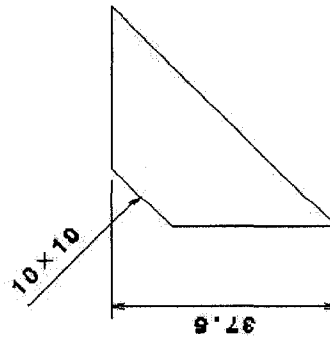




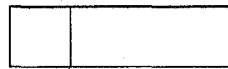
Note:  
80 deg angle is chamfered to allow some  
space for welding.



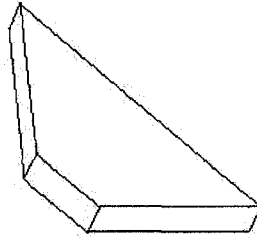
Bottom view



Front view

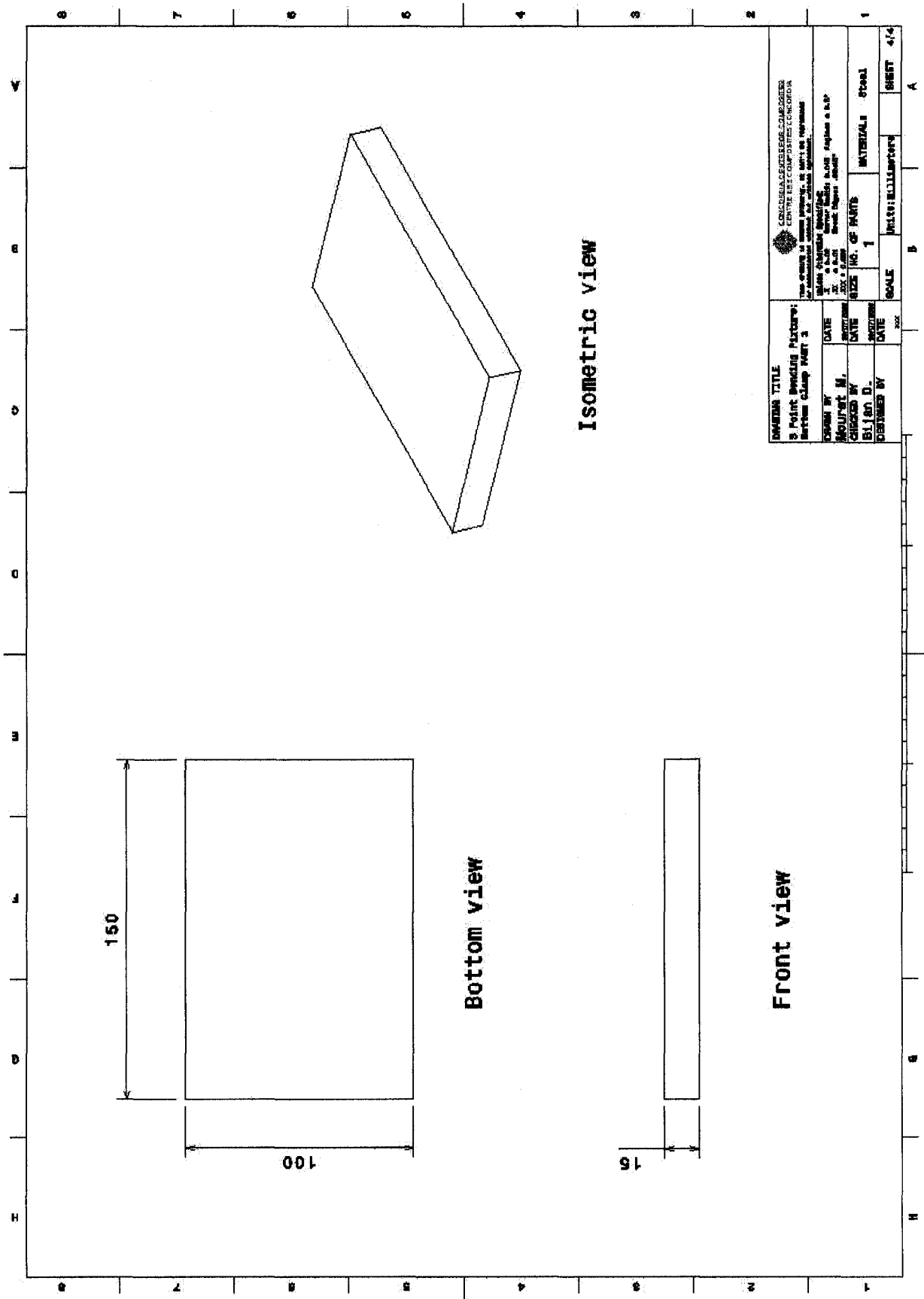


Left view



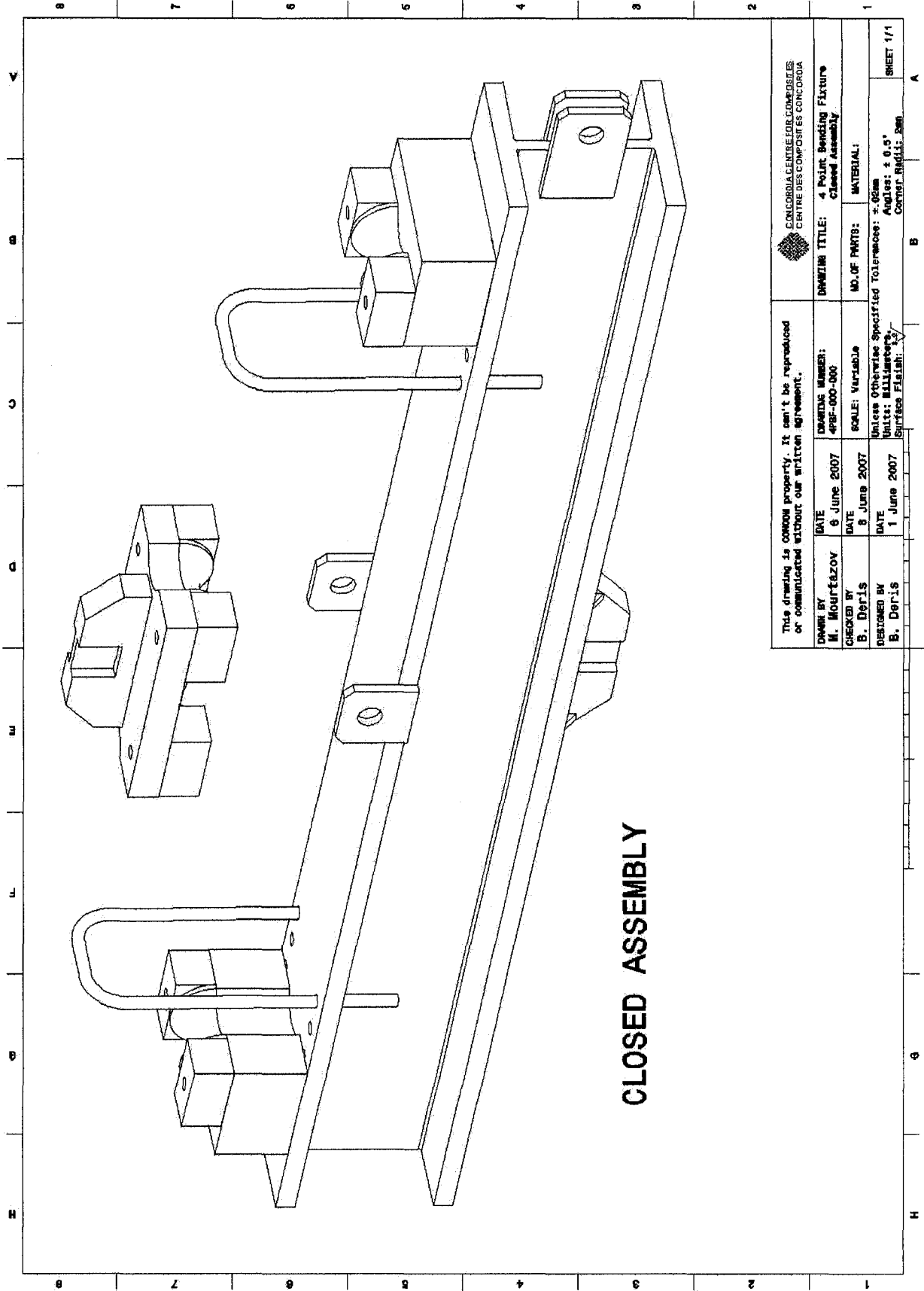
Isometric view

<b>COMPANY TITLE</b> S. Point Bending Factory Barham Camp Part 2		 CONCRETE REINFORCEMENT CENTRE FOR FOUR POINTS LOCATION 100, 101, 102, 103, 104, 105, 106, 107, 108, 109, 110, 111, 112, 113, 114, 115, 116, 117, 118, 119, 120, 121, 122, 123, 124, 125, 126, 127, 128, 129, 130, 131, 132, 133, 134, 135, 136, 137, 138, 139, 140, 141, 142, 143, 144, 145, 146, 147, 148, 149, 150, 151, 152, 153, 154, 155, 156, 157, 158, 159, 160, 161, 162, 163, 164, 165, 166, 167, 168, 169, 170, 171, 172, 173, 174, 175, 176, 177, 178, 179, 180, 181, 182, 183, 184, 185, 186, 187, 188, 189, 190, 191, 192, 193, 194, 195, 196, 197, 198, 199, 200, 201, 202, 203, 204, 205, 206, 207, 208, 209, 210, 211, 212, 213, 214, 215, 216, 217, 218, 219, 220, 221, 222, 223, 224, 225, 226, 227, 228, 229, 230, 231, 232, 233, 234, 235, 236, 237, 238, 239, 240, 241, 242, 243, 244, 245, 246, 247, 248, 249, 250, 251, 252, 253, 254, 255, 256, 257, 258, 259, 260, 261, 262, 263, 264, 265, 266, 267, 268, 269, 270, 271, 272, 273, 274, 275, 276, 277, 278, 279, 280, 281, 282, 283, 284, 285, 286, 287, 288, 289, 290, 291, 292, 293, 294, 295, 296, 297, 298, 299, 300, 301, 302, 303, 304, 305, 306, 307, 308, 309, 310, 311, 312, 313, 314, 315, 316, 317, 318, 319, 320, 321, 322, 323, 324, 325, 326, 327, 328, 329, 330, 331, 332, 333, 334, 335, 336, 337, 338, 339, 340, 341, 342, 343, 344, 345, 346, 347, 348, 349, 350, 351, 352, 353, 354, 355, 356, 357, 358, 359, 360, 361, 362, 363, 364, 365, 366, 367, 368, 369, 370, 371, 372, 373, 374, 375, 376, 377, 378, 379, 380, 381, 382, 383, 384, 385, 386, 387, 388, 389, 390, 391, 392, 393, 394, 395, 396, 397, 398, 399, 400, 401, 402, 403, 404, 405, 406, 407, 408, 409, 410, 411, 412, 413, 414, 415, 416, 417, 418, 419, 420, 421, 422, 423, 424, 425, 426, 427, 428, 429, 430, 431, 432, 433, 434, 435, 436, 437, 438, 439, 440, 441, 442, 443, 444, 445, 446, 447, 448, 449, 450, 451, 452, 453, 454, 455, 456, 457, 458, 459, 460, 461, 462, 463, 464, 465, 466, 467, 468, 469, 470, 471, 472, 473, 474, 475, 476, 477, 478, 479, 480, 481, 482, 483, 484, 485, 486, 487, 488, 489, 490, 491, 492, 493, 494, 495, 496, 497, 498, 499, 500, 501, 502, 503, 504, 505, 506, 507, 508, 509, 510, 511, 512, 513, 514, 515, 516, 517, 518, 519, 520, 521, 522, 523, 524, 525, 526, 527, 528, 529, 530, 531, 532, 533, 534, 535, 536, 537, 538, 539, 540, 541, 542, 543, 544, 545, 546, 547, 548, 549, 550, 551, 552, 553, 554, 555, 556, 557, 558, 559, 560, 561, 562, 563, 564, 565, 566, 567, 568, 569, 570, 571, 572, 573, 574, 575, 576, 577, 578, 579, 580, 581, 582, 583, 584, 585, 586, 587, 588, 589, 590, 591, 592, 593, 594, 595, 596, 597, 598, 599, 600, 601, 602, 603, 604, 605, 606, 607, 608, 609, 610, 611, 612, 613, 614, 615, 616, 617, 618, 619, 620, 621, 622, 623, 624, 625, 626, 627, 628, 629, 630, 631, 632, 633, 634, 635, 636, 637, 638, 639, 640, 641, 642, 643, 644, 645, 646, 647, 648, 649, 650, 651, 652, 653, 654, 655, 656, 657, 658, 659, 660, 661, 662, 663, 664, 665, 666, 667, 668, 669, 670, 671, 672, 673, 674, 675, 676, 677, 678, 679, 680, 681, 682, 683, 684, 685, 686, 687, 688, 689, 690, 691, 692, 693, 694, 695, 696, 697, 698, 699, 700, 701, 702, 703, 704, 705, 706, 707, 708, 709, 710, 711, 712, 713, 714, 715, 716, 717, 718, 719, 720, 721, 722, 723, 724, 725, 726, 727, 728, 729, 730, 731, 732, 733, 734, 735, 736, 737, 738, 739, 740, 741, 742, 743, 744, 745, 746, 747, 748, 749, 750, 751, 752, 753, 754, 755, 756, 757, 758, 759, 760, 761, 762, 763, 764, 765, 766, 767, 768, 769, 770, 771, 772, 773, 774, 775, 776, 777, 778, 779, 780, 781, 782, 783, 784, 785, 786, 787, 788, 789, 790, 791, 792, 793, 794, 795, 796, 797, 798, 799, 800, 801, 802, 803, 804, 805, 806, 807, 808, 809, 810, 811, 812, 813, 814, 815, 816, 817, 818, 819, 820, 821, 822, 823, 824, 825, 826, 827, 828, 829, 830, 831, 832, 833, 834, 835, 836, 837, 838, 839, 840, 841, 842, 843, 844, 845, 846, 847, 848, 849, 850, 851, 852, 853, 854, 855, 856, 857, 858, 859, 860, 861, 862, 863, 864, 865, 866, 867, 868, 869, 870, 871, 872, 873, 874, 875, 876, 877, 878, 879, 880, 881, 882, 883, 884, 885, 886, 887, 888, 889, 890, 891, 892, 893, 894, 895, 896, 897, 898, 899, 900, 901, 902, 903, 904, 905, 906, 907, 908, 909, 910, 911, 912, 913, 914, 915, 916, 917, 918, 919, 920, 921, 922, 923, 924, 925, 926, 927, 928, 929, 930, 931, 932, 933, 934, 935, 936, 937, 938, 939, 940, 941, 942, 943, 944, 945, 946, 947, 948, 949, 950, 951, 952, 953, 954, 955, 956, 957, 958, 959, 960, 961, 962, 963, 964, 965, 966, 967, 968, 969, 970, 971, 972, 973, 974, 975, 976, 977, 978, 979, 980, 981, 982, 983, 984, 985, 986, 987, 988, 989, 990, 991, 992, 993, 994, 995, 996, 997, 998, 999, 1000		DRAWN BY CHECKED BY DESIGNED BY		DATE DATE DATE		MATERIAL SIZE NO. OF PARTS		SCALE UNIT: MILLIMETRE		SHEET 5/4 A	
--	--	---	--	---------------------------------------	--	----------------------	--	----------------------------------	--	---------------------------	--	----------------	--



<b>INDIANA TITLE</b> 8 Point Bending Fixture Bottom clamp Part 3		UNIVERSITY OF ILLINOIS ENGINEERING EXPERIMENT STATION 2420 N. GREEN ST. URBANA, ILL. 61801		DATE: _____ DRAWN BY: _____ CHECKED BY: _____ DATE: _____		DATE: _____ DATE: _____ DATE: _____		SIZE: 11" x 17" NO. OF PARTS: 1 MATERIAL: Steel		SCALE: _____ SHEET: 4/4	
--	--	---	--	--	--	---	--	---	--	----------------------------	--

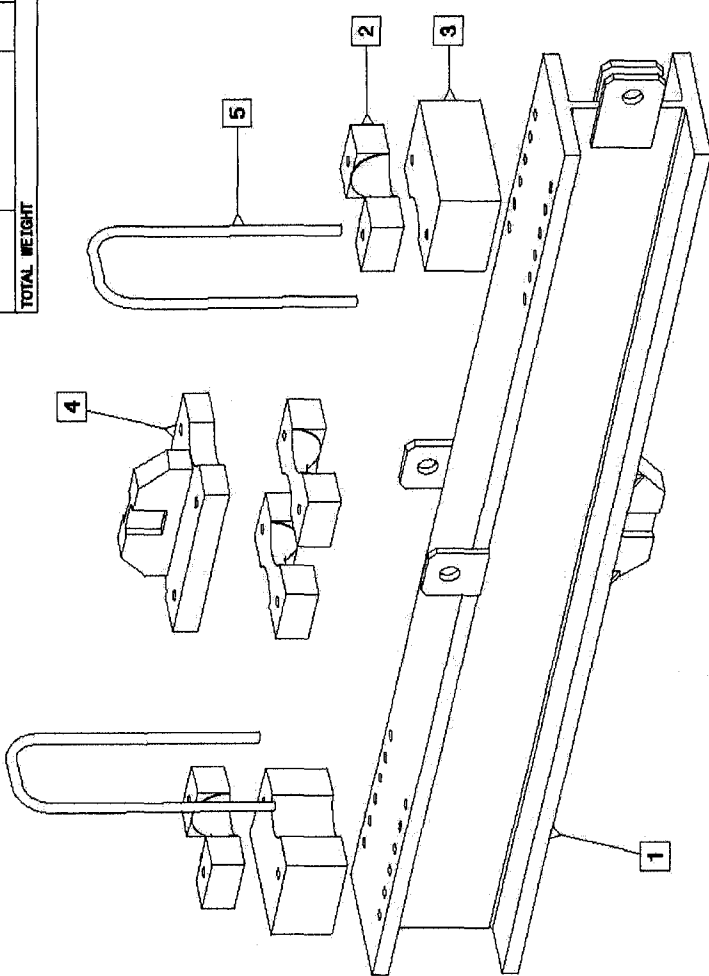
Appendix D:  
Four-Point Bending Fixture Drawings



**CLOSED ASSEMBLY**

<p>This drawing is CONCOR's property. It can't be reproduced or communicated without our written agreement.</p>		 <p>CONCOR/CENTRE DES COMPOSITES CENTRE DES COMPOSITES CONCORDIA</p>	
<p>DRAWN BY M. Mourfatzov</p>	<p>DATE 6 June 2007</p>	<p>DRAWING NUMBER: 4PRE-000-000</p>	<p>DRAWING TITLE: 4 Point Bending Fixture</p>
<p>CHECKED BY B. Deyris</p>	<p>DATE 8 June 2007</p>	<p>SCALE: Variable</p>	<p>NO. OF PARTS: MATERIAL:</p>
<p>DESIGNED BY B. Deyris</p>	<p>DATE 1 June 2007</p>	<p>Unless otherwise Specified Tolerances: ±.02mm Angles: ± 0.5° Surface Finish: 3.2</p>	
		<p>CONCOR/111</p>	

PT. No.	DESCRIPTION	QTY	MATL	WEIGHT (Kg)		REMARKS
				UNIT	TOTAL	
1	Bottom grip with I-beam	1	Steel ASTM-A36	400	400	Grip is welded to the center of the I-beam
2	Saddle	4	Stainless Steel AISI 304 Cold Rolled	10	40	
3	Spacer	2	Steel ASTM-A36	45	90	
4	Top Grip	1	Steel ASTM-A36	50	50	
5	Security Rod	2	Steel ASTM-A36	3	6	Nuts are used to secure the rods on the I-beam
TOTAL WEIGHT					588 Kg	



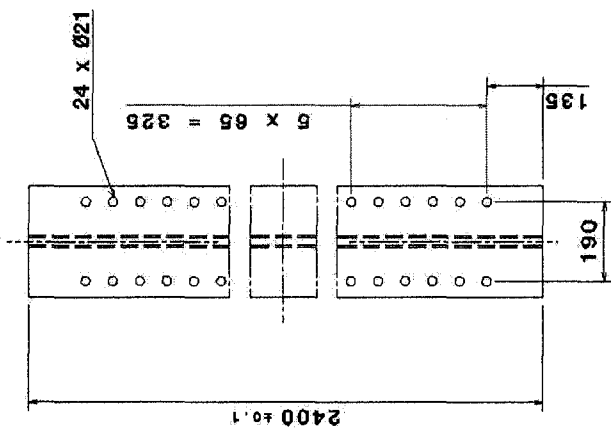
- Note:**
- Parts 2 and 3 must be fixed to the I-Beam with M20x2.5 hex bolts (250mm long), nuts and spring washers (Grade 8.8);
  - Part 4 must be fixed to Parts 2 with M20x2.5 hex bolts (150mm long), nuts and spring washers (Grade 8.8);
  - Assure assembly before delivering.
  - Slightly bevel all edges.

 CONCORDIA CENTRES COMPOSÉS CENTRES COMPOSÉS CONCORDIA	
This drawing is CONCORD property. It can't be reproduced or communicated without our written agreement.	DRAWING TITLE: 4 Point Bending Fixture Open Assembly
DRAWN BY M. MOUTAZOV DATE 5 June 2007	DRAWMAN NUMBER: 4PBF-001-000
CHECKED BY B. Derris DATE 8 June 2007	SCALE: Variable NO. OF PARTS:
DESIGNED BY B. Derris DATE 1 June 2007	MATERIAL: Unless otherwise Specified Tolerances: ±.05mm Holes: ± 0.0° Corner Radii: 2mm

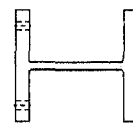


**Note:**

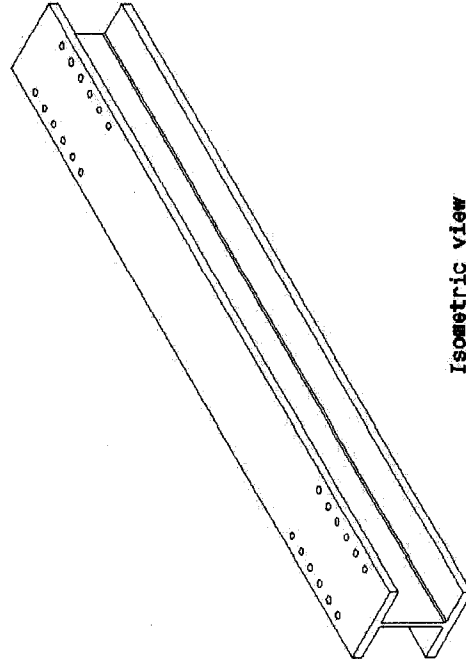
- I-beam: W250X167 ASTM-A36
- Holes must be aligned with Spacers and Saddles
- Ø21mm holes are for M20 Hex Bolts close feet. If other than metric bolts are chosen, close values should be selected and standardized throughout the other effected parts.



**Top view**

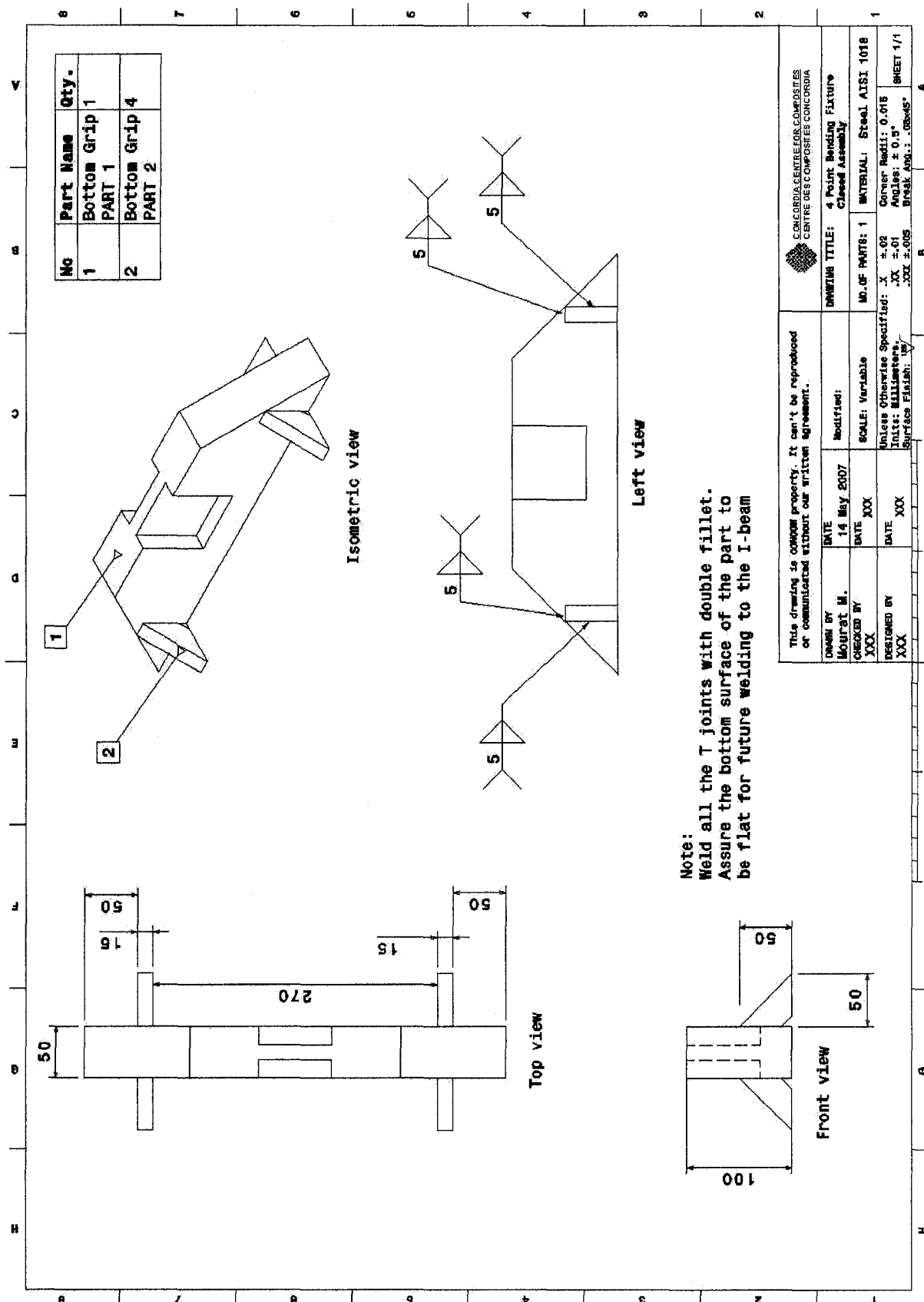


**Front view**



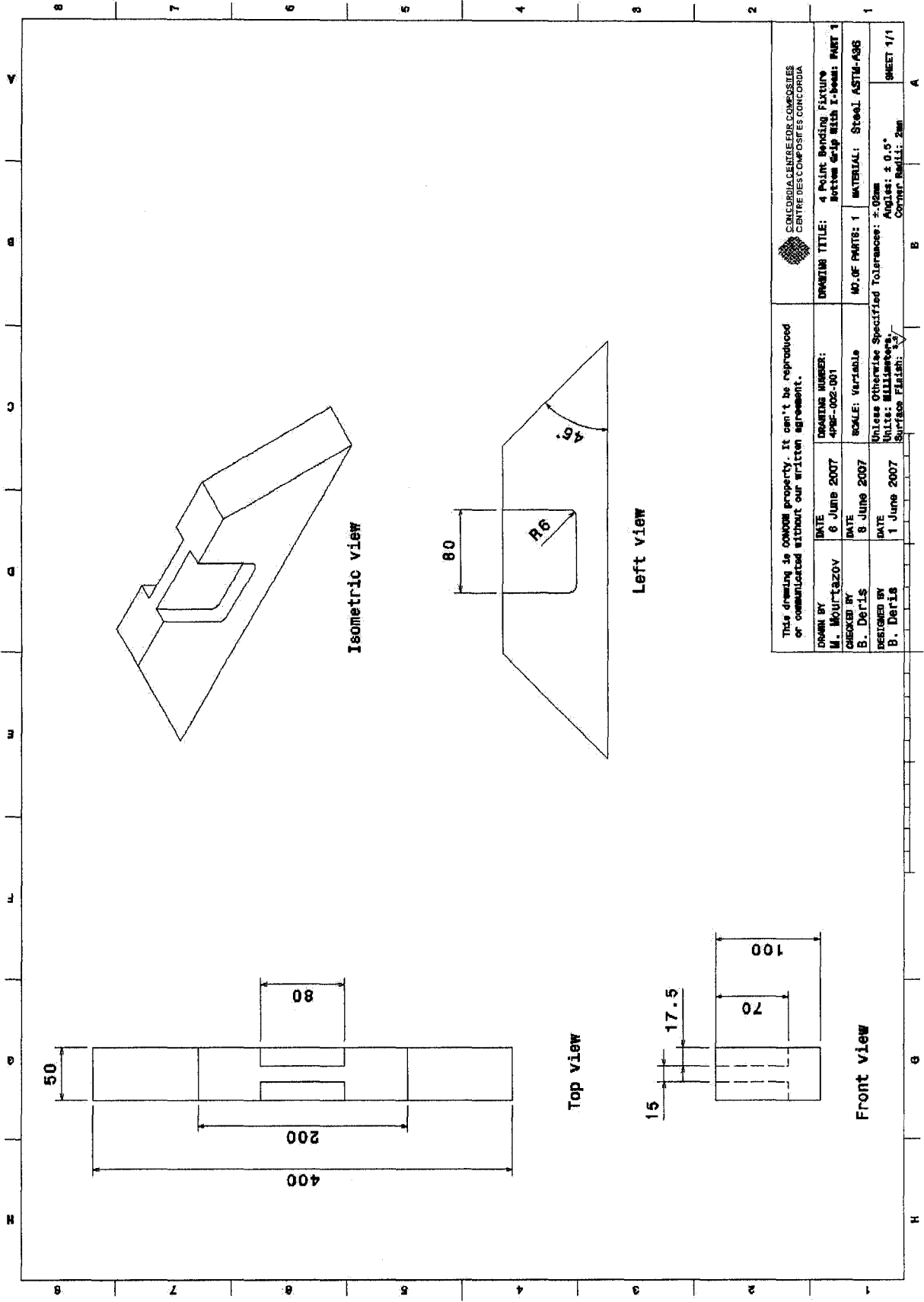
**Isometric view**

		CONCORDIA CENTRE FOR COMPOSITES CENTRE DES COMPOSITES CONCORDIA	
This drawing is CONCORD property. It can't be reproduced or communicated without our written agreement.		DRAWING TITLE: 4 Point Bending Fixture I-beam W250X167	
DRAWN BY M. MOULTEAZOV	DATE 6 June 2007	DRAWING NUMBER: 4PBF-022-003	M.O.F PARTS: 1
CHECKED BY B. DIERIS	DATE 8 June 2007	SCALE: Variable	MATERIAL: Steel ASTM-A36
DESIGNED BY B. Dieris	DATE 1 June 2007	Unless otherwise Specified Tolerances: ±.02mm Units: Millimeters Surface Finish:	
			SHEET 1/1



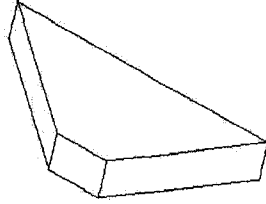
**Note:**  
 Weld all the T joints with double fillet.  
 Assure the bottom surface of the part to be flat for future welding to the I-beam

This drawing is CONCORDIA property. It can't be reproduced or communicated without our written agreement.		CONCORDIA CENTRE FOR COMPOSITES CENTRE DES COMPOSITES CONCORDIA	
DRAWN BY Mount M. XXX	DATE 14 May 2007	Modified:	DRAWING TITLE: 4 Point Bending Fixture Closed Assembly
CHECKED BY XXX	DATE XXX	SCALE: Variable	NO. OF PARTS: 1
DESIGNED BY XXX	DATE XXX	Unless Otherwise Specified: .X ±.02 Inits: Millimeters .XX ±.01 .XXX ±.005 Surface Finish: .005	MATERIAL: Steel AISI 1018
			Corner Radii: 0.015 Angles: ± 0.5° BRSAK APP.: .005/45° SHEET 1/1

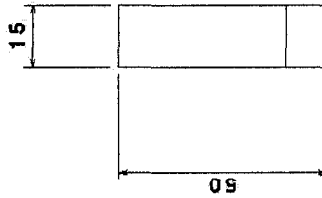


CONCORDIA CENTRE FOR COMPOSITES CENTRE DES COMPOSITES CONCORDIA		DRAWING TITLE: 4 Point Bending Fixture Bottom Grip with I-beam: PART 1	
DRAWN BY M. MOUTTAZOV	DATE 6 June 2007	DRAWING NUMBER: 4PBF-002-001	NO. OF PARTS: 1
CHECKED BY B. Deris	DATE 8 June 2007	SCALE: Variable	MATERIAL: Steel ASTM-A36
DESIGNED BY B. Deris	DATE 1 June 2007	Unless Otherwise Specified Tolerances: ±0.2mm Angles: ±0.5° Surface Finish:	
		OTHER FINISH: 2mm	

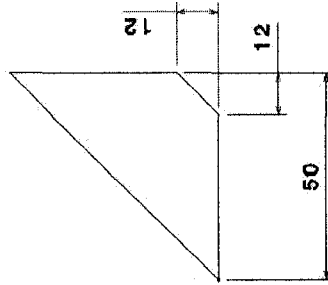
Note:  
90 deg corner is chamfered  
to allow space for welding



Isometric view



Front view

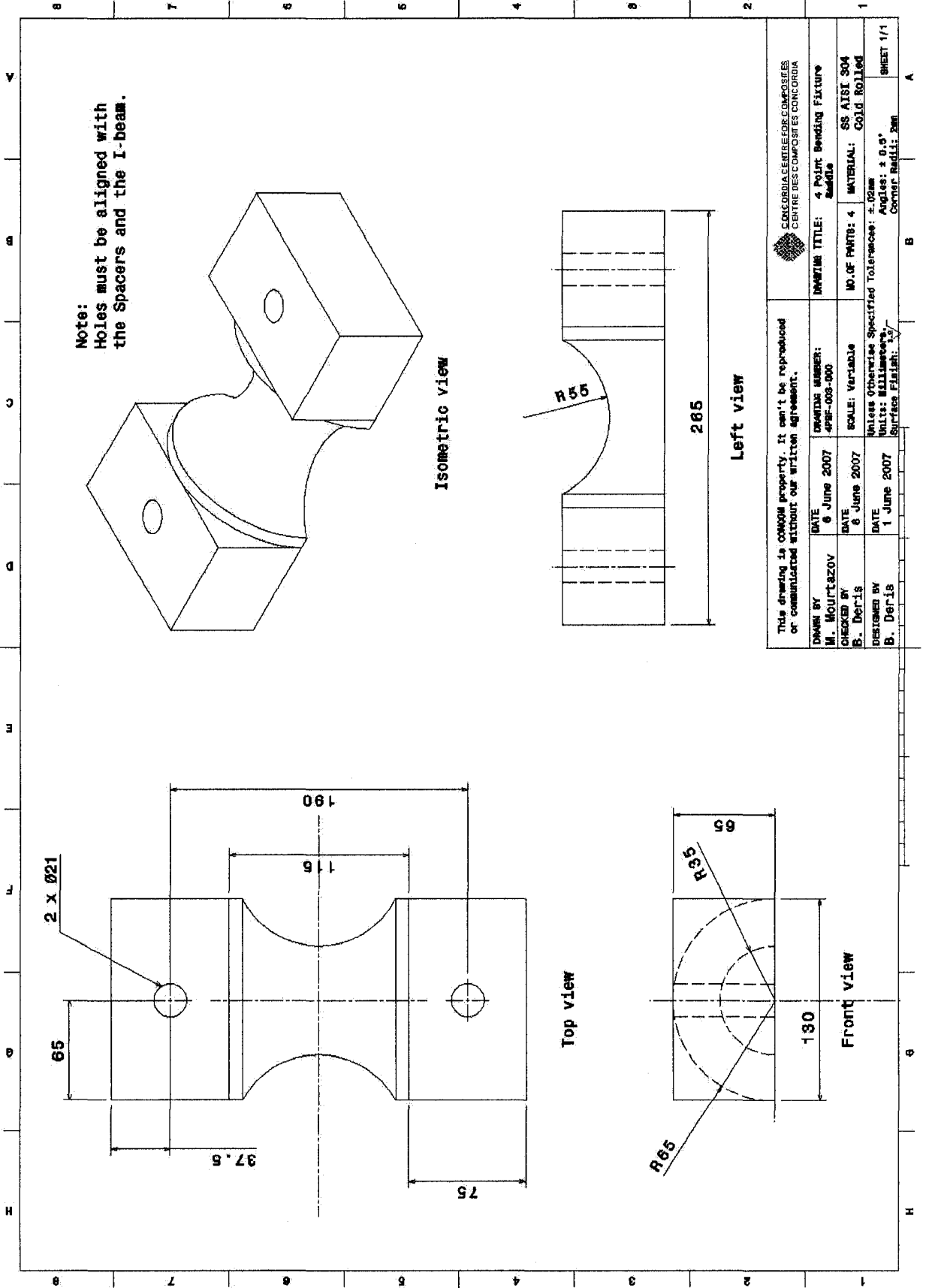


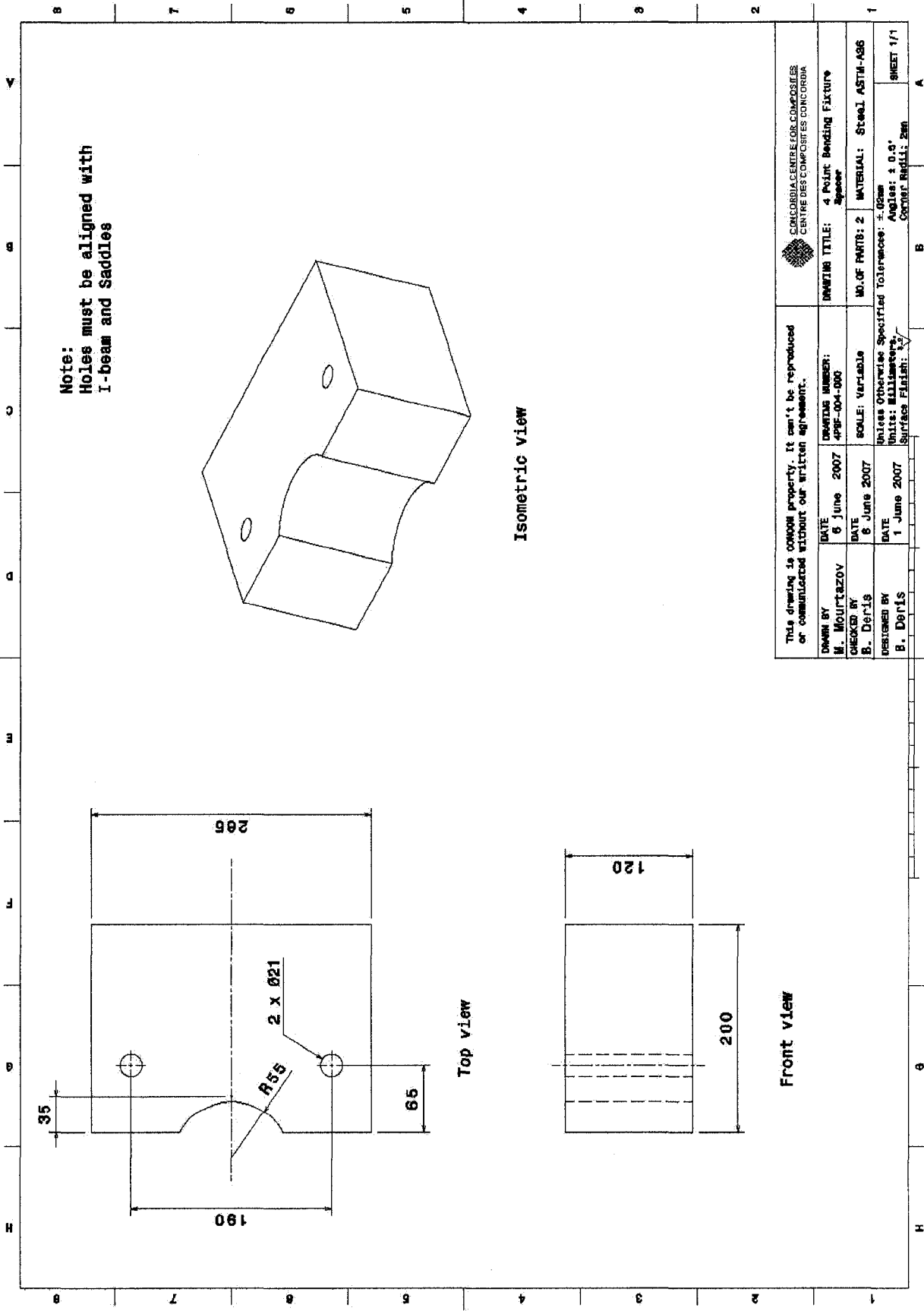
Left view

This drawing is CONCORD property. It can't be reproduced  
or communicated without our written agreement.

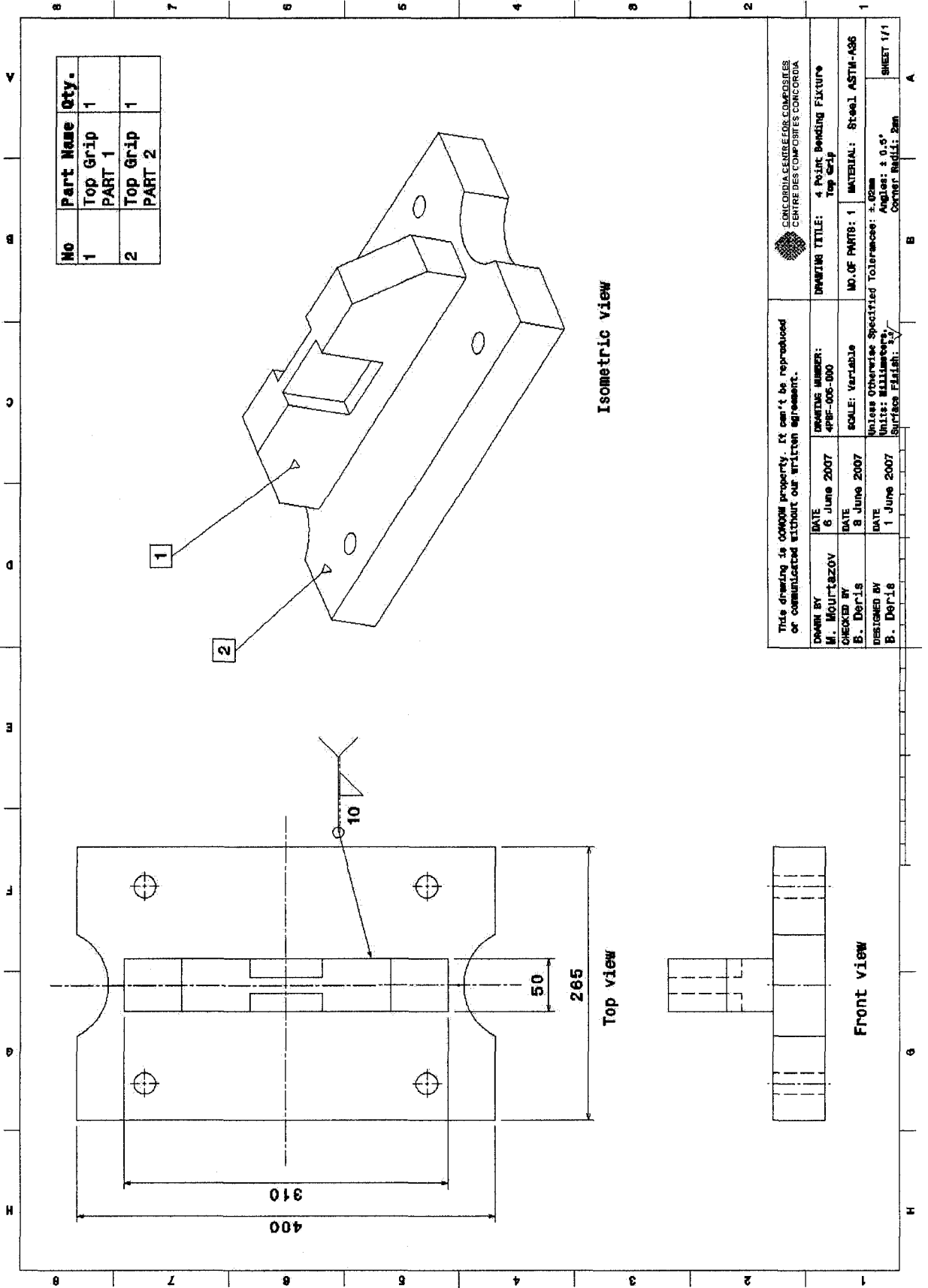


DRAWN BY M. MOURTAAZOV	DATE 6 May 2007	DRAWING NUMBER: 4PSE-002-002	ISSUING TITLE: 4 Point Bending Fixture Part 2 of 2
CHECKED BY B. Deris	DATE 8 June 2007	SCALE: Variable	NO. OF PARTS: 4
DESIGNED BY B. Deris	DATE 1 June 2007	MATERIAL: Steel (ASTM-A36)	
		Unless otherwise Specified Tolerances: ±.02mm	
		Units: Millimeters	
		Surface Finish: 3.2	
		Angles: ± 0.5°	
		Corner Radii: 2mm	

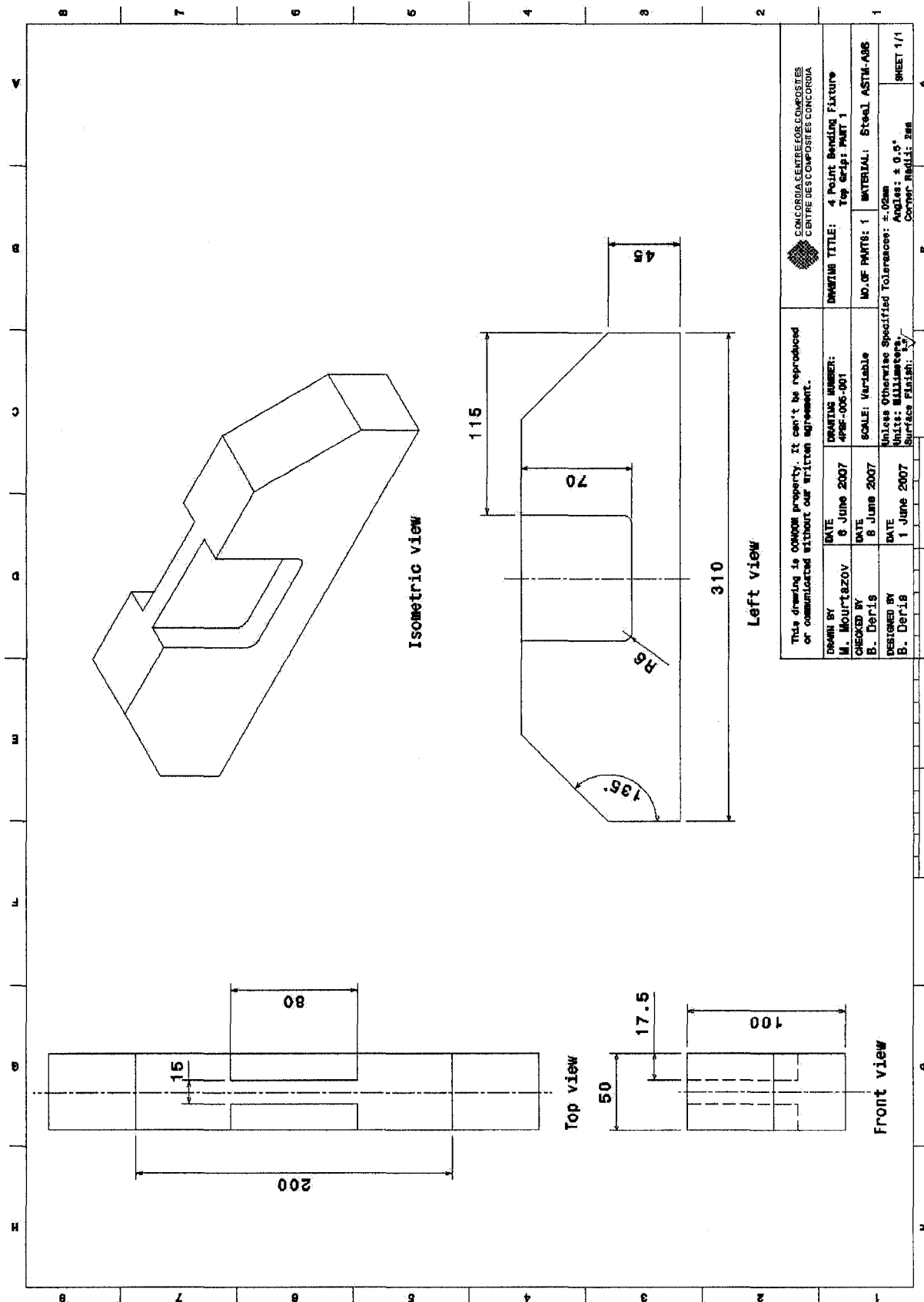




		This drawing is copyright property. It can't be reproduced or communicated without our written agreement.	
<b>DRAWN BY</b> M. MOURTASOV	<b>DATE</b> 6 June 2007	<b>DRAWING NUMBER</b> 493-04-000	<b>DRAWING TITLE</b> 4 Point Bending Fixture
<b>CHECKED BY</b> S. Dér-Is	<b>DATE</b> 6 June 2007	<b>SCALE</b> Variable	<b>NO. OF PARTS</b> 2
<b>DESIGNED BY</b> P. Dér-Is	<b>DATE</b> 1 June 2007	<b>MATERIAL</b> Steel ASTM-A36	
		<b>Unless Otherwise Specified Tolerances:</b> ±.02mm <b>Units:</b> Millimeters <b>Surface Finish:</b> 1/2 <b>Angles:</b> 1 0.0° <b>Corner Radii:</b> 2mm	
			<b>SHEET 1/1</b>

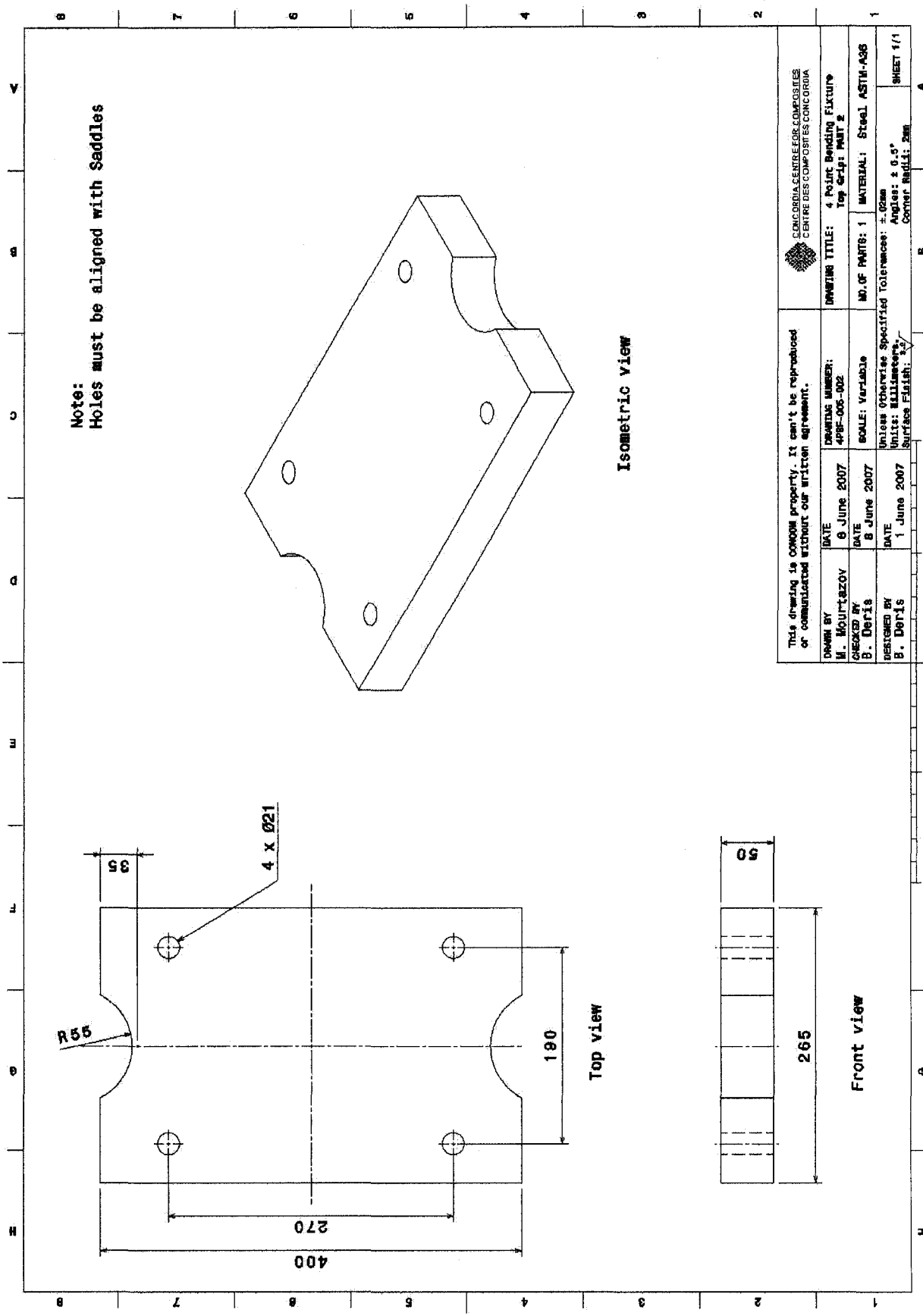


This drawing is CONCORDIA property. It can't be reproduced or communicated without our written agreement.		CONCORDIA CENTRE FOR COMPOSITES CENTRE DES COMPOSITES CONCORDIA	
DRAWN BY: M. MOURTAROV	DATE: 6 June 2007	DRAWING NUMBER: 498-006-000	DRAWING TITLE: 4 Point Bending Fixture top only
CHECKED BY: B. Doris	DATE: 8 June 2007	SCALE: Variable	NO. OF PARTS: 1
DESIGNED BY: B. Doris	DATE: 1 June 2007	Unless Otherwise Specified Tolerances: ±.02mm Units: Millimeters Surface Finish: 3.2	MATERIAL: Steel ASTM-A36
			Corner Radii: 2mm SHEET 1/1



This drawing is CONCOR's property. It can't be reproduced or communicated without our written agreement.

CONCOR/DA/CENTRE/FORM/COMPOSITES CENTRE DES COMPOSITES CONCORDIA	DRAWING TITLE: 4 Point Bending Fixture Top Grip: PART 1	
DRAWN BY M. Mourtafov	DATE 8 June 2007	DRAWING NUMBER: 4P2-005-001
CHECKED BY B. Deris	DATE 8 June 2007	SCALE: Variable
DESIGNED BY B. Deris	DATE 1 June 2007	NO. OF PARTS: 1
MATERIAL: Steel, ASTM-A36		UNLESS OTHERWISE SPECIFIED TOLERANCES: ±.02mm
Units: Millimeters		Angles: ± 0.5°
Surface Finish: N7		Corner Radii: 2mm



Note:  
Holes must be aligned with saddles

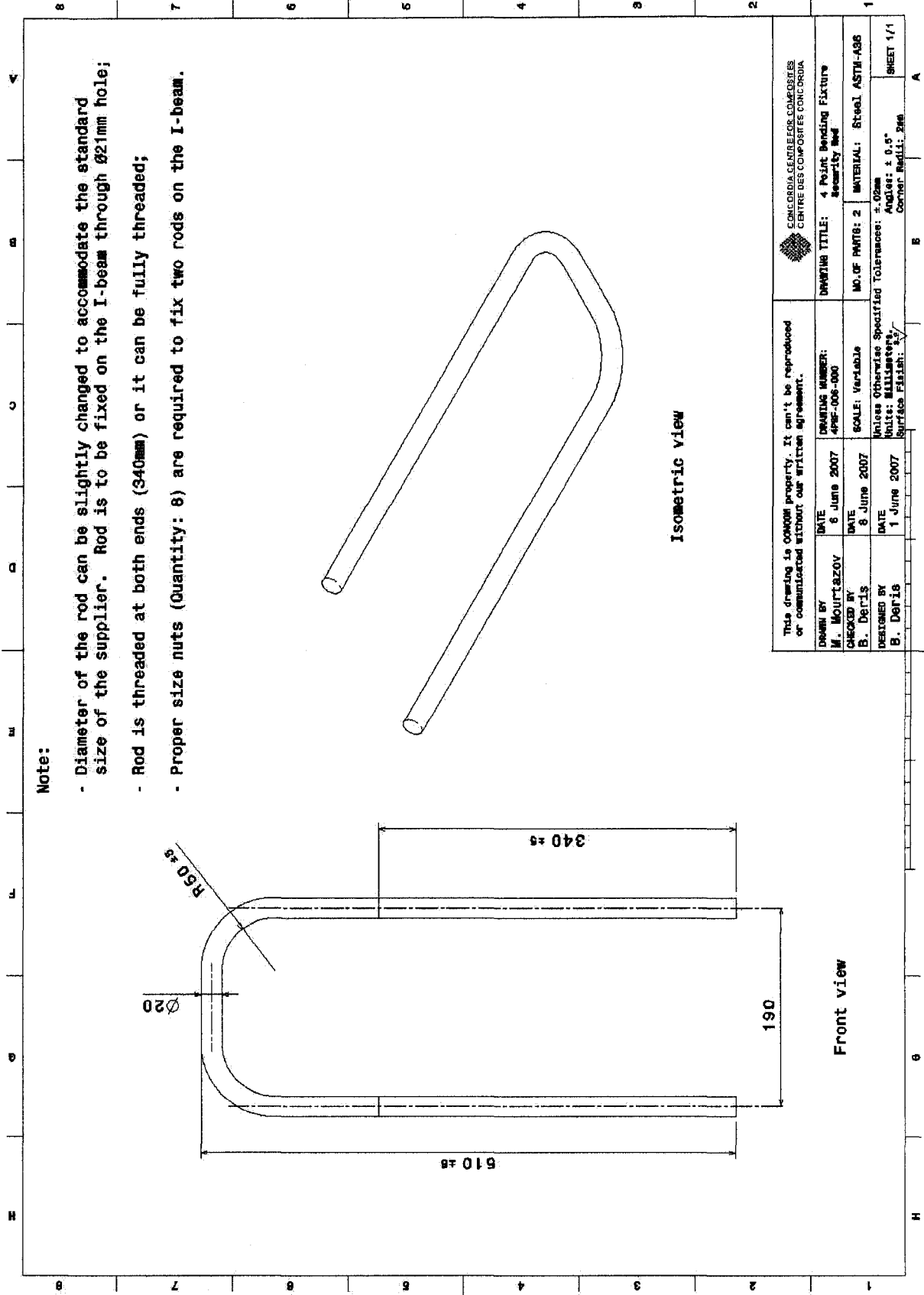
Isometric view

Top view

Front view

CONCORDIA CENTRE FOR COMPOSITES CENTRES COMPOSITES CONCORDIA		DRAWING TITLE: 4 Point Bending Fixture Top Grip: PART 2	
DRAWN BY M. MOURTALZOV	DATE 8 June 2007	DRAWING NUMBER: 4PBF-005-002	M.O.F PARTS: 1
CHECKED BY B. DORIS	DATE 8 June 2007	SCALE: Variable	MATERIAL: Steel ASTM-A36
DESIGNED BY B. DORIS	DATE 1 June 2007	Unless otherwise Specified Tolerances: ±.02mm Units: Millimeters Surface Finish: 3.2 Angles: ± 0.5° Corner Radii: 2mm	
			SHEET 1/1

This drawing is CONCORD property. It can't be reproduced or communicated without our written agreement.



**Note:**

- Diameter of the rod can be slightly changed to accommodate the standard size of the supplier. Rod is to be fixed on the I-beam through Ø21mm hole;
- Rod is threaded at both ends (340mm) or it can be fully threaded;
- Proper size nuts (Quantity: 8) are required to fix two rods on the I-beam.

This drawing is company property. It can't be reproduced or communicated without our written agreement.		CONCORDIA GENIE RESEARCH CENTRES CENTRE DES RECHERCHES CONCORDIA	
DRAWN BY M. MOURTIZOV	DATE 6 June 2007	DRAWING NUMBER: 4PSC-006-000	DRAWING TITLE: 4 Point Bending Fixture Security Nut
CHECKED BY B. Deris	DATE 8 June 2007	SCALE: Variable	NO. OF PARTS: 2
DESIGNED BY B. Deris	DATE 1 June 2007	MATERIAL: Steel ASTM-A36 Unless Otherwise Specified Tolerances: ±.02mm Units: Millimeters Surface Finish:	
			Corner Radii: 2R6 SHEET 1/1